The gametophyte specific ARM repeat protein AtARO1 is required for actin dynamics in *Arabidopsis* during pollen tube growth and double fertilization

DISSERTATION

A thesis submitted to the
Faculty of Natural Sciences, Biology and Preclinical Medicine,
University of Regensburg
for the degree of doctor of natural sciences (Dr. rer. nat.)

by Marina Gebert from Hamburg

5/2008

Promotionsgesuch eingereicht am:	21.05.2008
Tag des Kolloquiums:	11.07.2008
Die Arbeit wurde angeleitet von:	Prof. Dr. T. Dresselhaus
Prüfungsausschuß:	Vorsitzender: Prof. Dr. G. Längst
	Erstgutachter: Prof. Dr. T. Dresselhaus
	Zweitgutachter: Prof. Dr. E. Kerkhoff
	Drittprüfer: Prof. Dr. H. Tschochner

CONTENTS

ABBREVIATIONS

Amino Acids

Ala	A	Alanine	Leu	L	Leucine
Arg	R	Arginine	Lys	K	Lysine
Asn	N	Asparagine	Met	M	Methionine
Asp	D	Aspartic acid	Phe	F	Phenylalanine
Cys	C	Cysteine	Pro	P	Proline
Gln	Q	Glutamine	Ser	S	Serine
Glu	E	Glutamic acid	Thr	T	Threonine
Gly	G	Glycine	Trp	T	Tryptophan
His	H	Histidine	Tyr	Y	Tyrosine
Ile	I	Isoleucine	Val	V	Valine

Chemicals and solutions

Ca^{2+}	calcium
$CaCl_2$	calcium chloride
$Ca(NO_3)_2$	calcium nitrate
$CoCl_2$	Cobalt chloride
CSPD	3-(4.methoxyspiro{1,2-dioxetan-3,2´-(5´chloro)tricyclo[3.3.1.1^{3,7}]decan}-4-yl) Phenylphosphate, disodium salt
$CuSO_4$	copper sulfate
Dig	Digoxigenin
DMSO	Dimethylsulfoxide
EDTA	Ethylenediaminotetraacetic acid
EGTA	Ethylenglycol-bis-[β-aminoethyl-ether]-N,N,N´,N´-tetraacetic acid
$FeSO_4$	iron sulfate
H_3BO_3	boric acid
HCl	hydrogen chloride
Hg	mercury
H_2O	water
KAc	potassium acetate
KCl	potassium chloride
KH_2PO_4	monopotassium phosphate
KI	potassium iodide
KNO_3	potassium nitrate
LiAc	lithium acetate
LiCl	lithium chloride
LiDS	lithium dodecyl sulfate
Mg^{2+}	magnesium

$MgCl_2$	magnesium chloride
$MgSO_4$	magnesium sulfate
$MnCl_2$	manganese chloride
$MnSO_4$	manganese sulfate
NaCl	sodium chloride
Na_2EDTA	sodium ethylenediaminotetraacetic acid
Na_2MoO_4	sodium molybdate
NaOAC	sodium acetate
NaOH	sodium hydroxide
NH_4AC	ammonium acetate
NH_4NO_3	ammonium nitrate
^{32}P	radioactive phosphor isotope 32
PEG	polyethylene glycol
PI	propidium iodide
RbCl	rubidium chloride
SDS	sodium dodecyl sulfate
Tris	tris(hydroxymethyl)aminomethane
x-Gal	5-bromo-4-chloro-3-indolyl β-D-galactoside
$ZnSO_4$	zinc sulfate

Genetics and molecular biology

35S-Pro	CaMV 35S promoter
35Sp	CaMV 35S promoter
A	adenosine
aadA	Aminoglycoside 3´-adenyltransferase
Amp	ampiciline
BAC	bacterial artificial chromosome
bar	BASTA resistance
bp	base pair
C	cytidine
cDNA	complementary DNA
CDS	coding sequence
ColE1	colicinogenic factor E1- origin of replication
cRNA	complementary RNA
dCTP	2´-deoxycytidine 5´-triphosphates
DNA	deoxyribonucleic acid
DNAse	deoxyribonuclease
dNTPs	2´-deoxyribonucleoside 5´-triphosphates
dT	deoxythymidine
dUTP	2´-deoxyuridine 5´-triphosphate
E.coli	*Escherichia coli*

EST	expressed sequence tag
F-actin	filamentous actin
G	guanosine
G-actin	globular actin
gDNA	genomic DNA
GDP	guanosine-5´-biphosphate
GFP	green fluorescent protein
GTP	guanosine-5´-triphosphate
iF2	intron FAD2 (fatty acid desaturase 2)
int	intron
LB	left border
loxP	locus of X-over P1
mRNA	messenger RNA
NOS	nopaline synthase
Npt II	neomycin phosphotransferase
OCS	octopine synthase
OD_{600}	optical density at 600 nm
ORF	open reading frame
ori	origin of replication
pat	phosphinotricin-acetyltransferase
PCR	polymerase chain reaction
Q-PCR	quantitative PCR
RB	right border
mRFP	monomeric red fluorescent protein
RNA	ribonucleic acid
RNAse	ribonuclease
RT-PCR	reverse transcriptase PCR
SDS-PAGE	sodium dodecyl sulfate polyacrylamide gel electrophoresis
Sm/Sp	resistance against streptomycin/spectinomycin
ST-LS1	intron from the *Solanum tuberosum* LS1 gene
T	thymidine
T35S	terminator of the CaMV 35S gene
uidA	*β-glucuronidase*
UTR	untranslated region
YFP	yellow fluorescent protein

Standrad Units and Physical Parameters

℃	degree Celsius	nM	nanomolar
Ci	Curie, unit of radioactivity	nm	nanometer
cm	centimeter	Ω	Ohm
g	gram	Pa	Pascal
h	hours	pH	power of hydrogen
kb	kilobasepair	psi	pound-force per square inch
kDa	kilodalton	rpm	revolutions per minute
l	liter	µFD	microfarad
lx	lux	µg	microgram
M	molar	µJ	microjoule
mg	milligram	µl	microliter
ml	milliliter	µm	micrometer
mm	millimeter	µM	micromolar
mM	millimolar	U	unit
mmol	millimole	UV	ultraviolet light
M_r	molecular mass	V	volt
N	normal	xg	acceleration of gravity
ng	nanogram		

Other abbreviations

3D	three dimensional
Ac.	accession number
et al.	“et alia”, latin for “and others”
e.g.	“exempli gratia“, latin for “for example”
Fig.	figure
fw	forward
LP	long pass
rev	reverse
SD	synthetic defined

1. INTRODUCTION

1.1 Development of the female and male gametophytes

Great advances in microscopy were made in the middle of the 19th century, when scientists like the Italian mathematician and astronomer Giovanni Battista Amici or the german physicist Ernst Abbe, together with the mechanician Carl Zeiss, used new types of glass lenses and discovered the effects of immersion systems with water or oil. Together with these technical advances, great steps were made in the discovery of processes concerning the life cycles of both, animals and plants. The plants life cycle consists of a diploid sporophyte and the haploid gametophytes, which develop inside the sporophytic tissues in all angiosperms. While pollen grains are released from the sporophytic tissue and are easily visible on the stigma, fertilization itself takes place deeply embedded in maternal tissues. Thus, first observations of pollen tubes germinating on a stigma were already made by Amici in 1824, but identification of the fertilization processes was hindered by the enclosure of the female germ unit in sporophytic tissues. This was observed 60 years later, in 1884 by Strasburger (Strasburger, 1879), 9 years after first microscopic observations of the fertilization process in sea urchins by Oscar Hertwig (1875). It took another 14 years (Nawashin, 1898) to discover double fertilization, a form of reproduction unique to flowering plants (Lord and Russell, 2002). Double fertilization was since an object of thorough investigations, first on the morphological level (e.g. Faure et al., 2002; Schneitz et al., 1995 and references therein) and since recent years on the molecular level (Berger, 2008; Laux and Jürgens, 1997; Lord and Russell, 2002; Weterings and Russell, 2004). While only some underlying molecular processes are understood so far, structures and developmental steps detectable with the microscope are well described. In the model plant *Arabidopsis thaliana*, the pistil consists of the ovary, formed by the two fused carpels, the stylus and the stigma. The ovary is divided by a false septum that consists of transmitting tissue in its centre and is fused with the inner layer of the ovary wall at its margins (Mansfield and Bowman, 1994). At these margins the ovules emerge, producing the female gametophytes. The female gametophyte (embryo sac) of angiosperms is the essential structure that gives rise to and nourishes the embryo. The most common form of angiosperm female gametophytes observed in over 70% of the species examined is the monosporic-type megasporogenesis combined with *Polygonum*-type megagametogenesis (Yadegari and Drews, 2004). Ovular bulges emerge from the epidermal cell layer and the megaspore mother cell originates from one of the cells found in the extreme apex of these protrusions (Schneitz et al., 1995). During meiosis, four haploid megaspores arise from the one diploid megaspore mother cell, which are enclosed by a single cell layer called the nucellus. Three of the megaspores degenerate, while the fourth cell, the functional megaspore or mononuclear embryo sac, undergoes three more rounds of mitotic divisions to form an eight-nucleate cell. Meanwhile, the inner and outer integuments completely enclose the embryo sac and nucellus cells but forming a small opening, the micropyle, where the pollen tube will penetrate upon fertilization. Opposite of the micropyle the chalaza is positioned, where the nucellus is connected to the integuments and a vascular bundle provides nutrients to the ovule. After mitotic divisions and nuclear migration, four nuclei are situated at each pole of the embryo sac,

separated by a large vacuole. One nucleus from each pole starts to migrate into the center of the embryo sac and cellularization takes place. A seven-celled embryo sac is formed, consisting of two synergid cells, the egg cell, the central cell with two polar nuclei laying adjacent to each other, and three antipodal cells. In *Arabidopsis*, the two polar nuclei of the central cell fuse to form the diploid secondary endosperm nucleus and the three antipodal cells degenerate before fertilization (Christensen et al., 1997). In other plant species, as e.g. in grasses, the antipodal cells proliferate, forming a cell cluster of 20 to up to 60 cells (Huang and Sheridan, 1994). At maturity, all four remaining cells of the *Arabidopsis* female gametophyte are highly vacuolated and thus exhibit a strong polarity. In the mature embryo sac, the nuclei of the two synergid cells are situated at the micropylar end, while large vacuoles occupy the chalazal part of the cells. The egg cell is situated slightly above the synergids, towards the chalaza and presents the opposite polarity, with the large vacuole situated at the micropylar end and the cytoplasm and nucleus concentrated at the chalazal part of the cell. The large central cell likewise accumulates most of its cytoplasm around the secondary nucleus which is adjacent to the chalazal end of the egg cell, so that egg and central cell nuclei lie very close to each other (Christensen et al., 1997).

Male gametogenesis takes place within the anthers, which contain reproductive as well as non-reproductive tissues responsible for producing pollen grains and releasing them in order to allow fertilization processes (Goldberg et al., 1993). Male gametophytes (pollen grains) develop after mitosis of a diploid sporophytic cell that forms the tapetal initial and the sporogenous initial or pollen mother cell. This pollen mother cell undergoes meiosis, giving rise to a tetrad of haploid cells (McCormick, 1993). After the cells are released from their surrounding callose wall by degradation of the wall with callase secreted from the tapetum, the free microspores experience several cellular changes. First, the pollen cell wall, composed of two layers, is built. The inner layer, the intine, contains high amounts of pectocellulose, while the outer layer (exine) is built up from sporopollenin, a very complex and degradation-resistant substance that is mainly synthesized by the tapetum. The exine displays a complex sculpted pattern of spines, ridges or perforations that are unique to distinct species and make pollen grains of each plant species unmistakable.

Meanwhile, the microspore nucleus migrates from the center of the cell towards one side, and a large vacuole is formed. Consequently, an asymmetric mitotic cell division takes place resulting in a larger vegetative cell harbouring a smaller generative cell that is completely enclosed by the vegetative pollen grain (McCormick, 2004). The generative cell contains only little cytoplasm, few mitochondria and endoplasmatic reticulum (ER) compared to the vegetative cell and its chromatin is highly condensed. In 70% of all flowering plants, male gametophytes are released from the anthers as bicellular pollen grains. The second mitotic division of the generative cell that results in the formation of the two sperm cells takes place after pollination inside the growing pollen tube. In the remaining plant species, like *Arabidopsis*, the second mitotic division is completed before anther dehiscence (McCormick, 1993). In both cases, pollen grains have to partially dehydrate to become fully mature before being released from the anther tissues (McCormick, 2004). Dehiscence of anthers begins shortly after formation of the tetrads (Goldberg et al., 1993), including the degeneration of specialized cells, the so called circular cell clusters, at the borders of the two upper and lower pollen sacs within each anther, as well as breakdown of the tapetum cells and the connective. Decomposition of these

cells results in the fusion of two pollen sacs on each side of the anther into a single locule. Finally, the anthers brake open at the stomium and mature pollen is released. The pollen of cross-pollinating plant species is transported towards the female parts of the flower either by wind, insects, or birds, while it is shed directly onto the stigmas of self-pollinating flowers. Here, the pollen grain adheres, rehydrates, and a cascade of cellular events leads to the establishment of polarity in the male gametophyte and subsequent germination (Weterings and Russell, 2004). The emerging pollen tube grows through the stigma and style, guided by chemotropic and/or mechanical sporophytic guidance cues (Higashiyama and Hamamura, 2008). Amongst others, arabinogalactan proteins were proposed to guide the pollen tubes trough the transmitting tract and towards the ovule in different plant species (Sanchez et al., 2004). Further, gametophytic guidance of the pollen tube towards the ovule is governed by the female gametophyte in *Arabidopsis* and *Torenia fournieri* (Higashiyama and Hamamura, 2008). Short-range signals, secreted by the egg apparatus of maize or the synergids of *Torenia* were shown to be important in micropylar guidance, the last phase of gametophytic guidance of the pollen tube (Higashiama et al., 2001; Márton et al., 2005). The pollen tube finally grows through the micropyle and enters the receptive synergid. Here, the pollen tube tip bursts and releases its cytoplasmic content, together with the two sperm cells. The sperm cells migrate towards the egg and central cell to accomplish double fertilization. One sperm cell fuses with the egg to form the diploid zygote and the other sperm cell fuses with the central cell, to give rise to the triploid endosperm.

1.2 Roles of the actin cytoskeleton during fertilization

The actin cytoskeleton is essential to many cellular processes during plant gametophyte development, fertilization and embryogenesis (Drøbak et al., 2004; Ren and Xiang, 2007; Webb and Gunning, 1994). In recent years, great emphasis was placed on elucidating the pathways responsible for organizing, maintaining and rearranging the dynamic actin cytoskeleton in both male and female reproductive tissues during the fertilization process (e.g. Chen et al., 2002; Fu et al., 2000; Huang and Sheridan, 1998; Huang et al., 2003; Huang et al., 2007; Pawloski et al. 2006; Thomas et al. 2006b).
On the female side, actin seems to play a crucial role, although experimental data is still scarce. During megagametogenesis, extensive nuclear migrations take place, and microtubules as well as microfilaments are most likely involved in positioning these nuclei (Webb and Gunning, 1994). The cells within the embryo sac before and after fertilization are highly polarized (McCormick, 1993) and central cell and egg cell are known to contain randomly distributed actin filaments in their perinuclear regions (Webb and Gunning, 1994). In the synergids, high amounts of actin bundles are oriented parallel to the long axis of the cells. Extensive cytoskeletal modifications were observed along with the degeneration of one of the synergids and the pollen tube discharge (Fu et al., 2000). Subsequently, so-called “actin coronas” are formed at the chalazal region of the synergid and the interface between egg cell and central cell (Fig. 1.1; Fu et al., 2000).

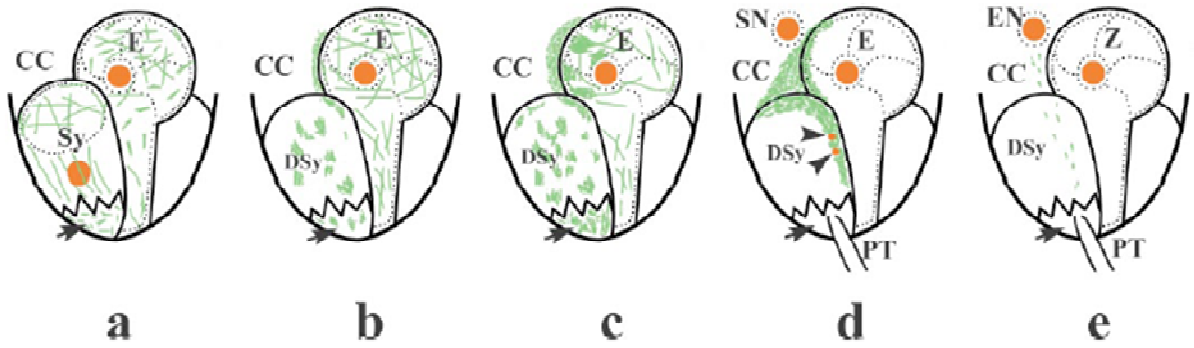

Fig.1.1. Diagrammatic reconstruction of actin organization (green) and nuclear position (red) during fertilization in *Torenia fournieri*. (a) Mature embryo sac with dense actin present near filiform apparatus (arrows); (b) onset of synergid degeneration with first evidence of corona formation; (c) actin reorganization just prior to pollen tube penetration; (d) pollen tube arrival, discharge, and transport of sperm nuclei (arrowheads); and (e) completion of fusion, dissolution of actin corona, initiation of post-fertilization actin pattern. CC, central cell; dSy, degenerated synergid; E, egg cell; EN, endosperm nucleus; PT, pollen tube; SN, secondary nucleus; Z, zygote. Figure and text from Fu et al. (2000)

These actin structures were found throughout plant species studied to date (Weterings and Russell, 2004 and references cited herein.). It is believed that the two sperm cells migrate along these actin structures towards their sites of fusion (Fu et al., 2000; Huang and Sheridan, 1998). Short, randomly oriented actin bundles were found in the egg and central cell of most plants examined, but their function in gamete fusion remains unclear to date. It is assumed, however, that they are necessary for the transport and fusion of the sperm nuclei with the egg and central cell nuclei (Fu et al., 2000; Huang et al., 1999; Ye et al., 2002).

During male gametophyte meiosis, cell polarity and predictable division planes are established jointly by the actin cytoskeleton and microtubules (Nacry et al., 2000 and references cited herein). Existence of actin in sperm cells was controversially discussed since F-actin was only found in some species examined, where in turn its presence was clearly proven. Possibly, these actin filaments might be involved in partly self-regulated sperm cell movement within the degenerating synergid (Ye et al., 2002 and references therein).

In addition, a functional actin cytoskeleton is a prerequisite for successful pollen germination and tube growth (Sheoran et al., 2006). According to morphological observations the growing pollen tube was described to contain four distinctive zones, namely the vesicle rich zone at the extreme apex of the pollen tube, followed by the organellar zone, the nuclear zone and the vacuolar zone (Fig 1.2A). In *Arabidopsis*, a first callose plug is formed after 2-3 hours of germination behind the cytoplasm that is pushed from the grain into the tube (Lennon and Lord, 2000). Filamentous actin is assembled starting from the subapex alongside the shank of the growing pollen tube (Fig. 1.2B) in parallel bundles and builds the backbone for organelle and sperm cell transport, reverse-fountain cytoplasmic streaming, and the delivery of secretory vesicles containing new membrane and wall material to the clear zone of the pollen tube tip (Vidali and Hepler, 2001). Dynamic endo-/exocytotic processes take place at the

pollen tube tip, where short actin filaments are present (Camacho and Malhó, 2003). Besides described processes it is now also well appreciated that dynamic changes in organization of tip-localized actin are indispensable for polar growth of tip growing cells like pollen tubes or root hairs (Cardenas et al., 2008). A cortical actin fringe was recently demonstrated to be present consistently in pollen tubes of lily and tobacco, due to an enhanced fixation protocol (Lovy-Wheeler et al., 2005). This fragile structure was only observed in few occasions beforehand, probably because of its fast degradation and formation of artefacts during fixation and staining procedures.

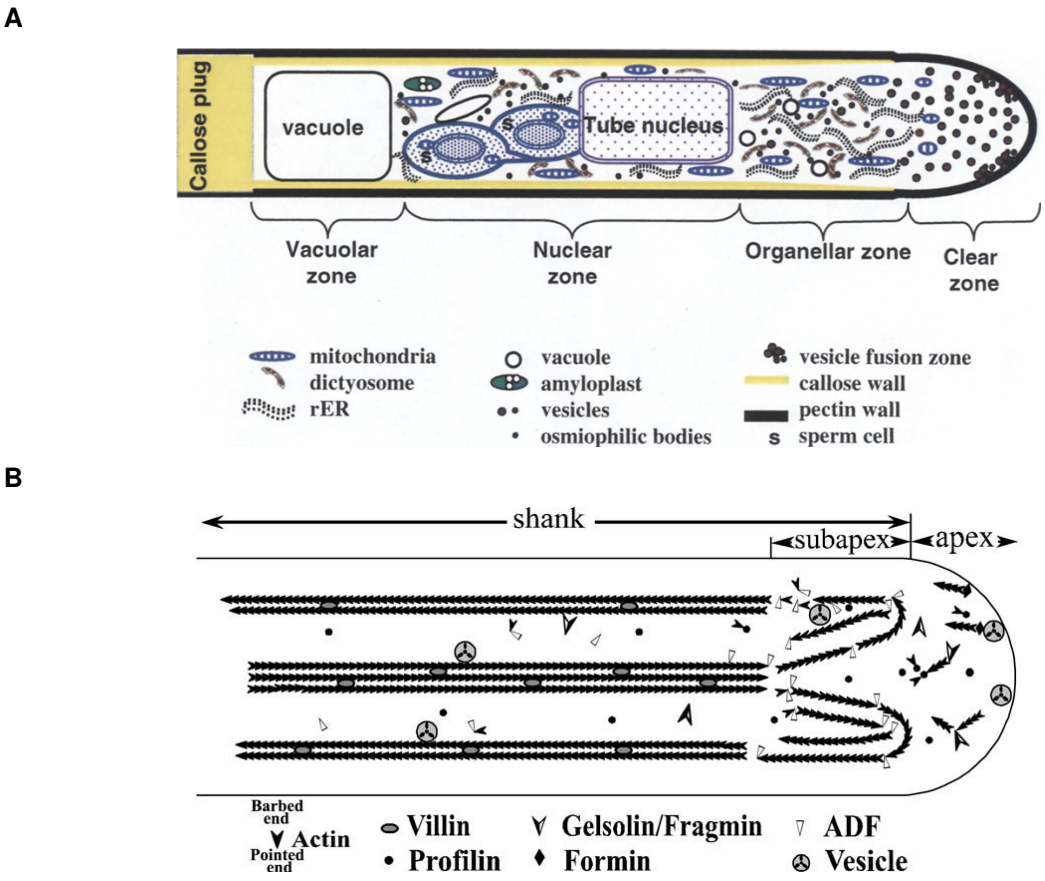

Fig. 1.2. Schematic representation of the pollen tube. (**A**) Diagram of an *in vivo* grown pollen tube cell of *A. thaliana* illustrating four distinct zones. Not to scale. Figure and text from Lennon and Lord (2000). (**B**) F-actin organization and the major sites of activity of actin-binding proteins in pollen tube. In the shank of the pollen tube, the actin filaments are often organized into bundles, connected by villins. At the subapex, where there exists an alkaline band, F-actin becomes less organized or forms a collar-like zone of fine filament bundles. ADFs are thought to play an important role in maintaining a high level of actin cycling activity by inducing filament severing and actin filament depolymerization. A dynamic meshwork of fine actin filaments may exist at the extreme apex, which is thought to organize vesicle docking and fusion. Gelsolin and fragmin may regulate Ca^{2+}-mediated dynamics of the actin cytoskeleton in the tip region of pollen tubes. Profilin is uniformly distributed in the pollen tube, but more actin-profilin complexes may form in the tip region. Formins might be important for the nucleation of short actin filaments in the tube tip, which facilitate targeting and fusion of vesicles. Figure and text modified from Ren and Xiang (2007).

Despite the fact that presence of dynamic forms of actin in the very apex of tip growing cells was controversially discussed in both, pollen tubes and root hairs, quite some progress was made in identifying a plethora of proteins involved in the organization, assembly and disassembly of the dynamic actin cytoskeleton in relation to oscillatory growth processes (e.g Bannigan and Baskin, 2005; Huang et al., 2007; Ingouff et al., 2005; Ren and Xiang, 2007; Staiger and Blanchoin, 2006; Thomas et al., 2006a; Zhao and Ren, 2006). For the pollen tube to grow through the female tissues and finally reach the ovule, it has to interact with a variety of different tissues and recognize a number of extracellular long and short range guidance cues and translate these molecules into intracellular signaling cascades that finally result in changes in the actin cytoskeleton and subsequent polarized growth. In this respect, tip growing cells of plants (e.g. pollen tubes, root hairs or fern/moss protonemata), fungi (fungal hyphae) and animals (axonal growth cones) exhibit similar intracellular molecules and pathways, although responding to different extracellular cues (Palanivelu and Preuss, 2000). In general, extracellular signals are brought forward into intracellular signaling pathways by receptor kinases, G-proteins, calcium-based signaling or signaling involving inositol phospholipids (Clark et al., 2001) and all these components also seem to play important roles in pollen tubes and appear to be interconnected with dynamic actin changes during tube tip growth (Malhó et al., 2006).

1.3 Signaling pathways of tip growth mechanisms

Small GTPases of the Rho-like family are known to be important regulators of signaling pathways that control growth processes involving actin. Since the early 1990ies it is known that surface receptors are linked to the cytoskeleton by Rho-like GTPases in animal cells (Hall, 1998). The Rho-like GTPases comprise Rho, Rac and CDC42 in animals and fungi (Hall, 1998; Palanivelu and Preuss, 2000) and belong to the Ras superfamily of small GTP-binding proteins (G-proteins). These small (20-25 kDa) molecules work as molecular switches to regulate a great variety of cellular processes. They are divided into six main families, namely Ras, Rho, Arf, Rab, Ran and Rad (Oxford and Theodorescu, 2003). While Rho proteins are involved in cytoskeletal dynamics and morphology, members of the Ras family are involved in cell proliferation (Boureux et al., 2007). Rab proteins and Arf GTPases have been implicated in vesicular trafficking and Ran is a regulator of nucleo-cytoplasmic transport (Konstantinopoulus et al., 2007).The general function of Rad still remains unclear (Oxford and Theodorescu, 2003). After post-translational modifications, Rho-like proteins associate with the membrane (Hussey et al., 2004) and are involved in signaling cascades that evoke rearrangements of the actin cytoskeleton, especially at the leading edges of motile cells, such as lamellipodia and filopodia in migrating mammalian cells (Sumi et al., 1999). More recently, small Rho-like GTPases, closely related to mammalian Rac, were also identified in plants and referred to as Rop (Rho of Plants) or Racs (Kost et al., 1999). Like their mammalian counterparts, Rop proteins are involved in actin organization and polar growth in pollen tubes and root hairs and accumulate in their apices. They seem to be activated at the growing tip by external cues, control intracellular levels of free Ca^{2+} and phosphoinositides, and are involved in exocytotic processes. In this respect, they exhibit a striking analogy to Rho proteins in guided axon growth in animals (Palanivelu and Preuss, 2000; Zheng and Yang, 2000). In *Arabidopsis* pollen tubes, two direct targets of tip-localized ROP1 were identified

recently (Gu et al., 2005). RIC3 (ROP-interactive CRIB motif-containing 3), which promotes the accumulation of tip-localized Ca^{2+}, and RIC4, involved in enhancing the assembly of apical F-actin, were found to operate in two counteracting pathways, regulating each other to control actin dynamics and pollen tube tip growth. In animals, one effector of CDC42 is WASP (Wiskott-Aldrich-Syndrome Protein), which is activated by CDC42 and phosphatidylinositol 4,5 bisphosphate (PtdIns4,5P_2) and binds to the ARP2/3 (actin related protein 2/3) complex. This complex is thereupon activated itself and drives nucleation of side branches on existing actin filaments. A plant Arp2/3 complex was recently identified and mutations of proteins from this complex in *Arabidopsis* resulted in abnormal F-actin organization and thereby affected growth of trichomes, pavement cells and root hairs (Li et al., 2003; Mathur et al., 2003a/b; Saedler et al., 2004)

Phospholipid signaling is another important factor regulating plant tip growth (Fischer et al., 2004). In this pathway, phosphatidylinositol (PtdIns) is sequentially phosphorylated by PtdIns-4-kinases and PtdIns-5-kinases (PIPKs) to form PtdIns4P and PtdIns4,5P_2, respectively. Upon specific stimuli, PtdIns4,5P_2 is hydrolyzed by Phospholipase C (PLC) and the second messengers diacylglycerol (DG) and Ins(1,4,5)P_3 (Inositol 1,4,5 triphosphate) are produced. Ins(1,4,5)P_3 mediates release of Ca^{2+} from internal stores while DG activates Protein kinase C to induce further downstream events (Clark et al., 2001; Perera et al., 2007). Phospholipids such as PtdIns4,5P_2 are thought to be recruited to specific membrane compartments at the growing tips of pollen tubes and root hairs, where they are considered to play important roles in cytoskeleton reorganization and membrane trafficking (Kusano et al., 2008). Members of the ADP-ribosylation factor (ARF) and Rab families of small GTPases seem to be involved in spatial regulation of PtdIns4,5P_2 and thus polarized secretion through regulation of a Ca^{2+} dependent PtdIns-4-kinase, PI4Kβ1, at tip-localized membrane compartments (Preuss et al., 2006). Thole et al. (2008) showed that a PtdIns4P phosphatase, RHD4 (Root hair defective 4), was recruited to RabA4B-labeled membranes and was required for proper root hair development. Here it might regulate levels of PI4Kβ1 generated PtdIns4P. Another enzyme recently found to be located in the tip membrane of growing root hairs is PIP5K3 (PtdIns-5-kinase 3; Kusano et al., 2008). It was proposed previously that PtdIns4,5P_2 might create “PIP landmarks” in the tip plasma membrane, that aid in the organization of the actin cytoskeleton and focus vesicle secretion to the extreme apex of root hairs (Vincent et al., 2005). In account with this model, *Arabidopsis* PIPK1 was shown to directly interact with F-actin and to recruit PI4Kβ1 to the cytoskeleton (Davis et al., 2007).

Many of the actin binding proteins (ABPs; Fig. 1.2B) found to date are regulated by Ca^{2+} (e.g. profilin, gelsolin / villin), pH (actin depolymerising factor (ADF) and actin interacting protein (AIP)) or in response to signaling molecules (Ren and Xiang, 2007). Ca^{2+} and pH gradients are formed along the pollen tube and an alkaline band was found to reside near the cortical fringe in the clear zone (Hepler and Lovy-Wheeler, 2006). Comprehensive models were proposed by Cole and Fowler (2006) and Cardenas et al. (2008) on how oscillatory tip growth could be achieved and in part be self-regulating. At high Ca^{2+} levels, ABPs of the gelsolin/villin family and profilin are activated. While gelsolins and villins stimulate depolymerisation and actively fragment F-actin, profilin is bound to monomeric actin and prevents spontaneous nucleation of new actin filaments. The activity of profilin is also in part modulated through the cleavage of PtdIns4,5P_2 by the Ca^{2+} sensitive PLC. In animals, PtdIns4,5P_2 and profilin build complexes that inhibit hydrolysis of PtdIns4,5P_2 by PLC. Upon phosphorylation, PLC

can overcome the inhibitory effect of profilin and cleave PtdIns4,5P_2, thereby releasing profilin, which is in turn free to bind G-actin (Drøbak et al., 1994). PLC was found to be localized laterally at the shank plasma membrane of rapidly growing *Petunia* pollen tubes, thus restricting PtdIns4,5P_2 to the membrane at the apex (Dowd et al., 2006). Upon high Ca^{2+} levels, polymerisation of new actin filaments is thus slowed down and exo-/endocytotic processes are reduced. While growth declines, stretch-activated Ca^{2+} channels close and free cytosolic Ca^{2+} is sequestered into the ER, mitochondria and the vacuole. The activity of gelsolin/villin and profilin is inhibited and actin polymerization increases. This process might be enhanced by ROP1/RIC4 activity. Further, Rho small GTPase-activated phosphorylation at a terminal region Ser residue plays an important role in regulating the actin binding and depolymerising activity of ADFs/cofilins in mammals and plants (Chen et al., 2003 and references therein; Edwards et al., 1999). NtRac1 seems to mediate phosphorylation of NtADF1, thereby inhibiting actin binding and depolymerisation (Chen et al., 2003). Pollen tube growth is enhanced by the assembly of new actin filaments and subsequent exocytotic processes, leading to a new growth spurt. Opening of stretch-activated Ca^{2+} channels and/or activation of the ROP1/RIC3 dependent pathway thereupon lead to a new increase in intracellular Ca^{2+} levels.

As members of the Rop/Rac family occupy a central position in the regulatory network of pollen tube tip growth, answers to the question on how these small GTPases are regulated and linked to the extracellular cues important during pollen tube guidance are fundamental (Fig. 1.3). In neuronal growth cones, upstream regulators of Rho-like GTPases have been identified, which control transduction of external signals. Well characterized positive regulators found in neurons include guanine nucleotide exchange factors (GEFs). These proteins promote accumulation of active Rho by exchanging GDP for GTP. Recently, a novel family of RopGEFs has been identified in *Arabidopsis thaliana*. They comprise a plant-specific Rop nucleotide exchanger (PRONE) domain shown to contain GEF activity, but with no sequence homology to classical catalytic domains of animal RhoGEFs (Berken et al., 2005; Gu et al., 2006). Interestingly, one RopGEF homologue from tomato, KPP (kinase partner protein), was shown to interact with the intracellular kinase domain of receptor-like protein kinases (RLKs) PRK1 and PRK2 (Kaothien et al., 2005) and overexpression of KPP induced isotropic growth of pollen tube tips. Thus, a first link between extracellular signaling and intracellular downstream events leading to polar pollen tube tip growth was given. Negative regulators are GTPase-activating proteins (GAPs) and guanine nucleotide dissociation inhibitors (GDIs), which have also been identified in plants (Fu et al., 2001; Wu et al., 2000). Here, Rop activity seems to be linked to Ca^{2+} concentrations through a calmodulin-like protein kinase found in *Petunia inflata* (PiCDPK1), which presumably phosphorylates RhoGDI in a Ca^{2+} dependent manner (Yoon et al., 2006).

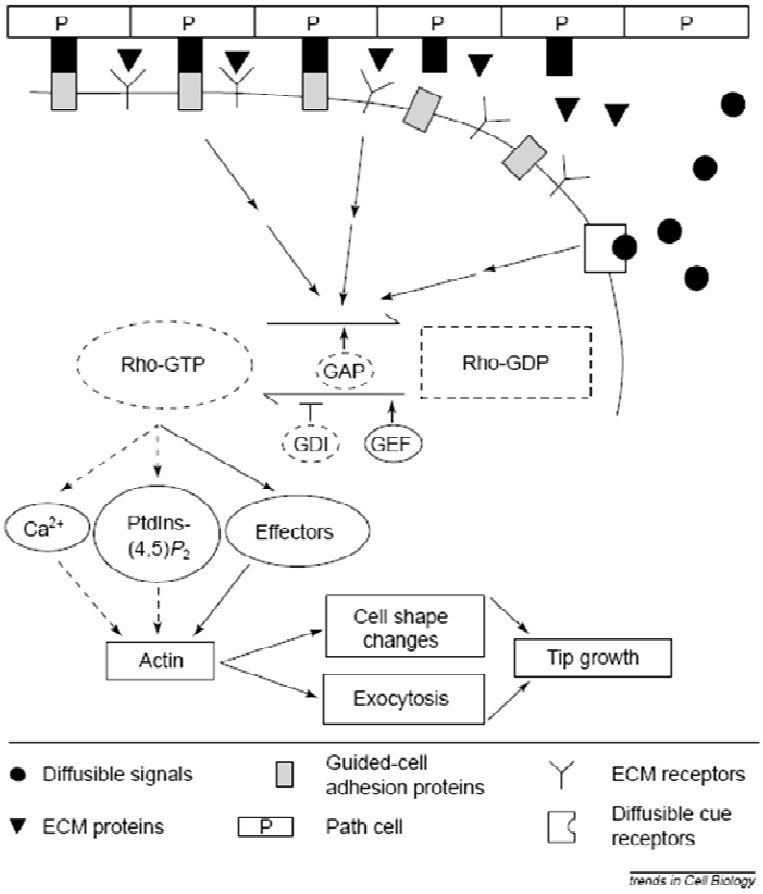

Fig. 1.3. Signal-transduction pathways involved in tip growth. Extracellular guidance cues are provided by diffusible signals (filled circles), extracellular matrix (ECM) proteins (filled triangles) and cell adhesion proteins on the guided cell (grey rectangles) and on cells in its path (P, black rectangles). Receptors for ECM proteins (Y) and for diffusible cues (open rectangle) are also indicated. Signals from the membrane are to upstream regulators [GTPase-activating protein (GAP), guanine nucleotide dissociation inhibitor (GDI) and GDP–GTP exchange factor (GEF)] of Rho GTPases. Activated Rho influences the actin cytoskeleton through phosphatidylinositol (4,5)-bisphosphate [PtdIns(4,5)P_2], calcium (Ca^{2+}) and other effector proteins. Actin cytoskeleton rearrangements result in downstream events (cell shape changes and directed exocytosis) that culminate in targeted tip growth. Components and processes recently identified in plants are indicated by dashed lines. Figure and text: Palanivelu and Preuss (2000).

In animals, Rho-GEFs and a RhoGAP (p190RhoGAP) have recently been found to interact with plakophilin, a member of the $p120^{ctn}$ (p120 catenin) superfamily of Armadillo repeat proteins, which are involved in cell adhesion and cytoskeleton assembly (Choi and Weiss, 2004; Hatzfeld, 2007; Niessen and Yap, 2006) through regulation of RhoGTPase activity (Yanagisawa et al., 2008). They therefore represent direct links between the cell adhesion proteins cadherins and actin regulating Rho GTPases. Although classical cell adhesion molecules like cadherins have not been identified in plants, homologues of another *Drosophila* cell-adhesion protein, Pollux, are present in *Arabidopsis* and rice (Zhang et al., 1996). Pollux is abundantly expressed in cells of the central nervous system along axon pathways, which use cell adhesion molecules to guide migrating axons. As many other parallels in

axon and pollen tube guidance, one can imagine that female transmitting tissues employ similar adhesion proteins to guide the pollen tube towards its goal, the ovule (Fig. 1.3).

1.4 Armadillo repeat proteins

Armadillo (ARM) repeat proteins are multifunctional proteins found to be involved in many developmental processes, including intracellular signaling and cytoskeletal regulation. In general, the degenerated ARM motif consists of about 42 amino acids forming three α-helices, which, in tandem repetition, give rise to a right handed superhelix of helices (Pfeifer et al., 1994). The resulting concave surface has previously been shown to mediate protein-protein interactions (Huber et al., 1997). The founding member of the ARM repeat family is *Armadillo*, a segment polarity gene from *Drosophila*. Its homologue in mammals, β-catenin was the first ARM protein found to be implicated in cytoskeletal regulation. It binds directly to cadherins to link the cell-cell adhesion molecules to the actin cytoskeleton via α-catenin. It is further important during embryonic development in animals and regulates cell differentiation and proliferation as key player in the Wnt signaling pathway.

In animals, extensive work has been published on the Wnt signaling pathway since the first Wnt genes were identified about 25 years ago (Wikramanayake and Wallingford, 2006). This signaling pathway, enabling an extensive array of transcriptional as well as non-transcriptional signal transduction mechanisms, is highly conserved from cnidarians to chordates. It coordinates mechanisms as diverse as cell adhesion, cancer development, differentiation of multiple cell lineages and polarity of single cells as well as of various tissues (Xiong and Kotake, 2006). Wnt signals are small, secreted and cystein-rich glycoproteins that activate downstream signaling events through binding to their membrane receptors. Their name is derived from the *Drosophila* segment polarity gene *Wingless* and the murine proto-oncogen *Int-1*. In mammals, 19 Wnt ligands were identified, most of which bind to receptors belonging to the family of seven-pass transmembrane receptors of the frizzled (Fz) family (Karner et al., 2006). Further, Wnt signals often bind to additional co-receptors of the LDL receptor-related protein (LRP) family. Dishevelled (Dsh), a protein found at the plasma membrane as well as in the cytoplasm, is activated by interaction with the transmembrane receptors. Probably depending on its subcellular localization, Dsh acts in two distinct branches of the Wnt pathway controlled by the different Wnt signals: the canonical and the non-canonical Wnt pathway. These two pathways diverge downstream of Dsh, probably with membrane bound Dsh functioning in the non-canonical and cytoplasmic Dsh working in the canonical pathway (Karner et al., 2006). In the absence of Wnt signals controlling the canonical pathway, the scaffolding protein axin and the tumor suppressor adenomatous polyposis coli (APC) bind newly synthesized β-catenin and recruit it to the so called “destruction protein complex” (Xiong and Kotake, 2006). Here, β-catenin is first phosphorylated by casein kinase 1 α (CK1α) and then by glycogen synthase kinase 3 β (GSK-3β). APC is probably phosphorylated in the same complex, enhancing its binding affinity to β-catenin. Subsequently, β-catenin is bound to and ubiquitinated by the $SCF^{\beta\text{-}TrCP}$ E3 ligase, formed by three subunits: Skp1, Cul1, and the F-box protein β-TrCP (Latres et al., 1999). Ubiquitination marks β-catenin for degradation in the proteasome. Activation of Dsh by binding of a Wnt signal to the Fz receptor in the canonical pathway leads to an inhibition of the “destruction complex” resulting in accumulation of β-catenin in the cytoplasm and

transport into the nucleus. Here it binds to transcription factors of the Lef/Tcf family, replacing the repressor Groucho and allowing transcription of target genes.

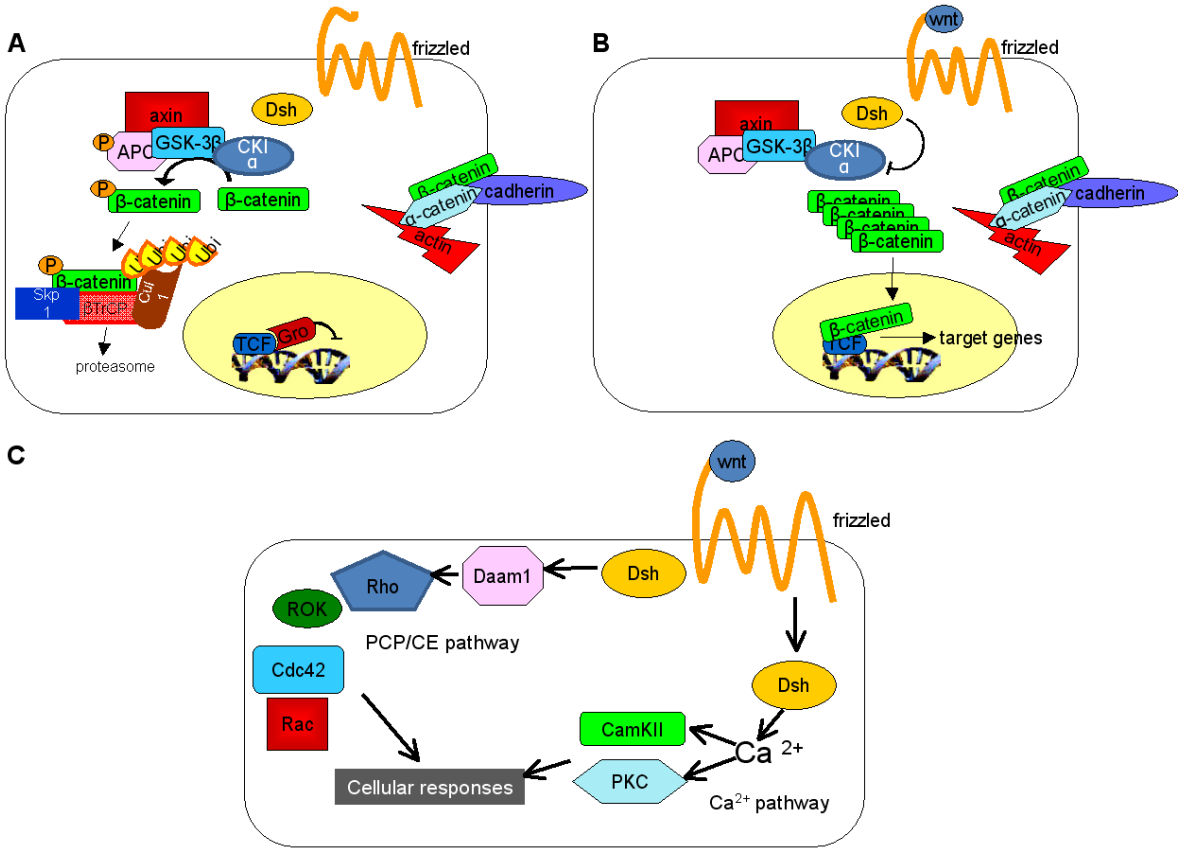

Fig. 1.4. The Wnt pathways. (**A**) Canonical pathway in absence of Wnt signals. β-catenin is found at cell adherens junctions. Cytosolic β-catenin is phosphorylated by the destruction complex (APC; Axin; CKI1α; GSK-3β) and marked for destruction in the proteasome by ubiquitination. (**B**) After Wnt binds to the receptor frizzled, Dsh inhibits the destruction complex and β-catenin accumulates in the cytoplasm. Cytoplsmic ß-catenin is transported into the nucleus and binds the transcription factor Tcf. Subsequently, transcription of target genes takes place. (**C**) The PCP/CE and Ca^{2+} non-canonical pathways. In the PCP/CE pathway, Rho and its effector ROK interact with Dsh through Daam1 and activate downstream GTPases and cellular responses in an yet unknown manner. In the Ca^{2+} pathway, Dsh leads to downstream events trough stimulating Ca^{2+} fluxes and thus activating kinases PKC and Cam KII.

The non-canonical Wnt pathway seems to be independent of β-catenin and can be divided into the Ca^{2+} pathway and the planar cell polarity/convergent extension (PCP/CE) pathway (Karner et al., 2006). These pathways affect cell polarity and shape as well as cell migration and involve the actin and microtubule cytoskeletons (Pfeifer and Polakis, 2000). In flies, the planar cell polarity pathway regulates the formation of single, actin-filled hairs at a defined location on each cell of the *Drosophila* wing. During the Wnt/Ca^{2+} pathway, Dsh stimulates Ca^{2+} fluxes and thus activates Ca^{2+}-sensitive kinases PKC and CamKII (Eisenmann, 2005). Similarly, Dsh is also needed in the PCP/CE pathway to activate small GTPases of the Rho family. Rho and its effector Rho-associated kinase (ROK) have

been shown to interact with Dsh through the bridging molecule Daam1, while the roles of other Rho family GTPases, like Rac and Cdc42, and further downstream mechanisms remain unclear. However, the Rho-like small GTPases seem to be the most obvious connection between the non-canonical Wnt signaling pathway and the cytoskeleton (Veeman et al., 2003). The PCP/CE pathway leads to diverse mechanisms controlling gastrulation movements, hair cell morphology or neuronal migration in vertebrates as well as the aforementioned cell polarity in *Drosophila*.

Besides ß-catenin/Armadillo, other proteins with ARM repeats were found to play important roles in many cellular processes in animals as well as in plants. Often, additional protein motifs can be found adjacent to several copies of ARM repeats, which contribute to their function and allow a classification into several subfamilies with a putative similar scope of duties (Coates, 2003). Some ARM repeat proteins have conserved functions in animals, plants and fungi, like importin-α. However, other plant ARM repeat proteins have been shown to have plant specific novel functions (Coates et al., 2003; Mudgil et al., 2004 and references cited therein). In *Arabidospis thaliana*, over 100 predicted proteins containing ARM repeats have been identified, but only few of them have been characterized so far (Mudgil et al., 2004). However, over the past decade, ARM repeat proteins have been discovered to play important plant-specific roles in signaling pathways such as the self-incompatibility response in *Brassica rapa* (Gu et al., 1998; Liu et al., 2007; Stone et al., 2003), the gibberellic acid signaling pathway in potatoes (Amador et al., 2001) or the abscisic acid response in *Arabidopsis* (Kim et al., 2004). Further roles of ARM repeat proteins were shown in trichome development (Downes et al., 2003), cell death and activation of defence mechanisms (González-Lamothe et al., 2006; Yang et al., 2006a; Zeng et al., 2004), as well as promoting lateral root development (Coates et al., 2006) and root-hair tip growth (Sakai et al., 2008; Yang et al, 2007).
The function of the U-box containing ARM repeat protein ARC1 (Armadillo repeat containing 1) during the *Brassica* self-incompatibility (SI) pathway is particularly well understood (Stone et al., 2003). Upon landing of an incompatible (self) pollen on the stigma, the male determinant SCR binds to the female determinant of SI, the transmembrane receptor SRK, and mediates auto-phosphorylation of the receptor. ARC1 binds to the activated receptor via its ARM repeats and is in turn phosphorylated by SRK. Thereupon, ARC1 presumably ubiquitinates an unknown substrate(s) as functional E3 ubiquitin ligase and relocalizes to the proteasome, where the substrate is degraded. During the absence of self-incompatible pollen, ARC1 actively shuttles between the cytosol and the nucleus, where it might have additional functions. Another U-box containing ARM protein from plants shown to exhibit a dual cellular localization is PHOR1, which is involved in gibberellic acid signaling. It was the first plant ARM repeat protein shown to be transported into the nucleus upon an extracellular stimulus (Amador et al., 2001). Yet another ARM repeat protein, ARIA, containing a BTB/POZ sequence motif, was found to interact with a transcription factor in the nucleus, that regulates abscisic acid-dependent gene expression. Besides, it was also localized to the plasma membrane, where its function is still unknown (Kim et al., 2004). Like in animals, plant ARM repeat containing proteins exhibit a plethora of different functions, probably not only due to differences in ARM repeat binding specificities but also through their additional domains. Many of the ARM repeat proteins seem to have more than one function, depending on their status in the cell, as indicated, for example by their phosphorylation.

In summary, not much is known about most of the ARM repeat proteins discovered in the genomes of plants. The described multiple functions of animal ARM repeat proteins in mediating signaling, cytoskeletal rearrangements, establishment of polarity, transcriptional activation, and protein degradation but also the putative novel functions of plant specific ARM repeat proteins promises them to be fascinating candidates to address open questions in the context of polar cell growth, the fertilization process and early embryogenesis.

1.5 Aims of the work

In a previous study, novel egg cell specific transcripts were identified by a transcriptomics approach using isolated egg cells of *Triticum aestivum* (Sprunck et al., 2005). Besides others, one egg cell transcript (EC-123) was identified which encodes a novel ARM repeat containing protein (wheat ARM repeat only; TaARO1). The corresponding gene was found to be specifically expressed in the egg cell and mature anthers (Sprunck et al., 2005). BLAST searches revealed similarities to predicted ARM repeat proteins of *Arabidopsis thaliana* and *Oryza sativa*, which appear to form small protein families of four members in each of the plant species.

During this work, continuation of bioinformatic analyses should be performed to identify more ARO-like proteins in plant or non-plant species, and to detect putative common protein features. The expression of all four *Arabidopsis* ARM repeat protein encoding genes (*AtARO1* to *-4*) in vegetative and reproductive tissues should be examined by RT-PCR or quantitative RT-PCR. *AtARO1* will be considered for detailed studies in transgenic plants expressing AtARO1-promoter::GUS constructs, as AtARO1 was found to encode the protein with highest similarity to TaARO1. Furthermore, the subcellular localization of AtARO1 should be examined in female and male gametophytes as well as during the fertilization process. Therefore, transgenic plants will be generated which express the AtARO1-GFP fusion protein under the endogenous promoter. Functional analysis of *AtARO1* should be carried out by using T-DNA insertion lines from the SALK institute, by generating egg cell-specific knock-downs of *AtARO1* using the RNAi approach, and by mis-expression of *AtARO1* in vegetative tissues. Finally, putative interaction partners of AtARO1 should be identified via a yeast two hybrid screen to further elucidate its function in pollen tube growth and during the fertilization processes.

2. MATERIALS AND METHODS

2.1 Chemicals, Enzymes and other consumables

All chemicals used were of the purity level "p.A." (per Analysis) or pure and purchased from the following companies if not indicated otherwise:
Applichem (Darmstadt), BD Biosciences (Sparks, MD, USA), Fluka (Buchs), Invitrogen (Karlsruhe), Merck (Darmstadt), Roth (Karlsruhe), Serva (Heidelberg), Sigma-Aldrich (München) and USB corporation (Cleveland, OH, USA).
DNA polymerases, dNTPs, restriction endonucleases, DNA/RNA modifying enzymes and other proteins were purchased from Invitrogen (Karlsruhe) or MBI Fermentas (St. Leon-Roth) unless indicated in the text. DNA size markers used were Lambda DNA/*EcoRI* + *HindIII* Marker, 3; Lambda DNA/Eco47I (*AvaII*) Marker, 13; Lambda DNA/*Eco130I* Marker, 16; Lambda DNA/*PstI* Marker, 24; FastRuler™ DNA Ladder, Low Range, ready-to-use and GeneRuler™ 1 kb DNA Ladder, ready-to-use. All DNA markers were from MBI Fermentas (St. Leon-Rot).
Hybond-N+ nylon membranes and radionucleotides α-[^{32}P]-dCTP (6,000 Ci/mmol) were obtained from Amersham Pharmacia Biotech (Freiburg) and Amersham Hyperfilm™ MP X-ray film from GE Healthcare (München).
Usage of kits is indicated in the text. All kits, enzymes and reagents were used following the manufacturers´ protocols, if not indicated otherwise.

2.2 Primers

Primers were synthesized by the companies Invitrogen (Karlsruhe) and biomers.net (Ulm) and primer sequences are listed in the appendix (Tables 7.1.1-7.1.6). 100 µM stock solutions were prepared and diluted in deionized water to 10 µM before use. Primer stocks and working solutions were stored at -20°C.

2.3 Standard molecular biology methods

Standard methods of molecular biology, such as gel electrophoresis, precipitation of nucleic acids and DNA cloning were performed and general buffer and media were prepared according to Sambrook et al. (1989) if not described otherwise in the text. All buffer and media were prepared with distilled water of the quality "aqua bidest" (ddH_2O) from a water purification system (Milli-Q Water System, Millipore, Schwalbach/Ts.) or deionized water. For sterile work, hardware and media were autoclaved in a Varioclav steam sterilizer 75 S (H+P Labortechnik AG, Oberschleißheim) for 20 minutes at 121°C and 2 x 10^5 Pa or media filtered through a sterile filter (pore size: 0.2 µm, Renner GmbH, Darmstadt).
Documentation of agarose gels was achieved with the Gene Genius Bio Imaging System (Syngene, Cambridge, U.K.) and processed with the GeneSnap software (Syngene, Cambridge, U.K.) or with the BioDoc Analyze digital (Biometra, Göttingen) and its corresponding software and pictures printed on a thermal printer with K65HM-CE thermal paper (Mitsubishi, Kyoto, Japan).

2.4 Bioinformatical methods

The cDNA sequence and the corresponding CDS of the wheat clone EC-123 was used to run BLASTX 2.2.17 and TBLASTN 2.2.17 homology searches in the non-redundant nucleotide collection (nr/nt) database at NCBI (http://www.ncbi.nlm.nih.gov/). The *Arabidopsis* AtARO1 protein sequence (At4g34940) was used as query to search the non-redundant protein sequences (nr) database with BLASTP 2.2.17 algorithm and the non-redundant nucleotide collection (nr/nt) with TBLASTN 2.2.17 at NCBI. Further, it was used for TBLASTN searches using the *Zea mays* BAC (*Zmbac)* Plant Genome Database (http://www.plantgdb.org/) as well as the *Populus* genome release 1.1 (http://genome.jgi-psf.org/Poptr1_1/Poptr1_1.home.html) and the TGI databases of pine and spruce (http://compbio.dcfi.harvard.edu/tgi/tgipage.html), respectively. ORFs of corresponding genomic sequences or ESTs were identified and translated using Clone Manager 6 (©Scientific & Educational Software, Cary, NC, USA). Translated protein sequences and 5´upstream sequences of genomic regions were analysed using the programs ClustalW (http://www.ebi.ac.uk/Tools/clustalw) and the M-Coffee webserver (http://www.tcoffee.org/; Moretti et al., 2007). GeneDoc 2.7.000 (Nicholas and Nicholas, 1997) was used for manual editing of alignments. Phylogenetic relationships of ARO-like proteins were calculated importing a multiple sequence alignment obtained from the M-Coffee webserver into SplitsTree4 (Huson and Bryant, 2006). A maximum likelihood distance matrix was determined using a JTT model (Jones et al., 1992) and neighbour-joining method (Saitou and Nei, 1987). Statistic significance of single branches was verified with bootstrapping (1,000 replicates).

Phylogenetic relationships of ARO proteins from *Arabidopsis* were displayed as obtained from the ClustalW webpage using default parameters with TreeView 1.6.6. (http://taxonomy.zoology.gla.ac.uk/rod/rod.html, ©2001 by Roderic D. M. Page, Glasgow, U.K.)

ARM repeats were identified using NCBI Conserved Domain search service (http://www.ncbi.nlm.nih.gov/Structure/ cdd/wrpsb.cgi), the Pfam 22.0 and HMMPfam 2.3.2. data bases (http://pfam.sanger.ac.uk/; http://hmmpfam.ddbj.nig.ac.jp/top-e.html), and PSIPRED v2.5 secondary protein structure predictions (http://bioinf.cs.ucl.ac.uk/psipred/psiform.html). Potential transmembrane domains were analyzed on the ARAMEMNON (http://aramemnon.botanik.uni-koeln.de/) plant membrane protein database. Subcellular localizations of proteins were predicted with PSORT (http://psort.nibb.ac.jp/) and TargetP (http://www.cbs.dtu.dk/services/TargetP/).

Putative phosphorylation sites were predicted by ELM (http://elm.eu.org/), NetPhos2.0 (http://www.cbs.dtu.dk/services/NetPhos/) and PredictProtein (http://www.predictprotein.org/). Homologous modeling of the AtARO1 3D structure was made using the DeepView/ Swiss-Pdb viewer 3.7 (http://www.expasy.org/spdbv) and importin-α from mouse (*Mus musculus*; protein 1ialA). The AtARO1 promoter was analyzed using the plant cis-acting regulatory DNA elements database PLACE (http://www.dna.affrc.go.jp/PLACE/) and TAIR (http://www.arabidopsis.org/index.jsp).

T-DNA Express (http://signal.salk.edu/cgi-bin/tdnaexpress) from the SALK Institute Genomic Analysis Laboratory was used for identification and ordering of *Arabidopsis* T-DNA insertion lines as well as for primer design for PCR analysis of T-DNA lines.

All transgenic constructs were planned *in silico* with Clone Manager 6 (©Scientific & Educational Software).

Sequences of genes and proteins were visualized, sequencing data analyzed and primers designed using Lasergene Software (©1989-2000 DNAStar Inc., Konstanz).

The expression pattern of *OsAROl-1* and *OsAROl-2* genes were identified in the MPSS (Massively Parallel Signature Sequencing; http://mpss.udel.edu/rice/) database.

2.5 Plant material and growth conditions

Arabidopsis thaliana seeds (ecotype Columbia-0) were sown in a soil/sand mix (4:1), stratified at 4°C for two days and germinated under short day conditions (9 h light/ 15 h dark, 8,500 lx) at 22°C and 70% humidity. After 3–4 weeks, plants were grown in a 16-h-light/8-h-dark cycle at 22°C, 8,500 lx and 70% humidity. Seeds of T-DNA insertion lines generated by the Salk Institute Genomic Analysis Laboratory (SIGnAL; http://signal.salk.edu/cgi-bin/tdnaexpress; Alonso et al., 2003) were obtained from the Nottingham Arabidopsis Stock Center (NASC; http://arabidopsis.info/; Scholl et al., 2000). *AtARO1* T-DNA insertion lines used in this work were SALK_040310 (*aro1-1*), SALK_147528 (*aro1-2*), SALK_033785 (*aro1-3*) and SALK_112709 (*aro1-4*). For *AtARO2, AtARO3* and *AtARO4* insertion lines SALK_003387 (*aro2*), SALK_136769 (*aro3*) and SALK_122722 (*aro4*) were used, respectively. Seeds were surface-sterilized by treatment for 3 minutes in 700 µl 70% ethanol and 2 minutes in 700 µl 1% sodium hypochlorite with 2% of the bacteriostatic cleaning agent Mucasol® (Merz, Frankfurt am Main). Afterwards, seeds were washed 5 times in 700 µl ddH_2O, each. Each time the supernatant was removed after 1 minute centrifugation at maximum speed in a MiniSpin Plus centrifuge (Eppendorf, Hamburg). The seeds were dispersed on petri-dishes containing sterile MS-medium (1,65 g/l NH_4NO_3, 1,9 g/l KNO_3, 0,17g/l KH_2PO_4, 0,44 g/l $CaCl_2$* $2H_2O$, 0,37 g/l $MgSO_4$*7 H_2O,620 µg/l H_3BO_3, 1120 µg/l $MnSO_4$*H_2O, 580 µg/l $ZnSO_4$* 7H_2O, 25 µg/l Na_2MoO_4* 2 H_2O, 2.5 µg/l $CuSO_4$*5 H_2O, 2,5 µg/l $CoCl_2$* 6 H_2O, 80µg/l KI, 7.46 mg/l Na_2EDTA, 5.56 mg/l $FeSO_4$* 7H_2O, 60g/l Saccharose, pH 6.0; Murashige and Skoog, 1962) with 0,3% phytagel, stratified and germinated as described above. At growth stages 1.02 to 1.04 (Boyes et al., 2001), the plantlets were transferred into earth in single pots and grown as described. Progenies were directly sown in soil. All seeds used were of the ecotype Columbia-0.

Spring onions (*Allium fistulosum L.*) or onions (*Allium cepa L.*) were purchased from a local supermarket for biolistic transformations.

2.6 Standard PCR and Colony-PCR

Standard PCR reactions were performed in a volume of 50 µl in a TGradient or TPersonal thermocycler (Biometra, Göttingen) or in a Mastercycler® ep (Eppendorf, Hamburg). The reaction mixture contained: 200-400 nM of each forward (3´) and reverse (5´) primer, 200 µM dNTP mix, 1x PCR buffer, 1.5 mM $MgCl_2$, 1-2 U Taq-Polymerase and approximately 100-500 ng genomic DNA or ~10-50 ng plasmid DNA. For Colony-PCR, a single fresh colony from transformed *E. coli* strains was picked with a tooth pick and transferred to the PCR reaction mixture by moving the tooth pick up and down. If necessary, a final concentration of 2%- 5% DMSO and 1 M betain were added to the reaction.

The reaction mixture was vortexed and centrifuged briefly and placed into the thermocycler, preheated to 95°C. Standard conditions for a PCR reaction consisted of one initial denaturation at 95°C for 2 minutes and 15 seconds, followed by 30-40 cycles of denaturation (95°C, 45 seconds), annealing (45 seconds) and elongation (72°C). A final elongation step at 72°C ensured complete polymerization of all amplification products. The annealing temperature for each PCR reaction was depending on the melting temperature of the respective primer pair (Tables 7.1.1-7.1.6). The elongation time was estimated on the basis of the length of the fragment to be amplified. Generally, the *Taq* polymerase amplifies 1 kb of DNA in one minute under optimum conditions. The final elongation step was 2-3 times longer than the elongation time calculated. The PCR-reaction was kept at 4°C until further use.
Sequences of all primers, annealing temperatures, optional ingredients and length of the products are listed in the appendix, Tables 7.1.1-7.1.6

2.7 Analysis of T-DNA insertion lines, complementation and reciprocal crosses

T-DNA insertion lines were tested for their genetic background by PCR. Genomic DNA was isolated from leaves with the Invisorb® Spin Plant Mini Kit (Invitek GmbH, Berlin) or innuPREP Plant DNA kit (Analytik Jena, Jena). For each plant, two distinct PCR reactions were carried out using both two gene specific primers (ARO1-1LP to ARO1-4LP/ ARO1-1RP to ARO1-4RP and ARO2LP to ARO4LP/ ARO2RP to ARO4RP, respectively) flanking the putative insertion site and a combination of one gene specific and one T-DNA specific primer (LBa1). All primer sequences are listed in the appendix. T-DNA insertions of SALK_040310 (*aro1-1*), SALK_147528 (*aro1-2*) and SALK_122722 (*aro4*) were identified using the primer sets ARO1-1RP/LBa1, ARO1-2RP/LBa1 and ARO4RP/LBa1 respectively, while primer combinations of either ARO1-3LP, ARO2LP or ARO3LP with LBa1 were used for identification of SALK_033785 *(aro1-3)*, SALK_003387 (*aro2*) and SALK_136769 (aro3). SALK_112709 (*aro1-4*) was tested with both combinations ARO1-4RP/LBa1 and ARO1-4LP/LBa1. T-DNA specific primers T-D fw and T-D rev were used to verify the existence of a T-DNA insertion in plants of line *aro1-4*. PCR products of *aro1-1* to *aro1-3* were sequenced to confirm the insertion locus within the 5´ upstream or coding sequence of *AtARO1* using primers LBb1 for line *aro1-1* and *aro1-2* and LBa1 for line *aro1-3*.
For reciprocal crosses, the heterozygous insertion line *aro1-3/+* was used as egg donor and wild type (WT) plants as sperm donor and *vice versa*. For complementation tests homozygous *AtARO1p::AtARO1-GFP* pollen was used to fertilize heterozygous *aro1-3/+* plants. Closed flower buds from *Arabidopsis* flowers of floral stage 12 (Smyth et al., 1990) were emasculated and pollinated 48 hours later by hand using freshly dehiscent anthers. Pollen from at least two different anthers was used to pollinate each pistil. Progenies of reciprocal crosses were analyzed for T-DNA integration as described above.

2.8 Expression analysis

Tissues for RT-PCR were collected and immediately frozen in liquid nitrogen. Up to 5 mg of tissue was used for mRNA isolation using the Dynabeads® mRNA DIRECT™ Micro kit (Dynal® Biotech,

Invitrogen, Karlsruhe) according to the manufacturers' instructions but scaled down to 50 µl in case of very small amounts of tissues. mRNA annealed to the magnetic Dynabeads was transferred using a PickPen™ (Bio-Nobile, Turku, Finland). Before RT-PCR, the isolated mRNA was treated with 1U DNAse I (RNAse free; MBI Fermentas, St. Leon-Roth) in a volume of 12.5 µl for half an hour at 37°C. Subsequently, the DNAse I was inactivated by incubation with 1 µl of 25 mM EDTA for 10 minutes at 65°C. First-strand cDNA synthesis was carried out using Oligo$(dT)_{18}$ primers (MBI Fermentas) and RevertAid™ M–MuLV Reverse Transcriptase (MBI Fermentas), following the manufacturers' protocol but adding 40 U RiboLock™ Ribonuclease Inhibitor (MBI Fermentas). Quality and amount of generated cDNAs was checked by PCR using intron-flanking primers against *Actin 3* (At2g37620, Act 3fw/ Act3rev). Expression of genes *ARO1 to ARO4* was analysed using gene specific primers ARO1fw to ARO4fw and ARO1rev to ARO4rev respectively. As template 2 µl of cDNA were used for both, PCR and Q-PCR reactions. Q-PCR analysis was performed using the iQ™ SYBR Green Supermix and the iQ™ 5 Real-time PCR detection system (BioRad, München).The experiment was performed in triplicate for each sample. Each sample consisted of three anthers of the corresponding floral stage or pollen from one single freshly dehiscent anther. Mean values and standard deviation for each triplicate were calculated by the iQ™ 5 optical system software provided with the detection system. The efficiency of the two PCR reactions with Act3 and ARO1 primers was calculated with the software by comparison of standard curves produced by PCR reactions using serial dilution of gDNA (1:1, 1:10, 1:100, 1:1,000, 1:10,000, 1:100,000, 1:1,000,000).

2.9 Generation of constructs

2.9.1 *AtARO1p::GUS*

A 723 bp genomic fragment ranging from +6 to -717 upstream of the predicted start codon of *AtARO1* was amplified from genomic DNA. The PCR reaction was performed using "proof-reading" ACCUZYME™ DNA Polymerase (Bioline, Luckenwalde) and modified primers including *BglII* sites (ARO1p fw, ARO1p rev). The promoter fragment was cloned into pCR®-Blunt II-TOPO® vector (Invitrogen, Karlsruhe), creating plasmid *AtARO1p*::TOPO. Cloning of the *AtARO1* promoter fragment upstream of the intron containing *ß-glucuronidase* gene (*GUS-INT*; Vancanneyt et al., 1990) was achieved using the vector pMG2002 (M. Gahrtz, unpublished), which has the vector backbone of binary vector pB-AB (DNA cloning service, Hamburg) and comprises a cassette of *CaMV-35Sp::bar::nost* as well as *GUS-INT* under control of the maize ubiquitin (*UBI*) promoter (*ZmUBIp::GUS-INT::nost*). pMG2002 was digested with *PstI* to remove the maize *UBI* promoter and religated. Thereupon, it was digested with *BglII* and dephosphorylated with calf intestine alkaline phosphatase (MBI Fermentas, St. Leon-Roth). The *AtARO1* promoter fragment was cut from pCR®-Blunt II-TOPO® vector by *BglII* and ligated into the digested vector pMG2002 with T4 DNA ligase (Invitrogen) to create the binary vector *AtARO1p::GUS*. The junction between *AtARO1* promoter and *GUS* were verified using the primer GUS start rev.

2.9.2 *UBIp::AtARO1-GFP* and *UBIp::AtARO2-GFP*

For cloning of AtARO1-GFP and AtARO2-GFP fusion proteins under control of the maize *UBI* promoter, *e-GFP* (enhanced green fluorescence protein; Pang et al., 1996) was C-terminal fused to the coding sequences of AtARO1 and AtARO2. The open reading frames of *AtARO1* and *AtARO2* were amplified from genomic DNA using Advantage Genomic Polymerase Mix (Clontech, Saint-Germain-en-Laye, France) and primers ARO1GFP fw/ ARO1GFP rev and ARO2GFP fw/ ARO2GFP rev, all including *AvrII* restriction sites, thereby simultaneously removing the stop codon at the 3´ restriction site. After cloning into pCR®-Blunt II-TOPO® vector (Invitrogen, Karlsruhe), creating the plasmids *AtARO1-GFP*-TOPO and *AtARO2-GFP*-TOPO, the *AvrII* digested fragments of *AtARO1* and *AtARO2* were transferred into the vector pLNU-*GFP* (DNA Cloning Service, Hamburg), likewise digested with *AvrII*, but dephosphorylated with shrimp alkaline phosphatase (MBI Fermentas, St. Leon-Roth). Successful cloning of *AtARO1*- and *AtARO2-GFP* fusions were verified by sequencing cloning sites with primers GFP seq and UBI 1. The resulting plasmids, *UBIp::AtARO1-GFP* and *UBIp::AtARO2-GFP*, were used for transient transformation assays. The vector pLNU-*GFP* (*UBIp::GFP*) without modifications was used as control.

2.9.3 95P-Nos*AtARO1p::AtARO1-GFP*

All cloning steps described in this section were performed by the DNA cloning service (Hamburg). The *AtARO1* promoter was amplified from *AtARO1p::GUS* using primers PAro1F (*Not I* site included) and PAro1R (*SpeI* site included) with *Pfu* DNA Polymerase (MBI Fermentas, St. Leon-Roth). After digesting the plasmid *UBIp::AtARO1-GFP* with *NotI* and *SpeI* the *UBI* promoter was replaced by ligating the *NotI/SpeI* digested *AtARO1* promoter fragment. Afterwards, the cloned cassette of *AtARO1p::AtARO1-GFP* was transferred into the binary vector 95P-Nos (DNA Cloning Service, Hamburg) via *Sfi* digest and ligation. The resulting plasmid was named 95P-Nos*AtARO1p::AtARO1-GFP* and the junctions of the *AtARO1* promoter with the plasmid were verified by sequencing with the primers A1prom5´ and A1prom3´.

2.9.4 95P-*Nos35Sp::AtARO1-GFP*

The vector *UBIp::AtARO1-GFP* was used by the DNA cloning service (Hamburg) for cloning of an AtARO1-GFP fusion protein under the control of the *35S* promoter. For this purpose, the *UBI* promoter was replaced by the *35S* promoter, which was isolated from the vector *p35*OCS-BM (DNA cloning service). *UBIp::AtARO1-GFP* and *p35*OCS-BM were both digested with *NotI* and *SpeI*, respectively and the *35S* promoter ligated in front of the *AtARO1-GFP* fusion. The whole cassette of *35Sp::AtARO1-GFP* was transferred into the binary vector 95P-Nos (DNA Cloning Service, Hamburg) via *Sfi* digest and ligation. The resulting plasmid was named 95P-Nos*35Sp::AtARO1-GFP*.

2.9.5 p7N*EC1p::ARO1-RNAi*

An RNAi construct directed against *AtARO1* under the control of the egg cell specific *EC1* promoter was cloned by the DNA cloning service (Hamburg) using the plasmid pUBI-iF2 (DNA Cloning Service).

In a first step, the *EC1* promoter (*EC1p*) was amplified using primers EC1-PF and EC1-PR, thereby introducing *EagI* and *BamHI* restriction sites, and *Pfu* DNA Polymerase (MBI Fermentas, St. Leon-Roth). Further, a 292 bp fragment specific for *AtARO1* ("spacer", see Fig. 3.3) ranging from +939 to +1231 downstream of the predicted start codon was amplified using *Pfu* DNA polymerase and two different primer pairs: primers ARO-Eco and ARO-Mlu, including *EcoRI* and *MluI* sites respectively, were used to amplify the DNA fragment in sense orientation and primers ARO-Bam and ARO-Eco, the former including a *BamHI* restriction site were used to amplify the fragment in antisense orientation. As *NotI* and *EagI* produce compatible overhangs, the vector pUBI-iF2 was restricted with enzymes *NotI* and *BamHI*, removing the *UBI* promoter and ligated with the *EagI/BamHI* digested *EC1* promoter (*pEC1*-iF2). The plasmid *pEC1*-iF2 and the *ARO-Bam/ARO-Eco* amplified fragment of *AtARO1* were digested with *EcoRI* and *BamHI*, each and ligated (*pEC1-ARO1*-AS). After digestion of the plasmid *pEC1-ARO1*-AS with *MunI* (creating an overhang compatible to *EcoRI*) and *MluI* and digestion of the *ARO-Eco/ARO-Mlu* fragment of *AtARO1* with *EcoRI* and *MluI,* they were ligated, creating the plasmid *pEC1-ARO1*-RNAi. The whole cassette of *EC1p::ARO1as-iF2-ARO1s* was finally transferred into the binary vector p7N via *Sfi* digest and ligation and the resulting plasmid was named p7N*EC1p::ARO1*-RNAi.

The plasmids *AtARO1p::GUS*, 95P-Nos*AtARO1p::AtARO1-GFP*, 95P-Nos*35Sp::AtARO1-GFP* and p7N*EC1p::AtARO1*-RNAi were transferred into *Agrobacterium tumefaciens* as described in section 2.10.3 and used to transform *Arabidopsis thaliana* plants as described in section 2.13.
Vector maps of all original and generated plasmids are shown in the Appendix section 7.3.

2.10 Preparation and transformation of competent cells

2.10.1 Chemically competent *E. coli* cells

A single fresh colony of *E. coli* strain DH5α (Woodcock et al., 1989) or XL1-blue MRF´ (Bullock et al., 1987) was used to inoculate 5 ml LB medium (10g/l Bacto-Tryptone, 5g/l Bacto-Yeast, 10g/l NaCl, pH 7.0), containing 20 µg/ml tetracycline (LB_{tet}) in the case of XL1-blue MRF´ cells, and grown over night at 37°C with vigorous shaking at 220 rpm in a laboratory incubator. 50 ml LB_{tet} medium were inoculated with 100 µl from the over night culture. The bacteria were grown at 37°C shaking at 220 rpm to an OD_{600} of ~0.5. The cells were immediately cooled on ice for 10 minutes and centrifuged 5 minutes at 2,500 rpm (~755xg) and 4°C in a Sorvall RC5B or Sorvall Superspeed RC2-B (Du Pont Instruments, Wilmington, DE, USA), using a SS34 rotor. The pellet was resuspended in 15 ml ice cold TfB I (30 mM KAc, 50 mM $MnCl_2$, 100 mM RbCl, 10 mM $CaCl_2$, 15% glycerol) and incubated on ice for 2 minutes. After a second centrifugation step of 5 minutes at 2,500 rpm and 4°C, the pellet was resuspended in 2 ml ice cold TfB II (15 mM $CaCl_2$, 10 mM RbCl, 15% glycerol) and divided into aliquots of 100 µl. The aliquots were frozen in liquid nitrogen and stored at -80°C for further use.
5 µl of ligated plasmids were used directly or dissolved 1:5 with sterile ddH_2O to transform 100 µl competent cells, previously thawed on ice. The mixture was incubated 30 minutes on ice, heat-pulsed for 45 seconds at 42°C and transferred into an ice bath. After the addition of 250 µl 37°C warm LB medium, the suspension was incubated for 1 hour at 37°C, shaking with 220 rpm. 50-100 µl of

bacteria solution was then plated on selective LB plates (LB medium containing 20g/l Agar) containing the appropriate antibiotic for the corresponding plasmid and incubated over night at 37°C.

Table 1: Concentrations of antibiotics used for selective LB and YEP plates

Antibiotic	Stock (mg/ml)	Final concentration (µg/ml)	
		E. coli	*Agrobacterium*
Ampicilin	50	100	-
Gentamycin	30	-	30
Kanamycin	50	50	50
Spectinomycin	50	50	100
Tetracyclin	2	20	-

2.10.2 Electro-competent *E. coli* cells

5 ml LB_{tet} medium was inoculated overnight at 37°C with a single fresh *E.coli* XL1-blue MRF´ colony and used to inoculate 500 ml LB_{tet} medium the next day. The bacteria culture was incubated for another 2-5 hours until an OD_{600} of 0.5-0.7 was reached and thereafter cooled on ice, along with all materials that were used for the procedure. The suspension was divided into two 500 ml centrifuge tubes and centrifuged at 5,000xg and 4°C for 10 minutes in a Sorvall centrifuge. The supernatant was discarded and the cells in each tube were resuspended in 250 ml ice-cold sterile ddH_2O (resistivity: 18 megaohms per cm). After a second centrifugation under the same conditions, the pelleted cells were resuspended in 1/10 of the original volume ice-cold ddH_2O. Again, the suspension was centrifuged (4,000xg, 15 minutes, 4°C), the supernatant discarded and the cells resuspended in 1/20 of the original volume ice-cold ddH_2O. Another centrifugation step of 15 minutes at 6,000xg and 4°C was followed by resuspension of the pellet in 5 ml ice-cold 10% glycerol. Finally, the cell suspension was centrifuged at 7,000xg and 4°C for 10 minutes and the pellet resuspended in 500 µl ice-cold 10% glycerol. The cells were frozen in aliquots of 50 µl in liquid nitrogen and stored at -80°C until use. For transformation, one aliquot of cells was slowly thawed on ice, carefully mixed with 200-300 ng plasmid and incubated for one minute on ice. The mixture was transferred into an ice-cold electroporation cuvette (2mm gap; Peqlab, Erlangen) and elektro-porated with GenePulser (BioRad, München) at 200 Ω, 2.5 µFD and 2.5 V. Immediately, 1 ml SOC medium (20 g/l Bacto-Tryptone, 5 g/l Bacto-Yeast extract, 0.5 g/l NaCl, 2.5 g, 2.5 mM KCl, 10 mM $MgCl_2$, 20 mM glucose, pH 7.0) was added to the cells and the suspension transferred into a 15 ml reaction tube. The cells were incubated at 37°C and 220 rpm for 1 hour. Subsequently, 50-100 µl were plated on selective plates containing appropriate antibiotic and incubated over night at 37°C.

2.10.3 Competent *Agrobacterium tumefaciens* cells

A single colony of *Agrobacterium tumefaciens* strain GV3101 pMP90RK (Koncz and Schell, 1986) was grown in 2 ml YEP medium (10g/l yeast extract; 10 g/l peptone; 5 g/l NaCl; pH 7.0), containing 30 µg/ml gentamycin, 50 µg/ml kanamycin and 100 µg/ml spectinomycin, at 28°C over night and used to inoculate 50 ml YEP medium. The culture was grown to an OD_{600} of ~ 0.5 and pelleted for 5 minutes at 5,000 rpm (~3,000xg) in a Sorvall centrifuge with SS 34 rotor. The cells were resuspended in 10 ml 0.15 M NaCl and centrifuged at the same conditions as before. After the pellet was resuspended in 1

ml of 20 mM ice cold $CaCl_2$, the cells were frozen in 200 µl aliquots in liquid nitrogen and stored at -80°C or immediately used for transformation with 1 µg of DNA. 200 µl competent cells were mixed with the DNA and incubated 30 minutes on ice, frozen for 1 minute in liquid nitrogen and thawed in a 37°C water bath. After the addition of 1 ml YEP medium, the cells were incubated at 28°C for 2-4 hours with gentle shaking. The cells were pelleted for 1 minute at maximum speed and resuspended in 100 µl fresh YEP medium. The suspension was then streaked onto a selective YEP plate (YEP medium containing 20 g/l Agar) containing the appropriate antibiotic for each plasmid used and incubated at 28°C for 2-3 days. Single colonies were used to inoculate medium for the transformation of *Arabidopsis thaliana*.

Glycerol stocks of transformed *E.coli* or *Agrobacterium tumefaciens* were prepared for long-time storage by mixing 350 µl of a freshly grown liquid bacteria culture with 150 µl 50% glycerol through vortexing and immediately freezing them in liquid nitrogen. Glycerol stocks were then stored at -80°C.

2.11 Preparation of plasmid DNA

Different methods for the isolation of plasmid DNA were used to optimize the quantity and quality of plasmids for each application. Small amounts were isolated from 3- 4.5 ml culture with the peqGOLD Plasmid Miniprep Kit I (Peqlab, Erlangen), while more DNA in a higher concentration was isolated from 25-80 ml over night culture with the peqGOLD HP Plasmid Midi Kit (Peqlab) or QIAfilter Midi cartdriges (Qiagen, Hilden) using solutions prepared according to the manufacturers´ specifications.
Alternatively, plasmids were isolated “by hand” from 70 ml over night culture. The cells were spun down in 2 centrifuge tubes at 6,000 rpm for 15 minutes (~4,300xg; Sorvall, SS34 Rotor) at 4°C. Each pellet was resuspended in 4 ml buffer I (50 mM glucose; 25 mM Tris; 10 mM EDTA; pH 8.0; stored at 4°C) combined with 40 µg/ml RNAse A. Afterwards, 8 ml buffer II (0.2 N NaOH; 1% SDS) was added and the lysate was incubated for 10 minutes at room temperature. 6 ml buffer III (3 M potassium acetate; 11.5% acetic acid, pH 4.8) was admixed each by gently inverting the tubes 6-8 times and genomic DNA and cell debris precipitated for 15 minutes on ice. The precipitate was removed by a 15 minutes centrifugation at 13,000 rpm (~20,400xg) and 4°C and filtration of the supernatant trough a paper filter, which was previously moistured with ddH_2O. Nucleic acids were precipitated with 0.7 volumes isopropanol for 15 minutes on ice and separated for 12 minutes at 10,000 rpm (~12,000xg) and 4°C. The two air-dryed pellets were resuspended and combined in a total volume of 2 ml ddH_2O and mixed with 2 ml 5 M LiCl. After 30 minutes on ice, the RNA was removed (8 minutes, 6,000 rpm/~4,300xg, 4°C) and the supernatant transferred into a fresh tube. To precipitate the plasmid DNA, the suspension was incubated with 2.5 volumes 96% ethanol for 15-20 minutes on ice. The DNA was pelleted 15 minutes at 15,000 rpm (27,000xg) and 4°C, air-dryed, resuspended in 500-800 µl TE buffer (10 mM Tris, pH 8.0; 0.1 mM Na_2EDTA; pH 8.0) and transferred to a 2 ml reaction tube. Residual RNA was removed with 2.5 µl RNase A (40 mg/ml) for 20 minutes at 37°C and the DNA was purified by adding phenol/chloroform/isoamyl alcohol (25:24:1), mixing and 2-3 minutes incubation on ice. After a 5 minute centrifugation at maximum speed (~21,500xg) in a Sigma 3K15 centrifuge with Rotor 12154, the upper phase was transferred into a new reaction tube, mixed with 1 volume

chloroform/isoamyl alcohol (24:1) and incubated and centrifuged as above. This step was repeated and the upper phase was precipitated with 1/10 volume sodium acetate (3 M, pH 5.2) and 1 volume isopropanol for 15-20 minutes at -20°C. The DNA pellet, obtained by centrifugation (15 minutes, 15,000 rpm/~20,600xg, 4°C) was washed with 70% EtOH (10 minutes, 15,000 rpm/~20,600xg, 4°C). The air-dry pellet was then carefully resuspended in 100 µl ddH_2O or TE buffer (10 mM Tris, pH 8.0; 0.1 mM Na_2EDTA; pH 8.0).
Quantity and quality of all DNA preparations were measured using an Eppendorf BioPhotometer Spectrophotometer (Eppendorf, Hamburg) or NanoDrop ND-1000 spectrophotometer (Thermo Fisher Scientific, Schwerte).

2.12 Transient transformation of epidermal onion cells

Particle bombardment was performed modified from Dresselhaus et al. (2006). 60 mg/ml gold particles (0.4-1.2 µm, Heraeus) were washed twice in absolute ethanol and once in ddH_2O by resuspending the gold particles with vigorous vortexing and ultrasound, following 10 seconds centrifugation at 10,000xg, each. The pellet was again resuspended in 1 ml ddH_2O and 50 µl aliquots were used for each assay. Extant aliquots were stored at -20°C. All following work was done on ice. 5-10 µg plasmid DNA were added to the gold suspension and vortexed carefully. 50 µl 2.5 M $CaCl_2$ and 20 µl 0.1 M Spermidin were thoroughly mixed in the lid of the same reaction tube and then added to the gold suspension by vortexing. The DNA-coated gold particles were pelleted (20-30 seconds centrifugation at maximum speed), washed in 250 µl ethanol and resuspended in a final volume of 240 µl 96% ethanol. 7-10 µl were spread onto plastic macrocarrier discs for each biolistic transformation (Particle Delivery System-1000/He; BioRad, München). The bulbs of onions or spring onions were quartered, the innermost layers removed and the concave side bombarded under 28 inch Hg, a pressure of 1,100 psi and at 6 cm distance from the support of the macrocarrier. Bombarded onions were placed with the concave side down on MS-medium (formula see section 2.5) and maintained over night in the dark at room temperature until microscopic examination.

2.13 Transformation of *Arabidopsis thaliana*

Agrobacterium tumefaciens strain GV3101 pMP90RK (Koncz and Schell, 1986) transformed with corresponding binary vectors was used for transformation of *Arabidopsis* wild type (Columbia-0) plants. Transformations were performed by a “floral dip” procedure according to Clough and Bent (1998). Seeds obtained from transformations were germinated on soil, as described in section 2.5. Three days after germination, transgenic seedlings using phosphinotricin-acetyltransferase (*bar/pat*) as selection marker were selected by spraying 200 mg/l BASTA® (Bayer Crop Science, Langenfeld) supplemented with 0.1% Tween. BASTA® treatment was repeated two times after three days, each. Kanamycin resistant transgenic plants transformed with 95P-Nos*AtARO1p::AtARO1-GFP* were selected by a protocol modified from Xiang et al., 1999. Plants were sprayed for 2 days with 100 mg/l kanamycin, followed by two days with 200 mg/l kanamycin, followed by three days with 500 mg/l

kanamycin, each kanamycin solution containing 0.1% Triton X-100. Surviving plantlets were transferred to single pots and cultured as described.

2.14 Southern blot analysis

Copy numbers of gene constructs were determined using southern blot analysis. Genomic DNA (gDNA) was isolated from transgenic plants with the Invisorb® Spin Plant Mini Kit (Invitek GmbH, Berlin) and 5 µg gDNA was restricted with *EcoRI*. After precipitation of the digested gDNA with 1 µl glycogen, 1/10 volume 3 M NaOAc and 2.5 volumes 96% ethanol and 15 minutes centrifugation at 20,000xg, the pelleted gDNA was washed with 70% ethanol (20,000xg, 10 minutes), air-dryed and resuspended in 20 µl TE buffer (10ml/l 1M Tris, pH 8.0; 200 µl/l 0.5 M Na_2EDTA (pH 8.0)). gDNA was separated in 0.8% agarose gel and gels treated as described in Sambrook et al. (1998). The DNA was transferred onto Hybond N+ nylon membrane by capillary transfer with 20x SSC over night and crosslinked to the membrane with 1,200 µJ using Stratalinker™ 1800 UV crosslinker (Stratagene, La Jolla, CA, USA). Digoxigenin (DIG)-11-dUTP-labelled probes of the *PAT* gene, which encodes resistance against the herbicide BASTA® (Bayer Crop Science, Langenfeld), were made by standard PCR with primers bar biV fw and bar biVrev, additionally adding 70 µM DIG-11-dUTP. After separation on a 1.5% agarose gel, the fragment was purified with EasyPure® DNA Purification Kit (Biozym Diagnostik GmbH, Hess. Oldendorf). Hybridisation of the filter with 28.5 ng labelled probe/ml hybridisation solution was carried out at 42°C using DIG Easy Hyb solution (Roche, Penzberg) and chemiluminescent detection was performed with CSPD® (Roche) according to the manufacturers´ guidelines. The washing buffer from the CSPD® protocol was slightly modified and was prepared with 0.1 M maleic acid and 0,3% Tween only, omitting 0.15 M NaCl. Hybridisation signals were detected by exposing Amersham Hyperfilm™ MP X-ray film to membranes wrapped in plastic film for 2 ½ hours at 37°C or 48 hours at 4°C.

2.15 *In vitro* pollen germination

Pollen from open flowers were placed on small petri dishes (4 cm) with pollen germination medium (PGM) containing 18% sucrose, 0.01% H_3BO_3, 1 mM $CaCl_2$, 1 mM $Ca(NO_3)_2$, 1 mM $MgSO_4$, pH 7 (Li et al., 1999) and 0,5% purified agar (BD Biosciences, Sparks, MD, USA). Wild type (WT) and *aro1-3/+* pollen was each placed separately on the two halves of the same petri dish. Pollen was germinated in a wet chamber at 22°C and 8,000-9,000 lux for 5-28 hours. For analysis by confocal laser scanning microscopy (CLSM), a small block of PGM, carrying the pollen, was cut from the petri dish and placed upside down on a self-made object holder that allows observation with the inverted microscope. This object holder consists of a cover slip fixed to the lower side of a special metal slide (76mm x 26mm) provided with an opening (ø 20 mm) in the center.

For expression analysis, mRNA was isolated from germinated pollen (5 hours after germination) that was placed on PGM containing petri dishes by carefully dabbing single freshly dehiscent anthers, harvested from mature flowers of stage 13 (Smyth et al., 1990), onto the medium. The germinated

pollen was resuspended in a drop of sodium phosphate buffer (100 mM, pH 7.0), collected in a 0.5 ml reaction tube and immediately frozen in liquid nitrogen.

For cDNA library construction, larger amounts of germinated pollen were necessary. For harvesting plenty of pollen, a pipette tip version of an "*Arabidopsis* vacuum cleaner" was constructed according to Johnson-Brousseau and McCormick (2004). A 1 ml pipette tip was cut two times and assembled with two different-sized gaze nets (30 µm and 10 µm) as shown in Fig. 2.1. The side of the pipette tip holding the 10 µm gaze was inserted into a rubber tubing attached to a water jet vacuum pump. Pollen from freshly opened flowers of 12 individual plants were collected using the pipette tip vacuum cleaner. Pollen from each two plants was transferred on petri dishes containing PGM by disassembling the vacuum pollen collector and placing the 10 µm mesh with the pollen containing side onto the PGM. The pollen was transferred by gently dapping the gaze onto the medium. Subsequently, the pollen was germinated for 6 hours as described above. Germinated pollen was then resuspended in 100 mM sodium phosphate buffer and pollen from each two petri dishes collected in a 0.5 ml reaction tube and centrifuged at 600xg for 5 seconds in a MiniSpin Plus centrifuge (Eppendorf, Hamburg). As much supernatant as possible was removed without disturbing the pollen pellet and the pollen immediately frozen in liquid nitrogen.

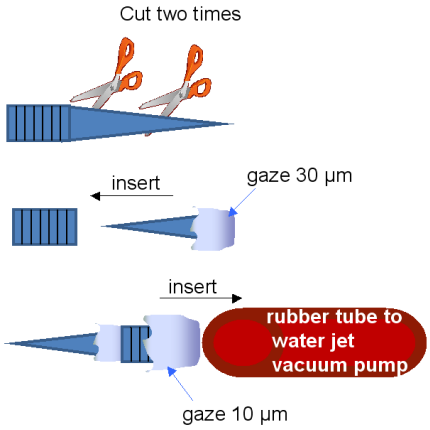

Fig. 2.1. Schematic drawing of assembly of the "*Arabidopsis* vacuum cleaner" modified from Johnson-Brousseau and McCormick (2004). A 1 ml pipette tip was cut two times, the middle part discarded and the tip assembled with a 30 µm gaze net and inserted backwards into the wide part of the pipette tip. This part was then again wrapped with a 10 µm gaze net and plugged into a rubber tube connected to a water jet vacuum pump.

2.16 Drug treatments

Latrunculin B (Lat B; Sigma-Aldrich, München) was dissolved in 100% DMSO at a concentration of 2.5 mM and added at a final concentration of 20 nM to liquid PGM (recipe see 2.15). 500 µl of LatB containing PGM were added to pollen tubes previously germinated for three hours. Control pollen tubes were treated with PGM containing 8% DMSO only. Brefeldin A (BFA; Applichem, Darmstadt) was dissolved at a concentration of 5 mg/ml in methanol and diluted to a final concentration of 5 µg/ml

in liquid PGM. Treatments were performed by adding 500 µl BFA containing PGM to pollen tubes grown for three hours. Control pollen tubes were treated with PGM containing 0.1% methanol. Treated pollen was incubated for another 2 hours, each. The membrane dye FM® 4-64 FX (Invitrogen, Karlsruhe) was dissolved to a concentration of 1 mM in 100% DMSO and added at a final concentration of 4 µM in liquid PGM to germinating pollen 30 minutes prior to actin staining.

2.17 Staining procedures

2.17.1 Actin staining

Actin staining of *in vitro* germinated pollen tubes and ovules was modified after Sonobe and Shibaoka (1989) and Monteiro et al. (2005). Briefly, pollen was fixed by adding 500 µl A-MSB Buffer (100 mM Piperazin-1,4-bis[2-ethansulfonic acid] (PIPES), 10 mM EGTA, 5 mM Magnesiumsulfate, 0.05% Triton X) containing 0.1 mM freshly added Maleimidobenzoyl-N-hydroxysuccinimid-ester (MBS) to the germinated pollen for half an hour. Ovaries were cut open with a hypodermic needle (0.4 x 20mm, Braun, Melsungen), immersed in 500 µl A-MSB buffer containing MBS and vacuum infiltrated for 30 minutes. The tissues were washed twice with 500 µl W-MSB (100 mM PIPES, 10 mM EGTA, 5 mM Magnesiumsulfate) each and incubated for 10-15 minutes in 100 µl W-MSB containing 5% rhodamine-phalloidin. Ovaries were again subjected to vacuum infiltration during this time. The ovules were subsequently fetched from the ovaries with a hypodermic needle and mounted on glass slides for microscopic observation.
For microscopy of pollen tubes using CLSM, a small block of PGM, carrying the pollen, was cut from the petri dish and placed upside down on a cover slip fixed to the lower side of a special metal slide (76mm x 26mm) provided with an opening (ø 20mm) in the center. This allowed direct observation of pollen tubes under the inverted CLSM without the need of transferring the pollen onto a glass slide.

2.17.2 Aniline-blue staining

Aniline-blue staining of pollen tubes was modified from Huck et al. (2003). 24 hours after hand pollination, pistils were cut open with a hypodermic needle and fixed over night in ethanol/ acetic acid (9:1) at 4°C. The tissues were rehydrated in an ethanol series (70%, 50%, 30%; 5 minutes each), washed with sodium phosphate buffer (100 mM, pH 7.0) and softened with 10% chloralhydrate for 5 minutes at 65°C. Pistils were washed again twice in sodium phosphate buffer and incubated in 5 M NaOH at 65°C for 10 minutes. The samples were then mounted on glass slides with 0.1% aniline blue (Fluka, Seelze) in sodium phosphate buffer.

2.17.3 Staining of nuclei

To visualize the nuclei of embryo sac cells and pollen grains, ovules and dehiscent anthers were stained with 10 µg/ml 4',6-Diamidino-2-phenylindol (DAPI), 10 µM Draq5™ (Biostatus Limited, Leicestershire, U.K.) or 15 µg/ml propidium iodide (PI) for 10-30 minutes directly on a microscope slide and observed under a fluorescent microscope or CLSM. All fluorescent stains were dissolved in water.

Nuclei, cytoplasm and cell boundaries were visualized using a fixation protocol from Christensen et al. (1997).

2.17.4 Pollen viability test

To estimate pollen vitality, freshly dehiscent anthers were immersed in 50 µg/ml fluorescein diacetate (5 mg/ ml stock solution in 98% acetone) and 15 µg/ml PI in 100 mM sodium phosphate buffer (pH 7.0) on a microscope slide to detach pollen grains. Green fluorescent pollen were scored as vital and red fluorescent pollen as dead.

2.17.5 GUS staining

For GUS assays inflorescences, siliques, leaves, and stems from soil-grown plants were transferred into wells of microtiter plates containing 300 µl of GUS staining buffer (Vielle-Calzada et al., 2000). Ovaries and siliques were cut open lengthwise with a hypodermic needle before transferring into GUS staining buffer. Microtiter dishes were placed under vacuum for 2 min. After release of vacuum, plates were covered with a lid and incubated at 37°C in the dark over night. All tissues were washed briefly in sodium phosphate buffer (100 mM, pH 7.0) before observation. Ovules were isolated on glass slides by dissecting the ovaries or siliques and embryos isolated from older ovules with a hypodermic needle in a drop of clearing solution. Whole mount ovules were cleared using either Hoyers solution (Liu and Meinke, 1998) or lactatic acid clearing buffer (Vielle-Calzada et al. 2000).

2.18 Microscopy

Specimens were observed under a Zeiss Axioskop FL equipped with an epifluorescence UV-filter set and differential interference contrast (DIC). Filters used for imaging were filter set 02 (365 nm excitation, LP 420 nm) for specimens stained with DAPI and filter set 09 (450-490 nm excitation, LP 515 nm) for GFP samples and pollen viability measurements. Images were captured and processed and length of pollen tubes was measured using the Zeiss AxioVision software, release 4.6 and ImageJ 1.38x (Wayne Rasband, National Institutes of Health, USA, http://rsb.info.nih.gov/ij/). Tissues for confocal pictures were observed on a Zeiss Axiovert 200 M microscope equipped with a confocal laser scanning unit LSM 510 META. The 488 nm laser was used with band pass filter BP505-530 for detection of GFP fluorescent probes. All other fluorophores were excited with the 543 nm laser and the following filter sets used for recording: rhodamine-phalloidin, LP560; Draq5™ and PI**,** LP 650. Simultaneous detection of FM®4-64 FX and rhodamine-phalloidin was achieved by recording emission maxima for each 10 nm ranging from 552 nm to 798 nm and subsequent linear unmixing. Pictures were made with an AxioCam HRc camera and the Zeiss LSM 510 META software. Images were processed using Adobe photoshop CS3 (Adobe Systems, München). Stacks of pictures, co-localization plots, fluorescence intensity profiles and further processing of CLSM pictures were made with the Zeiss LSM Image Browser Version 3.5.0.359 (Carl Zeiss GmbH Jena, ©1997-2005).

2.19 Yeast two hybrid screen

The yeast two hybrid screen was performed using the Matchmaker™ GAL4 Two Hybrid System 3 (Clontech, Saint-Germain-en-Laye, France) according to the manufacturers´ protocol. A cDNA library from germinated pollen was constructed using the Matchmaker™ Two-Hybrid Library Construction and Screening kit (Clontech).

2.19.1 Pollen cDNA library

mRNA for the cDNA first strand synthesis was isolated using the Dynabeads® mRNA DIRECT™ Micro kit (Dynal® Biotech, Invitrogen, Karlsruhe). For this purpose, a volume of approximately 30 µl of germinated pollen were collected in three reaction tubes (see section 2.15) and grinded while frozen in liquid nitrogen. 50 µl lysis buffer from the Dynabeads® mRNA DIRECT™ Micro kit was then added to the first reaction tube, the content thawn, mixed and transferred to the second and, after the same treatment, to the third reaction tube. The manufacturers' protocol was then carried out for a scaled down version of 50 µl lysis puffer: 20 µl Dynabeads were transferred into 20 µl fresh lysis buffer with a PickPen™. The pollen containing lysate was shortly centrifuged and the supernatant added to the Dynabeads. These were incubated for 5 minutes on a DynalMixer (Rettberg Laborbedarf, Göttingen) at room temperature. mRNA annealed to the dynabeads was washed twice in 100 µl Buffer A (10 mM Tris-HCl, pH 7.5; 0.15 M LiCl; 1 mM EDTA; 0,1% LiDS) and twice in 100 µl Buffer B (10 mM Tris-HCl, pH 7.5; 0.15 M LiCl; 1 mM EDTA). After the second washing step in Buffer B, the Dynabeads were transferred into 10 µl Tris-HCl (10 mM, pH 7.5) and heated for 2 minutes at 90°C to release the mRNA from the beads, which were removed immediately. All following steps are described elaborately in the Matchmaker™ Library Construction & Screening Kits User Manual. First strand cDNA was synthesized using 38.5 ng pollen tube mRNA and random primer CDSIII/6, and double stranded (ds) cDNA was generated by Long Distance PCR (26 cycles). 1 µg of human placenta PolyA$^+$ RNA was used as control. The ds cDNAs were purified using a CHROMA SPIN™ TE-400 Column. The pollen cDNA was transformed into yeast strain AH109 together with the vector pGADT7-Rec, thus restoring the circular plasmid by homologous recombination. Transformants carrying the circularized plasmid were selected on SD/-Leu plates and subsequently harvested and pooled. 1 ml aliquots of the cDNA library were immediately frozen in liquid nitrogen and stored at -80°C. The library titer was determined by spreading 1:100, 1: 1,000 and 1:10,000 dilutions of one aliquot on SD/-Leu plates and counting the colonies appearing after 3 days incubation at 30 °C.

2.19.2 Generation of constructs

AtARO1 and candidate genes for direct interaction test, i.e. *AtActin3* (*Act3,* At3g53750), *AtActin4* (*Act4,* At5g59370), *AtActin7* (*Act7,* At5g09810) and *GFP* were amplified from cDNA generated from several tissues of *Arabidopsis* plants. *Act3* and *Act7* were amplified from cDNA of *Arabidopsis* WT leaves, *AtARO1* and *Act4* from WT pollen, while *GFP* was amplified from pollen of a transgenic plant expressing the *AtARO1p::AtARO1-GFP* construct described in section 2.9.3.

The cDNA was generated as described in section 2.8. 1 µl of cDNA was used in a 50 µl PCR reaction using primers containing *Nco I* and *Sma I* restriction sites for each gene and the TripleMaster PCR system (Eppendorf, Hamburg) with 10x high fidelity buffer+ Mg^{2+}. Additionally, 5% DMSO and 1 M betain was added. Primers were Y2H/ARO1 NcoI and Y2H/ARO1 SmaI for *AtARO1*, Y2H/Act3 NcoI and Y2H/Act3 SmaI for *Act3*, Y2H/Act4 NcoI and Y2H/Act4 SmaI for *Act4*, Y2H/Act7 NcoI and Y2H/Act7 SmaI for *Act7* and Y2H/GFP NcoI and Y2H/GFP SmaI for *GFP*. Thereby, restriction sites were introduced in frame in front and behind the coding sequence of all five genes, allowing the construction of a fusion protein with the GAL4 binding domain (BD) or the GAL4 activation domain (AD) of vectors pGBKT7 and pGADT7 respectively, supplied with the Matchmaker™ GAL4 Two Hybrid System 3. For this purpose, the amplified PCR products were separated using a 1.5% agarose gel (peqGOLD Universal agarose, Peqlab, Erlangen), isolated from the gel and purified with the EasyPure® DNA Purification Kit (Biozym Diagnostik GmbH, Hess. Oldendorf). After determining the quantity and quality of the obtained fragments with the NanoDrop ND-1000 spectrophotometer, these and the two vectors pGADT7 and pGBKT7 were consecutively digested with *SmaI* and *NcoI*. 500 ng vector and 150- 330 ng of the different fragments were digested over night with 5U *SmaI* in buffer Tango™ Y at 30°C. Thereafter, 5U *NcoI* were added and incubated for 4 more hours at 37°C. The digested DNA was separated in an 1.5% agarose gel, isolated and purified with the EasyPure® DNA Purification Kit. Approximately 100 ng vector DNA and three times equimolar concentration of insert DNA was used to ligate the coding sequences of *AtARO1*, *Act3*, *Act4*, *Act7* and *GFP* into both, prey vector pGADT7 and bait vector pGBKT7 using T4 DNA ligase. Additionally, all genes were ligated with 50 ng pCR®2.1 vector (Invtrogen, Karlsruhe) at equimolar ratios using T4 DNA ligase. All constructs were transformed into cells as described in section 2.10.1 and 2.10.2 and tested for successful ligation by digestion with *NcoI* and *SmaI* or Colony-PCR using primers M13 fw/ M13 rev for the pCR® 2.1 vector, T7 seq/ 3´DNA-BD seq for pGBKT7 and T7 seq/ 3´AD seq for pGADT7, respectively. All constructs were sequenced with primers T7 seq and 3´ AD seq for vector pGADT7, primers T7 seq and 3´ DNA-BD seq for vector pGBKT7 and primers M13 fw and M13rev for pCR® 2.1 vector.

2.19.3 Yeast transformation

The constructs of *AtARO1*, *Act3*, *Act4*, *Act7* and *GFP* in pGADT7 and pGBKT7 were transformed into yeast strains AH109 and Y187 (provided with the kit), respectively. For each transformation, a single fresh colony of the corresponding strain was inoculated in 5 ml YPD (20 g/l Difco peptone, 10 g/l Yeast extract, 20 g/l Agar (for plates only)) at 30°C over night, shaking at 250 rpm, to an OD_{600} of 0.5- 4.0. Cells from 1.5 ml of the culture were harvested in a 1.5 ml reaction tube by 30 seconds centrifugation at maximum speed in a MiniSpin Plus centrifuge (Eppendorf, Hamburg) and the supernatant removed completely. The pellet was briefly vortexed, 100 µg herring sperm DNA was added and the solution was mixed again. Successively, the following components were added, mixing in between each reagent: 1-2 µg plasmid DNA, 500 µl LP-Mix (40% PEG 4,000; 0.1 M LiAc; 10 mM Tris-HCl, pH 7.5; 1 mM EDTA, stored at 4°C) and 55 µl pure DMSO. The cells were first incubated at room temperature for 15 minutes and then heat shocked at 42°C for further 15 minutes. Meanwhile, YPD plates containing appropriate selective medium were dried under a laminar airflow cabinet. Yeast cells were mixed with 500 µl TE-buffer (10 mM Tris-HCl, pH 7.5; 1 mM EDTA) and centrifuged at 4,000xg for 3

minutes. The pellet was washed in 1 ml TE-buffer, centrifuged again at 4,000xg for 2 minutes and finally resuspended in 100 µl TE-buffer. The cells were plated on selective medium with 10-20 glass beads and incubated for 2 days at 30°C.

2.19.4 Western blot analysis

All fusion proteins were tested for their expression in yeast by western blot analyses. Transformed yeast colonies, positive for each construct, respectively, were inoculated over night at 30°C in 5 ml SD/-Trp selective medium (Clontech, Saint-Germain-en-Laye, France). Yeast strain Y187 containing the control plasmid pGBKT7 and yeast strain AH109 were used as controls and inoculated in 10 ml SD/-Trp and YPDA medium (adenine-supplemented YPD with 0.003% adenine hemisulfate), respectively. Cell suspensions were transferred into a final volume of 50 ml of the corresponding medium and grown to an OD_{600} of 0.4 -0.6. Protein extracts were prepared for SDS-PAGE as specified in the Yeast Protocols Handbook, supplied from Clontech.

A "mini" SDS-polyacrylamide gels was casted as follows:

	Seperating gel		Stacking gel
	10%	12%	4,5%
ddH_2O	4.0 ml	3.2 ml	-
3x separating gel buffer	4.0 ml	4.0 ml	-
Stacking gel buffer	-	-	4.5 ml
Acrylamide solution	4.0 ml	4.8 ml	0.8 ml
TEMED	6 µl	6 µl	4 µl
10% APS	120 µl	120µl	32 µl
Total Volume	12.126 ml	12.126 ml	5.336 ml

The corresponding amounts of 3x separating gel buffer (1.126 M Tris-HCl, pH 8.8; 0.3% SDS, stored at 4°C), acrylamide solution (30% acrylamide; 0,8% bisacrylamide, stored at 4°C), 10% APS (Ammoniumpersulfate, stored at 4°C), TEMED (N,N,N´,N´,-Tetramethylethylenediamine) and ddH_2O were mixed and polymerized in a "mini" gel sandwich (BioRad, München) for 20 minutes, overlayed with water to ensure an even surface of the separating gel. The water was removed with a paper tissue and the stacking gel poured on top of the separating gel. A comb was inserted carefully into the stacking gel and the gel polymerized for another 30 minutes. After removing the comb, 20 µl of each protein extract was loaded into the gel slots next to SDS7B2 Prestained Molecular Weight Marker (Sigma-Aldrich, München) and separated at 100 V in the stacking gel and at 200 V in the separating gel until the dye front reached the bottom of the gel.

After separation, the stacking gel was removed and the separating gel was placed on two layers of fleece and two layers whatman paper (Whatman, Dassel) into a sandwich clamp for "wet blot" western blotting (Mini Trans-Blot System, BioRad). A cellulose nitrate (Schleicher & Schuell, Dassel) membrane was placed on top of the gel and covered with two layers whatman paper and fleece,

respectively. The sandwich clamp was than placed into the transfer apparatus (BioRad), which was filled with 1x transfer buffer (20% Methanol, 20 mM Tris, 150 mM Glycin, 2% SDS) and the gel blotted for 25 minutes at 400 mA. After disassembling the blot, the membrane was stained for 10 minutes in Ponceau S (0,1 % Ponceau S in 5 % acetic acid) and washed on a glass plate until protein bands were clearly visible. The size standards and lanes were marked with a pencil and red colour removed by washing in 1x TBS (10x TBS: 0.5 M Tris-HCl, pH 7.5; 1.5 M NaCl).

Before immunostaining, the membrane was incubated 1 hour at room temperature in blocking buffer (50 mM Tris-HCl, pH 7.5; 150 mM NaCl, 1% milk powder, 0.1% Triton X-100) with slow rotation to block unspecific binding sites. The rabbit polyclonal antibody α-c-myc SC789 (Santa Cruz Biotechnology, Santa Cruz, CA, USA) was diluted 1/1,000 in blocking buffer and added to the membrane. Antibody binding was carried out over night at 4°C with slow rotation. Afterwards, the membrane was washed twice in blocking buffer and moved slowly in fresh blocking buffer for 10 more minutes. The secondary donkey anti-rabbit antibody (Amersham ECL™ Western blotting system, GE Healthcare, München), coupled to horseradish peroxidase (HRP-conjugated antibody) was diluted 1/4,000 in blocking buffer and swayed with the membrane for 1 hour at room temperature. The membrane was again washed twice and incubated for 10 minutes in blocking buffer, followed by four brief washings with ddH_2O. 1 ml of each detection reagent 1 and 2 from the Amersham ECL™ Western blotting detection reagents and analysis system (GE Healthcare) were mixed and dispersed on the membrane. After 2 minutes incubation time, the membrane was wrapped in cling film and placed in a Hypercasette™ (Amersham Pharmacia Biotech, Freiburg), together with a x-ray film. After 10 minutes, the film was developed in an Optimax 2010 x-ray film processor (Protec, Oberstenfeld). For detection of the more weakly expressed AtARO1, the x-ray film was exposed directly after addition of the detection reagents, without former 2-minutes incubation.

2.19.5 Yeast mating

Direct interaction tests of proteins were carried out by mating as specified in the Yeast Protocols Handbook. The following yeast strains containing corresponding plasmids were used:

	prey (pGADT7) in strain AH109	bait (pGBKT7) in strain Y187	bait (pGBKT7) in strain AH109	prey (pGADT7) in strain Y187
	pGADT7-AtARO1	pGBKT7-AtARO1	pGBKT7-AtARO1	pGADT7-AtARO1
	pGADT7-AtARO1	pGBKT7-Act3	pGBKT7-AtARO1	pGADT7-Act3
	pGADT7-AtARO1	pGBKT7- Act4	pGBKT7-AtARO1	pGADT7-Act4
	pGADT7-AtARO1	pGBKT7-Act7	pGBKT7-AtARO1	pGADT7-Act7
	pGADT7-AtARO1	pGBKT7-GFP	pGBKT7-AtARO1	pGADT7-GFP
Negative control	pGADT7-AtARO1	pGBKT7		
Negative control	pGADT7-AtARO1	pGBKT7-Lam		
	pGADT7-GFP	pGBKT7-Act3	pGBKT7-GFP	pGADT7-Act3
	pGADT7-GFP	pGBKT7-Act4	pGBKT7-GFP	pGADT7-Act4
	pGADT7-GFP	pGBKT7-Act7	pGBKT7-GFP	pGADT7-Act7
	pGADT7-GFP	pGBKT7-GFP	pGBKT7-GFP	pGADT7-GFP
Negative control	pGADT7-GFP	pGBKT7		
Positive control	pGADT7-RecT	pGBKT7-53		
Negative control	pGADT7-RecT	pGBKT7-Lam		

After mating, diploid cells were picked from four independent colonies for each mating combination with a 100 µl filter pipette tip and resuspended in 30 µl ddH_2O in a 96 well microtiter plate. A replica plater with 48 prongs was used to plate the cell suspensions onto selective media SD/-Leu/-Trp, SD/-Leu/-Trp/-His and SD/-Leu/-Trp/-His/-Ade, respectively (SD media from Clontech, Saint-Germain-en-Laye, France).

2.19.6 Two-hybrid library screen

pGBKT7-*ARO1* was used as a bait in the host strain AH109 and mated with the cDNA library from germinated pollen (section 2.19.1) according to the Matchmaker™ Library Construction & Screening Kit User Manual.

2.19.7 X-Gal assay

After selection on low and high stringency SD media (Clontech, Saint-Germain-en-Laye, France), colonies surviving high stringency conditions were tested for activation of the *MEL1* reporter gene. Colonies were replica plated on 150 mm petri dishes and grown for 3 days at 30°C. For each plate, 20 ml 1% bacto agar were dissolved in ddH_2O by boiling and cooled to 60°C. 20 ml 1 M sodium phosphate buffer (pH 7.0), 2.4 ml N,N-Dimethylformamide (DMFA), 200 µl 20% SDS and 400 µl x-Gal (20 mg/ml in DMFA) were carefully mixed and added to the bacto agar. After mixing by gentle swirling, the solution was carefully distributed over the whole petri dish without disturbing the yeast colonies. Plates were incubated at 30°C. After 30 minutes, plates were placed upside down to prevent

condensate accumulation on the agar. After over night incubation at 30°C, positive colonies were evaluated by eye according to the strength of blue precipitate observed in the colony.

2.19.8 Plasmid isolation

Plasmids of clones that were able to grow on SD/-Ade/-His/-Leu/-Trp selection medium (Clontech, Saint-Germain-en-Laye, France) and showed β-galactosidase activity were extracted from 1.5 ml cell suspension grown over night in SD/-Leu/-Trp at 30°C. Pelleted cells were resuspended in 100 µl STET buffer (8% saccharose, 50 mM Tris, pH 8.0; 50 mM EDTA, 5% Triton-X 100) and <1 Volume of glass beads (ø 0.5 mm) were used to homogenize the cells for 40 seconds at speed 5 in a Fastprep FP120 Homogenizer (Thermo Fischer Scientific, Schwerte). Another 100 µl STET buffer were added and after brief mixing, the suspension was incubated for 3 minutes at 95°C. The liquid was then cooled on ice and centrifuged at maximum speed and 4°C for 10 minutes. 100 µl of the supernatant were precipitated with 75 µl 5 M NH_4Ac at -20°C over night. The precipitate was pelleted (10 minutes, 4°C, maximum speed) and 100 µl of the supernatant mixed with 200 µl ice-cold 96% ethanol. After mixing and centrifugation (10 minutes, 4°C, maximum speed), the supernatant was removed, the pellet washed in 70% ice-cold ethanol, the pelleted DNA dryed in a Speedvac (Thermo Fisher Scientific) and resuspended in 20 µl ddH_2O.

5 µl of isolated plasmid was transformed into *E.coli* XL-1 blue MRF´ as described in section 2.10.1 and bacteria containing the plasmid with cDNA library insert selected on LB_{amp} selective medium. Plasmids of representative clones from each construct were isolated from *E.coli* cells (see section 2.11) and cDNA inserts were analysed by restriction enzyme digestion with 5U *EcoRI* and 5U *BamHI* at 37°C for 4 hours. cDNA inserts from plasmids that could not be transformed into *E. coli* were amplified by PCR using primers 5´LD amplier and 3´LD amplier and all inserts were sequenced using primers 5´LD amplier and 3´LD amplier.

For each gene identified, one representative plasmid containing the corresponding cDNA was retransformed (see 2.20.3) into yeast strain AH109 and validated by mating with yeast containing pGBKT7-ARO1 or pGBKT7 empty vector as negative control.

3. RESULTS

3.1 Identifying the ARO gene family

Previously, cDNA libraries of isolated egg cells as well as two-celled pro-embryos from wheat were constructed and used for a transcriptomics approach (Sprunck et al., 2005). 735 expressed sequence tags (ESTs) from wheat egg cells were generated and analysed bioinformatically. Novel transcripts, which did not match any annotated ESTs but showed significant similarities to hypothetical proteins from *Arabidopsis thaliana* or rice (*Oryza sativa*) were considered as especially interesting for expression analysis. The transcript EC-123 (Acc. no. EU662204) was found to be specifically expressed in the egg cell and anthers of wheat and to encode a novel ARM domain containing protein with similarity to hypothetical proteins from *Arabidopsis* (At4g34940; E-value= $1e^{-91}$) and rice (Os08g0548500; E-value= $9e^{-123}$).

In the present work, TBLASTN searches were carried out using the At4g34940 protein sequence as a query in the NCBI non-redundant (nr) database. These BLAST searches revealed the presence of small gene families of 4 members each in *Arabidopsis* and in rice (Fig. 3.3). In *Arabidopsis*, approximately 108 predicted ARM repeat proteins, containing between two and 32 ARM repeats each, were identified previously (Coates, 2003; Mudgil et al., 2004). Additional protein motifs have been found in the majority of these proteins and for some of them a function could be specified (Fig. 3.1B; Amador et al., 2001; Andersen et al., 2004; Coates et al., 2006; Downes et al., 2003; González-Lamothe et al., 2006; Gu et al., 1998; Kim et al., 2004; Liu et al., 2007; Sakai et al., 2008; Stone et al., 2003; Yang et al., 2006a; Yang et al., 2007; Zeng et al. 2004). One group of 28 proteins appears to contain no further known motif despite two to 10 ARM repeats (Fig. 3.1A, B; Mudgil et al., 2004). Most of these proteins represent hypothetical proteins and for none of them a function was identified so far. The four proteins from *Arabidopsis* with similarity to EC-123 belong to this subgroup (Fig. 3.1C) and were named Armadillo Repeat Only (*ARO*) proteins. Therefore, the wheat cDNA EC-123 was renamed as *TaARO1* and the genes from *Arabidopsis* were denominated *AtARO1 to AtARO4*, according to their descending similarity to *TaARO1*. Members of the rice family were named *OsAROl-1* to *OsAROl-4* (*OsARO-like 1* to *4;* Fig. 3.3).

A

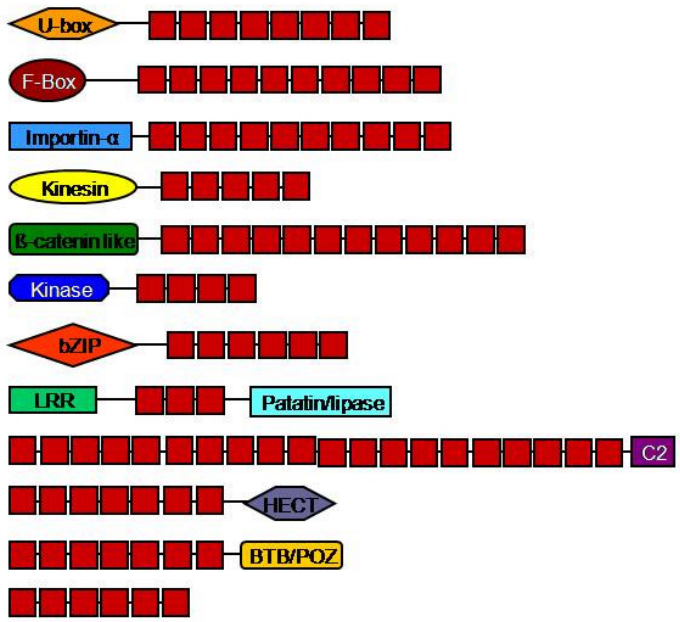

B

Additional motives	Identified proteins in *A. thaliana*	Characterized ARM repeat proteins in plants
U-box	41	ARC1; AtPUB14; AtPUB17; CMPG1; PHOR1; PUB8; SPL11
F-box	2	ARABIDILLO1/2
Importin-α	8	-
Kinesin	3	ARK1, MRH2
β-catenin like	2	-
Kinase	4	-
bZIP	1	-
LRR-Patatin/Lipase	3/1	-
C2	2	-
Hect	1	UPL3
BTB/POZ	2	ARIA
-	28	AtARO1 to -4

C

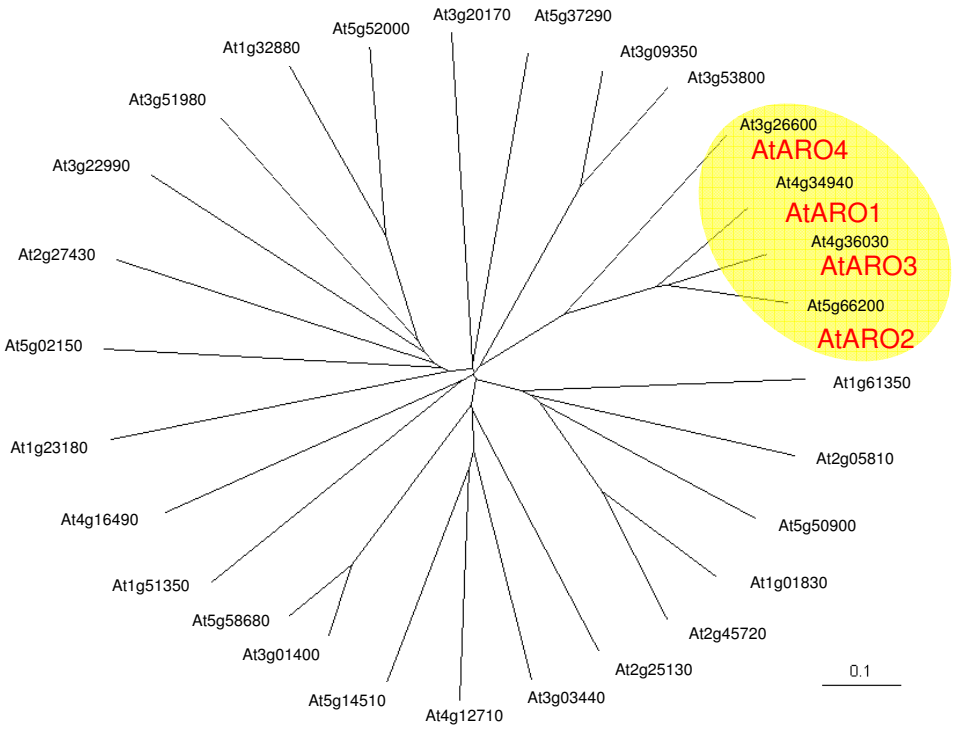

Fig. 3.1. ARM repeat proteins in plants. (**A**) Schematic representation of ARM repeat containing proteins in *Arabidopsis thaliana* modified after Coates, 2003 and Mudgil et al., 2004. Red boxes represent ARM tandem repeats; colored geometric forms represent additional known protein motifs. BTB/POZ (Pfam 00651): bric-a-brac tramtrack, broad complex/pox viruses and zinc fingers; bZIP (pfam00170): basic Leucine Zipper Domain; C2 (pfam00168): Protein kinase C conserved region 2; F-box (pfam00646): domain first found in cyclin-f; HECT (pfam00632): Homologous to the E6-AP Carboxyl Terminus; LRR (pfam00560): Leucin rich repeat; U-box (pfam 04564): involved in ubiquitination; Kinase (pfam00069): serine/threonine kinase domain; Patatin/lipase

(pfam01734): patatin-like phospholipase domain. Numbers of ARM repeats can vary within the different groups. (**B**) Total numbers of identified hypothetical and known ARM repeat domain proteins in *A. thaliana*, grouped according to their additional known protein motifs. Characterized ARM domain containing proteins of plants are: ARC1 (Stone et al., 2003), AtPUB14 (Andersen et al., 2004), AtPUB17 (Yang et al., 2006a), ARC1 (Gu et al., 1998), CMPG1 (González-Lamothe et al., 2006), PHOR1 (Amador et al., 2001), PUB8 (Liu et al., 2007), SPL11 (Zeng et al. 2004), ARABIDILLO1/2 (Coates et al., 2006), ARIA (Kim et al., 2004), ARK1 (Sakai et al., 2008), MRH2 (Yang et al., 2007), UPL3 (Downes et al., 2003). AtARO1 to -4 belong to a subgroup of ARM repeat proteins apparently lacking additional known motifs. (**C**) Phylogenetic relationship of ARM repeat proteins. Sequences of ARM proteins lacking additional known motifs were aligned with ClustalW and an unrooted phylogenetic tree was generated using TreeView 1.6.6. Distances of proteins are displayed as numbers of nucleotide substitutions per site. Scale bar: 0.1 nucleotide substitution per site

Although two of the ARO-like proteins from the rice gene family, Os08g0548500 (OsAROl-1) and Os09g0536200 (OsAROl-2), show highest similarity (92% and 85% respectively) to the deduced amino acid sequence from the wheat cDNA (Fig. 3.3), further studies were focused on the model plant *Arabidopsis,* due to the abundance of scientific tools for this organism. At4g34940 (AtARO1) shows 67% identity and, with 82%, the highest similarity to the partial amino acid sequence of wheat. At5g66200 (AtARO2) shows 59% identity and 77% similarity, At4g36030 (AtARO3) 57% identity and 77% similarity and the most distant member of the family, AtARO4 (At3g26600) features only 40% identity and 60% similarity to TaARO1. All four *Arabidopsis* proteins are encoded by single exons and are between 615 (AtARO4) and 670 (AtARO3) amino acids in length, which corresponds to molecular weights of 67.8 to 73.0 kDa.

Despite the lower sequence conservation of AtARO4, all four *Arabidopsis* proteins share a highly similar overall structure (Fig. 3.2A). Although only two to three *bona fide* ARM repeats were identified in each protein by the Pfam database, sequence alignments of the protein motifs from AtARO1 to AtARO4 in combination with predicted secondary structure analysis revealed a total of 6 complete and 3 incomplete ARM repeats (Fig. 3.2B) in all four proteins. Despite the fact that the sequence conservation between ARM repeats from different protein families in general is only about 25%, the sequences of corresponding ARM repeats of homologous proteins and especially the structural organization and chemical properties are quite highly conserved (Hatzfeld, 1999). This is also true for the ARM repeats of AtARO1. The consensus sequence for the ARM repeats (Fig.3.2B) was calculated by the Pfam database with a Hidden-Markow-Model (HMM). Comparing each ARM repeat of AtARO1 with the consensus sequence makes obvious that only few amino acids in the ARM repeats exactly match the consensus, but several chemical properties are conserved throughout in all ARM repeats. Except repeats R1, R5 and R8, all ARM repeats of AtARO1 further show a typical secondary architecture, comprising three α-helices, H1, H2 and H3 (Fig. 3.2B). The ARM repeats are separated in two ARM repeat containing domains (ARD1 and ARD2) by a highly divergent “spacer” region of 30 (AtARO4) to 90 (AtARO1 and AtARO3) amino acids. ARD1 is preceded by a 143 to 153 amino acid long N-terminal domain and ARD2 is followed by a 55 to 59 amino acid long C-terminal region (Fig. 3.2A).

It is known from the animal as well as from the plant kingdom, that ARM repeat domain containing proteins have a plethora of functions in protein-protein interactions. To understand how these proteins

bind their ligands, the 3-dimensional structure of ARM repeat proteins like β-catenin, plakophilin 1 or importin-α were resolved using X-ray diffraction and NMR-spectroscopy (Choi and Weis, 2004; Huber and Weis, 2001; Kobe, 1999). In single ARM repeats, a conserved Gly residue between H1 and H2 was found to bend the two α-helices at 70°-90°C to each other (Choi and Weis, 2004). This Gly residue could also be identified between H1 and H2 of R2, R3 and R9 of AtARO1 (Fig.3.2B). Several conserved Leu residues, found to participate in intra- and inter-repeat hydrophobic interactions and in orientating H3 antiparallel to H2 (Choi and Weis, 2004), are also present in most of the AtARO1 H2 and H3 helices (Fig. 3.2B). Although variations in sequences of individual repeats entail minor alterations in the 3-dimensional structure, tandem repetition of ARM domains results in the formation of a right-handed superhelix of helices with a hydrophobic core, that gives rise to a concave protein binding surface. In β-catenin, this shallow groove contains most of the positive charges and presumably provides the binding site for its acidic interaction partners (Hatzfeld, 1999). The architecture of proteins with unknown 3-dimensional structure, like AtARO1, can be predicted aligning its amino acid sequence with similar proteins of known conformation (Fig. 3.2C). The DeepView/ Swiss-Pdb viewer 3.7 was used to compare the first 388 amino acids of AtARO1, comprising the N-terminal extension, the ARM repeats R1 to R4 and the "spacer", with murine importin-α (*Mus musculus*, PDB accession 1ialA). Despite the fact that the N-terminal domain as well as the spacer region do not contain any recognized ARM repeats, the whole sequence aligns very well with importin-α and reveals an elongated superhelical conformation.

Sequence alignments and phylogenetic studies of proteins AtARO1 to -4 revealed, that especially AtARO2 and AtARO3 share a very high overall sequence similarity to AtARO1 (Fig. 3.2A). Putative phosphorylation sites for AtARO1 were detected using the programs ELM, NetPhos2.0 and PredictProtein and many of these sites were found to be conserved in all three proteins, AtARO1 to AtARO3. Only one Protein Kinase A (PKA) recognition site could be identified in all four proteins (Fig. 3.2A, boxed arrow). Additionally, there was an especially high number of predicted GSK3 phosphorylation sites particularly present in the spacer region of all four proteins and in the N- and C-terminal region of AtARO4. Although sequence similarity is quite low in the spacer and the positions of GSK3 phosphorylation sites are not aligned in this model, the spacer region displays less densely packed α-helices (Fig. 3.4) and is therefore likely to be a contact point for modifying enzymes. Another motif found in the spacer regions of AtARO1 to AtARO3, but not in AtARO4 is a KEN box. This short sequence motif is found in several key cell cycle proteins where it acts as a signal for cell cycle-dependent proteolysis.

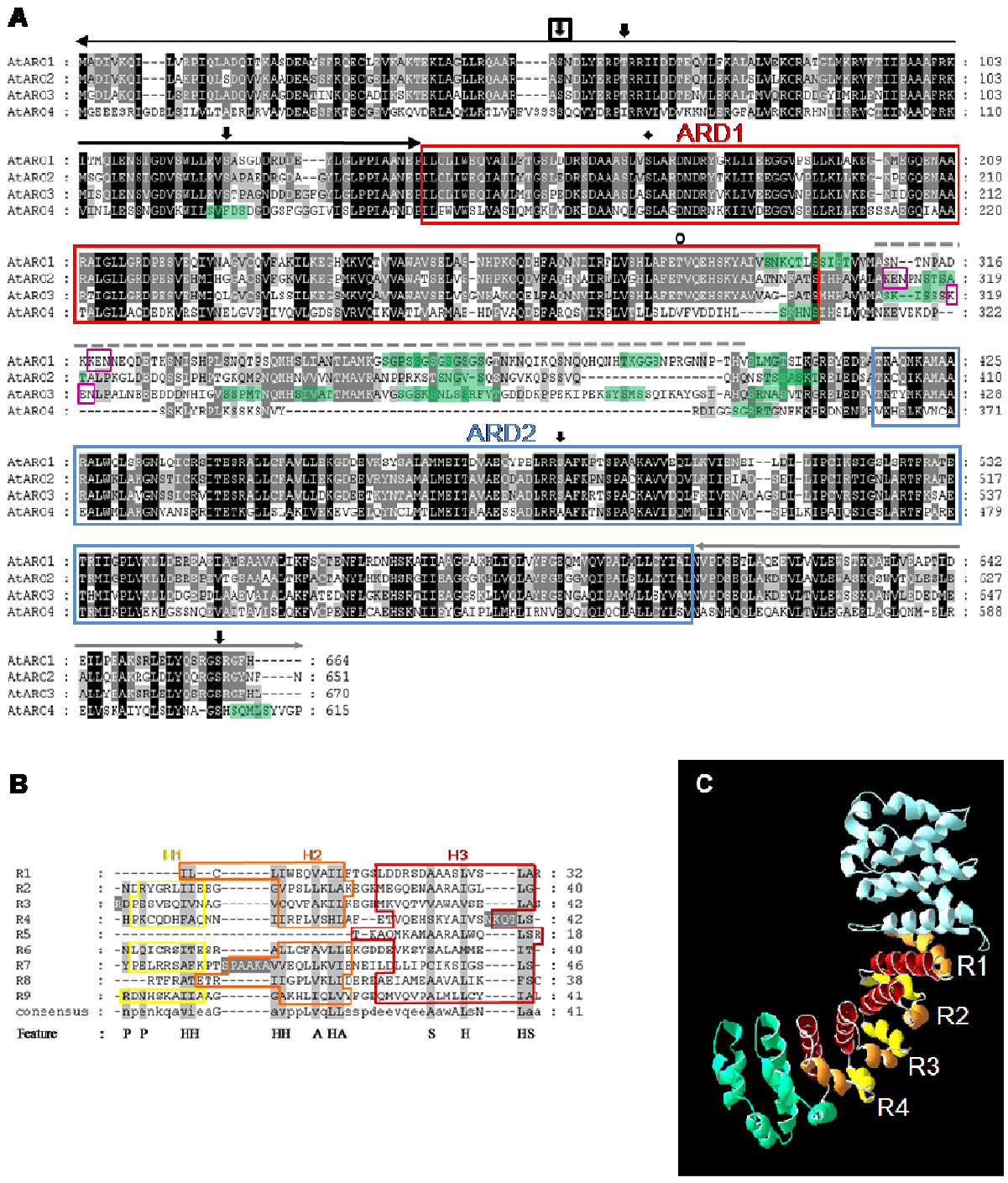

Fig. 3.2. *Arabidopsis* AtARO proteins. (**A**) Primary structure of AtARO1 to AtARO4. The predicted protein sequences encoded by *AtARO1* (At4g34940), *AtARO2* (At5g66200), *AtARO3* (At4g36030), and *AtARO4* (At3g26600) were aligned and processed using M-Coffee and GeneDoc. Two conserved ARM repeat domains (ARD1, ARD2) are located in the first and second half of each protein. ARD1 and ARD2 are separated by a highly divergent "spacer" region of variable length (dashed line). A conserved domain of 143 to 153 amino acids is located at the N-terminus (black arrow) and a short stretch of 55 to 59 amino acids follows ARD2 at the C-terminus (grey arrow). Phosphorylation sites were predicted by ELM, NetPhos 2.0 and PredictProtein. Putative Protein Kinase A (PKA, arrow), Casein Kinase (CK) II (open circle) and CK I (diamond) sites conserved in AtARO1-AtARO3 are indicated above the alignment. A PKA site conserved at the N-terminus of all four proteins is boxed. Putative GSK3 phosphorylation sites are highlighted in green. KEN boxes found in proteins AtARO1 to

AtARO3 are boxed in magenta. (**B**) Sequence alignment of the nine putative ARM repeats (R1–R9) identified in AtARO1 with the HMM consensus sequence of ARM repeats calculated by the Pfam data base (PF00514). Putative helices H1 (yellow), H2 (orange) and H3 (red) of AtARO1 were identified by PSIPRED secondary protein structure predictions. Note that R1, R5 and R8 represent incomplete ARM repeats. Conserved amino acid features are indicated below the alignment. P, polar; H, hydrophobic; A, aliphatic; S, small. (**C**) Predicted 3D structure of AtARO1 (amino acids 1–388), by homologous modeling with murine importin-α (*Mus musculus*; PDB accession 1iaIA). AtARO1 reveals a typical three-helical composition, forming a right handed superhelix of α-helices similar to importin-α. Although the N-terminal domain (blue) and the „spacer" (green) region do not contain recognized ARM repeats, their overall structure resembles the superhelical conformation of importin-α.

In order to identify ARO1-like sequences in genomes of other angiosperms, in gymnosperms and in mosses, the AtARO1 protein sequence (At4g34940; NP_195220) was used as query to run TBLASTN searches in the Plant Genome Database (*Zmbac database*) and the nucleotide collection (nr/nt) database at NCBI as well as the *Populus* genome release 1.1. ARO-like genes from *Zea mays (ZmAROl-1 to -4)* as well as *Lotus japonicus* (*LjAROl-1*), *Medicago truncatula* (*MtAROl-1* and *MtAROl-2*), *Vitis vinifera* (*VvAROl-1/-2*), *Populus trichocarpa* (*PtAROl-1*) and *Physcomitrella patens* (*PpAROl-1to -4*) could be identified (Fig. 3.3). Additionally, TBLASTN searches in the EST data collection of TGI databases from pine and spruce were performed. Tentative consensus sequences of assembled ESTs encoding putative ARO1-like transcripts (*Pinus ssp.*: *PuAROl-1* and *Picea ssp.*: *PiAROl-1*) were identified in the two gymnosperms. A multiple sequence alignment of all newly identified ARO-like putative proteins was obtained using the web server M-Coffee (Moretti et al., 2007) and the resulting output used to create a maximum likelihood distance matrix with SplitsTree4 (Fig. 3.3; Huson and Bryant, 2006). The resulting cladogramm shows that the divisions of angiosperms, gymnosperms and mosses each form independent groups, whereas the orders of monocotyledonous and dicotyledonous plants further divide clearly into two independent branches. Only AtARO4, the most distant member of the AtARO1 to -4 family did not group into any of the defined branches.

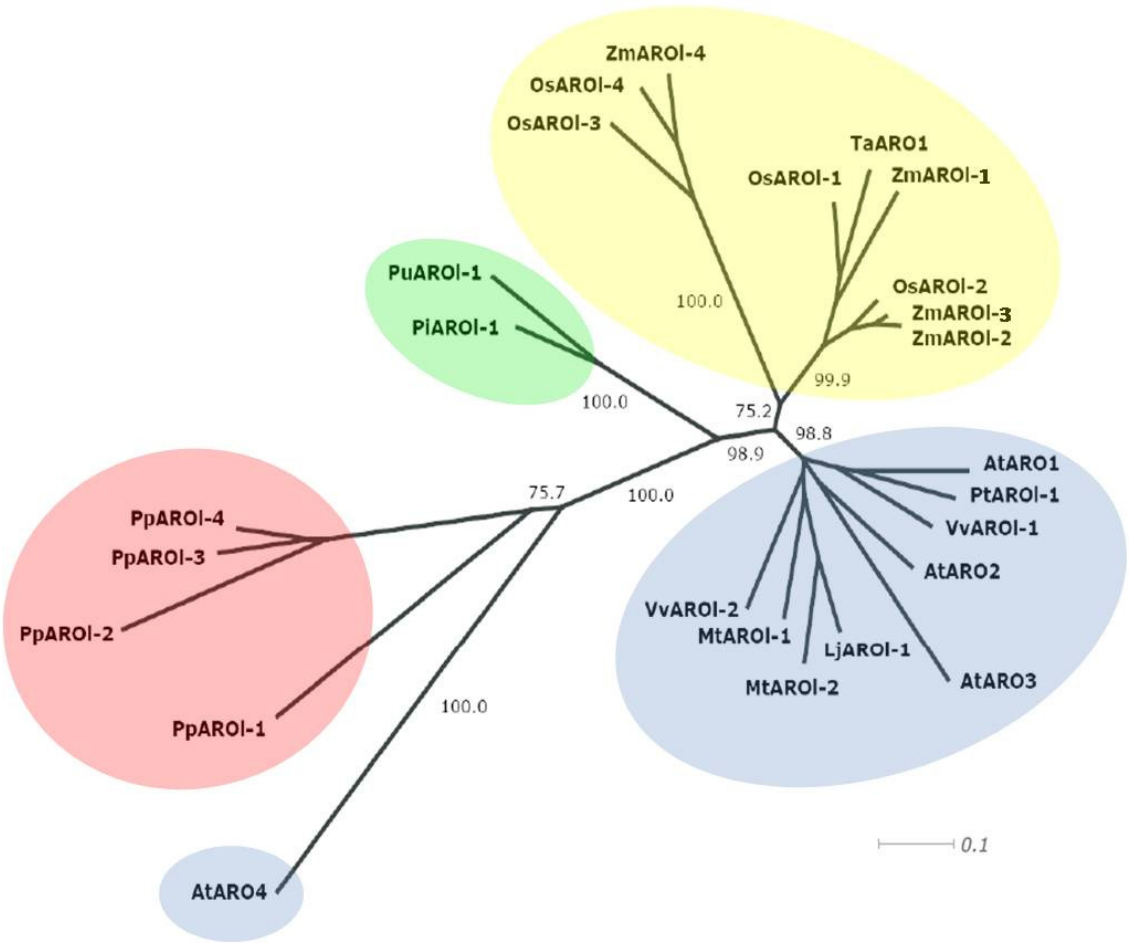

Fig. 3.3. Phylogenetic relationship of members of the ARO protein family. *Arabidopsis thaliana* AtARO1 to -4, *Triticum aestivum* TaARO1 (GeneBank Acc. no. EU662204) and identified ARO-like proteins of *Lotus japonicus* (LjAROl-1; GeneBank Acc. no. BK006563), *Medicago truncatula* (MtAROl-1, GeneBank Acc. no. BK006558; MtAROl-2; GeneBank Acc. no. BK006562), *Oryza sativa* (OsAROl-1 to -4; GeneBank Acc. no. Os08g0548500, Os09g0536200, Os03g0244700, Os10g0147900), *Vitis vinivera* (VvAROl-1, GeneBank Acc. no. BK006560; VvAROl-2, GeneBank Acc. no. BK006561), *Picea spp.* (PiAROl-1, TC39011), *Pinus spp.* (PuAROl-1, BK006559), *Populus trichocarpa* (PtAROl-1, Scaffold LG_IX, contig_31), *Physcomitrella patens* (PpAROl-1 to -4; GeneBank Acc. no. XP_001775927, XP_001774233, XP_001784239, XP_001766369), and *Zea mays* (ZmAROl-1 to –4; GeneBank Acc. no. BK006566, BK006564, BK006567 and BK006565) were aligned using M-Coffee. A maximum likelihood distance matrix was calculated with SplitsTree. The clade formed by AROs from dicotyledonous plants is colored in blue, the monocotyledonous clade is highlighted in yellow, gymnosperm AROs are highlighted in green, and the clade of moss AROs is colored in red. Please note that TaARO1 and PuAROl-1 represent partial protein sequences. Distances of proteins are displayed as numbers of nucleotide substitutions per site. Scale bar: 0.1 nucleotide substitution per site.

Despite the fact that proteins of same plant orders did show higher sequence similarities amongst each other than proteins with putative similar function from different orders, proteins from each plant genus with highest similarities to AtARO1 were selected to analyse analogies in secondary structure and domain architecture and to detect putative conserved phosphorylation sites or other binding motifs.

The secondary structure of all ARO1-like proteins was predicted by PSIPRED and the structure for AtARO1 is displayed below the alignment in Fig. 3.4. The α-helical stretches which are conserved in all ARO-like proteins are shaded. The 139 to 143 amino acid long N-terminal domain is strongly conserved in primary as well as secondary structure and is predicted to fold into one long (AtARO1, VvAROl-1 and PiAROl-1) or two separated (OsAROl-1, PtAROl-1, ZmAROl-1 and PpAROl-1) α-helices. It is followed by ARD1, consisting of one incomplete and three complete ARM repeats. Although less conserved, the spacer was predicted to contain several α-helices as well and the alignment with the 3-dimensional structure of importin-α mentioned above (Fig. 3.2C) revealed that it probably does not interfere with the overall superhelical conformation of AtARO1. ARD2 consists of two partial and three conserved ARM repeats and the C-terminal region of ARO1-like proteins was found to contain three more α-helices resembling the design of ARM repeats in architecture. However, no known protein domain was identified in this region. AtARO1, OsAROl-1 and ZmAROl-1 were further predicted to fold into a short β-sheet of three or four amino acids directly behind the last α-helix.

Several phosphorylation sites were found to be conserved either in all ARO1-like proteins (boxed icons; Fig. 3.4.), or in all angiosperms (unboxed icons; Fig. 3.4). Furthermore, a putative 14-3-3 protein binding site was identified in the angiosperm ARO1-like proteins. 14-3-3 proteins are adapter molecules that mediate protein-protein interactions, alter the subcellular localization of their binding partners and regulate enzyme activity. More than one hundred binding partners of 14-3-3 proteins have been identified so far, but their exact function is still largely unknown.

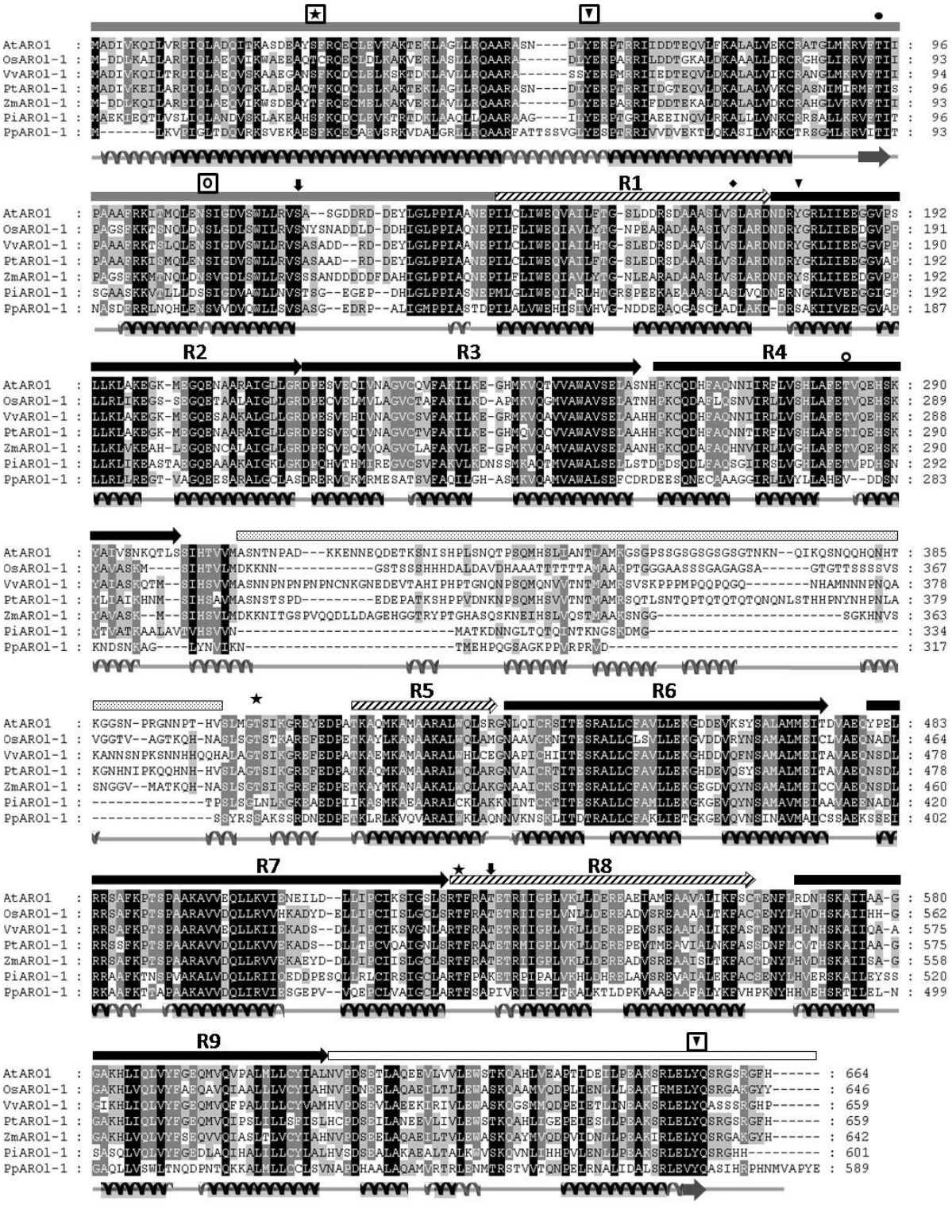

Fig. 3.4. Conserved secondary structure and phosphorylation sites of ARO1-like proteins. The amino acid sequence of AtARO1 (At4g34940) was aligned with most similar ARO-like proteins from *Oryza sativa* (OsAROl-1; Os08g43500), *Zea mays* (ZmAROl-1; BK006566), *Vitis vinifera* (VvAROl-1; BK006560), *Populus trichocarpa* (PtAROl-1; Scaffold LG_IX, contig_31), *Picea ssp.* (PiAROl-1; TC39011), and *Physcomitrella patens* (PpAROl-1; XP_001775927). Multiple sequence alignment and processing were performed using M-Coffee and GeneDoc. Letters in black blocks indicate identical amino acid residues/conserved substitutions found in all proteins, amino acid residues with ≥ 80% conservation are highlighted in dark grey, and those with ≥ 60% conservation are shown as light grey boxes. Secondary structures of ARO1-like proteins were predicted by PSIPRED. Twisted lines and

broad arrows below the alignment denote α-helices and β-sheets, respectively. Conserved secondary structure elements found in all ARO1-like proteins are shaded. Phosphorylation sites were predicted by NetPhos, ELM, and PredictProtein. Protein kinase C (PKC) sites are marked by asterisks, arrows indicate PKA sites, tyrosine phosphorylation sites are indicated by closed triangles, casein kinase (CK) II sites are marked by open circles, the CK I site is marked by a diamond. A possible 14-3-3 protein binding site is indicated by an open circle. Boxed icons indicate phosphorylation sites conserved in all proteins, unboxed icons are sites conserved in angiosperms. Positions of ARM repeats (R1 to R9) are depicted by arrows above the alignment. Black arrows: conserved ARM repeats; white arrows with diagonal stripes: incomplete ARM repeats. N- and C-terminal extensions are depicted as grey and open bars, respectively. The spacer region is labeled as a white bar with black dots.

3.2 Expression studies of *AtARO1-4* genes in *Arabidopsis*

3.2.1 Transcript analysis

All four members of the *Arabidopsis AtARO1* to *-4* family were analyzed for their expression pattern in different vegetative and generative tissues by reverse transcription mediated PCR (RT-PCR, Fig. 3.5). Only *AtARO1*, the gene with highest similarity to *TaARO1* from wheat, showed a similar expression pattern as *TaARO1*, which was exclusively detected in wheat egg cells, in the female gametophyte containing pistil, as well as in anthers (Sprunck et al., 2005). Transcripts of *AtARO1* were also found in reproductive tissues like buds and flowers and more specifically in anthers and unpollinated ovaries, which contain the unfertilized egg cells. The other three members of the gene family were found to be expressed ubiquitously in all tissues tested (Fig.3.5A). More detailed expression analysis of all four *AtARO* genes revealed however, that *AtARO1* is the only member of the gene family to be expressed in isolated mature pollen grains (Fig. 3.5B), while transcripts of all four genes can be detected in egg cells (Fig. 3.5C). In microarray experiments, an ATH1 GeneChip® was hybridized with fluorescently labelled cRNA from isolated egg cells of *Arabidopsis* (L. Soljic, unpublished). Relative fluorescence intensities resulting from hybridizing transcripts of *AtARO1* to *-4* were analyzed and compared with those of other genes, considered as positive and negative controls, respectively. Although transcripts of *AtARO2* to *-4* are present at much higher levels, the p-value of 0.000244 for *AtARO1* shows the high significance of the detected signal. Further, *WOX2* (At5g59340), a gene shown to be expressed in the egg and central cell by *in situ* hybridization (Haecker et el., 2004), shows a comparable fluorescence intensity (FI) together with a higher p-value (p=0.023926). *PGA3*, a gene known to be exclusively expressed in anthers (Torki et al., 1999) was used as negative control and transcripts were scored as absent due to its low fluorescence intensity and high p-value (FI=1.6;p= 0.753906).

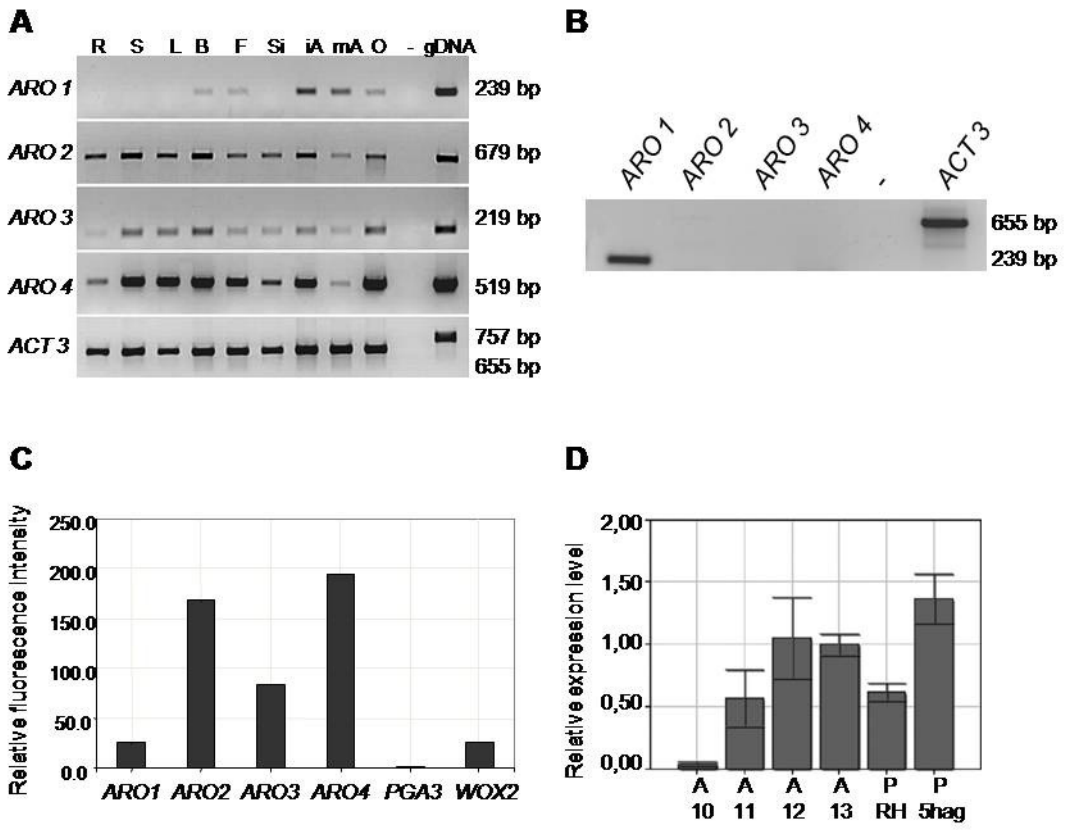

Fig. 3.5. Expression of *AtARO1* to *-4*. (**A**) RT-PCR analysis of *AtARO1* to *-4* in different tissues of *Arabidopsis thaliana*. RT-PCR was performed using cDNA from roots (R), stem (S), leaves (L), buds (B), flowers (F), siliques (Si), immature anthers (iA), mature anthers (mA) and ovaries (O) and gene-specific primers each for *AtARO1* to *-AtARO4*. *Actin3* (*ACT3*) primers were used as control. While *AtARO2* to *-4* appear to be expressed ubiquitously, transcripts of *AtARO1* were exclusively detected in tissues containing the male and female gametophytes. (**B**) RT-PCR using cDNA generated from mature pollen. In contrast to *AtARO1*, *AtARO2* to *-4* are not expressed in tricellular pollen grains. (**C**) Expression of *AtARO1* to *-4* in egg cells. Relative signal intensities (p-values < 0.05) of an ATH1 GeneChip® experiment using fluorescently labeled amplified RNA (cRNA) of isolated egg cells for hybridization. *AtARO2, -3* and *-4* show stronger fluorescence, compared to *AtARO1* or *WOX2* (At5g59340), a transcription factor known to be expressed in egg cells. No significant signals were obtained for the pollen-specific *PGA3* (At3g07830) which was considered as negative control. (**D**) Relative expression levels of *AtARO1* during anther development and in *in vitro* germinated pollen, estimated by Q-PCR. Highest transcript levels were detected in anthers at floral stages 12 and 13. After *in vitro* pollen germination, expression of *AtARO1* increased compared to its expression in rehydrated pollen. A10-A13, anthers at floral stages 10-13; RH, rehydrated; hag, hours after germination. Flower stages according to Smyth et al. (1990).

Real-time PCR was carried out to quantify the relative mRNA levels of *AtARO1* in different developmental stages of anthers as well as in mature and germinated pollen grains (Fig. 3.5D). Relative expression levels were calculated using *Actin3* (*ACT3*) as the reference housekeeping gene. During maturation of anthers, the mRNA levels of *AtARO1* increased significantly in flower stages 11 to 12 (flower stages according to Smyth et al., 1990) and showed highest accumulation in mature male gametophytes. According to the general classification of pollen-expressed genes, *AtARO1* can thus be

related to the group of late pollen-specific genes (Chiang et al., 2006). At 5 hours after germination (5hag), an increase of expression by 2.25 fold was found in pollen tubes compared to mature, freshly rehydrated (RH) pollen grains.

3.2.2 Promoter-GUS studies

For a more detailed view on tissue specificity and to verify the expression analysis obtained by RT-PCR, a 706 bp long fragment upstream of the start codon of *AtARO1* was chosen as putative promoter region and cloned in front of the reporter *β-glucuronidase* (*GUS*). The construct *AtARO1p::GUS* was stably transformed into *Arabidopsis* via *Agrobacterium* mediated transformation and homozygous F_2 plants were analyzed for GUS activity. After screening of seedlings at principal growth stages 1.04- 1.08 (Fig. 3.6A, stages after Boyes et al., 2001) and different tissues from principal growth stage 6 (Fig. 3.6B-F), GUS staining could exclusively be detected in flowers at stages 11 to 13 (Fig. 3.6E; stages after Smyth et al., 1990). There, the activity of the promoter was restricted to generative tissues and more specifically, a blue staining could only be detected inside anthers of flowers from stage 11 onwards (arrows in Fig. 3.6J and K), in the transmitting tract of the ovary (arrowhead in Fig. 3.6L) and inside embryo sacs (arrow in Fig. 3.6L).

A closer inspection at female gametophytes of developing ovules from Meiosis I until maturity (Fig. 3.7A-D) revealed that the promoter is switched on exclusively and specifically in the mature egg cell (Fig. 3.7D). During megasporogenesis and megagametogenesis (Fig. 3.7A-C), no traces of the reaction product from GUS activity were visible. After fertilization, GUS activity was still detectable in the zygote 18 hours after hand pollination (Fig. 3.7E), but quickly faded after the first cell division (Fig. 3.7.F). In older embryos from the four-celled to bent cotyledon stage the *AtARO1* promoter was switched off (Fig 3.7G-L). In the anthers, promoter activity is restricted to trinucleate and mature, tricellular pollen grains (Fig. 3.7M-R) and growing pollen tubes (Fig. 3.7S). These results underline the expression data obtained by RT-PCR and microarray and make it very likely that *TaARO1* and *AtARO1* are not only homologues in amino acid sequence but also analogues in function.

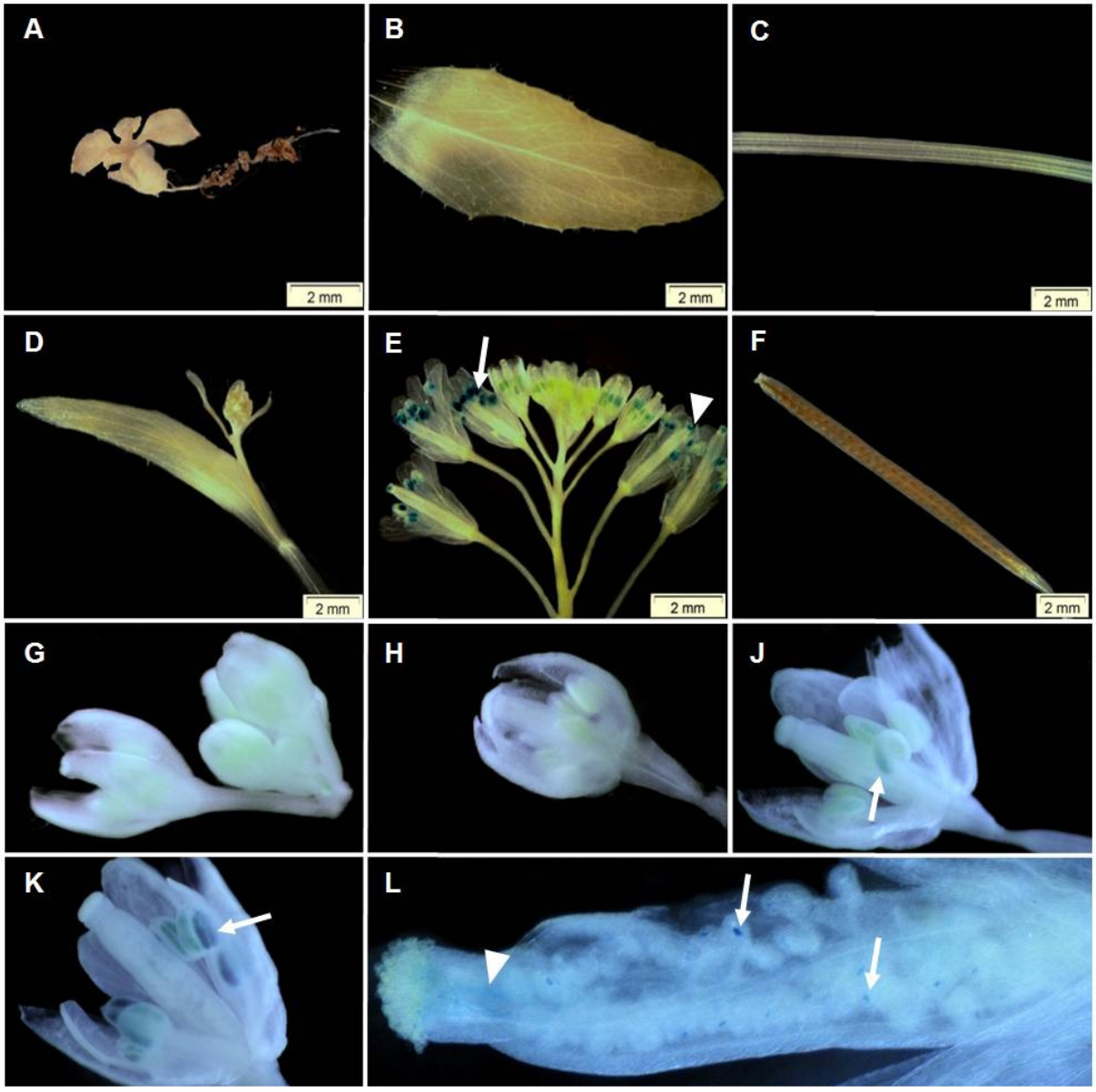

Fig. 3.6. *AtARO1* promoter activity in homozygous *AtARO1p::GUS* plants. (**A**) No GUS staining is detected in young seedlings (principal growth stage 1.06), rosette leaves (**B**), stem (**C**) or young inflorescences (**D**). (**E**) In older inflorescences, GUS staining accumulates in the maturing anthers, starting form floral stage 11 (arrow) and is visible on the stigmata of pollinated flowers (arrowhead). (**F**) In siliques, no GUS activity is visible. (**G**-**L**) *AtARO1* promoter activity in flowers of homozygous *AtARO1p::GUS* plants. (**G**) Flower buds of floral stages 1-9 show no GUS activity. (**H**) Flower bud at floral stage 10. No GUS staining is visible in any tissues of the bud. (**J**) Flower at floral stage 11. The GUS activity starts to become obvious in maturing anthers (arrow). (**K**) Clear GUS staining is visible in mature pollen inside the tapetum of the anthers (arrow) from a flower of stage 12. (**L**) Open flower after pollination with self pollen. Blue precipitate can be detected in pollen grains on the stigma, in pollen tubes growing through the style (arrowhead) and inside the ovules (arrows). Floral stages according to Smyth et al. (1990).

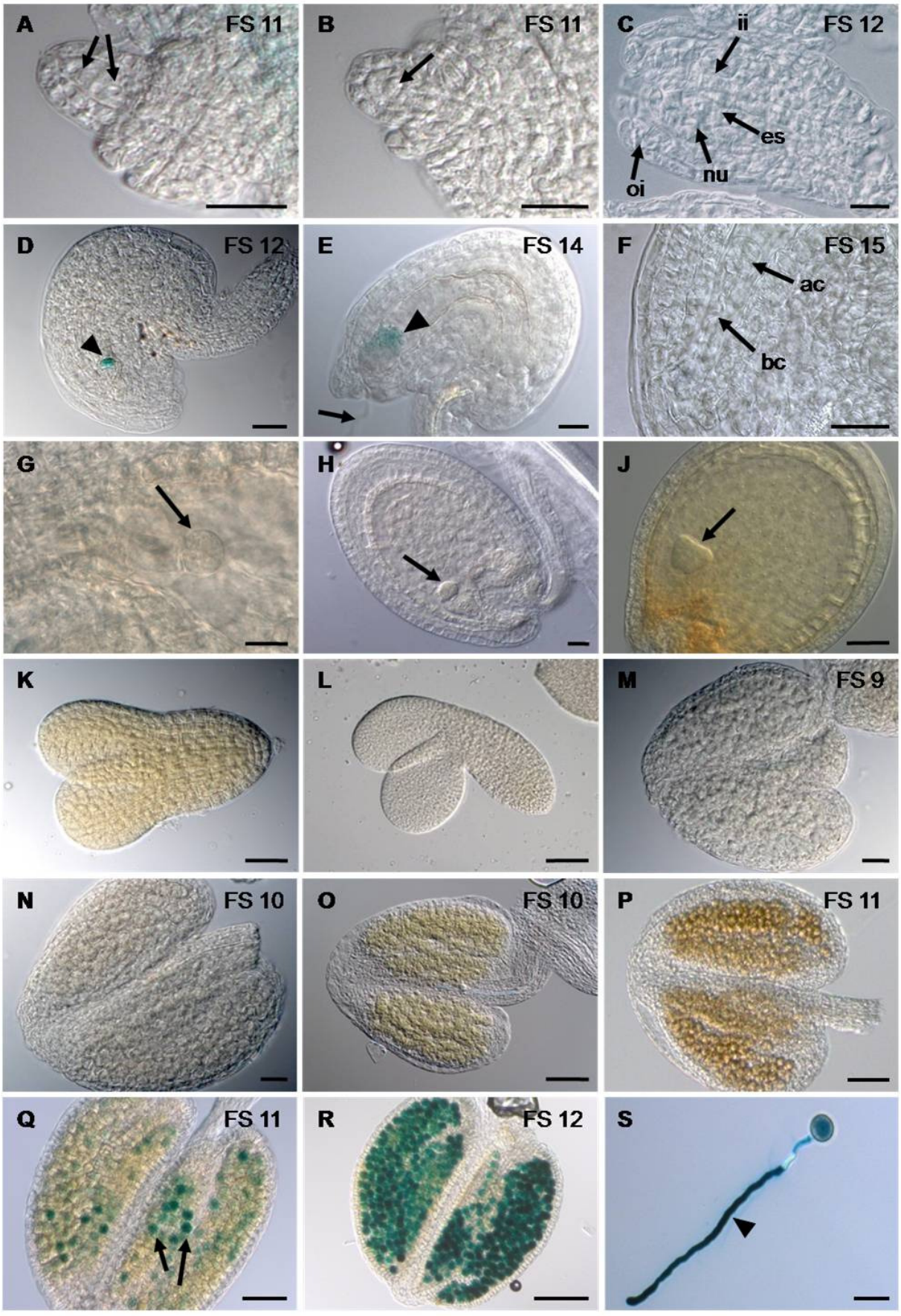
A
FS 11
B
FS 11
C
ii
FS 12
es
nu
oi
D
FS 12
E
FS 14
F
FS 15
ac
bc
G
H
J
K
L
M
FS 9
N
FS 10
O
FS 10
P
FS 11
Q
FS 11
R
FS 12
S

Fig. 3.7. *AtARO1* promoter activity in the female and male gametophytes of homozygous *AtARO1p::GUS* plants. (**A**-**C**) No GUS staining is detected in the immature embryo sac before cellularization. (**A**) Megasporogenesis: Ovule at Meiosis I. Two megaspores and their nuclei are visible inside the nucellar tissue (arrows). (**B**) Megagametogenesis: Three of the four tetrads degenerated while the functional megaspore develops into the mononuclear embryo sac. (**C**) The first of three rounds of mitosis takes place in the embryo sac (es), while the inner (ii) and outer integuments (oi) grow around the nucellus cells (nu). (**D**) Mature ovule, 2 days after emasculation. GUS staining is detected exclusively in the egg cell (arrow). (**E** and **F**) *AtARO1p::GUS* ovules, hand-pollinated with WT pollen (arrow in **E** points at pollen tube). (**E**) 18 hours after pollination, GUS activity is still visible in the zygote (arrowhead). (**F**) In the two-celled embryo (ac, apical cell; bc, basal cell), the GUS signal is no longer detectable. (**G**-**L**) During embryo development, the *AtARO1* promoter is no longer active. Four-celled embryo (**G**), embryo at globular stage (**H**) and heart stage (**J**) inside ovules (arrows). Isolated embryos at torpedo stage (**K**) and early bent cotyledon stage (**L**). (**M**-**S**) *AtARO1* promoter activity in the male gametophyte. (**M**) Anther at floral stage 9. At the end of meiosis, in the tetrad stage, the reporter gene can not be detected yet in developing pollen. (**N**) Anther at floral stage 10. The *AtARO1* promoter is not active in microspores, during pollen mitosis I (**O**) or pollen mitosis II (**P**). (**Q**) As the pollen grains successively become mature in floral stage 11, GUS activity becomes visible. (**R**) In mature, tricellular pollen (floral stage 12), strong GUS activity is detected. (**S**) After 6 hours of *in vitro* germination, the pollen tube (arrowhead) shows intense GUS staining. FS, floral stage. Scale bars: (**A**-**G**) 20 µm; (**H**, **K**, **O**, **P**, **Q**) 50 µm (**J**, **L**, **R**) 100 µm; (**M**, **N**) 10 µm; (**S**) 25 µm. Floral stages according to Smyth et al. (1990).

3.3 Functional analysis

To analyze the function of AtARO1 in the egg cell and pollen grain, two different approaches were chosen. On the one hand, T-DNA insertion lines were ordered for each, *AtARO1* to - *AtARO4* from the SALK institute (Alonso et al., 2003). Since a complete knock out of *AtARO1* is likely be lethal, due to the fact that it is expressed in both, the haploid female and male gametophytes, an RNAi approach was chosen in addition, to specifically downregulate the expression of *AtARO1* exclusively in the egg cell.

3.3.1 Specific knock down of *AtARO1* in the egg cell with RNA interference

An RNAi construct was designed to specifically downregulate *AtARO1* expression in the egg cell. For this purpose, a fragment from the central “spacer” region of *AtARO1* with very low homology to the other members of the *ARO* family was selected for cloning in sense and antisense orientation into an RNAi vector (pEC1-iF2). As the dicer enzyme cleaves double-stranded RNA into 20-25 nucleotides long guide strands for the RISC complex, a fragment of *AtARO1* was chosen (+939 to +1231 downstream of the predicted start codon), where less than 20 consecutive bp matched to the sequences of *AtARO2* to *AtARO4*. For egg cell specific expression, the *Arabidopsis EC1* promoter was used, which is only active in mature egg cells and switched off shortly after the first zygotic division (S. Sprunck, personal communication).

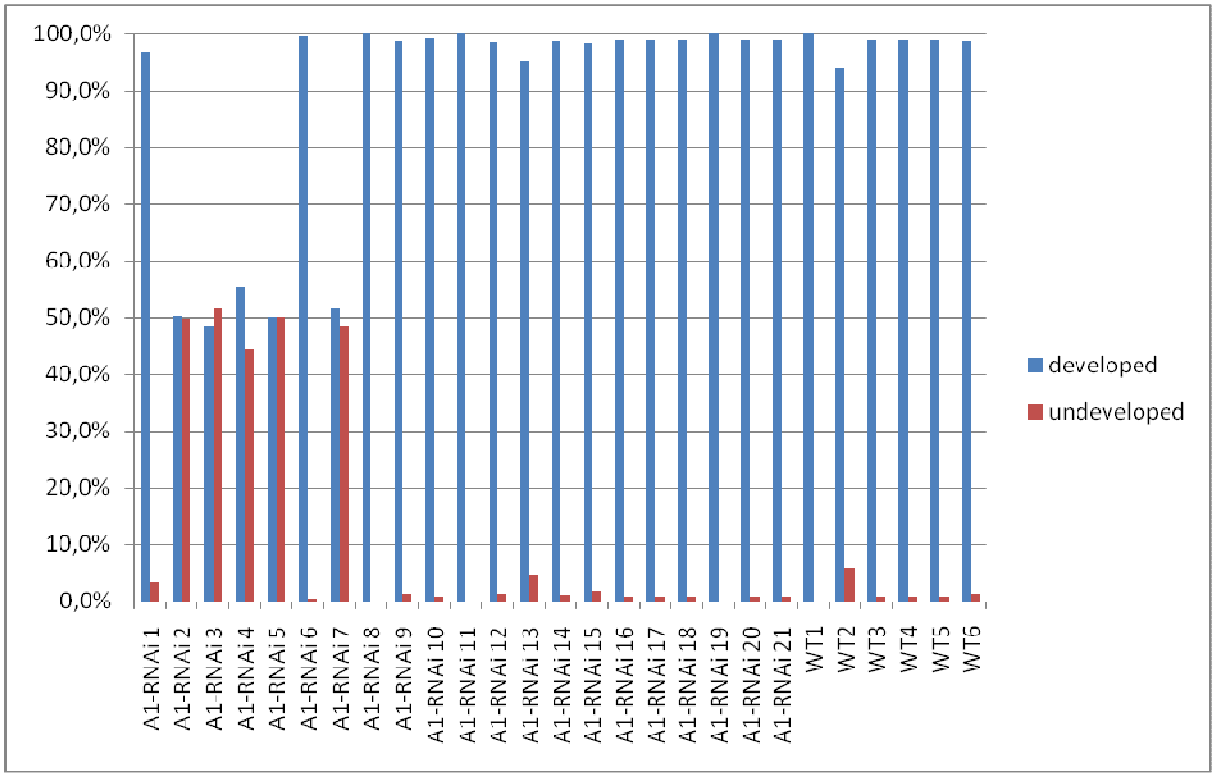

Fig. 3.8. Numbers of developed and undeveloped seeds (expressed in percentage) from a total of 21 independent lines containing the ARO1-RNAi transgene (A1-RNAi). For each, ARO1-RNAi and WT plants, 10 siliques from the main branch were harvested, opened and developed and undeveloped seeds were scored. 5 out of 21 lines (Lines 2, 3, 4, 5 and 7) showed an approximately 50% aborted seed set.

In total, 21 independent lines containing the vector p7N*EC1p::ARO1*-RNAi (referred to as *ARO1*-RNAi hereafter) were analyzed. As the *ARO1*-RNAi construct specifically is switched on in the mature egg cell, the lines were examined for phenotypic anomalies in reproduction processes. A reduced seed set is a criterion often used to identify female gametophyte mutations, as in plants heterozygous for such a mutation, approximately half of the female gametophytes are most probably nonfunctional (Drews and Yadegari, 2002). Thus, 10 siliques at principal growth stage 8.0 (Boyes et al., 2001) from the main branch of each line were opened and developed and undeveloped seeds were scored. 5 of the independent lines actually showed a reduced seed set of approximately 50% aborted ovules while the rest of the lines did show no phenotype (Fig. 3.8). To correlate the aborted ovule phenotype with a downregulation of the endogenous *AtARO1* gene through the *ARO1*-RNAi transgene, progeny from one line displaying the abortion phenotype as well as from several *ARO1*-RNAi lines not showing a phenotype and from WT plants were analyzed by Q-PCR. Progeny plants used in this Q-PCR study were as well scored for aborted ovules. 5 out of ten progeny plants of line 7 (plants 7-1 to 7-10) again showed the abortion phenotype (Fig. 3.9A), while progeny plants of lines 16 to 21 and all WT controls developed full seed set (not shown). For Q-PCR analysis, cDNA was generated from single, unfertilized pistils two days after emasculation. *AtARO1* specific primers were used for Q-PCR and relative expression levels calculated using *Act3* as housekeeping gene for normalization.

As shown in Fig. 3.9B and C, the variation of *AtARO1* transcripts is very strong among *ARO1*-RNAi plants but also among WT controls and does not correlate with the abortion phenotype. Plant 7-10 showed the highest levels of *AtARO1* transcript (relative expression level, REL: 44.2) but a reduced seed set while plant 7-2, an outcrossed plant not containing the *ARO1*-RNAi cassette and showing full seed set, exhibited a quite weak expression of the *AtARO1* gene (Fig. 3.9B; REL 6.5). Transcript levels also varied widely in control WT plants (REL between 1.0 and 34.3) and *ARO1*-RNAi plants not displaying the phenotype (Fig. 3.9C; REL between 4.9 and 68.6). Arithmetic mean values of relative expression levels for *ARO1*-RNAi progeny from lines 16-21 were 16.4 ± 17.0 and for WT plants 12.8 ± 11.4.

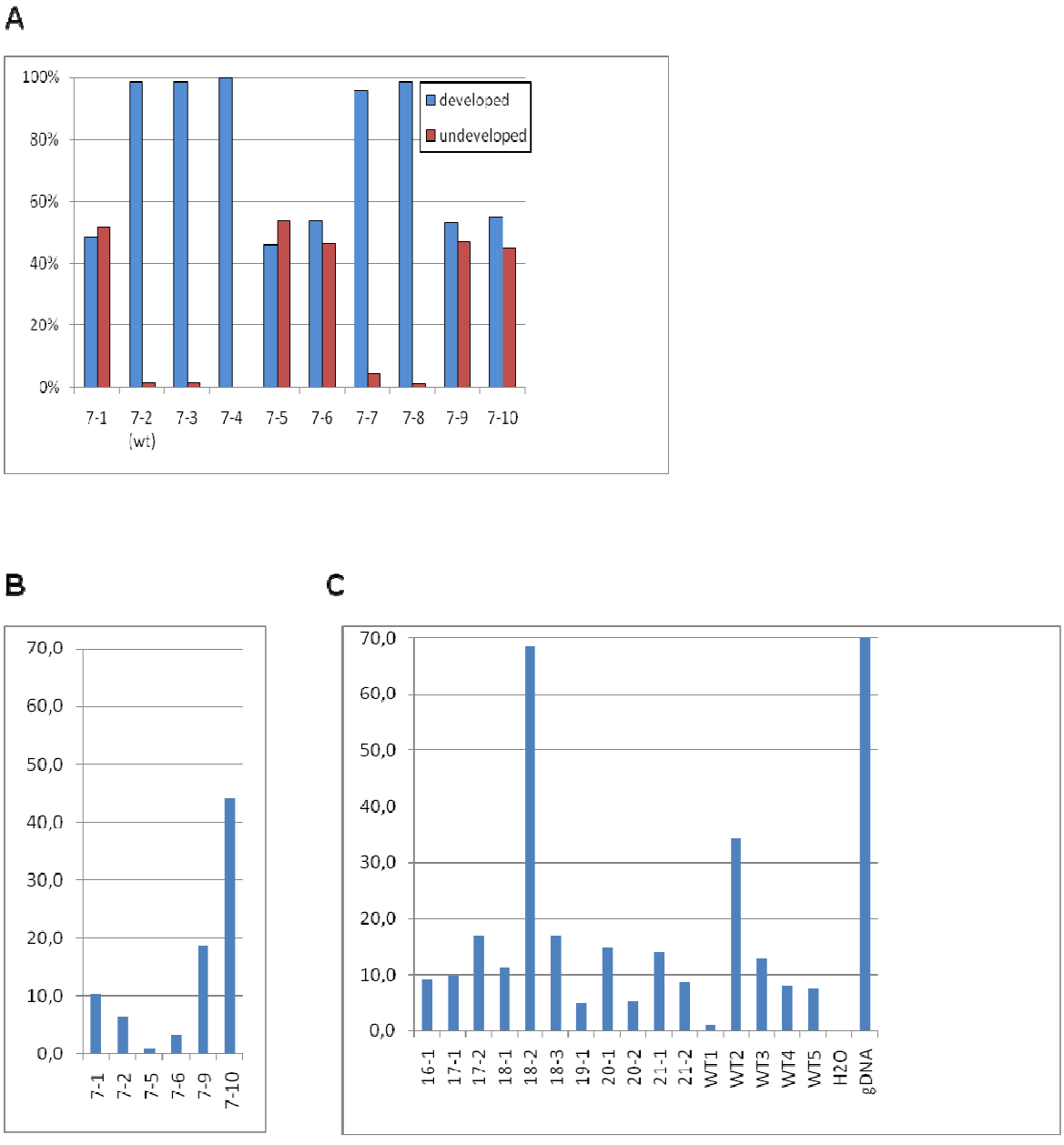

Fig. 3.9. Correlation of the aborted seed set phenotype of progeny plants from *ARO1*-RNAi lines with relative expression levels of endogenous *AtARO1*. (**A**) Ten progeny plants from *ARO1*-RNAi line 7 were analyzed for aberrant seed set. 10 siliques from the main branch of each plant were harvested, each opened and developed and undeveloped seeds were scored. Numbers of seeds expressed in percentage. Plants 7-1, 7-5, 7-6, 7-9 and

7-10 showed an approximately 50% reduced seed set. (**B**) and (**C**) Relative expression levels of endogenous *AtARO1* in *ARO1*-RNAi and WT pistils estimated using quantitative PCR. δ-δ-C_t method was used to calculate relative expression using *Act 3* for normalization. gDNA was used as positive control. Detected relative expression levels of *AtARO1* varied strongly between *ARO1*-RNAi as well as WT lines.

It was shown before, that independent single-copy RNAi lines from *Arabidopsis* targeting one gene generally reduce transcript levels to the same extent, whereas multi-copy RNAi lines differ in the degree of target reduction and never exceed the effect of single-copy transgenes (Kerschen et al., 2004). To determine the copy number of the inserted *ARO1*-RNAi transgene, southern blotting was carried out with *EcoRI* digested genomic DNA from progeny plants of different independent lines. The *EcoRI* enzyme cuts once inside the cassette containing the *PAT* gene under the control of the *NOS* promoter and the *ARO1*-RNAi construct under the control of the *EC1* promoter (Appendix 7.3.13). Thus, each band detected in the southern blot experiment with a probe against the *PAT* gene represents one integration of the transgene. Two to three integrations of the *ARO1*-RNAi transgene could be detected in all plants analyzed with exception of progenies from line 17 which displayed 7 copies of the transgene cassette (Fig. 3.10) but no single-copy lines were identified amongst all lines analyzed. Plant 20-3 was an outcrossed plant with WT background and used as negative control in the southern experiment. The *EcoRI* restricted plasmid p7N*EC1p::ARO1*-RNAi was used as positive control. Between individual sister plants from one line, no segregation of the multiple integrates could be detected, indicating that they are inserted in tandem repetition at one locus and thus linked.

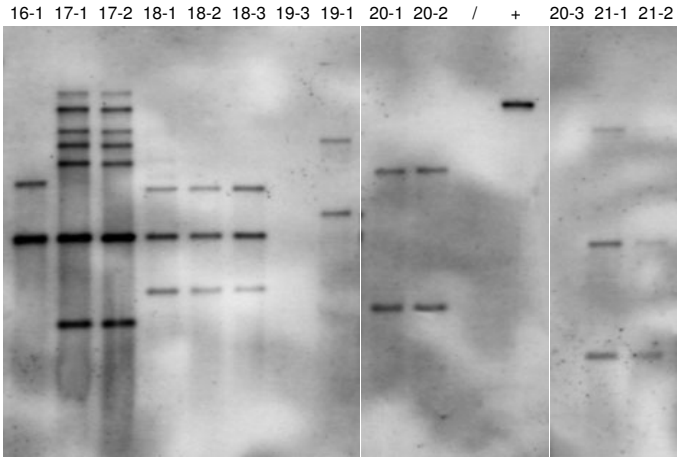

Fig. 3.10. Estimation of copy numbers of integrated T-DNA in progenies of transgenic lines 16 to 21. Southern blots of genomic DNA from *ARO1*-RNAi plants digested with *EcoRI* and hybridized with a probe against the *PAT* gene. 2-3 copies of the transgene were found in each plant, except for progenies from line 17, which carried 7 copies. Plant 20-3 was an outcrossed WT plant and used as negative control. The restricted plasmid p7N*EC1p::ARO1*-RNAi was used as positive control (+). Plant 19-3 did not reveal any hybridization signal.

Although no direct correlation between downregulation of *AtARO1* and seed abortion could be detected, aborted seeds were analyzed microscopically. The phenotypic appearance of the undeveloped ovules in siliques displaying aberrant seed set was of small size and white color (Fig. 3.11A). This phenotype is an indication for very early ovule abortion due to a defect in gametophyte development or fertilization (Acosta-García and Vielle-Calzada, 2004). For this reason, cytoplasm, nucleoli and vacuoles of *ARO1*-RNAi ovules from floral stages 8 to 12 were visualized according to Christensen et al. (1997) and analyzed under the CLSM. At the beginning of megagametogenesis (ovule stage 3-I, after Schneitz et al., 1995), no phenotypic variations could be observed between ovules of RNAi plants and WT plants (Fig. 3.11B, C). In mature ovules of stage 3-VI, however, approximately half of the ovules from such plants displaying a reduced seed set showed an arrest in embryo sac development (Fig. 3.11E-G). Only one (Fig. 3.11E), in rare cases two nuclei (Fig. 3.11F) could be observed in these embryosacs, while the inner and outer integuments were fully developed, enclosing the nucellus cells (arrow in Fig. 3.11G). A strong white staining could occasionally be observed at the position of the former mononuclear embryo sac cell (dashed arrow in Fig. 3.11G), that probably represent degraded cells. Obviously, the embryo sac development of ovules displaying the aberrant phenotype arrested either after the functional megaspore developed at stage FG1 (stages after Christensen et al., 1997), or at stage FG2 after the first mitotic division of the mononuclear embryo sac (Fig. 3.11E, F). Upon the time point where fertilization normally would take place (ovule stage 4-I), the cells arrested in their development seemed to induce apoptosis (Fig. 3.11G). The other half of ovules developed normally as in these embryo sacs the nuclei of the two synergids, the egg cell and the central cell were clearly visible in stage FG 7 (Fig. 3.11D, H-N) and the ovules were able to develop seeds after fertilization (Fig.3.11O).

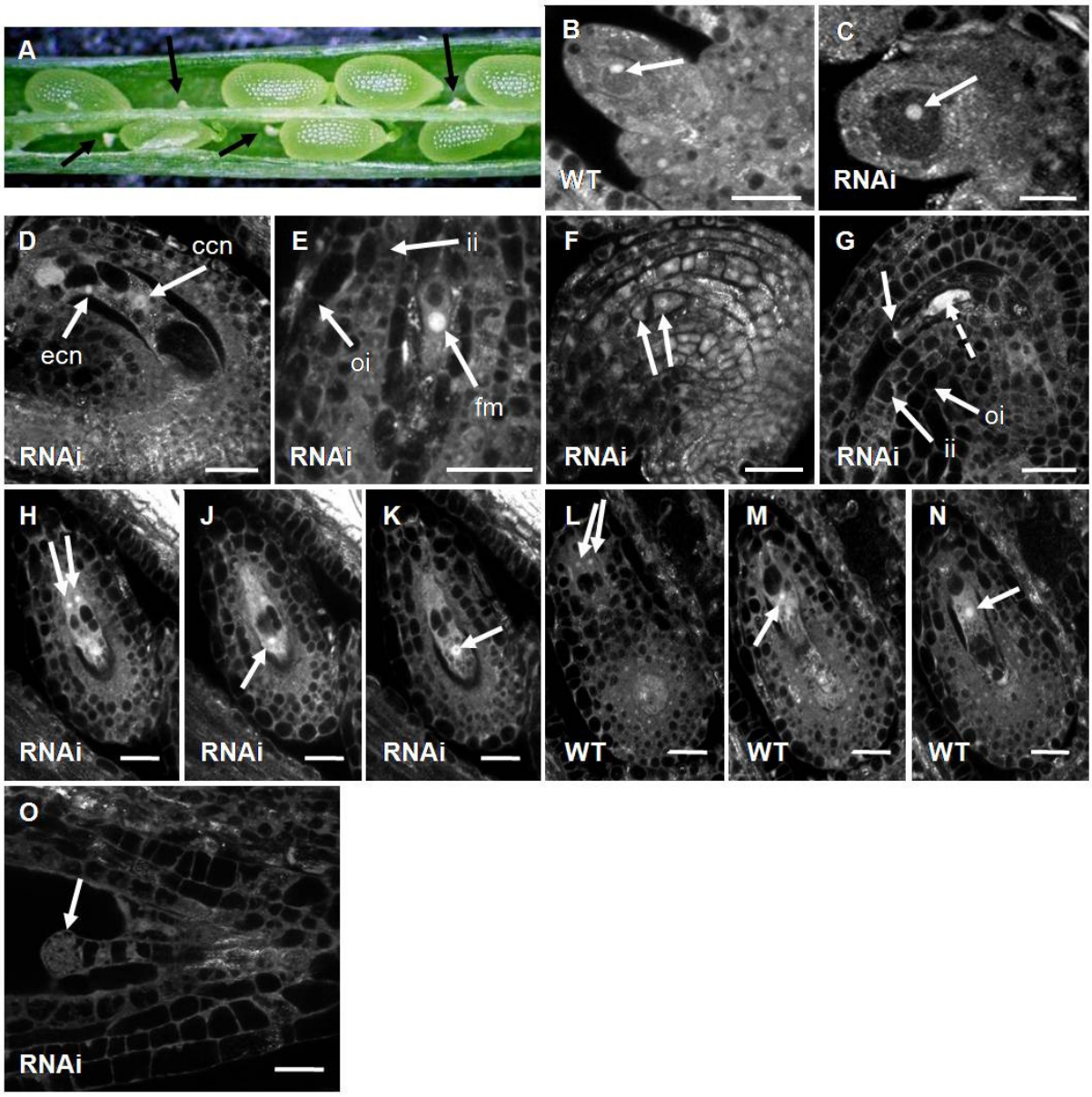

Fig. 3.11. Phenotypic analysis of ovules from progenies of the p7N*EC1p::ARO1*-RNAi lines 2 and 4. (**A**) Opened silique of plant 2-2 showing normally developed seeds and small, white and shriveled ovules arrested during development (arrows). (**B**-**O**) CLSM images of WT and *ARO1*-RNAi ovules at different stages of development (single 0.39 µm optical section, each). Cytoplasm displays weak, nucleoli a high auto-fluorescence after fixation. Vacuoles and cell boundaries do not show fluorescence. (**B**, **C**) WT and *ARO1*-RNAi female gametophytes at developmental stage FG0 before meiosis (stages after Christensen et al., 1997). (**B**) In the developing WT female gametophyte (**B**) as well as in the *ARO1*-RNAi female gametophyte (**C**), the megaspore mother cell (MMC, arrow) is visible at stage FG0. (**D**) Mature, normally developed *ARO1*-RNAi embryo sac at stage FG7. The nuclei of the egg cell (ecn) and central cell (ccn) are visible in this focal plane. (**E**) Arrested embryo sac of an *ARO1*-RNAi ovule corresponding to stage FG7. Development of the embryo sac is arrested at the uninucleate stage (FG1). The functional megaspore is teardrop-shaped and one nucleus is visible (arrow). The mononuclear embryo sac is completely enclosed by the inner (ii) and outer integuments (oi). (**F**) Occasionally, the female gametophyte of ARO1-RNAi ovules arrested at stage FG2. Two nuclei are visible (arrows), separated by a small vacuole. (**G**) At stage FG8 the arrested female gametophytes started to degenerate inside the mature ovule (dashed arrow). Degenerating cells exhibit a strong auto-fluorescence and lack a distinguishable nucleolus. The inner (ii) and

outer integuments (oi) completely enclose the degenerating immature embryo sac and the nucellus cells (arrow). (**H**-**K**) Three optical sections of a normally developed ARO1-RNAi embryosac at stage FG7. (**H**) The nuclei of the two synergids are visible (arrows). Vacuoles are visible at the chalazal end of each synergid. (**J**) The next optical section shows the nucleus of the egg cell (arrow). (**K**) In the third section the large central cell with several vacuoles and the secondary nucleus (arrow) is visible. (**L**-**N**) Three optical sections of a WT female gametophyte. (**L**) The synergid cells are visible, with vacuoles each at the chalazal end and the nuclei (arrows). (**M**) The egg cell nucleus (arrow) and a large vacuole at the micropylar pole can be seen in the second optical section. (**N**) In the last section, the secondary nucleus of the central cell (arrow) is clearly visible. (**O**) Approximately 50% of the *ARO1*-RNAi ovules display normally developed globular embryos (arrow) 2 days after fertilization. Scale bars: (**B**, **C**) 10 µm; (**D**-**O**) 20 µm

3.3.2 Analysis of T-DNA insertion lines

3.3.2.1 Segregation analysis of T-DNA insertion lines

To examine the T-DNA insertion phenotypes of all four genes of the *AtARO* gene family, three T-DNA insertion lines with different insertion sites for *AtARO1* (*aro1-1* to *aro1-3*) and one insertion line for each *AtARO2* (*aro2*), *AtARO3* (*aro3*) and *AtARO4* (*aro4*) were obtained from the SALK institute (Alonso et al., 2003). Plants were analyzed by PCR for their genetic background as described in section 2.7. For all insertion lines, except *aro1-3*, homozygous plants could be identified (Fig. 3.12). In the fourth insertion ordered for *AtARO1* (*aro1-4*), the T-DNA integration was shown to be elsewhere than in the *AtARO1* gene by PCR and was excluded from further work.

Legend for Fig. 3.12. *AtARO1 to -4* T-DNA insertions. Seeds of corresponding plant lines were obtained from the SALK collection. (**A**) Genomic structure of *AtARO1*. The ORF of *AtARO1* is encoded by a single exon, containing six complete and three incomplete ARM repeats (red boxes). The positions of T-DNA integrations in lines *aro1-1*, *aro1-2* and *aro1-3*, determined by sequencing, are indicated by yellow arrowheads. (**B**-**H**) Genotypic analysis of T-DNA insertion lines by PCR. Plants from all lines were tested with two gene specific primers flanking the T-DNA insertion (upper panel) as well as one gene and a T-DNA specific primer (lower panel), respectively. WT plants show a signal with gene specific primers only, while in plants homozygous for the T-DNA insertion (marked by asterisks), a signal is solely detected with a combination of gene specific and T-DNA specific primer. Heterozygous plants show amplification products in both PCR reactions. (**B**) PCR of progenies of line *aro1-1*. Progenies of plants *aro1-1 1*, *aro1-1 4* and *aro1-1 6* are homozygous for the insertion, while five descendants of plant *aro1-1 2* seem to be heterozygous for the T-DNA insertion. (**C**) Segregating progenies of line *aro1-2*. From 9 plants tested, only *aro1-2-8* is homozygous. (**D**) Segregating progenies of line *aro1-3*. No homozygous progeny could be obtained for the allele *aro1-3*. 7 of 16 plants are heterozygous. For plant *aro1-3 7-2-1* no PCR product was obtained in this PCR reaction. (**E**) Segregating progenies of line *aro2*. Three WT, one heterozygous and 11 homozygous plants were identified from 16 analyzed progeny plants of insertion line *aro2*. (**F**) Progenies of line *aro3*. Only homozygous progeny were obtained. (**G**) Segregating progenies of line *aro4*. One homozygous plant (*aro4-4*) could be detected among 16 tested plants.

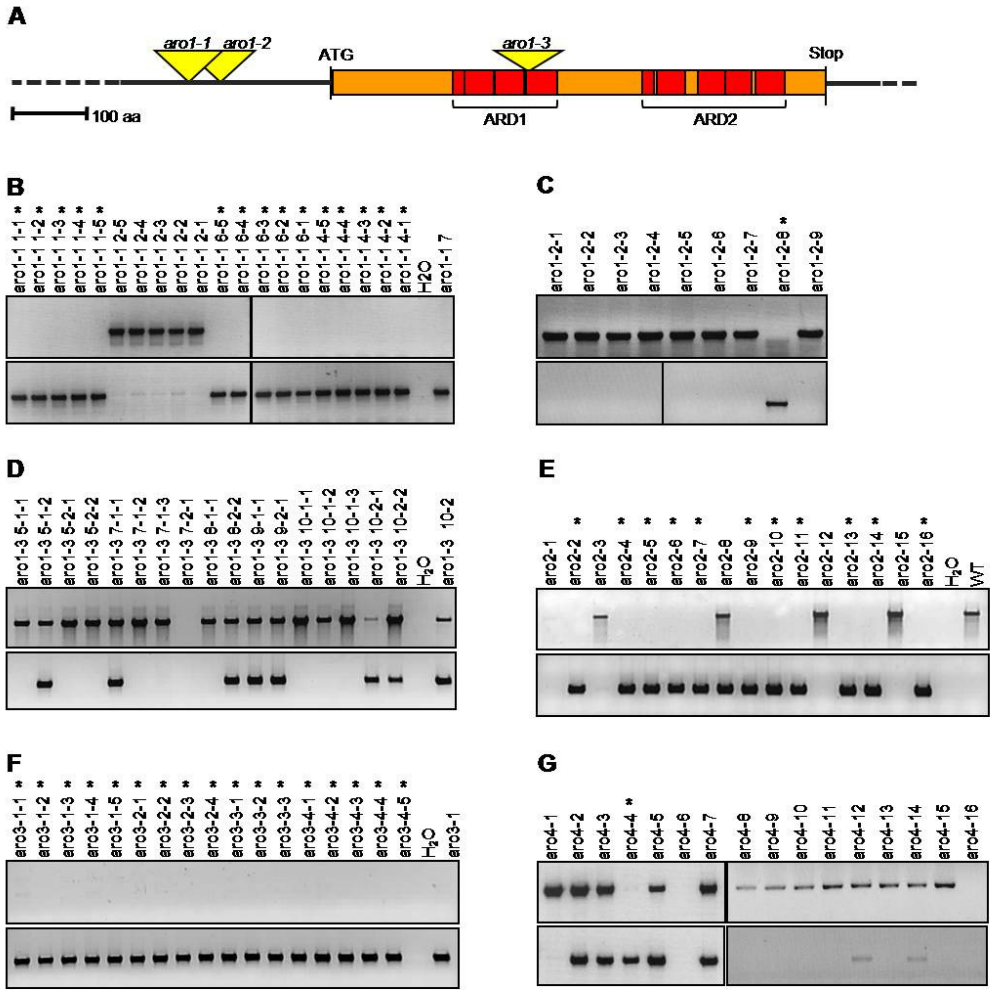

Fig. 3.12 Legend see previous page

The mutant allele *aro1-3* (insertion at +791 bp, corresponding to amino acid position 263) segregated in a ration of 1:1.02 (+/+ : *aro1-3/+*) and no homozygous plant was detected amongst 178 *aro1-3* progenies, indicating a gametophytic effect (Fig. 3.12D). Insertion lines *aro1-1* (insertion -360 bp 5´ upstream of the start codon) and *aro1-2* (insertion -327 bp 5´ upstream of the start codon) in the potential promoter region of *AtARO1* on the other hand, did have homozygous progeny (Fig. 3.12B, C). It is therefore very likely that neither the T-DNA insertion of *aro1-1* nor of *aro1-2* affect the expression of *AtARO1* to an extent that reproduction processes are hampered.

3.3.2.2 Phenotypic analysis of T-DNA insertion lines

Heterozygous plants from line *aro1-3* as well as homozygous individuals from lines *aro1-1*, *aro1-2*, *aro2*, *aro3* and *aro4* were examined for their phenotypes during vegetative and generative development. All lines examined showed normal growth, flower development and seed set, indistinguishable from the WT. In Fig. 3.13, phenotypes of a heterozygous *aro1-3 (aro1-3/+)* plant and homozygous plants of the lines *aro2* and *aro3* are shown in comparison to WT plants. Closer examination of flowers and siliques revealed normal development and full seed set (Fig. 3.13 B-K).

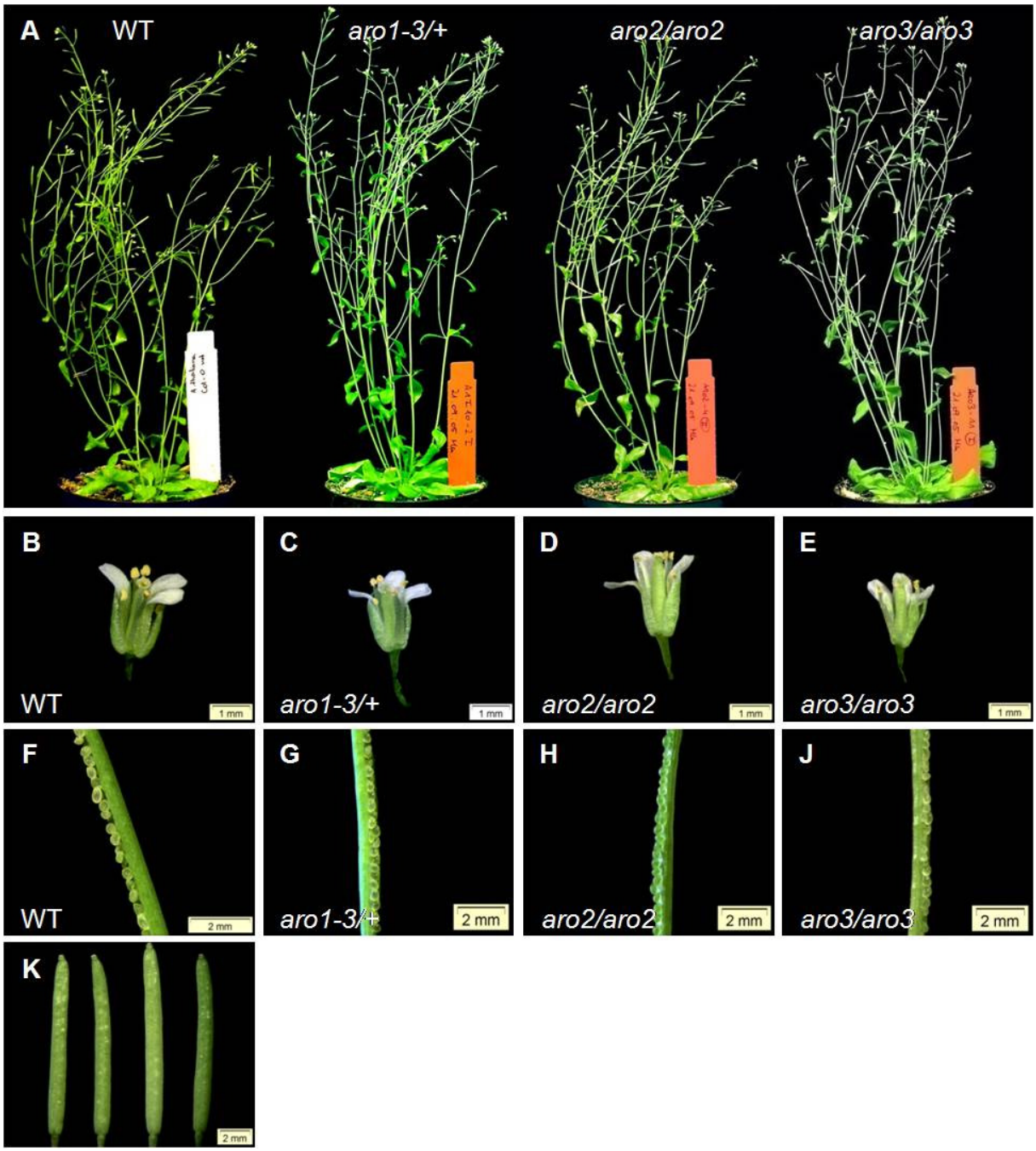

Fig. 3.13. Phenotypic analysis of AtARO1 to -3 T-DNA insertion lines in comparison to WT. The plant of line *aro1-3/+* is heterozygous, while the plants of lines *aro2* and *aro3* are homozygous for the T-DNA insertion. (**A**) All insertion lines grew at same rates and without any obvious changes in overall morphology compared to WT. (**B**-**E**) Phenotypic comparison of flowers from the T-DNA insertion lines and WT. All flowers show the same morphology, similar to WT flowers. (**B**) WT flower. (**C**) Heterozygous *aro1-3/+* flower. (**D**) Flower of homozygous *aro2* plant. (**E**) Flower of homozygous *aro3* plant. (**F**-**K**) Phenotypic analysis of opened siliques from the T-DNA insertion lines and WT. All siliques are normally developed and show full seed set. (**F**) WT silique, showing a full row of developed seeds. (**G**) Silique from a heterozygous *aro1-3/+* line. (**H**) Silique of homozygous *aro2* (**J**) *aro3* silique from a homozygous plant. (**K**) Siliques of WT and T-DNA insertion lines have the same length. From left to right: WT, *aro1-3/+*, *aro2,* and *aro3*.

3.3.2.3 Promoter analysis of AtARO1

As the T-DNA in *aro1-2* is integrated 327 bp upstream of the start codon, all promoter elements important for development- and tissue-specific expression of *AtARO1* are very likely to be located downstream of this insertion site. The 711 bp *AtARO1* promoter region used for promoter-GUS studies was analyzed *in silico* using the plant cis-acting regulatory DNA elements database PLACE (Fig. 3.14). The transcription start point (TSP) of the *AtARO1* mRNA was predicted to be located 162 bp upstream of the start codon. Several general as well as tissue-specific binding sites for transcription factors and enhancer elements were found mainly up to 480 bp upstream of the start codon. 54 bp upstream of the TSP, a TATA-box and a TATA-like motif were found on the (+) and (-) strands of the promoter sequence, respectively. Besides these general promoter motifs, several putative (C)CAAT-boxes and Initiator elements were found before and after the TSP, but none of them was located at typical distances from the transcription start. (C)CAAT-boxes are usually found about 75 bp upstream of the TSP, while Initiator elements are found at -1 to +6 from the TSP. Some elements for transcriptional activators, namely the ARR1-binding element and a CT-rich motif, which can enhance gene expression, were found throughout the length of the putative promoter sequence and 5´UTR. Two promoter elements of late pollen specific genes (GTGA-motif and Pollen1 LAT52-motif) were also present in several copies on the (+) and (-) strands of the AtARO1 promoter and 5´ UTR. Further, three copies of a motif for seed-specific expression were found at 218 to 209 bp upstream of the TSP. Many other binding sites for transcription factors could be identified, like the core site for plant-specific Dof transcription factors (Yanagisawa and Schmidt, 1999) or several Myb transcription factor recognition sites. Additionally, several motifs for stress-induced and light regulated transcriptional activation were found, but for better overview not included in figure 3.14.

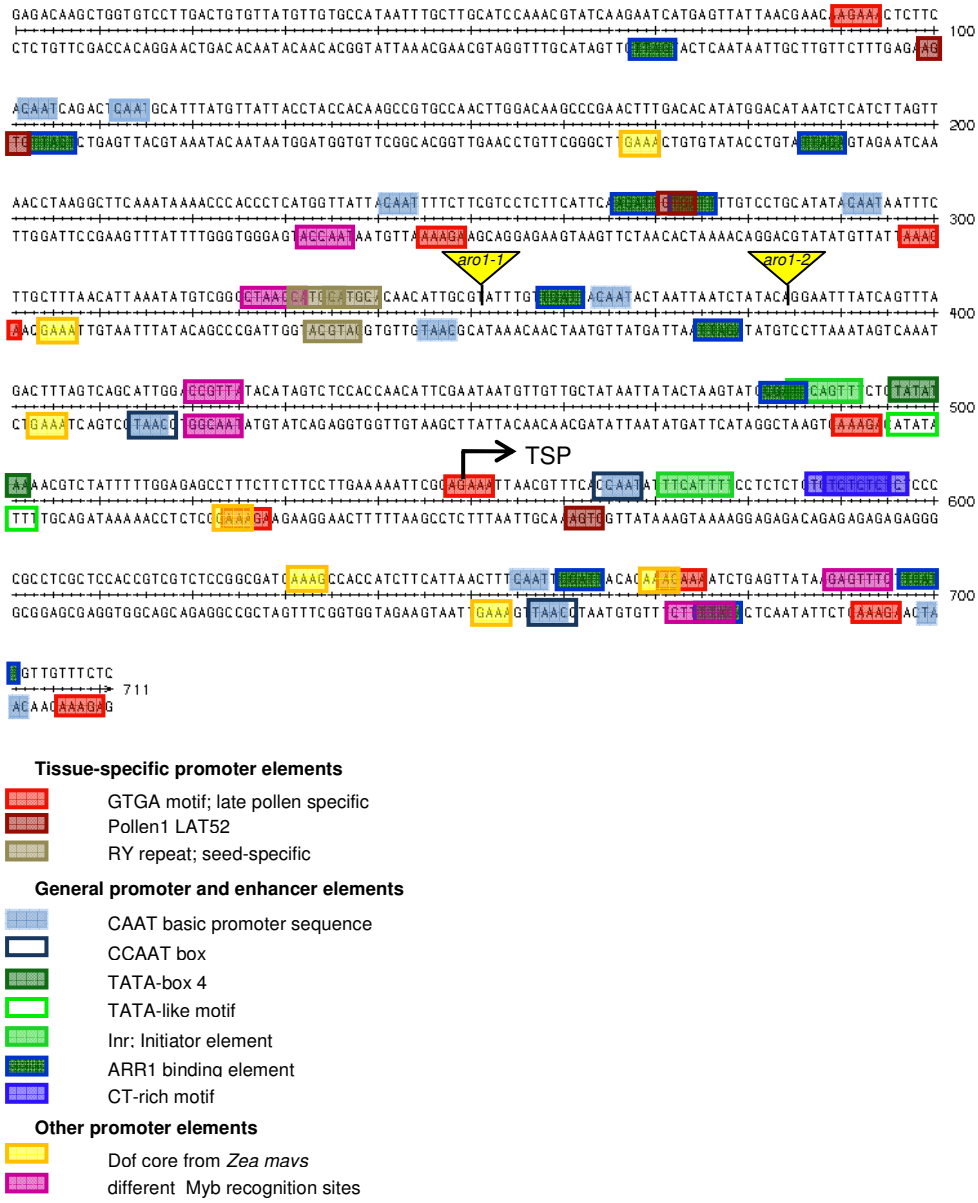

Fig. 3.14. 711 bp promoter fragment and 5´ UTR of *AtARO1* displaying some putative cis-acting elements. Putative cis-acting elements are in colored boxes and each colored box is described beneath. Angled arrow indicates the putative transcription star point (TSP). Yellow arrows indicate the position of the T-DNA insertions of *aro1-1* and *aro1-2*.

3.3.3 Analysis of line *aro1-3/+*

3.3.3.1 Microscopic examination of female and male gametophytes of line *aro1-3/+*

The fact that segregation distortion and reduced seed set give evidence for gametophytic mutations (Drews and Yadegari, 2002), that only heterozygous progenies of the *aro1-3* allele was obtained and the seed set of *aro1-3/+* plants was not altered pointed at a male gametophytic effect in *aro1-3/+* plants. However, mature but unfertilized *aro1-3/+* ovules and ovules 2 days after pollination were

examined under the DIC microscope for phenotypical anomalies. No obvious alterations, compared to WT ovules could be observed (Fig. 3.15A-C). As the other members of the *AtARO* gene family, *AtARO2* to *AtARO4*, are expressed in the egg cell too (see chapter 3.2.1), a complementation of AtARO1 in the female gametophyte is feasible. Closer inspection of the morphology of *aro1-3/+* male gametophytes after DAPI staining did not reveal any alterations compared to WT (Fig. 3.15D, E). Further, pollen vitality was analyzed by staining mature pollen grains with PI and fluoresceindiacetate. Only living cells can hydrolyse fluoresceindiacetate and therefore only those show green fluorescence under UV-light. PI in turn can only stain the cytoplasm of dead pollen grains. The pollen viability for WT pollen was 84% (n=461), compared to 82% (n=501) for *aro1-3/+* pollen, thus no significant difference was observed. Consequently, female as well as male gametophytes of insertion mutant *aro1-3/+* are able to develop to maturity without any obvious alterations.

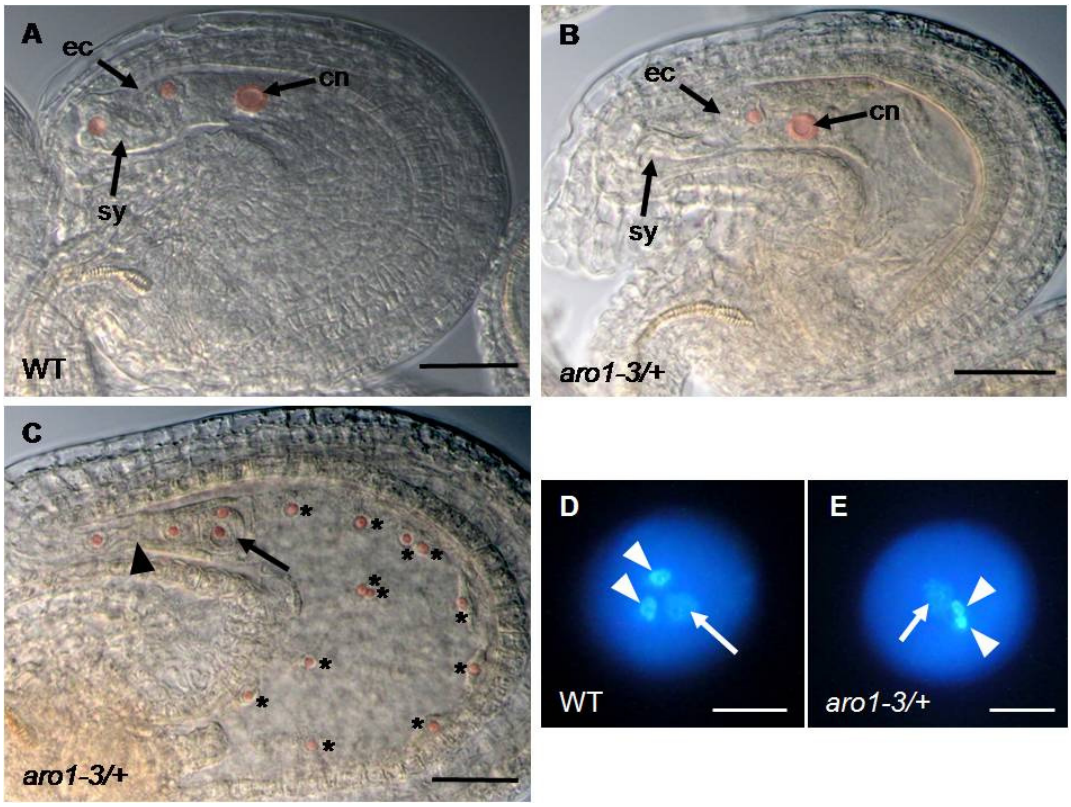

Fig. 3.15. Microscopic examination of WT and *aro1-3/+* mature female and male gametophytes using DIC (**A**-**C**) and epifluorescence (**D** and **E**). Nuclei of female gametophytes are false coloured in red, for better contrast. (**A**) Mature, unfertilized whole-mount WT ovule, after clearing in Hoyers solution. One synergid (sy), the egg cell (ec) and the central cell with the secondary nucleus (cn) are visible. (**B**) Mature, cleared whole-mount *aro1-3/+* ovule from an emasculated flower. The nucleus of the synergid (sy) is not in focus. Egg cell (ec) and central cell nucleus (cn) are indicated. (**C**) Cleared *aro1-3/+* ovule, 2 days after fertilization. Syncytical endosperm nuclei are dispersed throughout the embryo sac (asterisks). A 2-celled embryo proper (arrow) and 2-celled suspensor (arrowhead) are visible. Embryonic and endosperm development is not altered, compared to the WT (not shown). (**D**) WT pollen grain stained with DAPI. The two densely packed sperm cell nuclei (arrowheads) show a strong fluorescent DNA signal, while the vegetative nucleus (arrow) is stained diffusely. (**E**) DAPI stained *aro1-3/+* pollen grain. Vegetative (arrowheads) and generative (arrow) nuclei show similar staining intensities, compared to WT pollen. Scale bars: (**A**, **B**) 20 µm; (**C**) 50 µm; (**D**, **E**) 10 µm

3.3.3.2 Transmission efficiency of the *aro1-3* allele

The transmission efficiency (TE) of the *aro1-3* allele through the female and male gametophytes was determined by reciprocal crosses of *aro1-3/+* lines with WT (+/+) plants. Table 3.1 undoubtedly shows that *aro1-3* can only be transmitted via the female gametophyte, as pollinating WT plants with pollen from heterozygous *aro1-3/+* plants only yielded WT progeny (0% TE for *aro1-3/+* through the male gametes), while fertilization of *aro1-3/+* with WT pollen or selfing of *aro1-3/+* plants gave rise to almost equal numbers of +/+ and *aro1-3/+* plants (TE 50.7% and 45.16% through male gametes respectively). However, the TE in selfed *aro1-3/+* plants is slightly below the TE of those fertilized with WT pollen. Hence, evidence for a functional role of *AtARO1* in either pollen germination or post-pollination events was given.

Table 3.1. Gametophytic transmission efficiency of the *aro1-3* allele

	Progeny		
Crosses[a] (♀ x ♂)	*aro1-3/+*	+/+	TE (%)
+/+ x *aro1-3/+*	0	38	♂ 0 (n=38)
aro1-3/+ x +/+	36	35	♀ 50.70 (n=71)
aro1-3/+ x *aro1-3*	42	51	45.16 (n=93)

[a] Reciprocal crosses of WT (+/+) and heterozygous *aro1-3/+* plants were carried out by hand-pollination of emasculated WT pistils with *aro1-3/+* pollen, and *vice versa*. As control, *aro1-3/+* plants were pollinated with self-pollen. Progenies were analyzed for T-DNA integration. Values represent absolute numbers of *aro1-3/+* and WT progeny plants as well as the transmission efficiency (TE) of the *aro1-3* mutant allele through the male and female gametophytes. Numbers between parentheses indicate total number of analyzed plants (n). TE of the *aro1-3* mutant allele in self-pollinated *aro1-3/+* plants is slightly below the TE in *aro1-3/+* plants pollinated with WT pollen.

3.3.3.3 *In vitro* pollen germination

Pollen from freshly dehiscent WT and *aro1-3/+* anthers was germinated *in vitro* to study the growth rate and morphology of pollen tubes. An interesting phenotype could be observed (Fig. 3.16B). In pollen germination cultures, 28% of the heterozygous pollen tubes were considerably broader and shorter than both, pollen tubes with normal morphology (51.6%) and control WT pollen tubes. A high number of *aro1-3/+* pollen grains (20.4%) burst immediately after germination (Table 3.2). Large vacuoles were found throughout the morphologically aberrant pollen tubes and grains. Widths of these pollen tubes ranged from 15 µm to 35 µm with an average of ~ 23 µm, compared to 5-7 µm in WT pollen tubes. These short and plump pollen tubes are referred to hereafter as "*aro1-3* pollen tubes".
Pollen germination rates (Table 3.3) and pollen morphology (not shown) were also tested for lines *aro1-2*, *aro2*, *aro3* and *aro4*, but no significant differences to WT pollen were observed.

Table 3.2. Pollen tube phenotypes of wild type (+/+) and *aro1-3/+* pollen, observed 5 hours after *in vitro* germination.

Phenotype[a]	normal	short&plump	burst pollen
aro1-3/+ pollen	51.6% (n=1608)	28.0% (n=874)	20.4% (n=634)
+/+ pollen	98.8% (n=3956)	0.01% (n=3)	1.1% (n=44)

[a]Pollen of WT and heterozygous *aro1-3/+* plants were germinated on the two halves of the same petri dish. 5 hours after germination, phenotypes of germinated pollen were scored.

Table 3.3. Germination rates of T-DNA insertion lines *aro1-2*, *aro2*, *aro3* and *aro4* in comparison to WT.

Line	germinated pollen	non-germinated pollen	germination rate[a]
aro1-2	1051	423	71%
aro2	929	278	77%
aro3	1079	317	77%
aro4	1180	368	76%
WT	991	332	75%

[a] Pollen of WT and T-DNA insertion lines were germinated *in vitro* on the two halves of the same petri dish, each. 5 hours after germination, visible pollen tubes were scored. Germination rates of WT pollen tubes were reproducible in all replicates and thus numbers for only one replicate are given.

Tube lengths of *aro1-3* pollen tubes and WT controls were measured 3, 6 and 28 hours after *in vitro* germination. Most of the *aro1-3* pollen tubes did not grow beyond an average length of 21.96 µm, ranging from 7.8 µm to 50.57 µm (Table 3.4) at 28 hours of germination. In contrast, WT pollen tubes showed variations in tube length from 14 µm to 287.94 µm, with a mean value of 101.48 µm. These high variations in growth rates of *in vitro* germinated *Arabidopsis* pollen tubes have been described before (Taylor and Hepler, 1997; Boavida and McCormick, 2007). However, comparing the average numbers of WT and *aro1-3* pollen tube lengths, the severe growth retardation of *aro1-3* pollen tubes is obvious (Table 3.4).

Table 3.4. Average length of wild type (+/+) and *aro1-3/+* pollen tubes measured after 3, 6 and 28 hours of *in vitro* germination.

	Tube length[a] (µm)		
Pollen	3 hag	6 hag	28 hag
+/+ pollen	37.52 ± 21.43	85.65 ± 44.45	101.48 ± 46.09
aro1-3/+ pollen; normal phenotype	34.09 ± 21.95	89.30 ± 38.29	102.80 ± 43.53
aro1-3/+ pollen; short and plump phenotype	16.90 ± 9.15	19.39 ± 10.14	21.96 ± 10.47

[a]Pollen of WT and heterozygous *aro1-3/+* plants were germinated on the two halves of the same petri dish, each. After indicated incubation time, germinated pollen were captured and measured with the Zeiss AxioVision software, release 4.6.

In vivo pollination experiments with limited amounts of pollen showed that *aro1-3* pollen tubes could not enter the cell wall of stigmatic cells. The short and plump pollen tubes were found to adhere to the papillae, hydrate and germinate normally but failed to grow into the cell walls of papillae and further into the style and often formed small protuberances around the stigmatic cells (Fig.3.16H). The aberrant pollen tubes were never found to grow through the female transmitting tissues towards the ovules (Fig. 3.16D, F). Thus, only *aro1-3/+* pollen with WT genetic background is able to fertilize the female gametophytes.

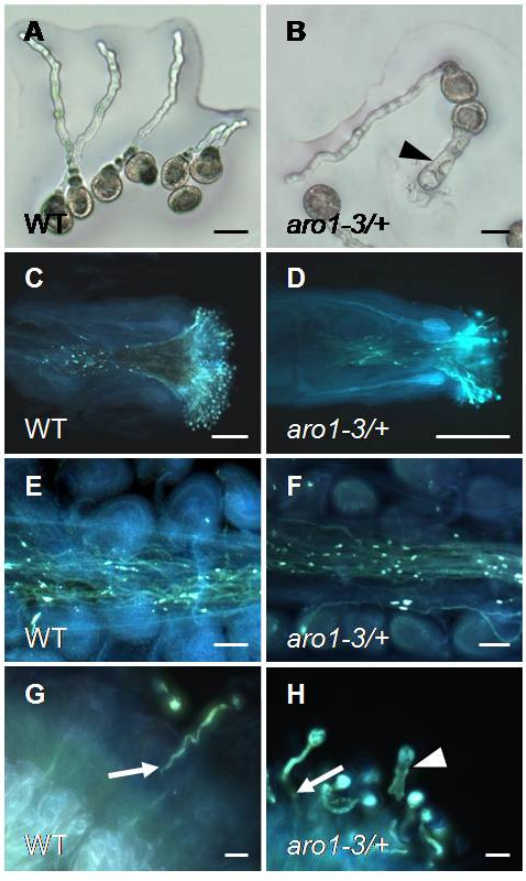

Fig. 3.16. *aro1-3/+* T-DNA insertion line shows defective pollen tube growth. Phenotypes of heterozygous *aro1-3/+* knock out plants (**B**, **D, F, H**) in comparison to WT (**A**, **C, E, G**). (**A**, **B**) *In vitro* germinated pollen tubes. WT pollen tubes show normal germination and pollen tube growth (**A**), while approximately 50% of the pollen of *aro1-3/+* plants either burst immediately after germination or exhibited a short and swollen phenotype (**B**; arrowhead). (**C**-**H**) Aniline blue staining of growing pollen tubes in *Arabidopsis* pistils, 24 hours after hand-pollination with self pollen. (**C**, **D**) Pollen tubes of *aro1-3/+* (**D**) appear to grow through the pistil comparable to WT pollen tubes (**C**). (**E**, **F**) Close up of the transmitting tract. (**E**) WT pollen tubes in transmitting tract. (**F**) Obviously, only *aro1-3/+* pollen tubes with wild type morphology can enter the female tissues. (**G**, **H**) *aro1-3* pollen tubes fail to penetrate stigmatic cells. WT pollen tubes grow into the stigmatic cells and throughout the style (arrows in **G, H**), while short, plump *aro1-3* pollen tubes remain on the surface of the stigmatic cells (arrowhead, **H**). Scale bars: (**A**, **B, G, H**) 20 µm; (**E**, **F**) 50 µm; (**C**, **D**) 200 µm.

3.3.3.4 Staining of the actin cytoskeleton of *aro1-3/+* pollen tubes

As the actin cytoskeleton is known to be essential for pollen tube growth (Ren and Xiang, 2007), actin staining experiments of *in vitro* germinated WT and mutant *aro1-3/+* pollen tubes were performed. WT and *aro1-3/+* pollen tubes were fixed and incubated with rhodamine-phalloidin for observations under a confocal laser scanning microscope (CLSM). In germinated WT pollen, actin filaments oriented towards the germination pore, and strong, parallel actin bundles are arranged longitudinally to the axis of the outgrowing pollen tube (Fig. 3.17A, B, C). In the tube tip of WT pollen tubes, diffuse actin staining or thicker actin bundles invading the tip were observed. Contrary to WT, *aro1-3* pollen showed a sever disorganization and fragmentation of the actin cytoskeleton over the whole length of the pollen grain and pollen tube (Fig. 3.17D, E, F). Short and thick actin fragments were found at random orientations in the pollen grain and tube (Fig. 3.17D). Most of the very short *aro1-3* pollen tubes revealed an unsystematic network of disordered actin filaments (Fig. 3.17E) that was found to be strongly intertwining in the few cases when *aro1-3* pollen tubes grew over longer distances (Fig. 3.17F).

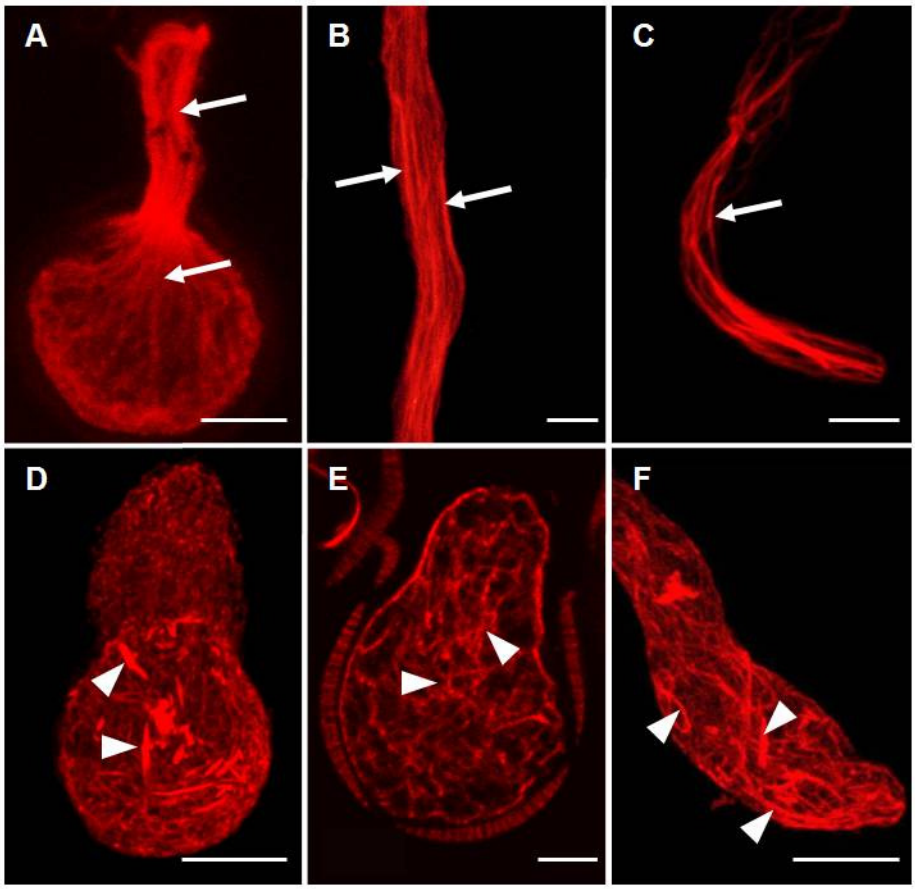

Fig. 3.17. Actin cytoskeleton of *in vitro* germinated WT and *aro1-3* pollen, stained with rhodamine-phalloidin. (**A-C**) WT pollen grains and pollen tubes display thick actin bundles with a highly organized orientation, parallel to the growth axis (arrows). (**D-F**) Parallel organization and polar orientation of actin bundles is disturbed in germinating *aro1-3* pollen. Rather unorganized short actin bundles (**D**) or networks (**E**, **F**) were observed inside germinating pollen grains and pollen tubes (arrowheads). Scale bars: (**A**, **D, F**) 10µm, (**B**, **C, E**) 5µm

3.3.3.5 Functional complementation of *aro1-3/+* plants

To prove the causal correlation of the *aro1-3* allele and the observed pollen tube phenotype and demonstrate the functionality of an *AtARO1p::AtARO1-GFP* fusion construct *in vivo*, *aro1-3/+* plants were crossed with homozygous *AtARO1p::AtARO1-GFP* plants (Fig. 3.18A) to achieve complementation of the mutant allele. Amongst progenies, the *aro1-3* allele containing plants were selected for *in vitro* pollen germination tests via PCR. In the F_1 generation, approximately half of the pollen tubes should contain a copy of the *AtARO1-GFP* fusion (Fig. 3.18A: 50% with AtARO1-GFP). Given the fact that the AtARO1-GFP fusion protein could not complement the function of the mutant allele, half of these fluorescently labelled pollen tubes (Fig. 3.18A: 25% of total) should exhibit a short and plump phenotype, similar to pollen tubes without AtARO1-GFP (Fig. 3.18C, Table 3.6). The numbers of fluorescently labelled WT pollen stayed with 40% underneath the theoretically expected number of 50%, while progeny of *aro1-3/+* x AtARO1-GFP crossings showed 54% of fluorescent pollen. However, all *in vitro* germinated fluorescent pollen tubes looked phenotypically normal (Fig.

3.18B, Table 3.6 and Fig. 3.19). Only little pollen (2%) burst shortly after germination and in the WT control 4 pollen tubes (3%) grew broader pollen tubes of approximately 15 to 20 µm diameter compared to the normal diameter of ~5 to 7µm. These few escapes might be due to stress during germination *in vitro*. On the other hand, 46% of *aro1-3/+* x AtARO1-GFP progeny showed no fluorescence. Little less than half of these pollen tubes displayed the *aro1-3* phenotype (18%; Fig. 3.18C, Table 3.6 and Fig. 3.19). In the WT control, a higher number of pollen tubes burst shortly after germination and showed no GFP fluorescence (10%), while 50% of the germinated control pollen tubes showed no fluorescent signal. Although the percentages of observed phenotypes did not exactly match the expected theoretical segregation, the overall result demonstrates that AtARO1-GFP can complement the *aro1-3* phenotype and thus is functional *in vivo*.

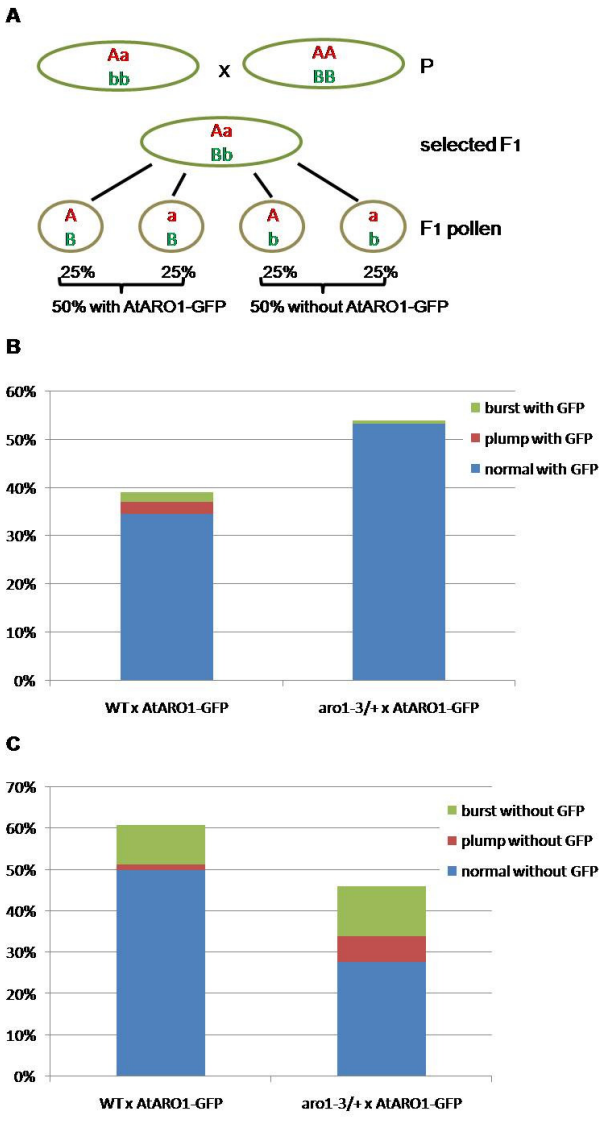

Fig. 3.18. Complementation of the *aro1-3* phenotype with the AtARO1-GFP fusion protein. (**A**) Scheme of the transmission of the *aro1-3* and the *AtARO1-GFP* allele. Heterozygous *aro1-3/+* plants (Aa bb) were crossed with homozygous AtARO1-GFP plants (aa BB), where A/a represents the *aro1-3* alleles and B/b represents the AtARO1-GFP alleles. Progenies containing the *aro1-3* allele were selected for *in vitro* pollen germination tests (F_1; Aa Bb). Possible genotypic combinations in pollen are *ARO1-3* without AtARO1-GFP (A b), *aro1-3* without

AtARO1-GFP (a b), *ARO1-3* with AtARO1-GFP (A B) and *aro1-3* with AtARO1-GFP (a B) should be represented by 25% of total pollen. (**B**) Percentages of pollen (tube) phenotypes displaying GFP fluorescence. With few exceptions, all WT and *aro1-3/+* pollen tubes showed normal morphology. (**C**) Percentages of pollen (tube) phenotypes which did not show GFP fluorescence. All WT pollen tubes, apart from some exceptions (1%), show a normal growth phenotype. 10% of WT pollen tubes burst shortly after germination. *aro1-3/+* pollen tubes in contrast, show a normal growth phenotype in 28% and typical *aro1-3* phenotypes (either burst shortly after germination or short and plump) in 18% of total pollen tubes examined.

Table 3.6. Absolute numbers of pollen tube phenotypes scored from segregating pollen of F_1 progeny, after crossing WT (control) and *aro1-3/+* with AtARO1-GFP plants, respectively.

	WT x AtARO1-GFP	*aro1-3/+* x AtARO1-GFP
Burst without GFP	15	53
Plump without GFP	2	28
Normal without GFP	78	123
Burst with GFP	3	3
Plump with GFP	4	0
Normal with GFP	54	237
Total numbers	156	444

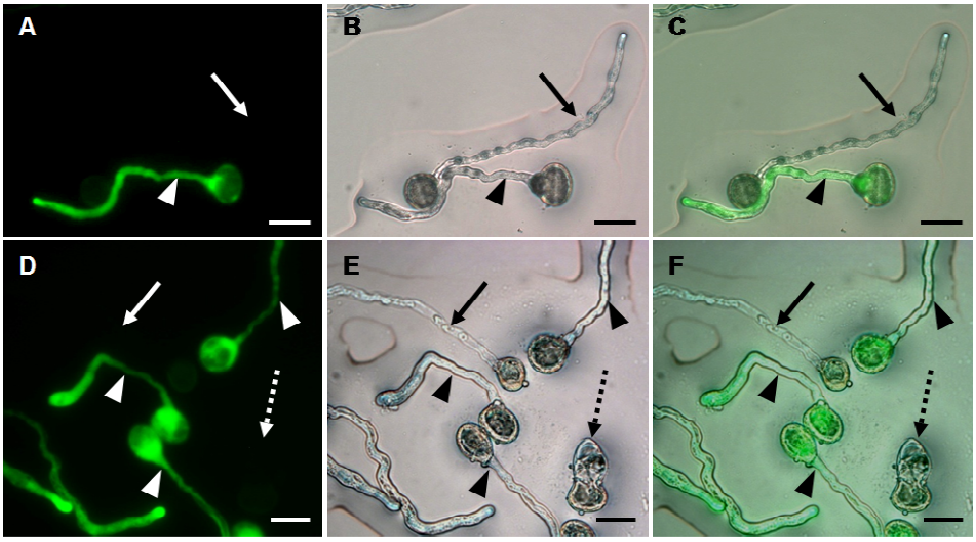

Fig. 3.19. Complementation of the *aro1-3* phenotype by expression of the AtARO1-GFP fusion protein. (**A**-**C**) In pollen from WT x AtARO1-GFP F_1 plants, approximately 40% of the pollen shows fluorescence (arrowhead), while in 60%, the fusion protein is absent (arrow). All pollen tubes showed normal morphology. (**D**-**F**) Pollen of F_1 progeny from *aro1-3/+* x AtARO1-GFP. All pollen tubes fluorescently labelled with AtARO1-GFP exhibit normal pollen tube growth (arrowheads), while pollen tubes without fluorescence show normal (arrow) as well as aberrant (dashed arrow) growth phenotypes. (**A**, **D**) GFP channel. (**B**, **E**) Bright field picture. (**C**, **F**) Merged image. Scale bars: 20 µm

3.3.4 Overexpression of AtARO1

AtARO1 was misexpressed in whole plants as an AtARO1-GFP (green fluorescent protein) fusion protein under the control of the 35S promoter. In total, 12 independent lines carrying the 35Sp::AtARO1-GFP construct were generated. The strength of expression of *AtARO1-GFP* was examined under the epifluorescent microscope using petals from freshly opened flowers. Three out of the 12 lines (lines 1, 6 and 17) showed a strong fluorescence, two lines (lines 2 and 7) showed an intermediate fluorescence and three lines (lines 5, 11 and 20) a weak fluorescence. In 4 lines (lines 12, 13, 14 and 21), although expressing the *AtARO1-GFP* fusion, no fluorescence could be detected that would be significantly different from background auto-fluorescence of the plant tissues tested. Analysis of homozygous F_2 plants from lines showing strong or intermediate fluorescence did not reveal any obvious changes in vegetative tissue morphology of *Arabidopsis* transgenes. Further, the plants showed normal development of generative tissues and full seed set (not shown). The fusion protein seems to accumulate strongly in the membranes and nuclei of most vegetative cells but is also weakly detected in the cytoplasm (Fig. 3.20A, B). According to the fact, that the *35S* promoter is not active in pollen (Wilkinson et al., 1997) or young embryos (Sunilkumar et al., 2002), the AtARO1-GFP fusion protein was not detected in these tissues (Fig. 3.20F-H). Surprisingly, AtARO1-GFP fluorescence was neither found in most cells of roots from plants at principle growth stage 6 (stages after Boyes et al., 2001). Only a weak staining in the columella cells of the root tip could be observed (Fig. 3.20C-E), although the 35S promoter was shown to be active throughout the surface of roots and in root hairs in cotton (Sunilkumar et al., 2002).

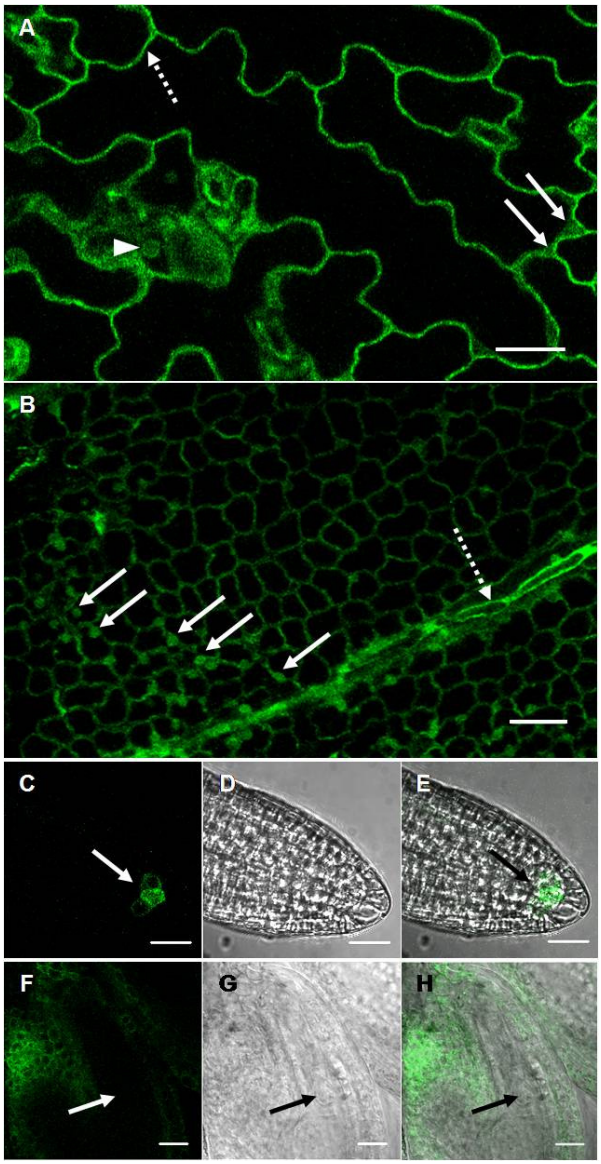

Fig. 3.20. Overexpression of an AtARO1-GFP fusion protein. *AtARO1* was fused to *GFP* and expressed under the control of the *35S* promoter (95P-Nos*35Sp::AtARO1-GFP*). Homozygous progeny plants (plants 2-1 and 6-3) were analyzed for morphological anomalies and subcellular distribution of the fusion protein. In all tissues examined, no morphological differences to WT tissues could be observed. (**A**) Epidermal cells of a rosette leave from a mature *35Sp::AtARO1-GFP* plant. AtARO1-GFP accumulates at the membranes (dashed arrow) and in the nuclei (arrowhead). In addition, it is detectable to a lesser extent in the cytoplasm (arrows). (**B**) Epidermal cells of a petal. The fluorescent signal can be found at the membrane as well as in the nuclei (arrows). In companion cells of the vascular bundles, expression of the fusion protein was found to be increased (dashed arrow). (**C**-**E**) Root tip of a young plant expressing AtARO1-GFP. (**C**) The fusion protein is only detectable in the columella cells (arrow). (**D**) Bright field picture of (**C**). (**E**) Merged picture of (**C**) and (**D**). (**F**-**H**) AtARO1-GFP ovule with a two-celled embryo (arrows). The embryo and suspensor, visible in the bright field picture (**G**) and in the merged image (**H**) do not show any GFP fluorescence (**F**), as the 35S promoter is inactive at this stage. The cells of the ovule in turn exhibit diffuse GFP-signals of the membrane, cytoplasm and nuclei. Scale bars: 20 µm

3.4. Subcellular localization of AtARO1/2-GFP fusions proteins

AtARO1 was predicted to have a putative transmembrane domain (TM) by 7 of 15 prediction programs from the Aramemnon database, while AtARO2, its closest relative, seems not to have a TM (only 1 of 15 programs predicted a TM at Aramemnon). However, bioinformatic prediction programs do not necessarily reflect the real *in vivo* situation and transmembrane regions of proteins are predicted based on different methods with more or less reliability. Bioinformatic analysis of proteins with prediction programs can therefore only be a first hint on how proteins might be distributed in a cell. To determine the subcellular localization of AtARO1 and AtARO2 *in vivo*, transient and stable transformation assays of the full-length proteins fused to the N-terminus of the reporter GFP were conducted.

3.4.1 Transient transformation of epidermal onion cells with AtARO1/2-GFP

For transient transformation assays in spring onion epidermal cells, the AtARO1-GFP and AtARO2-GFP fusions were expressed under the control of the maize *Ubiquitin* promoter. Interestingly, the subcellular localisation of AtARO1-GFP appeared to alternate. Most analyzed cells (73%) showed a dual localization in the cytoplasm and nucleus, although AtARO1 does not contain a classical nuclear localization signal (NLS; Fig. 3.21A, B and Table 3.5). Due to the high molecular weight of the AtARO1-GFP fusion protein (101.74 kDa), a passive diffusion into the nucleus is impossible. In 10% of the cells, nuclear localization could not be detected (Fig. 3.21C, D; Table 3.5) and the fusion protein was located exclusively in the cytoplasm. In the remaining 17% of analyzed cells AtARO1 was localized exclusively at the membrane (Fig. 3.21E, F; Table 3.5). Interestingly, these variations were neither observed in AtARO1-GFP overexpressing *Arabidopsis* plants (section 3.3.4) nor in epidermis cells transiently transformed with AtARO2-GFP. Here, the protein was detected in the cytoplasm as well as the nucleus in 100% of all analyzed cells (Fig. 3.21G, H; Table 3.5). AtARO2 neither has a NLS and the M_r of AtARO2-GFP is 99.59 kDa, which again exceeds the passive diffusion limit into the nucleus, which is around ~ 50 kDa (Macara, 2001). These results indicate that AtARO1 and AtARO2 are transported through the nuclear pore complex in an NLS-independent manner. Control GFP alone in turn is small enough (~27 kDa) to enter the nucleus by diffusion and was detected there as well as in the cytoplasm (Fig. 3.21J, K; Table 3.5).

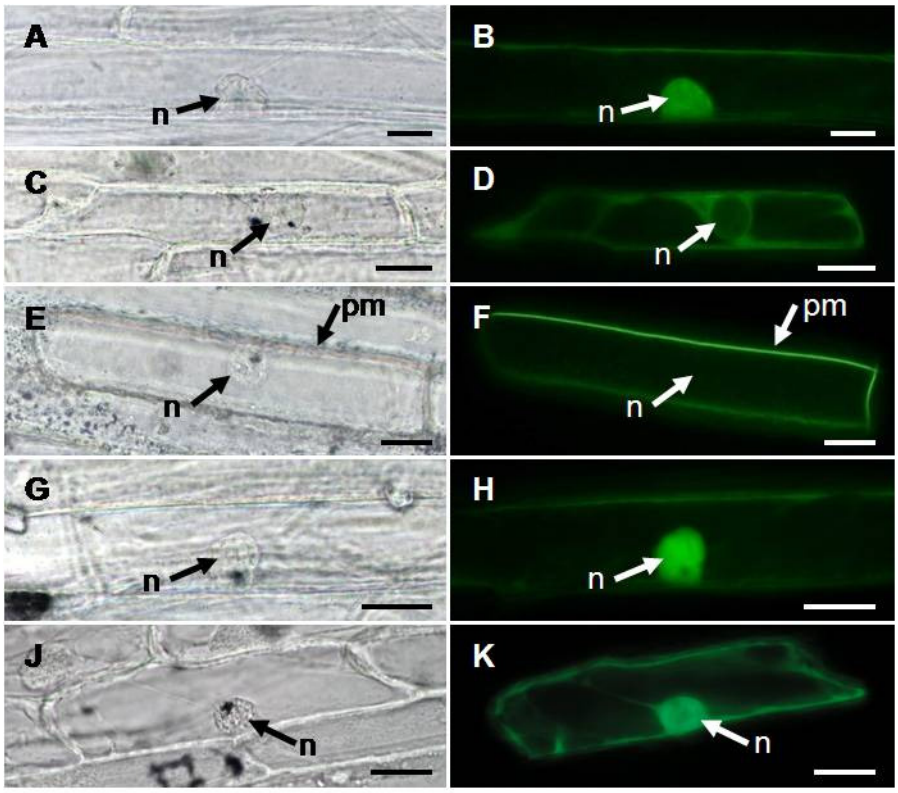

Fig. 3.21. Bright field and epifluorescent pictures of epidermal spring onion cells transiently transformed with AtARO1-GFP (**A**-**F**) and AtARO2-GFP (**G**, **H**) fusion proteins under control of the maize *UBI* promoter. *UBIp::GFP* was used as a control (**J**, **K**). (**A**, **B**) In 73% of all analyzed cells (see Table 3.5), the AtARO1-GFP signal was detected in the cytoplasm and the nucleus, although AtARO1 lacks a classical nuclear localization sequence. (**C**, **D**) In 10% of the cells, AtARO1-GFP was found in the cytoplasm but excluded the nucleus. (**E**, **F**) In 17% of all analyzed cells the AtARO1-GFP fusion protein was seen exclusively at the plasma membrane. (**G**, **H**) AtARO2-GFP was always found in both, cytoplasm and nucleus. (**J**, **K**) In cells expressing GFP only, fluorescence was always detected in the cytoplasm and in the nucleus. (n) nucleus, (pm) plasma membrane. Scale bars: 40 µm

Table 3.5. Subcellular localization of AtARO1- and AtARO2-GFP fusion proteins in transiently transformed spring onion epidermal cells

	Observed subcellular GFP fluorescence[a]		
Construct	Nucleus & cytoplasm	Cytoplasm	Plasmamembrane
UBIp::AtARO1-GFP	73% (n=450)	10% (n=65)	17% (n=107)
UBIp::AtARO2-GFP	100% (n=260)	0%	0%
UBIp::GFP	100% (n=34)	0%	0%

[a]Spring onion epidermal cells were transiently transformed with the plasmids *UBIp::AtARO1-GFP*, *UBIp::AtARO2-GFP* and *UBIp::GFP* using biolistic bombardment. 24 hours after transformation, expressing cells were scored for their subcellular localization of GFP fluorescence. Observed subcellular localizations are expressed as percentage. Numbers between parentheses indicate absolute numbers of analyzed cells.

3.4.2 Stable transformation of *Arabidopsis thaliana* with AtARO1-GFP

Stably transformed *Arabidopsis* lines expressing the AtARO1-GFP fusion driven by the endogenous *AtARO1* promoter were generated in order to examine the time-frame of expression and the subcellular distribution of AtARO1-GFP.

Evidence was given that AtARO1-GFP is functional *in planta* (Chapter 3.3.3.5). Therefore, female and male gametophytes of homozygous *AtARO1p::AtARO1-GFP* plants were analyzed for subcellular localization of the fusion protein under a CLSM. Ovules from emasculated *Arabidopsis* flowers showed fluorescent signals in the mature egg cell only, consistent with observations made in promoter-GUS constructs (compare Fig. 3.22B and D with Fig. 3.7D). Co-staining with Draq5 demonstrated that the GFP fusion protein is present in the cytoplasm of the egg cell but absent from the nucleus (Fig. 3.22A-C). Fig. 3.22D shows a close-up of a stack of CLSM optical sections from a mature unfertilized egg cell, demonstrating that AtARO1-GFP is evenly distributed throughout the cytoplasm but is excluded from the large vacuole (arrow). After self-fertilization, the expression of AtARO1-GFP is quickly switched off, as no fluorescence is detectable after the first zygotic division in the female gametophyte (Fig. 3.22E, F). Only remnants of GFP fluorescence are visible in the pollen tube entering the micropyle (Fig. 3.22F, arrowhead).

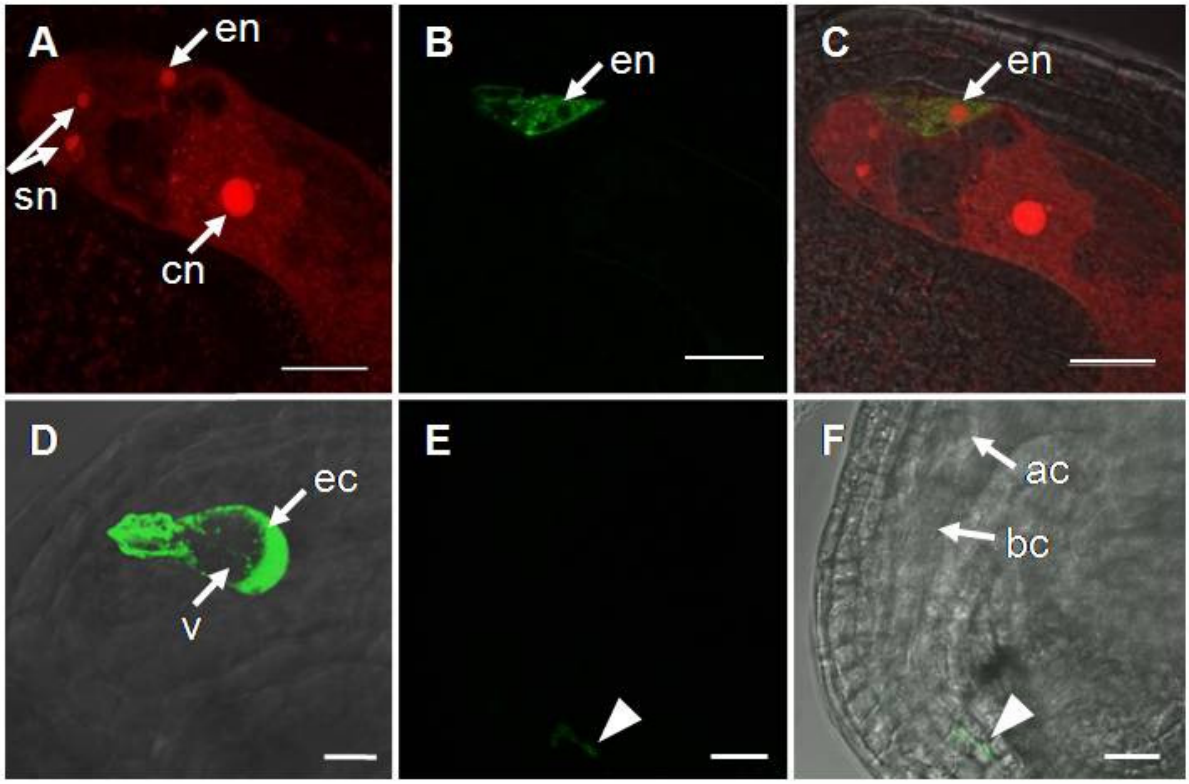

Fig. 3.22. Localization of the ARO1-GFP fusion protein in homozygous transgenic *AtARO1p::AtARO1-GFP* lines. CLSM images of female gametophytes. (**A**-**C**) AtARO1-GFP is localized in the egg cell of the mature embryo sac but is excluded from the egg cell nucleus (en; arrow). (**A**) Draq5 staining of the synergid nuclei (sn), the egg cell nucleus (en) and the central cell nucleus (cn) (stack of 30 optical sections, 0.34 µm each; 9.74 µm). (**B**) GFP signal of the fusion protein in the egg cell (single optical section). (**C**) Merged picture of (**A**), (**B**) and bright field.

(**D**) Close up view of a mature egg cell (ec) (3D projection of 75 0.36 µm sections; 26.95µm). The AtARO1-GFP fusion protein appears to be distributed throughout the cytoplasm but is excluded from the large vacuole (v). (**E**, **F**) Ovule, 24hap. After the first zygotic division, AtARO1-GFP is no longer detectable. Only a very weak fluorescence of the pollen tube can be seen in the micropylar region (**E**, arrowhead). (**F**) represents a merge of the bright field and GFP channel of (**E**). ac, apical cell; bc, basal cell. Scale bars: (**A-C**, **E, F**) 20 µm; (**D**) 10 µm

By contrast, a dual localization of AtARO1-GFP can be seen in the male gametophyte: in the vegetative cell the AtARO1-GFP fusion is situated in the cytoplasm as well as in the nucleus (Fig. 3.23A-F). The generative sperm cells in contrast completely lack any GFP signal (Fig. 3.23B). In merged images of the green and red channel of CLSM pictures, PI shows a co-localization in the vegetative but not in the two generative nuclei (Fig. 3.23C, F). After *in vitro* germination of pollen tubes, the AtARO1-GFP fusion protein was found to be dispersed in the cytoplasm, but also present in the vegetative nucleus. In addition, the fluorescence strongly accumulated in a cup-shaped fashion at the tip of the pollen tube. Few small fluorescent spots with a diameter of approximately 0.5 µm could be detected in the shank of the tube (Fig. 3.23G). Sometimes, filamentous fluorescent structures were detected in the grain or along the shank of the germinated pollen tube (Fig.3.23H). They are best visible near the membrane of the pollen grain, after most cytoplasm was pushed into the pollen tube by the big vacuole. AtARO1 was still absent from sperm cells after germination (not shown).

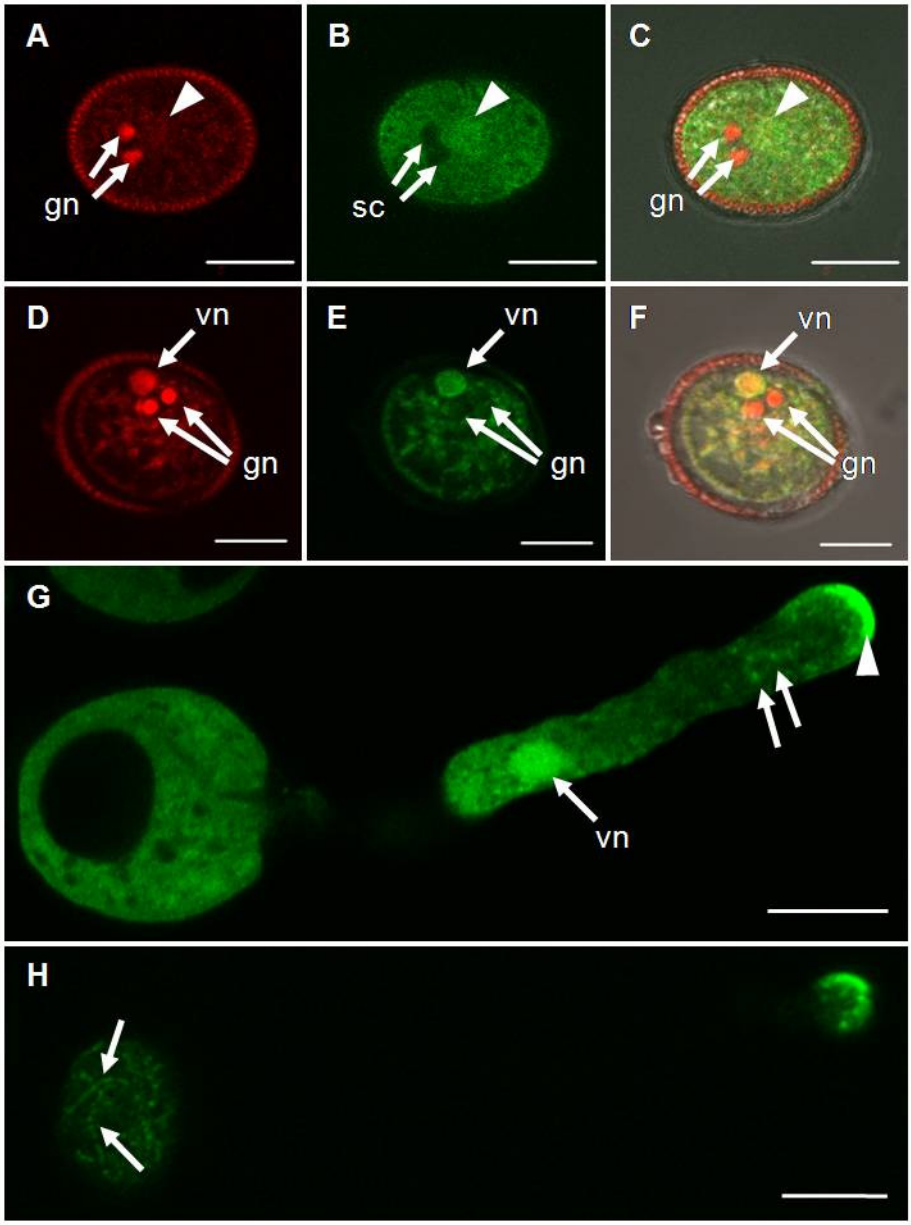

Fig. 3.23. Localization of the ARO1-GFP fusion protein in homozygous transgenic *AtARO1p::AtARO1-GFP* lines. CLSM images of male gametophytes. (**A**-**C**) Single 0.4 µm optical section of a pollen grain stained with propidium iodide (PI). The two generative sperm cell nuclei (gn) show a strong red staining (**A,** arrows); the vegetative nucleus (arrowhead) is not in focus. (**B**) ARO1-GFP is not localized at the position of the sperm cells (sc**,** arrows). (**C**) Merged picture of (**A**), (**B**) and bright field. (**D**-**F**) Single 0.5 µm optical section of a pollen grain. Vegetative nucleus (vn) and generative nuclei (gn) are stained with PI (**D**), but green fluorescence of AtARO1-GFP is only visible in the vegetative nucleus (**E,** arrow). In the merged picture of (**D**) and (**E**) with the bright field image, the co-localization of AtARO1-GFP in the vegetative nucleus can be seen as yellow color (**F,** arrow). (**G**-**H**) *In vitro* germinated pollen, expressing AtARO1-GFP. (**G**) The fusion protein is distributed throughout the cytoplasm of the pollen tube but clearly accumulates in the tip (arrowhead). GFP fluorescence can be detected in the vegetative nucleus (vn) and spots of higher fluorescence intensity are visible in the cytoplasm (arrows). Sperm cells are not in focus. (**H**) Single 0.36 µm optical section near the membrane of a germinated pollen. Filamentous fluorescent structures can be detected near the plasma membrane after most of the cytoplasm moved into the pollen tube. Scale bars: 10 µm

3.5 Co-localization studies using AtARO1-GFP expressing male and female gametophytes

3.5.1 AtARO1 co-localizes with the actin cytoskeleton of growing pollen tubes

Due to the severe phenotype of the actin cytoskeleton in pollen tubes of *aro1-3* knock out mutants, AtARO1-GFP expressing pollen tubes were used to carry out co-localization studies of AtARO1 with the actin cytoskeleton. After fixation and rhodamine-phalloidin labelling of pollen tubes, the distribution of AtARO1-GFP in the cytoplasm was found to be altered. More filamentous structures became visible throughout the shank while the tip-high accumulation remained (Fig. 3.24A, D). In merged images of AtARO1-GFP fluorescence and F-actin fluorescence, co-localization of AtARO1-GFP and actin can be detected. It is most obvious in the shank of the pollen tube (Fig. 3.24C, F), while in the tip the AtARO1-GFP signal often takes precedence (Fig. 3.24F). Over the width of the pollen tube, AtARO1 and F-actin obviously demonstrate very similar distribution patterns in a fluorescence intensity profile (Fig. 3.24G).

Co-localization of two signals can be demonstrated by a scatter plot of fluorescent signal intensities. In a scatter graph, values for two variables from a set of data, in this case green or red fluorescent signals at each pixel of a given picture, are displayed. If the pattern of pixels from a region of interest ascends from the lower left to upper right corner of the scatter plot, it suggests a positive correlation between the variables being studied. In the case of AtARO1-GFP and rhodamine-phalloidin labeled actin filaments, a clear correlation and thus co-localization can be seen (Fig. 3.24H). Closer inspection of the tip of germinated pollen revealed, that fluorescence of AtARO1-GFP is strongest at the extreme apex of the tube (Fig. 3.24J), where only short actin filaments and G-actin exist and dynamic changes in actin organization take place. As is visible in a fluorescence intensity profile of the tip, the intensity of the green AtARO1-GFP signal is much stronger than the fluorescence of rhodamine-phalloidin labelled actin, contrary to the rest of the pollen tube (Fig.3.24K, compare to Fig. 3.24G). However, weak and dispersed staining of the dynamic actin in the very tip of the pollen tube might also be due to the staining method used in this study, which was shown to often disrupt very fragile cytoskeletal elements (Lovy-Wheeler et al., 2005).

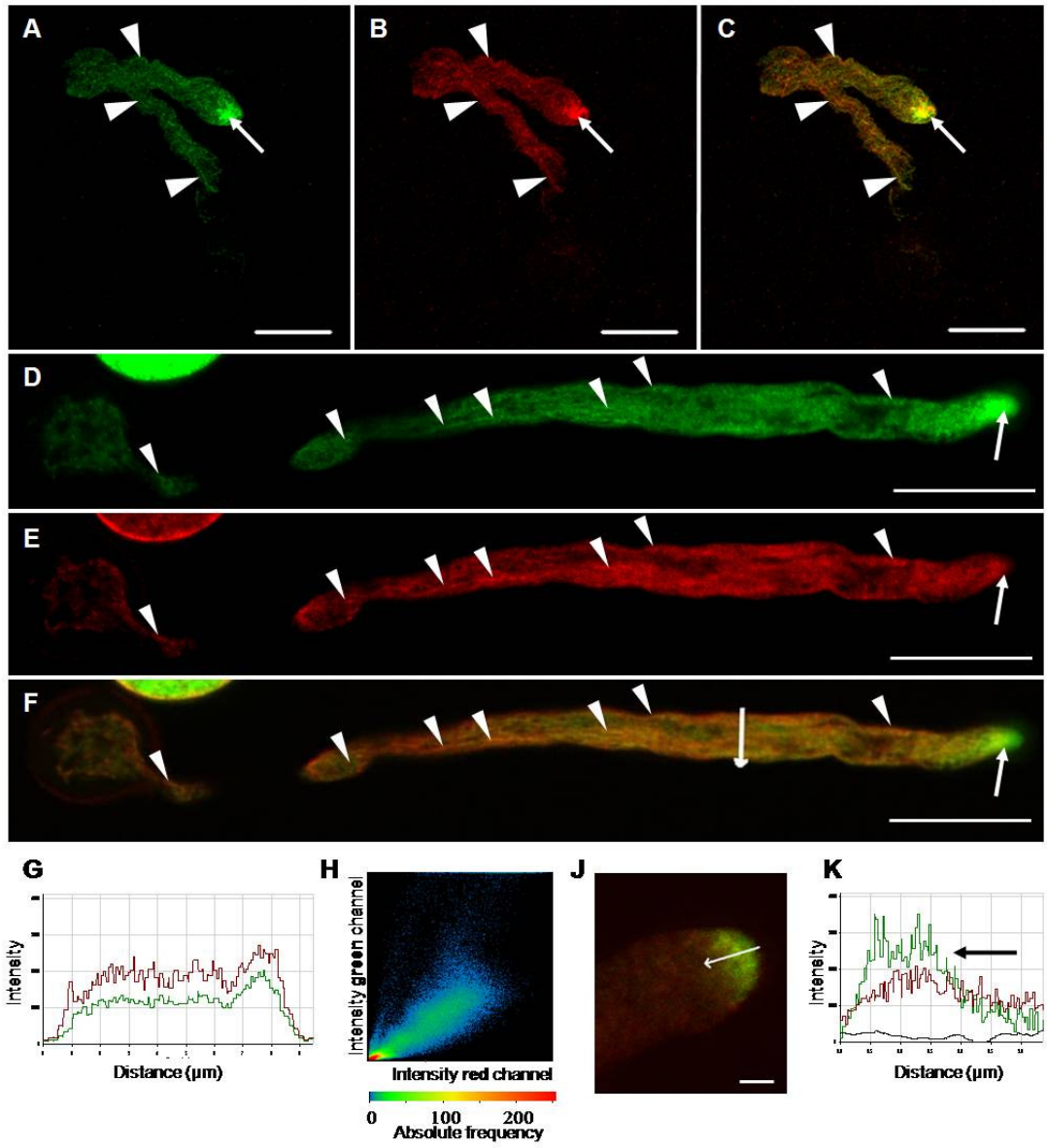

Fig. 3.24 Co-localization studies of AtARO1-GFP and actin in germinated pollen tubes. *In vitro* germinated pollen tubes were fixed, stained with rhodamine-phalloidin and analyzed using CLSM. The AtARO1-GFP fusion protein co-localizes with actin in the growing pollen tube. (**A**) Distribution of AtARO1-GFP after fixation (single 0.4 µm optical section). Filamentous structures of AtARO1-GFP fusion protein become visible (arrowheads). (**B**) Actin is organized in parallel bundles along the shank but has a more patchy appearance in the tip of the pollen tube (arrow). (**C**) Merged images of AtARO1-GFP fluorescence (green) and actin cytoskeleton (red) demonstrate the co-localization of the GFP fusion protein with actin at orange to yellow areas (arrowheads). (**D**-**F**) Single, 0.66 µm optical section of a germinated and stained pollen tube. Although AtARO1-GFP (**D**) is still distributed in the cytoplasm, it clearly accumulates along actin bundles (**E**, arrowheads) and shows a clear co-localization at orange areas of the merged image (**F**). (**G**) Fluorescence intensity profiles of red (actin) and green (AtARO1-GFP) signals show the same spatial distribution in a transverse section of the pollen tube (arrow in (**F**)). (**H**) Scatterplot of actin (red) and GFP (green) signals of the pollen tube shown in (**F**). Co-localization of signals is recognized as a nearly linear and increasing diagonal distribution of pixels. (**J**) Close up of a pollen tube tip (single 0.34 µm section). The fluorescence intensity profile (**K**) of a longitudinal section (arrow in (**J**)) shows high GFP accumulation in the very tip of the pollen tube where actin filaments are scarce. Scale bars: (**A**-**C**) 20 µm; (**D**-**F**) 10 µm; (**J**) 2µm

It is well established, that pollen tube growth is oscillatory and levels of components involved in the tip growth machinery oscillate at the same frequency, either in phase with growth, like the tip-focused Ca^{2+} gradient or in the opposite growth phase, as was shown for tip-localized actin (Fu et al., 2001). Interestingly, evaluation of AtARO1-GFP fluorescence in pollen tube tips revealed a variation in the area and the intensity of fluorescence. The area of the very tip, which was occupied by AtARO1-GFP varied between 0.7 to 5 µm, with respect to the apical plasma membrane. Further, a change in pollen tube growth direction was always accompanied by a relocation of AtARO1-GFP fluorescence towards the new growth site of the tip (Fig. 3.25), indicating a correlation between AtARO1-GFP accumulation and tip growth. Jointly, the localization of AtARO1-GFP fusion protein and the aberrant actin cytoskeleton in *aro1-3* knock out mutants strongly suggest the participation of AtARO1 in the assembly and/or maintenance of the dynamic actin cytoskeleton in the growing pollen tube tip.

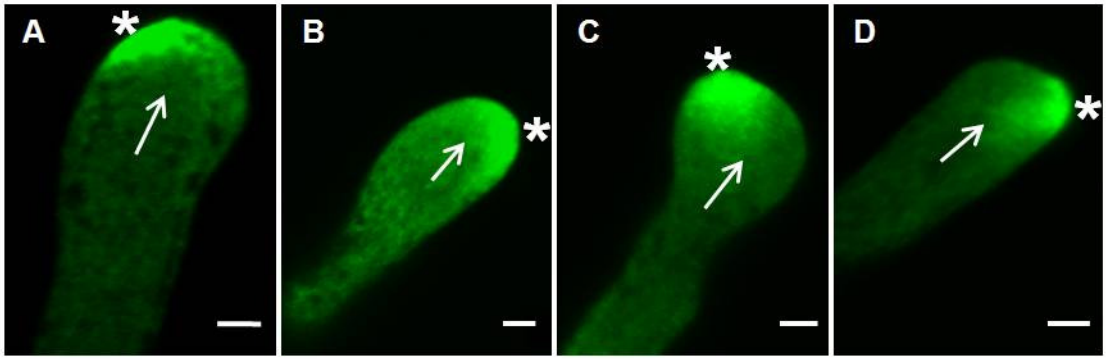

Fig. 3.25. Relocation of AtARO1-GFP in the tip of *in vitro* germinated *AtARO1p::AtARO1-GFP* pollen tubes during growth reorientation, analyzed by CLSM. (**A**-**D**) Lopsided fluorescence, accumulating at the future growth side of pollen tube tip (asterisks). Arrows indicate previous growth direction of pollen tubes. (**A**) Single 0.5µm optical section, (**B**) to (**D**) projection of three 0.34µm optical sections. Scale bars 2µm

3.5.2 AtARO1 localization in the tube tip is BFA dependent but LatB insensitive

To further verify the participation of AtARO1 in establishment of the actin cytoskeleton, the effect of the actin nucleation inhibitor Latrunculin B (LatB) from the red sea sponge *Latrunculia magnifica* on AtARO1-GFP distribution was investigated. Furthermore, the accumulation of AtARO1-GFP in spot-like structures (Fig. 3.23G) suggested another role of the protein in exo- and/or endocytotic processes. The transport of Golgi vesicles, filled with cell wall material, to sites of exocytosis was shown to be highly dependent on the actin cytoskeleton (Hepler et al., 2001). Brefeldin A (BFA), which is known to inhibit exocytosis and enhance endocytosis in pollen tubes (Wang et al., 2005), was used as another drug to analyze possible effects on AtARO1-GFP localization. Pollen were germinated *in vitro* for three hours and subsequently treated with LatB or BFA in liquid germination medium for two hours respectively. Control pollen tubes were incubated in liquid germination medium containing only the dissolvent dimethylsulfoxide (DMSO) or Methanol (MeOH), respectively. The control pollen tubes showed normal AtARO1-GFP distribution in the cytoplasm and vegetative nucleus of the pollen tube,

with the tip-high accumulation described above (Fig. 3.26A, C; compare to 3.23G). Intriguingly, BFA treatment led to a loss of accumulation of AtARO1-GFP in the pollen tube tip (Fig.3.26B) and the fusion protein was evenly distributed throughout the cytoplasm. Morphological changes of the pollen, like increased tube diameter, tip swelling or accumulation of vacuoles were observed. These effects of BFA treatment were also observed elsewhere (Wang et al, 2005) and therefore not regarded to be specific for altered AtARO1-GFP distribution but a consequence of inhibited exocytosis and enhanced endocytosis. LatB, in contrast, did not abolish the tip accumulation of AtARO1-GFP (Fig. 3.26D), although it was often weaker than in the controls (Fig.3.26C). A high number of bright fluorescent spots could be detected in pollen tubes treated with BFA and to a lesser extent, in pollen tubes treated with LatB (Fig. 3.26B and D). A few bright fluorescent spots were also observed in the control experiments or in non-treated pollen tubes (arrows in Fig. 3.26C, Fig.3.23G).

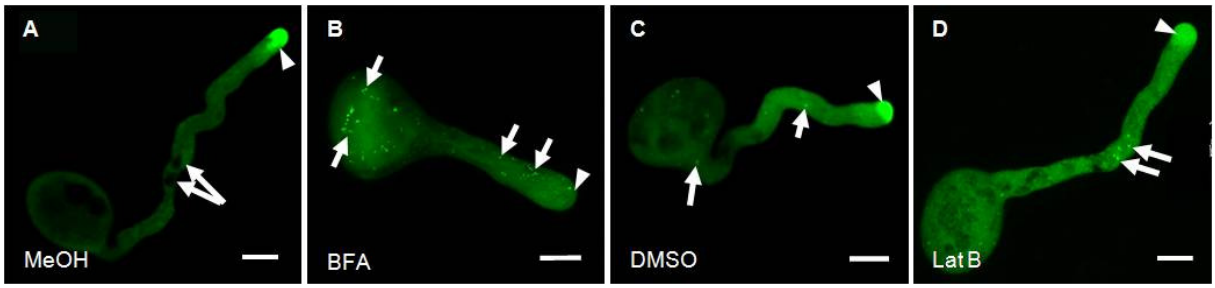

Fig.3.26. Localization of AtARO1-GFP in pollen tubes treated with Brefeldin A (BFA) or Latrunculin B (LatB), respectively. Control pollen tubes were treated each with the corresponding solvent. (**A**) Typical phenotype of a control pollen tube incubated with MeOH for two hours (single optical section; 0.50 µm). No alterations compared to non-treated pollen tubes were detected. AtARO1-GFP accumulates in the pollen tube tip (arrowhead), the two sperm cells, free of fluorescence, are visible (arrows). (**B**) BFA treatment leads to reduced growth rate as well as altered pollen tube morphology. The tip-high accumulation of AtARO1-GFP disappears (arrowhead) while bright fluorescent spots can be detected throughout the pollen tube and grain (arrows, 52 0.30 µm optical sections; 15.32µm). (**C**) Control pollen tube treated with DMSO (36 optical sections; 17.63 µm). Growth rate, pollen tube morphology and distribution of AtARO1-GFP were comparable to non-treated pollen tubes. The tip-high accumulation of AtARO1-GFP (arrowhead) and spots of lower fluorescence intensity are visible in the cytoplasm (arrows). (**D**) Treatment of pollen tubes with LatB (3D stack of 59 optical sections; 17.42 µm). Pollen tube morphology and the distribution of AtARO1-GFP fusion protein did not show strong alterations after LatB treatment. However, punctiform fluorescence (arrows) in the cytoplasm is brighter, while the amount of AtARO1-GFP in the tip seems to decrease (arrowhead). Scale bars: 10 µm

In a second set of experiments, the actin cytoskeleton was fixed and stained with rhodamine-phalloidin after treatments with BFA or LatB. While the control experiments showed the same co-localization of AtARO1-GFP and actin as non-treated cells (not shown), BFA treatment revealed even more severe changes in AtARO1-GFP distribution after fixation (Fig. 3.27A-C). The accumulation in the tip vanished as in unfixed BFA-treated cells, additionally the filamentous AtARO1-GFP distribution changed into a punctiform fluorescence of varying size and shape (on average 0.5 µm diameter). These accumulations of AtARO1-GFP mostly did not seem to be associated with thick actin bundles, as can

also be seen as an L-shaped scatterplot of red (actin) and green (AtARO1-GFP) fluorescence intensities in Fig. 3.27D. Instead, the fluorescent spots were often found to be distributed along fine actin filaments like pearls on a string (dashed arrow in Fig. 3.27A-C).

After the complete disruption of the actin cytoskeleton by LatB, labeling of remnants of F-actin by rhodamine-phalloidin was very weak (Fig. 3.27F). The disruption of actin filaments was accompanied by the disappearance of filament-like AtARO1-GFP signals in the shank of pollen tubes and AtARO1-GFP was dispersed through the cytoplasm (Fig. 3.27E). Again, several brighter AtARO1-GFP spots were detected throughout the cytoplasm, of which few co-localized with red fluorescent spots of actin. Co-localization was still present at the pollen tube tip, where both, AtARO1-GFP and actin accumulated to a weaker extent compared to non treated cells (Fig. 3.27G). This reduced co-localization is also reflected in a broader distribution of pixels in the scatterplot (compare Fig. 3.27H with Fig. 3.24H). Therefore, AtARO1-GFP accumulation in the pollen tube tip seems not or only to a low extent depend on an intact cytoskeleton.

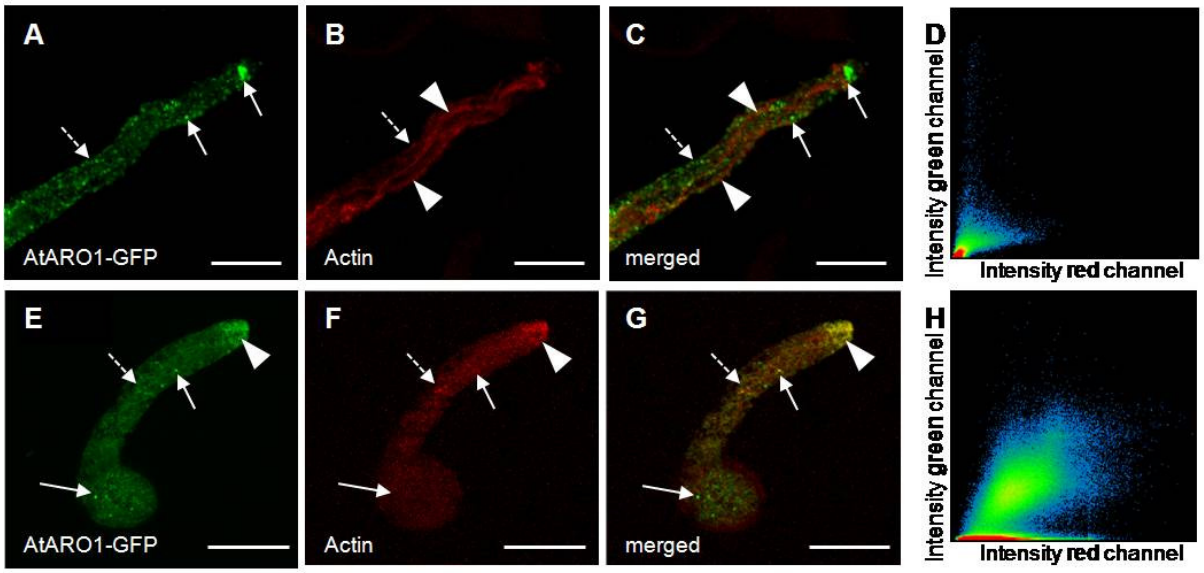

Fig. 3.27. Co-localization of AtARO1-GFP and actin after treatment with BFA and LatB, respectively. (**A**-**D**) Co-localization of AtARO1-GFP and actin after BFA treatment. (**A**) The distribution of the fusion protein is strongly altered compared to fixed pollen tubes without BFA treatment as well as compared to unfixed but BFA treated pollen tubes. AtARO1-GFP strongly accumulates as bright fluorescent structures of approximately 0.5 µm diameter (arrows) that are dispersed throughout the cytoplasm. (**B**) Thick actin cables (arrowheads) and finer filaments (dashed arrow) are visible in the red channel. (**C**) The merged image reveals that AtARO1-GFP seems to associate with finer actin filaments (dashed arrow). However, most AtARO1-GFP accumulations do not co-localize with actin bundles (arrowheads). (**D**) The scatterplot reveals only little correlation between red and green pixels, which are distributed in an L-shaped fashion. (**E**-**H**) Co-localization of AtARO1-GFP and the actin cytoskeleton after treatment with LatB. (**E**) The filamentous fluorescence of AtARO1-GFP which is found after fixation of untreated pollen tubes is lost as actin bundles are disrupted due to LatB treatment (**F**). Some bright fluorescent AtARO1-GFP spots are dispersed throughout the cytoplasm (arrows) but do not coincide with spots of actin accumulations (dashed arrow). (**G**) AtARO1-GFP and actin still co-localize, to a certain extent, in the pollen tube tip (arrowhead). (**H**) The reduced co-localization of actin and AtARO1-GFP is reflected in a broader distribution of pixels in the scatterplot.

Due to the presence of vesicle-like, fluorescent structures throughout the pollen tube shank and the accumulation of AtARO1-GFP in the vesicle-enriched tip region of the pollen tubes, a possible association of AtARO1 with transport vesicles was examined using the fluorescent membrane dye FM4-64 (Bolte et al., 2004; Ovečka et al., 2005) in combination with BFA. So called "BFA compartments" were reported to form from endosomes and Golgi derived endomembrane systems (Baluska et al., 2002) after BFA treatment and a localization of AtARO1-GFP to these compartments could point to an involvement of AtARO1 in vesicle trafficking. Before fixation, BFA treated and control pollen tubes were incubated for half an hour with the fixable derivative FM®4-64FX to visualize endomembrane compartments. In BFA-free control experiments, AtARO1-GFP co-localized with the actin cytoskeleton and bright fluorescent spots were visible, but these did not coincide with small endocytic vesicles stained by FM4-64 (Fig. 3.28A-D). Moreover, no co-localization was detected in BFA treated pollen tubes, where BFA induced compartments became visible as enlarged FM4-64 stained membrane compartments (Fig. 3.28E-H).

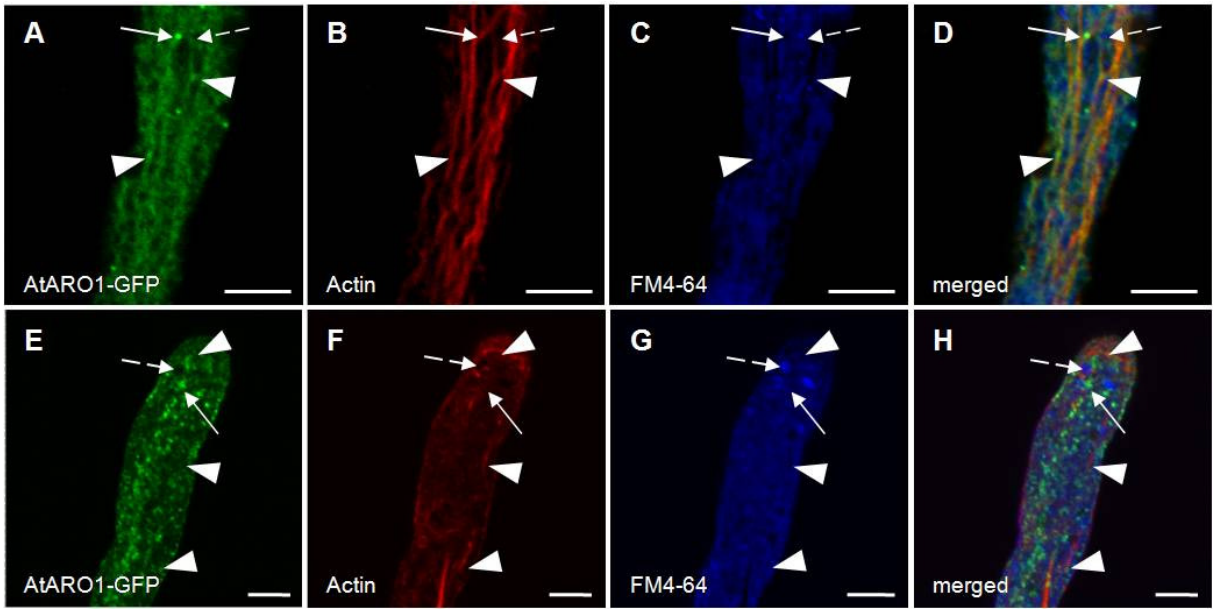

Fig. 3.28 Co-localization of AtARO1-GFP, endomembrane compartments and actin. AtARO1-GFP does not co-localize with endocytotic vesicles. (**A**) AtARO1-GFP co-localizes with actin bundles (**B**) in the pollen tube shank (arrowheads). Punctiform fluorescence of AtARO1-GFP (arrow) does not co-localize with endocytotic vesicles labeled by FM®4-64FX (dashed arrow, **C**, **D**). (**E**-**H**) BFA treated pollen tube. AtARO1-GFP no longer decorates thick actin bundles (arrowheads) but appears as fluorescent bodies (arrow). AtARO1-GFP does not co-localize with FM®4-64FX labeled BFA-induced membrane compartments (dashed arrow). Scale bars: 5 µm

Recapitulatory, the co-localization experiments clearly demonstrate that AtARO1-GFP is definitely associated with the actin cytoskeleton in the shank of the pollen tube but not with endocytotic vesicles, although it shares a common spatial distribution with endo- and exocytotic vesicles.

3.5.3 Distribution of AtARO1-GFP and actin in the female gametophyte before and after fertilization

Co-localization studies were also carried out in the female gametophyte, where AtARO1-GFP is expressed in the unfertilized egg cell. Ovules form emasculated flowers of *AtARO1p::AtARO1-GFP* plants were stained with rhodamine-phalloidin and observed under the CLSM. A strong actin cytoskeleton could be stained in the synergids, with parallel actin filaments oriented along the micropylar-chalazal axis of the cells. In the egg or central cell actin filaments were rarely visible (Fig. 3.29B-D). Only a weak staining at the chalazal cortex of the egg cell was visible in some instances (Fig. 3.29B, arrowhead). A co-localization of AtARO1-GFP and actin in the egg cell could therefore not be detected. After protein fixation, very fine green fluorescent filaments were sometimes visible in the egg cell (arrows in Fig. 3.29C), but they likely represent transvacuolar strands pervading the large vacuole. One hour after hand pollination, before pollen tubes reach the ovules, distribution of actin filaments in the synergids was not changed (Fig. 3.29E), but the AtARO1-GFP signal seemed to accumulate at the micropylar end of the egg cell. Small bright spots accumulated near the plasma membrane at this part of the cell (Fig. 3.29F, G).

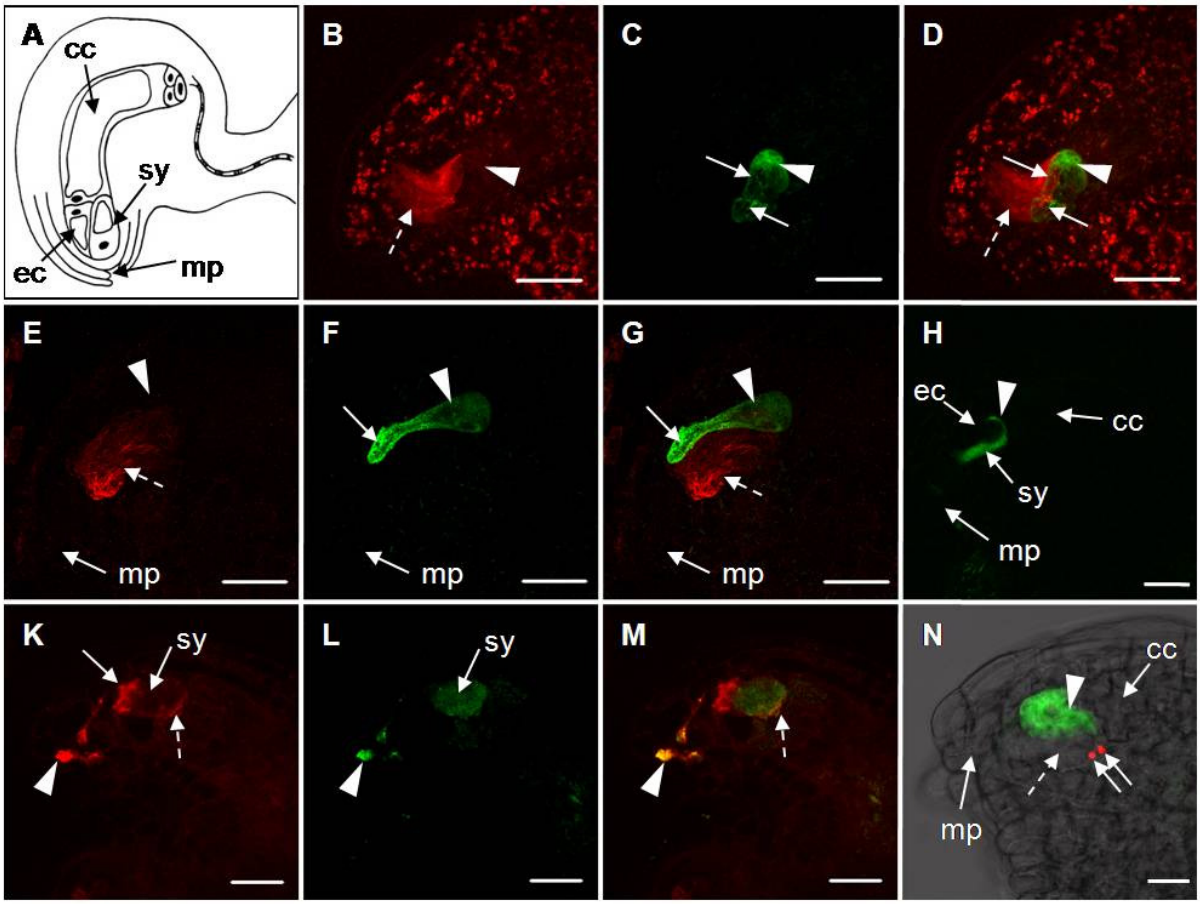

Fig. 3.29. Localization of AtARO1-GFP in the female gametophyte, before and during fertilization. (**A**) Scheme of an *Arabidopsis* ovule. The lateral view presents the egg cell (ec) and one of the two synergids (sy) near the micropyle (mp). The large central cell (cc) fills most of the embryo sac. (**B**-**D**) *AtARO1p::AtARO1-GFP* expressing ovule, stained for actin two days after emasculation (3D projection of 24 optical sections, 0.34 µm each). (**B**) The

synergid exhibits prominent axially orientated actin bundles (dashed arrow), while actin staining in the egg cell is scarce, basically visible at the cortex (arrowhead). (**C**) AtARO1-GFP is present in the cytoplasm of the mature egg cell (arrowhead). Fluorescence is also seen as fine filaments (arrows) that might represent transvacuolar strands. (**E**-**G**) *AtARO1p::AtARO1-GFP* ovule, one hour after hand pollination (3D projection of 55 optical sections, 0.40 µm each). (**E**) Actin staining reveals prominent axially actin bundles (dashed arrow) in the synergids, like in unpollinated pistils (arrowhead marks position of egg cell). (**F**) AtARO1-GFP is enriched at the micropylar part of the egg cell (arrow). (**G**) Merged picture of (**E**) and (**F**). (**H**) Distribution of pollen derived AtARO1-GFP after pollen tube discharge into a WT ovule (single 0.40 µm optical section). The fluorescence fills the degenerating synergid (sy) and spreads into the gap (arrowhead) between egg (ec) and the central cell (cc). (**K**-**M**) Actin organization, 7h after hand pollination with *AtARO1p::AtARO1-GFP* pollen (3D projection of 17 optical sections, 0.30 µm each). (**K**) Actin filaments in the lumen of the degenerating synergid (sy) disintegrate and aggregate as a dense patch at the micropylar part (arrow). A narrow band of actin is visible at the chalazal cortex (dashed arrow). (**L**) AtARO1-GFP fills the lumen of the degenerating synergid (sy); fluorescence is also visible in the pollen tube (arrowhead). (**M**) Merged picture of (**K**) and (**L**). Co-localization of actin and AtARO1-GFP appears in the pollen tube (arrowhead) and at the chalazal cortex of the degenerated synergid (dashed arrow). (**N**) *AtARO1p::AtARO1-GFP* expressing ovule, pollinated with sperm cell marker line *H3.3p::H3.3-mRFP1*. The two sperm cells (red) migrate towards the chalazal pole of the degenerating synergid (dashed arrow). mp, micropyle. Scale bars 20 µm

It is known from tobacco, maize and *Torenia fournieri* that so called “actin-coronas” are formed between the degenerating synergid, egg cell and central cell upon penetration of the pollen tube into the receptive synergid. This actin framework is thought to be important for the transport of the sperm cells towards the two female gametes. The nuclei of the two female gametes were shown to be positioned at the area where both, the egg and central cell are in contact with the receptive synergid (Russell, 1993). In order to examine whether pollen-tube derived AtARO1 is involved in reorganizing the actin cytoskeleton in the degenerating synergid, and whether AtARO1 in the egg cell plays a role in actin organization upon fertilization, reciprocal crosses of WT and AtARO1-GFP transgenic plants were carried out. In accordance with previous observations (Ingouff et al., 2007), first pollen tubes arrived at the ovules about 5 hours after hand pollination in our study. The typical distribution of male-derived AtARO1-GFP in the degenerating synergid, after the pollen tube released its cytoplasm and the two sperm cells, is shown in Fig. 3.29H. The fusion protein spreads into the space formerly filled by the receptive synergid and into the gap between egg cell and central cell. After staining the actin cytoskeleton of ovules at the time point of pollen tube discharge, the microfilaments of the degenerating synergid shows extensive rearrangements. Dense actin patches seem to accumulate at its micropylar end (Fig. 3.29K, arrow). Additionally, actin is located at the chalazal end of the synergid next to the egg as well as the central cell in a hook-like fashion, strongly resembling the actin coronas found in other plants (Fu et al., 2000; Huang et al., 1999; Russell, 1993; Ye et al., 2002). AtARO1-GFP is weakly visible throughout the whole synergid cell, but only co-localizes with the narrow actin band at the chalazal end (dashed arrow) as well as with remnants of actin in the pollen tube (Fig. 3.29M, arrowhead). In another set of experiments, AtARO1-GFP expressing pistils were crossed with pollen where the sperm cells are marked by H3.3-mRFP1, a male-gamete-specific histone variant fused to mRFP1 (Ingouff et al., 2007). The sperm cells were found to migrate towards the chalazal end of the degenerating synergid corresponding to the area where the actin band is located (Fig. 3.29N).

3.6 Yeast two hybrid

To substantiate the direct or indirect interaction of AtARO1 with the actin cytoskeleton, and to find additional possible binding partners of AtARO1, direct interaction assays and a yeast two hybrid screen were conducted. For the yeast two hybrid screen a cDNA library of germinated pollen tubes was cloned using the Matchmaker™ Two-Hybrid System 3. Further, the direct interaction of AtARO1 with different actins (ACT) from *Arabidopsis* was tested.

3.6.1 Direct interaction assays

AtARO1 and the ubiquitously expressed *ACT3* (At3g53750), pollen specific *ACT4* (At5g59370), and *ACT7* (At5g09810) which is only expressed in vegetative tissues, as well as *GFP* were cloned as bait and as prey into the yeast two hybrid expression vectors along with positive and negative controls provided with the kit. GFP was reported to have a low binding affinity to actin (J. Kuehnl, personal communication) and was therefore used as control to determine whether co-localization of AtARO1-GFP and actin was due to this low-affinity binding. All constructs were transformed into both AH109 and Y187 yeast strains provided with the Matchmaker™ Two-Hybrid System 3. Expression of the proteins in the two yeast strains was proven by protein extraction and western blotting of total protein extract with a polyclonal α-c-myc antibody (Fig. 3.30). Although cross reactions were detected with the polyclonal α-c-myc antibody in total protein extracts, distinct bands could be detected for ACT3, ACT4 and ACT7 fused to the Gal4 binding domain (BD) on a 10% gel. The observed size of ~ 65 kDa is close to the size of 57.5 kDa calculated for all three BD-ACTs (Fig. 3.30A, left panel, asterisk). AtARO1 fused to the BD of Gal4 was calculated to have a M_r of 93.1 kDa and could be detected on the same membrane but after direct exposure of an x-ray film to the detection reagents (see section 2.20.4). Although multiple unspecific bands were stained in all lanes, a distinct band at the appropriate size was visible in yeast strains expressing the BD-AtARO1 fusion (Fig.3.30A, right panel, asterisk). The smaller BD-GFP fusion protein and the empty pGBKT7 vector, used as positive control as well as the negative control (yeast strain AH109 without recombinant protein) were separated on a 12 % gel. Bands of appropriate sizes (GFP: 42.6 kDa; BD of pGBKT7 vector: 16.8 kDa) were detected.

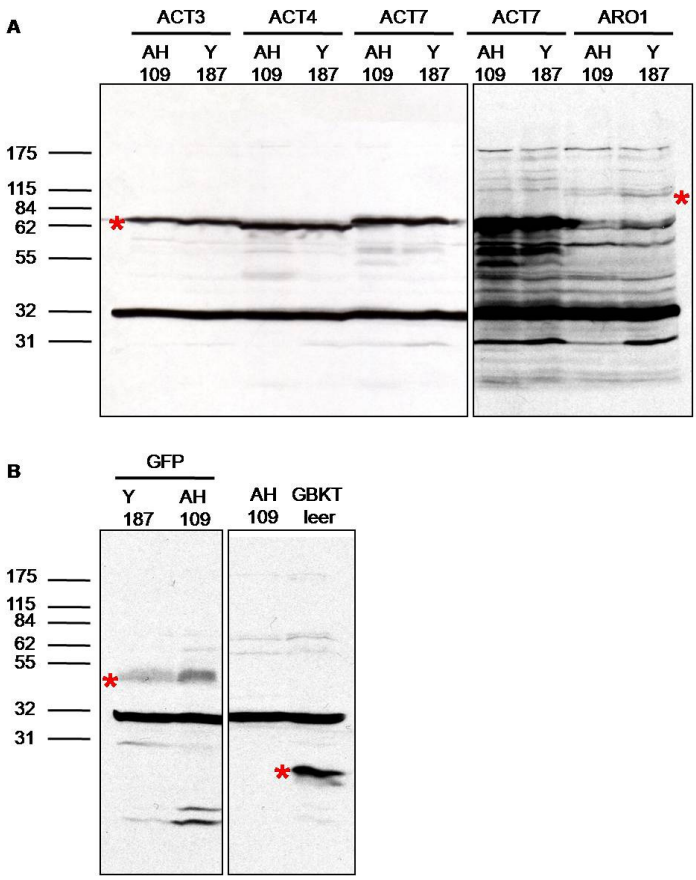

Fig. 3.30. Recombinant protein expression in yeast, detected by western blotting. Expression and translation of transgenic fusion constructs was verified by extracting total protein from yeast cells and western blotting using a polyclonal α-c-myc antibody. Each protein was expressed in the yeast strains AH109 and Y187, respectively. Bands of appropriate size (see text), representing the fusion proteins, are indicated by red asterisk. (**A**) Protein extracts of ACT3, ACT4, ACT7 and AtARO1 expressing yeast strains were separated on a 10% gel and proteins detected after a 10 minutes exposure on x-ray film. Stronger background on the blot showing AtARO1 is due to direct exposure of detection reagents to x-ray film (see section 2.20.4). Multiple unspecific bands are visible on the blot, due to cross reactions of the polyclonal antibody. However, only AtARO1 but not ACT7 expressing lines show a specific band at ~94 kDa (asterisk). (**B**) Protein extracts of GFP expressing yeast strains were separated on a 12% gel. Untransformed yeast strain AH109 and yeast strain Y187 expressing the BD of vector pGBKT7 only were used as negative and positive controls, respectively. Size markers indicate M_r in kDa.

The different transgenic yeast strains were mated with each other (Fig. 3.31A; section 2.20.5) and diploids were selected on SD/-Leu/-Trp plates. Four representative clones from each mating were picked and spotted on SD/-Leu/-Trp replica plates as well as on SD/-Leu/-Trp/-His plates selecting for protein interactions (Fig. 3.31B). None of the tested proteins showed a positive interaction, as only the diploids from the positive control could survive low stringency selection for activation of the nutritional marker *HIS3*. A direct interaction of AtARO1 with a pollen specific or with a ubiquitously expressed actin could not be observed by the yeast two hybrid assay neither could the low binding activity of GFP with actin be substantiated. Moreover, BD-AtARO1 does not show intrinsic transcriptional activation of the reporter genes and can thus be used for screening the pollen tube cDNA library.

A

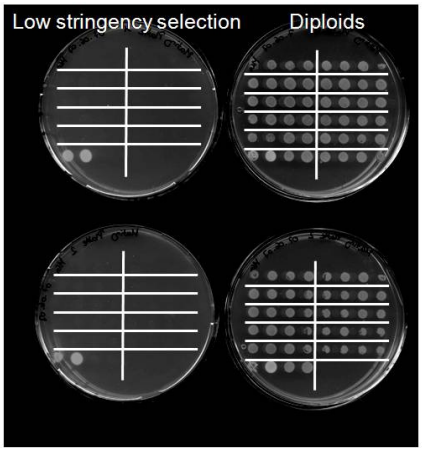

B

four replica clones	four replica clones
A1-BD x A1-AD	A1-AD x A1-BD
A1-BD x Act3-AD	A1-AD x Act3-BD
A1-BD x Act4-AD	A1-AD x Act4-BD
A1-BD x Act7-AD	A1-AD x Act7-BD
A1-BD x GFP-AD	A1-AD x GFP-BD
2 replicas +/ 2 replicas -	A1-AD x 0-BD

four replica clones	four replica clones
A1-BD x lam-BD	GFP-AD x GFP-BD
GFP-BD x GFP-AD	GFP-AD x Act3-BD
GFP-BD x Act3-AD	GFP-AD x Act4-BD
GFP-BD x Act4-AD	GFP-AD x Act7-BD
GFP-BD x Act7-AD	GFP-AD x 0-BD
2 replicas +/ 2 replicas -	

Fig. 3.31. Direct interaction test. Interaction of AtARO1 with ACT3, ACT4, ACT7 and GFP as well as intrinsic binding activity of AtARO1 and GFP each was tested via mating of transgenic yeast. (**A**) Low stringency selection of mated diploid yeast cells. Plates on the right hand side represent replica plates of diploid yeast cells, plated on SD/-Leu/-Trp. On the left hand side, clones from diploids were screened for protein interactions. Only positive controls could grow on low stringency SD/-Leu/-Trp/-His plates, indicating that none of the proteins investigated in this study interacted with each other or with itself. (**B**) Scheme of spotted yeast clones shown in (**A**). After mating, four representative clones from diploids were spotted onto selective media as indicated. A1, AtARO1; AD, activation domain; BD, binding domain; GFP, green fluorescent protein; lam, human lamin C (negative control); p53, murine p53; RecT, large T-antigen; 0-BD, empty pGBKT7 vector; +, positive control (=RecT-AD x p53-BD); -, negative control (=RecT-AD x lam-BD).

3.6.2 Yeast two hybrid screen of a pollen tube cDNA library

A screen for putative protein binding partners of AtARO1 was carried out with a cDNA library made from germinated pollen tubes (see section 2.20.1) using AtARO1 as bait. After amplification of the pollen tube cDNA and a human control cDNA by long distance PCR and subsequent purification, the integrity and average size of both probes was determined on an agarose gel. With 250 to 500 bp, the average size of cDNA fragments from pollen tubes was slightly lower than in human control cDNA, where most fragments ranged from 250 to 750 bp. The pollen tube cDNA and the vector pGADT7-Rec were co-transformed into yeast strain AH109. The transformation efficiency was 0.8 x 10^6 transformants for 3 µg vector used and therefore slightly lower than the expected 1x 10^6 transformants/3 µg vector. Accordingly, the library titer also was lower than the expected number of cells. Only 1.7 x 10^7 colonies/ml instead of the expected ≥2.0 x 10^7 colonies/ml were obtained. After mating the bait (pGBKT7-ARO1) with the host cDNA library (mating efficiency: 0,7%), diploids were plated onto SD/-Leu/-Trp/-His low stringency selection plates. 754 diploid clones able to activate the *HIS3* selective marker and therefore surviving this low stringency selection, were picked and spotted again on SD/-Leu/-Trp/-His (Fig. 3.32 A, B) as well as two times on SD/-Leu/-Trp/-His/-Ade (4x drop out medium, 4xDO; Fig. 3.32 C, D) selective plates. Colonies surviving the high stringency selection

on 4xDO medium, able to activate the *HIS3* and *ADE2* reporter genes, were tested for activation of a third reporter, *lacZ* with an x-Gal assay (Fig. 3.32E, F).

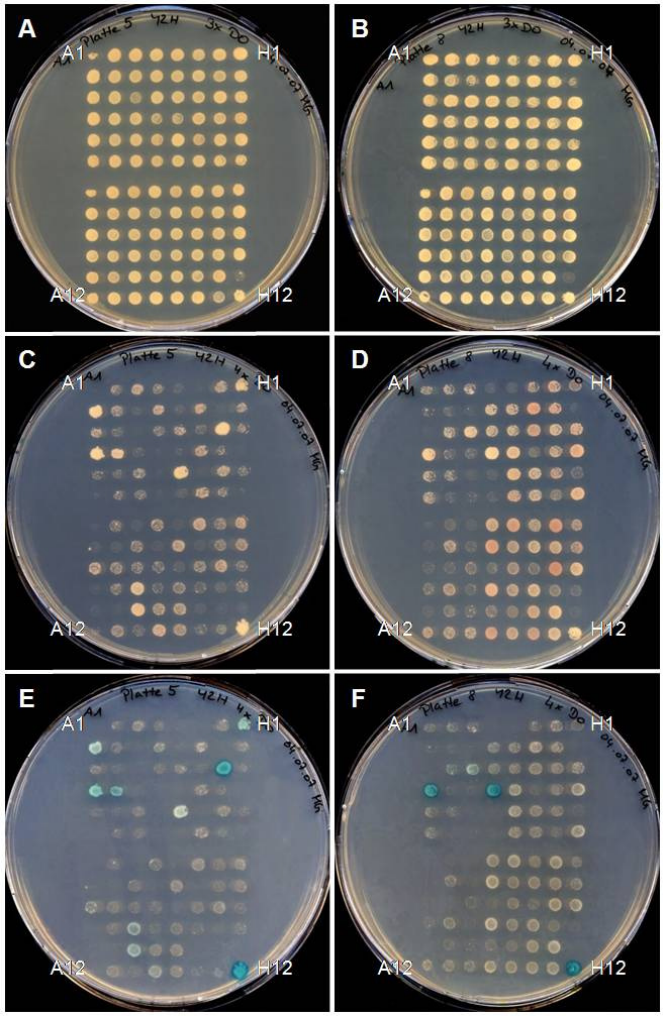

Fig. 3.32. Yeast two hybrid screening using AtARO1 as bait and a cDNA library from germinated pollen tubes. Diploids were tested for activation of reporter genes with low stringency (*HIS3* reporter gene) and high stringency (*HIS3* and *ADE2* reporter genes) selection plates and with an x-Gal assay (*HIS3*, *ADE2* and *lacZ* reporter genes). Two representative plates each are shown in this figure. A1, A12, H1 and H12 represent positions of clones on each plate (compare to Table 3.7). (**A**, **B**) Selection for *HIS3* on low stringency medium. (**C**, **D**) Selection for *HIS3* and *ADE2* on high stringency medium. (**E**, **F**) Selection for the third reporter, *lacZ*, using an x-Gal assay. Blue color indicates activation of *lacZ*.

As a result, 59 colonies showed a range of weak to strong activation of the *lacZ* reporter gene and were classified into 4 groups according to corresponding X-Gal activity: 0 = very weak staining, + = weak staining, ++ = intermediate staining, +++ = strong staining and - = negative control (Table 3.7).

Table 3.7 Very weak to strong activation of *lacZ* on 4xDO plates after the x-Gal assay. Colonies growing on 4xDO medium additionally show activation of *HIS3* and *ADE2* reporter genes.

Plate (1)	1	2	3	4	5	6	7	8	9	10	11	12
A						0						
B			0									
C												
D												
E					+							+
F												
G												
H												
											-	+++
Plate (2)	1	2	3	4	5	6	7	8	9	10	11	12
A			0					+	+			
B												
C						+						
D												
E												
F												
G	+											
H												
											-	+++
Plate (3)	1	2	3	4	5	6	7	8	9	10	11	12
A												
B								0				
C				+						0		
D												
E					+				0			
F												
G												
H							0					
											-	+++
Plate (4)	1	2	3	4	5	6	7	8	9	10	11	12
A		++										
B							++					
C	+											+
D												
E			+									
F											+	+
G							0					
H											-	+++

Plate (5)	1	2	3	4	5	6	7	8	9	10	11	12
A		+		++								
B				++								
C										+	+	
D												0
E												
F												
G			+++									
H	++											
											-	+++
Plate (6)	1	2	3	4	5	6	7	8	9	10	11	12
A		+	++									
B	++										+	+
C	++	++				+		+				
D												
E	+						+					
F								+		0		
G	+											0
H											-	+++
Plate (7)	1	2	3	4	5	6	7	8	9	10	11	12
A							+		+			
B												
C	0											
D		+	0		0							
E				+								
F												
G												
H		++									-	+++
Plate (8)	1	2	3	4	5	6	7	8	9	10	11	12
A				+++								
B			0									
C			0									0
D				+++								
E												
F												
G												
H											-	+++

On all plates, the negative and positive controls were spotted on positions H11 and H12 respectively, except for plate (1), where they were spotted by hand next to the full plate replica print. As shown in Table 3.7, 17 colonies showed a very weak staining and 29 colonies a weak staining, while intermediate staining could be observed in 10 colonies. A strong activation of the *lacZ* reporter, similar to that observed in positive controls, was only visible in 3 out of 754 analyzed clones. In order to identify the putative interacting proteins/protein fragments responsible for the activation of the reporter genes, 42 cDNAs of clones displaying a weak, intermediate or strong staining were sequenced, either after isolating plasmids and subsequent transformation in *E. coli* cells, or after direct amplification of the cDNA from the pGADT7 prey vector via PCR.

After sequencing the inserts from all 42 clones, the identified cDNA sequences were used for BLASTN searches of the *Arabidopsis thaliana* genome in the non-redundant nucleotide collection (nr/nt) at NCBI. 30 sequences matched to *PGA3* (At3g07820), a gene encoding polygalacturonase 3, which is highly expressed in germinating pollen and growing pollen tubes (Torki et al., 1999). The remaining cDNA fragments represented three more cDNAs for polygalacturonases (At5g48140 and At2g23900), each matching to two of the sequenced fragments, and two other genes. One of these genes encodes a SKS13 copper ion binding protein (4 clones, At3g13400), the other a member of the pectin esterase

family (1 clone, At5g07430). Two cDNAs gave no significant hit in the database, due to their length (132 bp and 64 bp). All cDNA clones identified in this screen are listed in the appendix (Table 7.2). Although polygalacturonases are known to be secreted (Niogret et al., 1991), and therefore an interaction with intracellular AtARO1 is highly unlikely, plasmids from one representative clone for each gene identified were retransformed into yeast strain AH109 and re-mated with the bait pGBKT7-ARO1, as well as with the empty pGBKT7 vector in order to examine possible auto-activation of the fragments. Positive and negative controls from the kit were included in the tests. All cDNA clones tested showed an activation of both reporter genes for nutritional selection *ADE2* and *HIS3* (Fig. 3.33). As the cDNA encoded peptides were able to activate the reporter genes independently of the bait protein, all cDNA fragments must be considered as false positives.

A

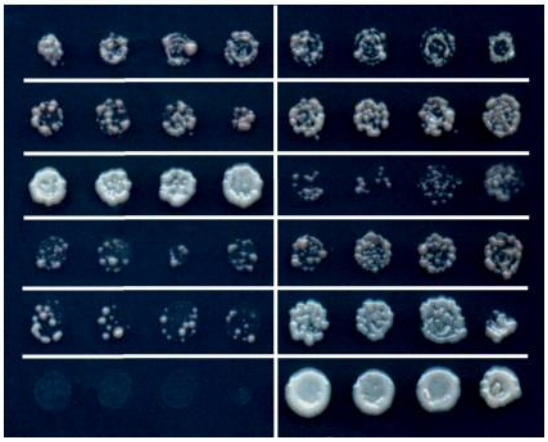

B

A1-BD x 6-A-2	A1-BD x 6-A-3
A1-BD x 6-E-7	A1-BD x 8-A-4
A1-BD x 8-D-4	0-BD x 6-A-2
0-BD x 6-A-3	0-BD x 6-E-7
0-BD x 8-A-4	0-BD x 8-D-4
BD-lam x AD-RecT	BD-53 x AD-RecT

Fig. 3.33. Verification of protein interactions found in the yeast two-hybrid screen using the pollen tube cDNA library. One representative cDNA clone of each gene identified as a putative positive was used to retest the activation of reporter genes on 4XDO medium. Each candidate was mated with the bait, AtARO1-BD, and with an empty pGBKT7 vector. Growth of diploids containing the empty pGBKT7 indicates auto-activation of candidate genes and thus false-positives. (**A**) All candidate genes showed activation of the reporter genes *HIS3* and *ADE2* with both, the AtARO1 bait and the empty vector control. (**B**) Table describing performed matings. Yeast cells were mated and diploids spotted onto 4xDO selective media as indicated in the table. A1, AtARO1; BD, binding domain; 0-BD, empty pGBKT7 vector; RecT, SV40 large T-antigen; 53, murine p53; lam, human lamin C.

4. DISCUSSION

4.1 The ARO family of ARM repeat proteins

Two small Armadillo (ARM) repeat protein encoding gene families were found in *Arabidopsis* and rice that display high homology to a novel transcript from wheat, which was found to be only present in wheat egg cells and anthers (Sprunck et al., 2005). Transcriptomic approaches (e.g Becker et al., 2003; Honys and Twell, 2004; Jones-Rhoades et al., 2007; Sprunck et al.,2005; Steffen et al., 2007; Yang et al., 2006b; Yu et al., 2005), transposon or T-DNA tagging mutant screens (e.g. Howden et al., 1998; Lalanne et al., 2004; Pagnussat et al., 2004;) and use of EMS mutagenesis (e.g. Schneitz et al., 1997) have been used to identify gametophyte-specific genes on a large scale. Although a number of genes have been characterized in the male (reviewed e.g in Cole and Fowler, 2006; Kost, 2008; McCormick, 2004) and female gametophytes (e.g. Drews and Yadegari, 2002; Yadegari and Drews, 2004), the molecular pathways underlying the fertilization process are only partly understood. Because only little is known about the signaling processes during pollen tube guidance and double fertilization, like e.g. sperm cell migration towards the egg and central cell, how the recognition and fusion of the gametes takes place, or the early events of embryogenesis, the identification and functional analysis of gametophyte specific genes is of special interest. This work reports on one of the first genes in *Arabidopsis* found to be expressed exclusively in the egg cell and the vegetative cell of the pollen, which was found to be switched off very shortly after fertilization. Due to the occurrence of ARM repeats, but no other known protein motifs (see below), the corresponding protein was named as AtARO1 (*Arabidopsis thaliana* Armadillo repeat only). The specific expression of *AtARO1* and the presence of ARM repeats, which are known to be present in proteins involved in developmental processes and signaling pathways, implicate an important role of this protein during the fertilization process. ARM repeat domains are tandemly arranged imperfect repeats of approximately 42 amino acids and were first identified in the segment polarity protein Armadillo from *Drosophila melanogaster* (Huber et al., 1997; Rigglemann et al., 1989), which was later found to be the homologue of mammalian β-catenin. These and several other animal ARM repeat containing proteins were shown to have important functions in protein-protein interactions necessary for cell adhesion, cytoskeletal regulation, intracellular signaling, nuclear transport, and transcriptional activation (Hatzfeld, 1999, 2007; Städeli et al., 2006; Zhurinski et al., 2000). ARM repeat proteins were found in the kingdoms of protists, fungi, plants and animals and thus represent a protein family with evolutionary ancient origins (Coates, 2003). In plants, ARM repeat containing proteins were found to have conserved functions, like e.g. importin-α, but besides those a great number of plant specific ARM proteins with novel functions was identified. In total, over one hundred proteins containing two to 32 ARM repeats were found in *Arabidopsis* (Mudgil et al., 2004). These proteins were divided into subfamilies according to their homology to each other and depending on additional protein motifs found. Interestingly, the biggest subfamily comprises plant specific U-box containing ARM repeat proteins (Coates, 2003; Mudgil et al., 2004). All proteins from this group analyzed so far were shown to be functional E3 ubiquitin ligases. These U-box containing ARM repeat proteins have been implicated in processes as

diverse as the regulation of self-incompatibility (Liu et al., 2007; Stone et al., 2003), in plant hormone signaling (Amador et al., 2001), and in cell death and activation of defense mechanisms (González-Lamothe et al., 2006; Yang et al., 2006a; Zeng et al., 2004). Other ARM repeat proteins with additional motifs like the BTB/POZ motif, a HECT domain, an F-box, kinase or kinesin domains were found to act in plant hormone signaling (Kim et al., 2004), in trichome development (Downes et al., 2003), in promoting lateral root development (Coates et al., 2006) , and in root-hair tip growth (Sakai et al., 2008; Yang et al, 2007), respectively.

However, 28 *Arabidopsis* ARM repeat proteins, including the novel small protein family analyzed in this work, contain no additional known protein motifs and the function of none of these proteins is known so far. Therefore, the four proteins of the family identified here were designated as *AtARO1* to *AtARO4* (Armadillo repeat only), with AtARO1 showing highest similarity to the protein encoded by the wheat egg cell cDNA clone *TaARO1*. AtARO2 and AtARO3 in turn share a high similarity to AtARO1, while AtARO4 represents the most divergent family member. Several other ARO-like proteins or putative open reading frames could be identified by BLAST searches all over the plant kingdom in as diverged plant species as the moss *Physcomitrella patens*, in gymnosperms like spruce and pine as well as in several monocotyledonous and dicotyledonous angiosperm species. By contrast, no ARO-like proteins were found in *Chlamydomonas*, yeast or animals, suggesting that the ARO-like proteins represent a plant specific but phylogenetically very old family.

Despite the fact that *Physcomitrella patens* is separated from flowering plants by more than 400 million years (Nishiyama et al., 2003), all ARO-like proteins identified show a very high degree of sequence conservation and the same overall structure. All proteins consist of two ARM repeat domains (ARD1 and ARD2), separated by a highly divergent spacer. Although only up to three ARM repeats were classified as significant hits by the Pfam database, six complete and three incomplete ARM repeats were identified in AtARO1 to -4 by combining all putative ARM repeats and secondary structure predictions of the four proteins. It is well known from ARM repeat proteins in animals, that the sequence conservation on the amino acid level is only about 25 % (Hatzfeld, 1999), while the three-dimensional structure is highly conserved. A minimum of six ARM repeats have been predicted to be necessary to form the basic superhelical structure of ARM repeat proteins (Huber et al., 1997). One ARM repeat consists of three α-helices, with the shorter H1 being arranged perpendicular to the antiparallel directed helices H2 and H3, and several higher conserved amino acid residues or physiochemical properties at pronounced positions within the repeats can be discerned (Choi and Weis, 2004). For example, a Gly residue is often found between H1 and H2 and several hydrophobic amino acids are highly conserved within H2 and H3 (Choi and Weis, 2004). These structural elements were also found in the repeats of AtARO1. Hence, homology modeling of AtARO1 with importin-α revealed a superhelical conformation of AtARO1, typical for ARM repeat containing proteins, without any amino acids of the AtARO1 sequence interfering sterically with this three-dimensional model.

Interestingly, the p120 catenins, a protein family found in animals involved in desmosome and cell adherens junction formation and signaling via RhoA, show a secondary structure comparable to the plant ARO proteins, although sharing no sequence similarities (Choi and Weis, 2004). β-catenin consist of a central region of 12 consecutive ARM repeats, preceded by an approximately 130 amino acid long N-terminus, containing the GSK-3β phosphorylation sites and followed by a ~100 amino acid

C-terminal region possessing transactivator function (Akiyama, 2000). The analysis of the three-dimensional structure of plakophilin, a member of the p120 catenin family, revealed however, that it contains two ARM repeat domains separated by an large insert (Choi and Weis, 2004). Besides that, plakophilin exhibits a long N-terminal domain comprising a coiled-coil domain and a regulatory phosphorylation domain as well as a C-terminal extension. Like in AtARO1, the second ARM repeat domain, directly following the large insert, is incomplete and only consists of helices H2 and H3 (Choi and Weis, 2004). Structural analysis of plakophilin showed that the space normally occupied by H1 in a standard ARM repeat is taken over by a part of the insert. Similarly, it is likely that the incomplete ARM repeat behind the spacer region in ARO-like proteins is completed by one of the α-helices predicted to be present in the spacer. The homologous modeling of importin-α with the first 388 amino acids of AtARO1, including the spacer region, revealed that the overall elongated superhelical conformation typical for ARM repeat proteins is maintained in AtARO1 and that the spacer region obviously does not interrupt the continuous packaging of the ARM repeats. An N-terminal domain of 133 to 153 amino acids precedes ARD1 in all ARO-like proteins. As the sequence and the secondary structure of this domain are also highly conserved, it likely constitutes another protein domain of yet unknown function. In p120 catenin, both the N- and C-terminal domains were shown to be essential for blocking GDP dissociation and inhibiting RhoA activity (Yanagisawa et al., 2008) and phosphorylation of p120 catenin was essential for RhoA binding (Castaño et al., 2007). AtARO1 and the ARO1-like proteins were also predicted to have one or two long α-helices at their N-terminus, thus resembling a coiled-coil domain. Besides that, several highly conserved putative phosphorylation sites were found in the N-terminal domain as well as at the C-terminal extension. Although AtARO1 downstream effectors are not known, phosphorylation of AtARO1 to regulate binding activity to its interaction partner(s) and conformational changes of the protein, especially of the long N-terminal α-helix are feasible.

4.2 Expression pattern and functional complementation of the AtARO gene family

Despite the high sequence conservation of the AtARO1 to -4 proteins, only *AtARO1* shows the same expression pattern as the wheat *TaARO1*. While *AtARO1* was shown to be expressed in mature, unfertilized egg cells and mature pollen grains by RT-PCR and promoter-GUS studies, *AtARO2 to AtARO4* were detectable in most tissues tested. Interestingly, while all transcripts of the family were detected in mature egg cells used for microarray GeneChip® hybridization experiments, only *AtARO1* was found to be expressed in mature, freshly rehydrated pollen grains. This might explain the fact that a severe phenotype was observed on the male side in the T-DNA insertion line *aro1-3* but no obvious malfunction was visible in *aro1-3* egg cells. Similarly, no phenotype was observed in ARO1-RNAi plants, where an RNAi construct was used to specifically downregulate *AtARO1* in the mature egg cells, using the egg cell specific *EC1* promoter. The overlapping expression patterns of *AtARO1 to -4* in the egg cell and the relative high levels of amino acid sequence conservation between the family members suggest that some level of functional redundancy exists among the four proteins. This redundancy might also account for the fact that overexpression of *AtARO1-GFP* in vegetative tissues did not result in any phenotypic anomalies, as *AtARO2* to *AtARO4* are already expressed at relatively

high levels in all tissues tested. However, only few lines were found showing a strong expression of the AtARO1-GFP fusion protein under the control of the 35S promoter, although the 35S promoter is known to be strongly and constitutively active in vegetative tissues (Odell et al., 1985). Further, the 35S promoter was shown to be active throughout the surface of roots and in root hairs of cotton (Sunilkumar et al., 2002) but *35Sp::AtARO1-GFP* lines showed no fluorescence in most cells of roots. As there is a putative proteolysis signal motif (KEN box, Fig. 3.2) present in AtARO1, AtARO1-GFP might be quickly degraded. On the other hand, although AtARO1 overexpression did not seem to influence any cellular growth processes of vegetative cells it might also be possible that very strong expression of the *AtARO1-GFP* fusion inhibits the growth and development of strongly expressing *35Sp::AtARO1-GFP* seedlings into mature plants. However, such assumptions have to be verified experimentally. On the other hand, neither homozygous T-DNA insertion lines *aro2*, *aro3* or *aro4* did show a phenotype, which is another strong argument for a mutual complementation. An egg cell specific triple or quadruple knock-down might be needed to reveal the function of this protein family in the female gamete. Another approach to identify the function of the AtARO1 to -4 protein family in vegetative tissues is to cross the homozygous lines of *aro2*, *aro3* and *aro4* and screen double or triple knock-down lines for phenotypes. Further, the *ARO1*-RNAi construct could be used to transform these double or triple knock-down plants and to study the effects of down-regulating several members of the AtARO family in the egg cell. However, downregulation of all functional redundant proteins in the egg cell or just as well in vegetative tissues might be lethal, as can be judged by the severe effect of *aro1-3* on pollen tube growth.

Surprisingly, few independent *ARO1*-RNAi lines and their progenies showed an approximately 50% reduced seed set. However, no correlation between this phenotype and a downregulation of *AtARO1* expression was detectable, due to the high variation of *AtARO1* transcript observed in Q-RT-PCR experiments using single, unfertilized pistils of WT as well as *ARO1*-RNAi plants as source for cDNA. As it was shown that *AtARO1* is only expressed in the fully mature egg cell, differences in maturity of the ovules within one ovary might explain the observed variations in transcript levels. Together with the fact that *AtARO1* is only expressed in one single cell in each ovule, surrounded by thousands of cells not expressing *AtARO1* but the housekeeping gene *ACT3* could make calculations using *ACT3* as normalization control quite inaccurate. Furthermore, the phenotype found in the aborted ovules was an arrest at stage FG1 or FG2 of ovule development (stages after Christensen et al., 1997). At this time point, the EC1 promoter is inactive (S. Sprunck, personal communication) but it is earliest switched on upon cellularization of the embryosac (FG5). Interestingly, our and other groups found similar arrests of female gametophyte development at FG1 or FG2 in ovules of lines transformed with a number of different RNAi constructs or overexpressing lines, independently of the promoters used or the target genes which were knocked down (B. Bellmann, G. Drews, R. Gross-Hardt, personal communications).Thus, several evidences point to the conclusion that the phenotype found in some of the *ARO1*-RNAi lines can not be attributed to a knock-down of the *AtARO1* gene. First of all, the *EC1* promoter is not active before stage FG5 or FG6 and it is specifically switched on in the egg cell. An arrest of gametophyte development at stage FG1 or FG2 is thus too early to be mediated by expression of *ARO1*-RNAi. Expression of transgenes in the haploid female gametophyte seems to often result in an untimely arrest of embryo sac development. Several putative female gametophyte

specific mutations were identified after T-DNA mutagenesis that showed the similar phenotype of an arrest of female gametogenesis at the one-nuclear stage (Johnston et al., 2007). Closer analysis revealed however, that these were not linked to the gene disruption and probably arose from maternal chromosome rearrangements or translocations during T-DNA integration. Further, a correlation between downregulation of *AtARO1* and *ARO1*-RNAi lines displaying aberrant ovule development was not observed. And finally, the overall number of plant lines displaying the embryo sac phenotype was very low (five out of 21 lines). Although severity of the RNAi effect may vary between independent transgenic lines due to copy number and/or positional effects, the overall number of lines displaying a phenotype was shown to be over 80% in several RNAi approaches directed against *Arabidopsis* genes (Chuang and Meyerowitz, 2000).

In the female gametophyte, *AtARO1* expression ceased very early after fertilization and was barely detectable after the first zygotic division and on the male side, *AtARO1* was only expressed in mature pollen grains and tubes, as was shown with *GUS* and the *AtARO1-GFP* fusion expressed under the endogenous *AtARO1* promoter. This very short expression window of *AtARO1* in the male and female gametophytes suggests an important role for AtARO1 either in the mature egg cell, during pollen tube growth, or in the fertilization process.
Analysis of putative promoter regulatory sequences revealed the presence of two pollen specific DNA-elements, the GTGA motif and the Pollen 1 LAT52 element. The pollen-specific activator element Pollen 1 LeLAT52 (AGAAA) is one part of a bipartite regulatory sequence which was first found in tomato and which consists of the 20 bp sequence AGAAATAATAGCTCCACCATA (Bate and Twell, 1998). This element was shown to enhance pollen specific transcriptional activity by 11.5-fold, but deletion or targeted mutation of either of the two sequence motifs in the Pollen 1 LeLAT52 activator abolished enhancement. The second motif (TCCACCATA) was not found in the promoter region of *AtARO1*, but only several copies of the first activator element could be detected. A regulatory role for this element during expression of *AtARO1* is thus doubtful. Anyhow, *in silico* identified regulatory sequences have to be validated experimentally to evidence their role in cell or tissue specific gene expression. As only very few egg cell specific genes have been published until now (Groß-Hardt et al., 2007; Le et al., 2005; Sprunck et al., 2005; Steffen et al., 2007), egg cell specific promoter elements are not known to date. But along the way of verifying pollen specific promoter elements through fusions of a truncated promoter to a reporter gene, sequences important for egg cell specific expression might be identified as well.

Similar to *AtARO1*, the rice gene *OsAROl-1* (MPSS annotation: LOC_Os08g43500) seems to be expressed only in mature pollen and ovary with mature stigma tissues, as revealed by the rice gene analysis MPSS (http://mpss.udel.edu/rice/) tool. It is likely that the rice gene with highest homology to the wheat *TaARO1* also shows a similar expression pattern in the egg cell and pollen grains. In contrast, sequence tags of a second rice ARO-like gene, *OsAROl-2* (MPSS annotation: LOC_Os09g36550), were found in several vegetative tissues like roots, leaves and meristems but also in ovary and mature stigma, while no expression was found in mature pollen. This pattern is highly similar to that found for *AtARO2 to -4*. It is therefore tempting to speculate that *OsAROl-1* has an

analogous function to *TaARO1* and *AtARO1*, while *OsAROl-2* might show analogy to *AtARO2* or other members of the family.

4.3 The subcellular localization of AtARO1 implicates a multifunctional role during the fertilization process

In transient as well as stable transformation assays of AtARO1-GFP fusion proteins, AtARO1 was shown to exhibit a dual localization in the cytoplasm and the nucleus, though not containing a nuclear localization sequence (NLS). As proteins >50 kDa were shown to generally require NLS or nuclear export sequences (NES) to pass through the nuclear pore complex of eukaryotic cells (Poon & Jans, 2005), and therefore a passive transport of the 101.74 kDa big fusion protein is unfeasible, an alternative way of active transport must be required to make accumulation of AtARO1-GFP in the nucleus possible. The best studied nuclear import pathway involves the importin-α/ß heterodimer of ARM repeat containing proteins, where importin-α serves as an adapter which recognizes NLS-containing cargo, whereas importin-ß interacts with the nuclear pore complex (Poon & Jans, 2005). It is imaginable that AtARO1 as a protein-interacting protein is co-transported into the nucleus by interacting with another, NLS-containing, protein. It is known that proteins change their subcellular localization in coordination with binding partners as was shown e.g. for the import of cyclin B1, which binds to cyclin F and utilizes the classical NLSs of cyclin F to “piggy-back” into the nucleus (Hood and Silver, 2000). Similarly, export of β-catenin out of the nucleus is dependent on the NES-containing proteins APC and Axin (Cong and Varmus, 2004; Willert and Jones 2006). Yet, several ARM repeat containing proteins have formerly been shown to be targeted to the nucleus in an NLS-independent manner. ß-catenin not only lacks a NES but also a classical NLS and is imported by competing with importin-ß for docking to components of the nuclear pore complex (Fagotto et al., 1998). Likewise, protein sorting studies with deletion mutants of the plant ARM repeat proteins PHOR1 (Amador et al., 2001) and ARABIDILLO-1 (Coates et al., 2006) indicated that the ARM repeats mediate their nuclear targeting. Nuclear targeting of AtARO1 might be mediated by its ARM repeats as well. Nevertheless, this remains to be tested by deletion mutants of AtARO1.

Despite its localization in the nucleus, AtARO1-GFP was also found in the cytoplasm, co-localizing with actin filaments in the shank of the pollen tube and accumulating in its very tip. Several other proteins binding directly or indirectly to the actin cytoskeleton have been found to display a dual localization in the nucleus and cytoplasm, including β-catenin (Willert and Jones 2006), proteins of the LIM family from tobacco and animals (Coghill et al., 2003; Thomas et al., 2006a), as well as mammalian myopodin (Weins et al., 2001). As actin was shown to be also present in the nuclei of plant cells (Paves and Truve, 2004), proteins binding to actin filaments could do so in the nucleus as well but they might also accomplish distinct functions in the two compartments.

However, AtARO1 is not present in the egg cell nucleus. Additionally, a small but reproducible portion of transiently transformed *UBIp::AtARO1-GFP* expressing cells exhibited either a preferential cytoplasmic localization of AtARO1-GFP, or an exclusive fluorescence at the plasma membrane. The fact that AtARO1 seems to be actively excluded from the egg cell nucleus, and the variable subcellular localization in transiently transformed epidermal onion cells rather implicates a multifunctional role for

AtARO1. Without much doubt, its nucleo-cytoplasmic shuttling is dynamically regulated, like it is e.g. known for ß-catenin/armadillo, and plakoglobin (Hatzfeld et al., 1999; Zhurinsky et al., 2000). β-catenin is phosphorylated at different positions to achieve its multiple functions, depending upon the Wnt signaling cascade (Willert and Jones, 2006). In resting cells, ß-catenin is observed mostly at the cell membrane, where it connects the cell junction protein E-cadherin and the actin cytoskeleton via α-catenin. Excess β-catenin is phosphorylated by GSK3/zw-3 (glycogen synthase kinase-3/ zeste-white-3-kinase), facilitating its degradation by the proteasome. Tyrosine phosphorylation of β-catenin modulates its association to adherens junctions. The presence of a non-phosphorylated Tyr142 in β-catenin is required for α-catenin binding, while phosphorylation of this residue aids in translocating β-catenin into the nucleus at particular developmental stages (Brembeck et al., 2004). In plants, ARC1 is recruited to different subcellular compartments depending on its phosphorylation state (Stone et al., 2003) and the phytohormone gibberellin was reported to induce the migration of PHOR1 into the nucleus (Amador et al., 2001). It is thus conceivable that changes in intracellular localization of AtARO1 are partly mediated by phosphorylation, induced trough exogenous signals or the physiological state of the individual cell. As mentioned before, several putative phosphorylation sites were found in AtARO1 and, amongst other phosphorylation sites, two tyrosine residues in the N- and C-termini of ARO1-like proteins are highly conserved.

4.4 AtARO1 is involved in the dynamic organization of actin filaments and probably also in the tip regulatory network of the growing pollen tube

The co-localization of AtARO1 with the actin bundles in the shank of the pollen tube and its high accumulation in the pollen tube tip suggests a role of AtARO1 in actin-mediated polar tip growth processes, as is also implied by the disrupted actin cytoskeleton and the arrested growth phenotype of *aro1-3* pollen tubes. Another allele of *aro1* (*seth4*) was previously identified as one out of nine male-specific progamic phase *Ds* transposon mutants, termed as "*seth1" to "seth9*" (Lalanne et al., 2004). The *Ds* insertion was found to be at position +550 bp, corresponding to amino acid position 183 in AtARO1. This is within the first helix of the second ARM repeat R2, while the insertion *aro1-3* is situated further downstream, within H1 of repeat R4. Interestingly, *seth4* mutant pollen showed a more severe phenotype and completely failed to germinate (Twell, unpublished). It is conceivable that truncated versions of *AtARO1* are still translated in the two different insertion lines and that the truncated protein expressed in *aro1-3* might retain at least some capabilities to bind one of its interaction partners. It has been speculated beforehand, that ARM motifs are at least partially independent and additive in their function, as was shown for β-catenin (Pfeifer and Wieschaus, 1990). However, a single ARM repeat does not seem to form a stable structure (Hatzfeld, 1999), and proteins found in *Arabidopsis* display at least two ARM repeats, each. Thus, the truncated AtARO1 protein in *seth4* mutants, containing only the first incomplete ARM repeat R1 (consisting of putative helices H2 and H3) is rather unlikely to show residual functionality.

It is well established that actin is organized in a very dynamic way during pollen germination and at the tip of polar growing pollen tubes and root hairs (Baluska et al., 2000; Ren and Xiang, 2007) and that it is involved in a highly complex and interconnected network. Upon hydration, pollen grains are

transformed from nonpolar cells to highly polarized cells and arrays of F-actin bundles focus towards the site of pollen tube emergence (Heslop-Harrison & Heslop-Harrison, 1992). Inhibition of actin polymerization by Latrunculin B (LatB) and cytochalasins hampers pollen germination and effectively blocks tube growth (Gibbon et al., 1999). If the ARM repeat domain ARD1 of AtARO1 would be mainly involved in actin organization during pollen germination, and if ARD2 would play a further important role during pollen tube tip growth, the differing phenotypes of *aro1-3* and *seth4* could be explained by the fact that the residual functionality of ARD1 in *aro1-3* mutants allows pollen grains to germinate but that further tip growth is inhibited, while *seth4* mutants already fail to undergo the initial steps of the germination process.

The co-localization of AtARO1-GFP along actin cables in the shank of the pollen tube and the *aro1-3* phenotype strongly suggest an involvement of AtARO1 in polar orienting actin filaments towards the germination pore and/or parallel to the growth axis of pollen tubes. Axially orientated actin cables in the shank of the pollen tube are fundamental for tip growth as they, together with myosins, cause cytoplasmic streaming and transport organelles and secretory vesicles directional towards the apex (Hepler et al., 2001). The observed growth depolarization and growth arrest of *aro1-3* pollen tubes might thus be a consequence of the breakdown of polar vesicle transport, caused by the loss of organized F-actin. However, in *aro1-3* pollen tubes we observed the disordered meshwork of short actin filaments to extend into the very tip. This breakdown of spatial regulation of F-actin dynamics suggests a close connection between AtARO1 and the tip growth machinery of *Arabidopsis* pollen tubes.

Precise analysis of the actin pattern in the apex of pollen tubes has manly been reported for lily and tobacco (Fu et al., 2001; Kost et al., 1998; Lovy-Wheeler et al., 2005; Vidali and Hepler, 2001). Only little information on the cellular organisation of the slowly growing pollen tubes from *Arabidopsis* is available to date *in vivo* or *in vitro* (Derksen et al., 2002 and references therein) and it is not known for sure, whether the actin cytoskeleton in *Arabidopsis* pollen tube tips is organized in a similar way than it is in pollen tubes of other, fast growing angiosperms (Gu et al., 2003). In both tobacco and lily pollen, short actin filaments are present in the extreme apex of the pollen tube tip and new staining and fixation techniques revealed a longitudinally-oriented cortical actin fringe, located few micrometers behind the tip (Wilsen et al., 2006). This actin fringe is thought to organize confined vesicle docking and fusion (Lovy-Wheeler et al., 2005), and thick actin bundles do not reach this region. By contrast, in the slow-growing pollen tubes of *Arabidopsis* and gymnosperms as well as in root hairs, evidence of diffuse actin clouds or short actin filaments in the extreme tip were reported (Gu et al., 2003; Samaj et al., 2006). In *Arabidopsis* root hairs, a tip-concentrated F-actin microfilament network was found in the vesicle rich zone (Vincent et al., 2005). In root hairs as well as gymnosperm pollen tubes, no actin fringe or cortical actin was observed so far and the spatial organization of the cytoskeleton and the interconnected endo- and exocytotic processes seem to be dependent on the individual growth characteristics of the tip growing cells (Samaj et al., 2006).

The intensity of AtARO1-GFP is strongest within the first few µm of the tip, where the short filaments or actin patches were detected, and the fluorescence fills the apex in a cup-shaped fashion. This fluorescent pattern does not correspond to the observed distribution of secretory vesicles in *Arabidopsis*, which, unlike the inverted cone shape found in lily or tobacco pollen tubes, appear to

evenly fill the whole clear zone of the pollen tube tip (Derksen et al., 2002; Lennon and Lord, 2000 and references therein).

The tip-enriched distribution of AtARO1 could implicate a role in either spatially restricted actin nucleating processes at the pollen tube tip, or in signal transduction from membrane-bound interaction partners of AtARO1 to e.g. actin binding proteins. Formins are a family of proteins that are involved in actin nucleation and the generation of new actin filaments *in vitro* as well as formation of unbranched, longitudinal actin bundles (Faix and Grosse, 2006). Formins bind actin filaments at their barbed ends and, as they antagonize capping proteins, are ideal for generating very long actin filaments. In yeast and plants, formins have been found to be important for cell polarity and cytokinesis (Ren and Xiang, 2007). In plants, a subset of plant-specific formins, referred to as group I formins, was identified (Cheung and Wu, 2004). They are distinct from animal and yeast formins in the respect that they contain an N-terminal signal peptide and a transmembrane domain. *Arabidopsis* AtAFH1 was found to locate to the plasma membrane of growing pollen tubes and overexpression of this formin resulted in formation of supernumerary actin cables and ballooned pollen tube tips (Cheung and Wu, 2004). It was proposed that cell-surface AtAFH1 and other group I formins might have analogous functions to integrins from animals in mediating extracellular stimuli to the cytoskeleton. Interestingly, the mammalian diaphanous-related formin mDia1 contains an ARM repeat region (ARR; Faix and Grosse, 2006; Kovar, 2006) that is involved in Rho GTPase signaling as well as auto-inhibition. In absence of Rho-GTP, ARR binds to a second domain within the same protein leading to auto-inhibition. Binding of active Rho and further unknown signaling molecules relieves this interaction, leading to actin nucleation and elongation by mDia1 (Faix and Grosse, 2006). As formins with ARM domains were not detected in plants yet, it is tempting to speculate that ARM repeat containing proteins, like AtARO1, might be involved in regulating ROP1 mediated activation of formins like, e.g., AtAFH1. Other ARM repeat containing proteins, like the aforementioned $p120^{ctn}$, were also shown to be involved in RhoA signaling as well as Rac and Cdc42 activity, leading to actin re-organization and an increase in cell motility in animals (Anastasiadis, 2007).

An involvement of AtARO1 in Rop GTPase dependent signaling would also be in agreement with the fact that tip-localized AtARO1 was shown to shift more laterally towards the future site of tip growth upon growth reorientation. ROP1 and RIC4 (ROP-interactive CRIB motif-containing 4), a downstream target of ROP1 in pollen tubes involved in apical F-actin assembly (Gu et al., 2005), were shown to relocate towards the future growth direction of pollen tube tips as well and thus indicate a spatial regulation of ROP1 in tobacco pollen tubes (Hwang et al., 2005). It was proposed that an increase in ROP1 activity and an increase of RIC4 at the apical plasma membrane is oscillatory and precedes a new burst of growth. Furthermore, AtARO1 was found in varying amounts in the pollen tubes observed, occupying between 0.7 µm and 5 µm of the apex, measured from the tip. Whether this variation can be attributed to an oscillatory increased accumulation of AtARO1 in the tip, correlating with growth oscillations, remains to be investigated experimentally. Anyway, this spatial regulation suggests a close connection between AtARO1 and the tip growth machinery of *Arabidopsis* pollen tubes.

The results obtained during this work indicate that AtARO1 is important for both, the formation of polar actin filaments in the pollen tube shank, and the complex regulatory system of the tip growth

machinery. Both processes require dynamic re-organization of F-actin. Binding of AtARO1 to actin is conceivable; however, we did not find a direct interaction with G-actin in the yeast two hybrid system. Other putative binding partners of AtARO1 could not be identified by an yeast two hybrid screen using a cDNA from germinated pollen tubes. Interestingly, a recent study of protein-protein interactions with TAP (tandem affinity purification) tagged protein kinases of rice revealed the presence of the rice OsAROl-1 (MPSS annotation/TIGR rice genome annotation: LOC_Os08g43500) in a protein complex together with a wall associated kinase (WAK), a serine/threonine kinase, a putative succinate dehydrogenase, a putative helicase protein, tubulin-α, a subunit of tubulin-β, as well as actin (Rohila et al., 2006). The plant specific WAK kinases have a cytoplasmic Ser/Thr kinase domain, span the plasma membrane and extend into the cell wall. The extracellular region has similarity to vertebrate epidermal growth factor (EGF)-like domains (Verica and He, 2002). WAKs are thought to link the extracellular matrix with the cytoskeleton and to mediate signaling between them. A large amount of WAKs is covalently linked to pectin (Kohorn, 2000). Until now, WAK or WAK-like kinases were not found to be expressed specifically in pollen (Deceux and Mesiaen, 2005), however, they would be interesting candidates to link the pectin containing extracellular matrix at the tip of pollen tubes to the actin cytoskeleton via ARM repeat containing proteins from the ARO-like family. In a complex similar to that found in the study of Rohila et al (2006), ARO-like proteins could be involved in recognizing extracellular signals and induce downstream events in response to these signals, as for example regulate actin dynamics.

If AtARO1 would interact directly with F-actin, or if its interaction partners would be membrane-bound proteins or members of a membrane-associated complex, a yeast two hybrid screen suited for soluble proteins is not apt for detecting such interactions (Wang et al., 2004). Instead, distinct approaches would be necessary, like e.g. the TAP-tag used in rice. Another possibility would be a Split-Ubiquitin Membrane Yeast Two-Hybrid System (Iyer et al., 2005) to detect membrane-bound interaction partners of AtARO1. A co-sedimentation assay would be required to analyze AtARO1s ability to directly bind to F-actin (Thomas et al., 2006a).

Due to its strong accumulation in the tip of the growing pollen tube, its connection to actin filaments in the shank and its localization to the nucleus, AtARO1 could enable a rapid coordination of cytoskeletal organization and gene expression throughout the pollen tube in response to signaling at the tip plasma membrane.

4.5 Tip-localization of AtARO1 is dependent on the secretory pathway

Root hair specific ROP2 was shown to localize to small intracellular spots in addition to its membrane localization, which was argued to be indicative for its vesicle associated transport towards the apex (Samaj et al., 2006). Further, the membrane associated ROP2 was shown to be recycled by co-localization experiments with the endocytic dye FM4-64 in root hairs. AtARO1 appeared to also localize to a few small spots which were dispersed throughout the cytoplasm. Strikingly the distribution of AtARO1 was affected by both, the depolymerisation of F-actin trough treatment with LatB and the inhibition of exocytosis mediated by BFA. While LatB treatment completely abolished the arrays of filamentous AtARO1-GFP structures upon actin depolymerisation in the shank, distribution of AtARO1-

GFP in the tip remained, but was weaker and more dispersed. Thus F-actin filaments might help in spatially restricting AtARO1-GFP accumulation at the tip. BFA in contrast completely removed AtARO1-GFP from the tip and the fusion protein was instead found in numerous bright spots throughout the cytoplasm. Neither the small spots visible before chemical treatment nor the fluorescent bodies appearing after BFA addition showed co-localization with the endocytic dye FM4-64 in small vesicles or with FM4-64 labelled BFA-induced compartments, known to appear in the subapical region of BFA treated pollen tubes (Baluska et al., 2002). In animal and plant cells, BFA was shown to inhibit exocytosis by inactivating Golgi-associated ARF-GEFs and thus impairing the formation of coated vesicles, cargo selection and packaging, as well as the maintenance of the Golgi structure (D´Souza-Schorey and Chavrier, 2006; Xu and Scheres, 2005). One BFA-sensitive ARF-GEF found in plants is GNOM, which was shown to be involved in establishing the apical-basal polarity of the *Arabidopsis* zygote and embryo (Steinmann et al., 1999). Another ARF-GEF protein related to GNOM, GNOM-like 2 (GNL2) was further shown to play a specific role in pollen germination and to accumulate in the growing pollen tube tip (G, Jürgens, unpublished). Here it is believed to be involved in exocytotic processes.

The subcellular localization of AtARO1-GFP upon BFA treatment implicates that AtARO1 is involved either actively or passively in formation or trafficking of exocytotic vesicles. AtARO1 might be associated with the plasma membrane of secretory vesicles and thereby transported to the apical clear zone of the growing tip but obviously is not recycled back as other membrane components. As AtARO1 localizes in part near or at the plasma membrane of transiently transformed cells and accumulates in a BFA-sensitive way at the tip-growth domain of pollen tubes, it is conceivable that AtARO1 is recruited to the tip of the growing pollen tube by an internal cue. This cue might be bound to the plasma membrane and thus be BFA-sensitive. Through such a mechanism, polar AtARO1 localization would change upon BFA treatment without AtARO1 itself being bound to the plasma membrane. Molendijk et al. (2001) proposed that Rop proteins might be targeted to the root hair initiation zone in a similar way. Another possibility is the passive transport of AtARO1. ß-catenin is for example known to bind to the cytoplasmic tail of the transmembrane receptor E-cadherin early in the biosynthetic pathway. Both proteins are then sorted, as a complex, for directional delivery to the adherens junction plasma membrane domains (Bryant & Stow, 2004).

Moreover, in mammals the GTPase-driven formation of actin coats on exo- and endocytotic vesicles has been described (Cao et al., 2005; Fernandez-Borja et al., 2005; Taunton, 2001), which are thought to be involved in the recruitment of proteins necessary for vesicle formation and/or budding, as well as in the actin-propelled motility of vesicles. Similarly, in plant root hairs Vincent et al. (2005) proposed from their analysis of *Atsfh1* (*Arabidopsis thaliana* Sec fourteen homolouge1) knock-outs, that PtdIns(4,5)P_2 “landmarks” are generated on emerging secretory vesicles, that drive F-actin assembly for polar vesicle secretion towards the apex. Thereby, the insertion of membrane-associated Ca^{2+}-channels might be restricted to the extreme apex of root hairs and the emerging tip-high Ca^{2+} gradient reinforces polarized actin assembly and thus tip-directed membrane trafficking (Vincent et al., 2005). If AtARO1 would be involved in targeting actin filaments to secretory but not endocytotic vesicles, the effect of BFA treatment on AtARO1-GFP distribution in pollen tubes could be explained by the inflicted disorder of the secretory system. Inhibition of the secretory pathway might result in a

redistribution of AtARO1-GFP from the vesicle-depleted tip to the trans-Golgi network, where formation of new vesicles is halted. Co-localization studies of AtARO1-GFP with fluorescent markers for the trans-Golgi network could further strengthen this hypothesis.

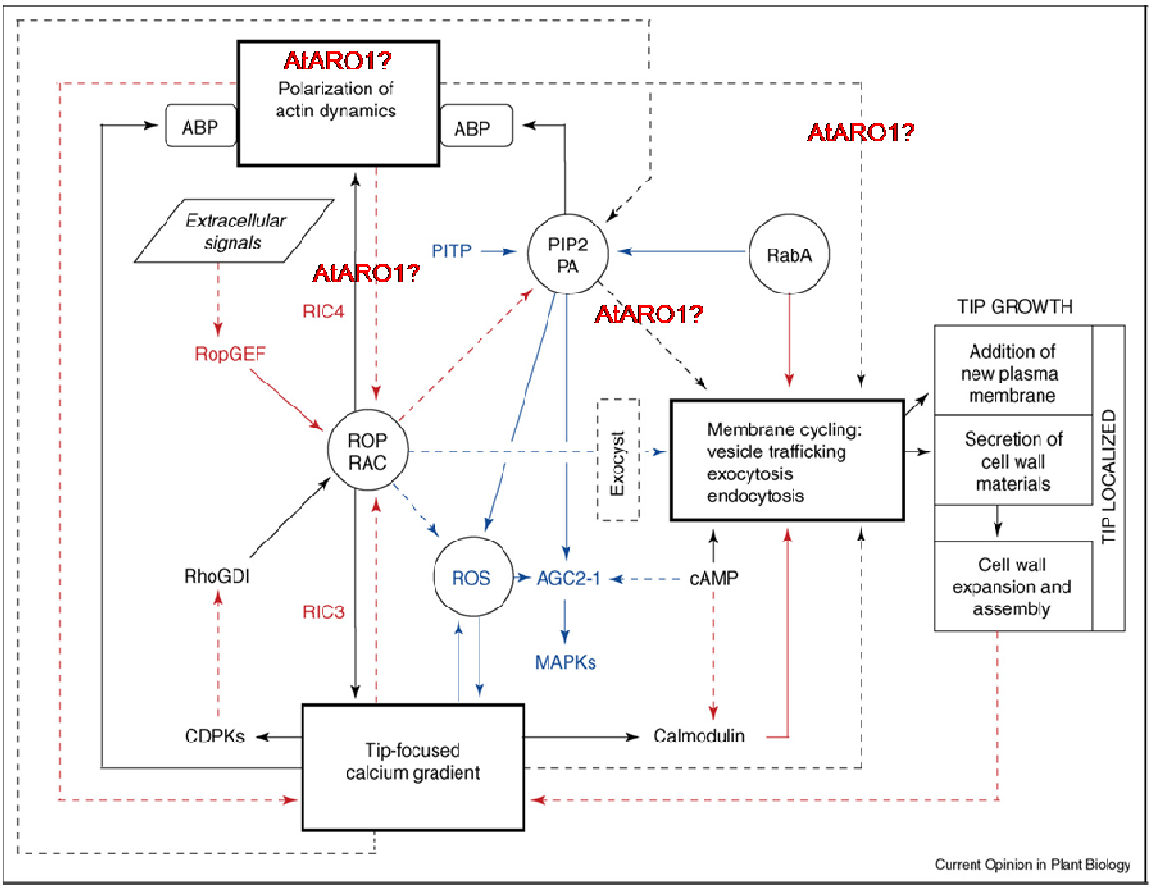

Fig. 4.1. Figure and text adapted from: Cole and Fowler (2006). A model of the tip growth LENS (for localization enhancing network, self-sustaining) in higher plants. Three major components of the tip-focusing machinery – a gradient of actin dynamics, a tip-focused calcium gradient, and membrane cycling (boxes with thick outlines) – are interconnected by a network of signaling pathways that lead to tip growth by the addition of new plasma membrane and cell wall to the tip. The circled components, ROP/RAC GTPases, phosphoinositides (PtdIns[4,5]P2 and PA), RabA GTPases, and ROS, represent key hubs of these signaling pathways. Solid interconnecting lines represent pathways that have been experimentally verified in tip-growing cells. Dotted lines represent hypothetical pathways for which there is some experimental evidence. Each line might represent multiple steps in a signaling pathway. Red lines indicate those pathways that have been identified in pollen tubes, blue lines are pathways identified in root hairs, and black lines are pathways identified in both types of tip-growing cells. The arrows indicate the direction of influence, but do not distinguish between positive and negative effects. AGC2-1, an AGC family protein kinase, also known as OXI1; cAMP, cyclic AMP; MAPK, mitogen-activated protein kinase. Feasible participation of AtARO1 in the signaling pathways is indicated.

4.6 What is the role of AtARO1 in the egg cell and during double fertilization?

Any evidence for the function of AtARO1 in the egg cell is still missing due to the lack of a phenotype, originating from the likely functional redundancy of the AtARO protein family. However, fascinating insights into a possible role of AtARO1 in dynamic actin organization in the receptive synergid and the egg cell were given from observations of the distribution of AtARO1 in the egg cell shortly after pollination as well as co-localization of actin and AtARO1 during the fertilization process.

In the mature embryo sac, extensive actin filaments arranged in parallel bundles longitudinally to the micropylar-chalazal axis were found in the synergids of *Arabidopsis*. The egg cell and central cell did not reveal strong actin staining with the staining procedure used in the present work, although in other plant species, like nun orchid (Ye et al., 2002) and *Torenia fournieri* (Fu et al., 2000), short actin bundles were found to be randomly distributed throughout the egg and central cell. However, microinjection was used to visualize F-actin in *Torenia fournieri*, and the embryo sacs of nun orchids were digested with cell wall degrading enzymes and dissected from ovules to allow better penetration of the actin dye rhodamine-phalloidin. Thus, an alternative method to visualize the delicate actin filaments inside the deeply embedded cells of the embryo sac will be necessary as well to better reveal the cytoskeleton structure in *Arabidopsis* female gametophytes.

Despite these difficulties of actin staining inside the female gametes, changes in actin organization in the degenerating synergid were clearly visible. Upon pollen tube arrival, the parallel actin bundles disintegrate and form aggregates at the chalazal end of the degenerating synergid. These rearrangements of the actin cytoskeleton were also observed in synergids from other plant species (Fu et al., 2000, Ye et al., 2002). Subsequently, so called actin coronas are formed at the interfaces between the synergids, egg and central cell in the female gametophytes of tobacco, maize, orchid and *Torenia fournieri* (Fu et al., 2000; Huang et al., 1999; Russell, 1993; Ye et al., 2002). Similarly, a narrow actin band was detected in this work, namely at the border of the degenerating synergid of *Arabidopsis* ovules, extending towards the egg and central cell. Strikingly, the pollen tube derived AtARO1-GFP co-localized with this narrow actin band. Moreover, H3.3-mRFP1 labeled sperm cells were found to migrate at the corresponding site, along the outer border of the degenerating synergid, towards their sites of fusion. Despite their immense role during sperm cell tracking and double fertilization, it is not known how actin coronas are formed in the environment of a degenerating synergid cell (Weterings and Russell, 2004). It is tempting to speculate that proteins from both, the synergid and pollen tube play important roles during this process, and that pollen tube derived AtARO1 is involved in dynamic reorganization of synergid-derived F-actin structures.

In the egg cell, AtARO1-GFP is evenly distributed throughout the cytoplasm, but excluded from the egg nucleus, as observed by live imaging. However, after fixation and staining for visualization of actin, AtARO1-GFP appeared as fine filaments inside the cytoplasm. These filaments might on the one hand represent transvacuolar strands which pervade the large vacuole at the micropylar end of the egg cell. On the other hand, although no actin filaments could be detected in this area, the fine green fluorescent filaments strongly resemble the filamentous structures of AtARO1-GFP bound to very fine actin filaments in the pollen tube. Whether AtARO1-GFP is associated with the actin cytoskeleton in the egg cell as well will need further, sophisticated experimentation.

A hint towards the involvement of egg cell derived AtARO1 in the fertilization process was given by the observation that AtARO1-GFP redistributes towards the micropylar end of the egg cell and is found in small fluorescent spots already one hour after pollination, before pollen tubes reach the ovules. It is well known that pollination can trigger a multitude of developmental events in the embryo sac, despite the long distance between the receptive tissue (stigma) and the ovule. Examples are the induction of final stages of megagametogenesis, synergid degeneration, or the establishment of calcium gradients, preparing the ovule for fertilization and embryogenesis (O´Neill, 1997; Wetering and Russell, 2004). Thus, AtARO1 might be involved in the actin organization necessary for a possible polar transport of vesicles towards the micropylar end of the egg cell, necessary for establishing e.g. calcium gradients or the secretion of signals for cell-cell communication (Dresselhaus, 2006). Another role for AtARO1 in the egg cell might be the fertilization induced actin re-organization to arrange F-actin for forming a membrane protrusion at the chalazal end of the egg cell for uptake of the sperm. Such an extension of the egg cell membrane, containing abundant actin filaments, was shown to be present in nun orchids (Ye et al., 2002), resembling the actin-driven formation of microvilli which participate in sperm-egg binding as well as sperm entry in animal oocytes (Sun & Schatten, 2006). Further processes in fertilization and early embryogenesis in *Arabidopsis*, which are likely to rely on actin dynamics are the movement of the egg cell/zygote nucleus after plasmogamy, or the elongation of the zygote as was e.g. shown for the fucoid brown algae (Hable et al., 2003).

4.7 Outlook

The most important step towards discovering the precise function of AtARO1 in the egg cell and pollen tube will certainly be to identify its interaction partners. As mentioned before, approaches other than conventional yeast two hybrid assays should be applied. Conceivable are e.g the Split-Ubiquitin Membrane Yeast Two Hybrid, which has been successfully applied to identifying previously unknown membrane bound interaction partners of e.g. ER-resident bait proteins of humans (Wang et al., 2004) or transmembrane receptors in plants (Pandey and Assmann, 2004). A method often used to analyze direct interaction of a given protein with F-actin is the co-sedimentation assay (for plants e.g. Thomas et al., 2006a). For this assay, a HIS-tagged AtARO1 could be expressed in bacteria, purified and pelleted together with F-actin. In a different approach, tandem affinity purification-tagged (TAP-tagged) proteins as AtARO1 to-4 can be expressed as transgenes in plants and isolated together with their interaction partners as was shown previously (Rohila et al., 2006). These proteins have to be separated with SDS-PAGE and can be analyzed by mass spectrometry. Membrane-associated and transmembrane proteins have been successfully isolated using this method (Rohila et al., 2006). Further, some proteins which are known to be involved in the growth signaling network at the pollen tube tip could be tested in direct interaction assays with AtARO1. Promising candidates are, for example, AtROP1 and AtRIC4, which were shown to work in the same pathway to promote actin assembly (Gu et al., 2005). Another possible candidate is the pollen specific formin AtAFH1, as inhibitory effects on the actin-nucleating activity of AtAFH1, similar to those mediated by intrinsic ARM domains in mammalian Diaphanous-related formins, might be achieved in plants by binding of AtAFH1 to an ARM repeat containing protein like AtARO1.

The fact that the two ARM domains of AtARO1 might have in part independent but additive roles can be assumed by the differing phenotypes of *aro1-3* and *seth4* mutants. More precise answers to the function of single domains of the AtARO1 protein will be given through deletion mutants of e.g the N-terminal domain of yet unknown function or the ARM repeat domains ARD1 or ARD2, respectively. The existence of phosphorylation sites can be shown by single amino acid substitutions of Ser, Thr or Tyr residues highly conserved in the ARO1-like proteins.

In addition, the nature of the fluorescent bodies, which appear in AtARO1-GFP expressing pollen tubes after BFA treatment, should be analyzed thoroughly. Transient transformation of AtARO1-GFP expressing pollen tubes with fluorescent markers for different compartments of the secretory pathway could be carried out. On the other hand, crossings of AtARO1-GFP expressing plants with marker lines expressing fluorescent proteins labeling different compartments of the secretory pathway could reveal a co-localization and thus strengthen the hypothesis that AtARO1 is involved in vesicle budding or transport. Additionally, live imaging of individual AtARO1-GFP expressing pollen tubes during a growth period will not only verify whether AtARO1 accumulation in the tip is oscillatory and precedes or follows a growth spurt but also uncover the changes in AtARO1 tip-localization upon growth reorientation of individual pollen tubes.

On the female side, the first aim should be to produce an egg cell specific triple knock-down of the genes *AtARO1*, *AtARO2*, and *AtARO3*. As AtARO4 is quite distant on the protein level from the other three members of the gene family, it is likely that a triple knock-down will be sufficient to induce a phenotype in the female gamete. However, it is also possible that a knock-down of the whole gene family will be needed to reveal its function in the ovule. This triple or quadruple knock-down might be achieved by using an RNAi construct directed against a highly conserved region of all four *AtARO1 to -4* genes under the control of the egg cell specific EC1 promoter. A knock-down of all *AtAROs* under the control of a ubiquitously expressed promoter or crossing of the homozygous *aro2*, *aro3* and *aro4* T-DNA insertion lines on the other hand might be lethal, as the strong phenotypic effect of *aro1-3* on the cytoskeleton in pollen tubes and the high conservation of ARO proteins amongst plant species implicates an important function for the ARO proteins in plant development. A further procedure to reveal the function of proteins often used in molecular biology is overexpression of the gene of interest. Overexpression of *AtARO1* in vegetative tissues under the control of the 35S promoter did not result in any phenotypes. Moderate overexpression of AtARO1-GFP under the control of the endogenous promoter in pollen tubes and egg cells did neither result in a visible phenotype. However, plants showing strong overexpression in all vegetative tissues, especially in roots, could not be generated. Thus, if only very strong overexpression of AtARO1-GFP results in inhibition of plant development, the use of the strong and egg cell specific *EC1* promoter identified in our group (B. Bellmann and S. Sprunck, unpublished) could lead to further insights into the function of AtARO1 in the egg cell.

Finally, new staining methods of the actin cytoskeleton, like those described by Lovy-Wheeler et al. (2005) might improve the labeling of the fragile actin cytoskeleton in the male and female gametophytes. Stable transformation of *Arabidopsis* with ubiquitously or specifically expressed adequate actin binding proteins (ABPs) fused to RFP or YFP might allow the live visualization of cytoskeletal changes in the egg cell and pollen tube upon pollination and fertilization and help to

unravel the role of AtARO1-GFP in these processes. Conceivable ABPs are on the one hand WLIM1 (Thomas et al., 2006a) or the actin binding domain 2 of fimbrin (Sheahan et al., 2004), which were already shown to interact with actin as a GFP fusion protein *in vivo*. On the other hand, ABPs known to bind to the long actin bundles in the shank of pollen tubes, like e.g. Vilin (Ren and Xiang, 2007) could be used.

5. SUMMARY

Plant gametogenesis, double fertilization and embryogenesis fascinate scientists since centuries. Microscopic analysis revealed the morphology of these processes, while the underlying molecular mechanisms are only previously starting to be unraveled. During the double fertilization process, a pollen tube lands on the female stigma and produces a long, polar outgrowth, the pollen tube. This pollen tube grows through the female tissues over a long distance, guided by different cues, to deliver the two sperm cells to the female gametophyte. This process requires a complex signaling network interconnected with the dynamic organization of the actin cytoskeleton.

The aim of this work was to identify the function of an ARM repeat protein encoding gene from *Arabidopsis*, whose homologous gene from wheat (*Triticum aestivum*) was found to be specifically expressed in egg cells and anthers. In the model plant *Arabidopsis thaliana* four proteins with similarity to the putative wheat ARM repeat protein were identified, and further putative homologues were found in several other plant species. As similar proteins are also present in the moss *Physcomitrella patens*, these newly identified proteins represent a phylogenetically old protein family. These proteins revealed no other known protein motifs in addition to the ARM repeats, and were thus named as Armadillo repeat only (ARO) proteins. All AtARO and ARO-like proteins showed a conserved amino acid sequence and overall structure. They comprise two ARM repeat containing domains (ARD1 and ARD2), which are separated by a highly divergent spacer sequence. Furthermore, they exhibit an N-terminal domain featuring one or two long α-helices and a C-terminal extension, both of which contain putative conserved phosphorylation sites. Expression studies via RT-PCR and QRT-PCR, evaluation of microarray data and promoter-reporter gene studies in transgenic plants revealed that *AtARO1* is specifically expressed in the mature egg cell, in mature pollen grains and in germinating pollen tubes. In contrast, the other members of the family (*AtARO2*, *AtARO3*, *AtARO4*) were found to be expressed more ubiquitously, including egg cells. However, their transcripts are absent in pollen.

The function of *AtARO1* was analyzed using two approaches. On the one hand three different T-DNA insertion lines, two insertions in the potential promoter (*aro1-1* and *aro1-2*) and one insertion at the end of ARD1 (*aro1-3*), were analyzed for aberrant phenotypes, especially in reproductive tissues. On the other hand, *AtARO1* was specifically knocked-down in egg cells using an egg cell specific promoter and the RNAi approach. The female gametophyte did not show any alterations upon downregulation through RNAi or in *aro1-3* T-DNA insertion lines. Similarly, overexpression of AtARO1-GFP in vegetative tissues did not alter the overall plant morphology. Both effects can be explained by a functional redundancy of the AtARO protein family, which in the egg cell results in functional complementation of AtARO1. A core promoter element necessary for cell-specific expression of *AtARO1* could be restricted to the length of 327 bp upstream of the start codon due to the fact that insertion lines *aro1-1* and *aro1-2* did not show any phenotype. Reciprocal crossings showed that the *aro1-3* allele could only be transmitted via the female gametophyte, indicating that the male gametophyte must be affected. Further analysis of the *aro1-3* pollen tube morphology and the actin cytoskeleton revealed depolarized growth, resulting in short and plump pollen tubes, which could be attributed to a severe disorganization of the actin cytoskeleton.

In coincidence with these findings, an AtARO1-GFP fusion protein expressed under the control of the endogenous *AtARO1* promoter was found to be localized in the cytoplasm of germinated pollen tubes and to co-localize with the rhodamine-phalloidin stained actin cytoskeleton. The fusion protein was shown to be functional *in planta*, as it could complement the *aro1-3* phenotype. In addition to its cytoplasmic localization, AtARO1-GFP localized in the pollens´ vegetative nucleus and accumulated at the pollen tube tip, while it was completely absent in sperm cells. As AtARO1-GFP was only detected in the cytoplasm of egg cells but not in the nucleus, it can be concluded that it is probably actively excluded from the nucleus in this cell type. The differential localization of AtARO1 was further emphasized by the finding that it localized exclusively to the plasma membrane in a small but reproducible number of transiently transformed epidermal onion cells.

A potential function of AtARO1 in the tip of growing pollen tubes can be assumed as AtARO1-GFP accumulates in the pollen tube tip, as this accumulation appears to oscillate, and as the tip localized AtARO1-GFP was found to reorient towards the future site of tip growth upon a directional change of the pollen tubes growth track. The co-localization of AtARO1-GFP and actin was further substantiated by treatments of AtARO1-GFP expressing pollen tubes with the F-actin disrupting drug LatB, which abolished both, the actin bundles and the filamentous distribution of AtARO1 in the shank of the pollen tube. However, the apical accumulation of AtARO1 was only affected to a minor extend, implicating that actin might aid in restricting AtARO1 to the tube tip. Upon treatment with the exocytotic inhibitor BFA, the distribution of AtARO1-GFP changed dramatically into accumulations of strong fluorescent bodies throughout the shank, and a complete evanescence of AtARO1-GFP from the tip. From these results it can be concluded that the accumulation of AtARO1 in the tube tip is dependent on exocytosis, and that AtARO1 not only is important to establish polar orientated F-actin bundles necessary for polar tip growth, but might participate in the highly active and polarized secretory machinery of growing pollen tubes.

The localization of AtARO1-GFP in the female gametophyte upon pollen tube arrival revealed that pollen-derived AtARO1 co-localizes with a narrow F-actin band emerging in the degenerating synergid of *Arabidopsis*. It is known that the pollen tube releases its contents into the receptive synergid of the ovule, and that the sperm cells migrate along emerging actin coronas towards their sites of fusion, the egg and central cell. The present results of this work indicate that AtARO1 might be involved in establishing F-actin structures necessary for sperm cell migration. The role of AtARO1 in the egg cell however, needs to be elucidated in future studies. Due to the functional redundancy of AtAROs in the egg cell, sophisticated experiments will be necessary to reveal their function in the female gametophyte, before or during the fertilization process.

To reveal the precise function of AtARO1 in both, the egg cell and pollen tube, the identification of interaction partners is indispensible. As conventional yeast two hybrid assays did not lead to any results, other approaches, taking in account the possibility of membrane bound interaction partners of AtARO1, might give valuable hints on AtARO1 function in the future.

6. LITERATURE

Acosta-García, G., Vielle-Calzada, J.-P. (2004). A classical arabinogalactan protein is essential for the initiation of female gametogenesis in Arabidopsis. *Plant Cell* **16**, 2614-2628

Akiyama, T. (2000). Wnt/β-catenin signaling. *Cytokine Growth Factor Rev* **11**, 273-282

Alonso, J.M., Stepanova, A.N., Leisse, T.J., Kim, C.J., Chen, H., Shinn, P., Stevenson, D.K., Zimmermann, J., Barrajas, P., Cheuk, R. et al. (2003). Genome-Wide insertional mutagenesis of *Arabidopsis thaliana*. *Science* **301**, 653-657

Amador, V., Monte, E., García-Martínez, J., Prat, S. (2001). Gibberellins signal nuclear import of PHOR1, a photoperiod-responsive protein with homology to *Drosophila* armadillo. *Cell* **106**, 343-354

Andersen, P., Kragekund, B.B., Olsen, A.N., Larsen, F.H., Chua, N., Poulsen F.M., Skriver, K. (2004). Structure and biochemical function of a prototypical *Arabidopsis* U-box domain. *J Biol Chem* **279**, 40053-40061

Baluska, F., Salaj, J., Mathur, J., Braun, M., Jasper, F., Samaj, J., Chua, N.-H., Barlow, P.W., Volkmann, D. (2000)**.** Root hair formation: F-actin-dependent tip growth is initiated by local assembly of profilin-supported F-actin meshworks accumulated within expansin-enriched bulges. *Dev Biol* **227,** 618-632

Baluska, F., Hlavacka, A., Samaj, J., Palme, K., Robinson, D. G., Matoh, T., McCurdy, D. W., Menzel, D., Volkmann, D. (2002). F-actin dependent endocytosis of cell wall pectins in meristematic root cells. Insights from Brefeldin A-induced compartments. *Plant Phys* **130**, 422-431

Bannigan, A., Baskin, T.I. (2005). Directional cell expansion- turning toward actin. *Curr Opin Plant Biol* **8 (6)**, 619-624

Bate, N., Twell, D. (1998). Functional architecture of a late pollen promoter: pollen-specific transcription is developmentally regulated by multiple stage-specific and co-dependent activator elements. *Plant Mol Biol* **37 (5)**, 859-869

Becker, J.D., Boavida, L.C., Carneiro, J., Haury, M., Feijó J.A. (2003). Transcriptional profiling of *Arabidopsis* tissues reveals the unique characteristics of the pollen transcriptome. *Plant Phys*. **133**, 713-725

Berger, F. (2008). Double-fertilization, from myths to reality. *Sex Plant Reprod* **21**, 3-5

Berken, A., Thomas, C., Wittinghofer, A. (2005). A new family of RhoGEFs activates the Rop molecular switch in plants. *Nature* **436**, 1176-1180

Boavida, L.C., McCormick, S. (2007). Temperature as a determinant factor for increased and reproducible *in vitro* pollen germination in *Arabidopsis thaliana. Plant J* **52 (3)**, 570-582

Bolte, S., Talbot, C., Boutte, Y., Catrice, O., Read, N.D., Satiat-Jeunemaitre, B. (2004). FM-dyes as experimental probes for dissecting vesicle trafficking in living plant cells. *J Microsc* **214**, 159-173

Boureux, A., Vignal, E., Faure, S., Fort, P. (2007). Evolution of the Rho family of Ras-Like GTPases in eukaryotes. *Mol Biol Evol* **24 (1)**, 203-216

Boyes, D.C., Zayed, A.M., Ascenzi, R., McCaskill, A.J., Hoffman, N.E., Davis, K.R., Görlach, J. (2001). Growth stage–based phenotypic analysis of *Arabidopsis*: A model for high throughput functional genomics in plants. *Plant Cell* **13**, 1499–1510

Brembeck, F.H., Schwarz-Romond, T., Bakkers, J., Wilhelm, S., Hammerschmidt, M., Birchmeier, W. (2004). Essential role of BCL9-2 in the switch between β-catenin's adhesive and transcriptional functions. *Gene Dev* **18**, 2225-2230

Bryant, D.M., Stow, J.L. (2004). The ins and outs of E-cadherin trafficking. *Trends Cell Biol* **14,** 427-434

Bullock, W.O., Fernandez, J.M., Short, J.M. (1987). XL-1 blue: A high efficiency plasmid transforming recA *Escherichia coli* strain with β-galactosidase selection. *Biotechnology* **5 (4)**, 376-379

Camacho, L., Malhó, R. (2003). Endo/exocytosis in the pollen tube apex is differentially regulated by Ca^{2+} and GTPases. *J Exp Bot* **54 (380)**, 83-92

Cárdenas, L., Lovy-Wheeler, A., Kunkel, J.G., Hepler, P.K. (2008). Pollen tube growth oscillations and intracellular calcium levels are reversibly modulated by actin polymerization. *Plant Physiol* **146**, 1611-1621

Cao, H., Weller, S., Orth, J.D., Chen, J., Huang, B., Chen, J.-L., Stamnes, M., McNiven, M.A. (2005). Actin and Arf1-dependent recruitment of a cortactin-dynamin complex to the Golgi regulates post-Golgi transport. *Nat Cell Biol* **7**, 483-492

Castaño, J., Solanas, G., Casagolda, D., Raurell, I., Villagrasa, P., Bustelo, X.R., García de Herreros, A., Duñach, M. (2007). Specific phosphorylation of p120-catenin regulatory domain differently modulates its binding to RhoA. *Mol Cell Biol* **27 (5)**, 1745-1757

Chen C.Y., Wong, E.I., Vidali, L., Estavillo, A., Hepler, P.K., Wu, H.-M., Cheung, A.Y. (2002). The regulation of actin organization by actin-depolymerizing factor in elongating pollen tubes. *Plant Cell* **14**, 2175-2190

Chen C.Y.-H., Cheung A.Y., Wu, H.-M. (2003). Actin-depolymerizing factor mediates Rac/Rop GTPase-regulated pollen tube growth. *Plant cell* **15**, 237-249

Cheung, A.Y., Wu, H.-m. (2004). Overexpression of an *Arabidopsis* formin stimulates supernumerary actin cable formation from pollen tube cell membrane. *Plant Cell* **16**, 257-269

Chiang, J.-Y., Balic, N., Hsu, S.-W., Yang, C.-Y., Ko, C.-W, Hsu, Y.-F., Swoboda, I., Wang, C.-S. (2006). A pollen-specific polygalacturonase from lily is related to major grass pollen allergens. *Plant Physiol Biochem* **44**, 743–751

Choi, H.-J., Weiss, W.I. (2004). Structure of the armadillo repeat domain of Plakophilin 1. *J Mol Biol* **346**, 367-376

Christensen, C.A., King, E.J., Jorda, J.R., Drews, G.N. (1997). Megagametogenesis in *Arabidopsis* wild type and the *Gf* mutant. *Sex Plant Reprod* **10**, 49-64

Chuang, C.-F., Meyerowitz, E.M. (2000). Specific and heritable genetic interference by double-stranded RNA in *Arabidopsis thaliana*. *PNAS* **97 (9)**, 4985-4990

Clark, G.B., Thompson Jr., G., Roux, S.J. (2001). Signal transduction mechanisms in plans: An overview. *Curr Sci* **80 (2)**, 170-177

Clough, S.J., Bent, A.F. (1998). Floral dip: a simplified method for *Agrobacterium*-mediated transformation of *Arabidopsis thaliana*. *Plant J* **16**,735-743

Coates, J.C. (2003). Armadillo repeat proteins: beyond the animal kingdom. *Trend Cell Biol* **13 (9)**, 463-471

Coates, J.C., Laplaze, L., Haselhoff, J. (2006). Armadillo-related proteins promote lateral root development in *Arabidopsis*. *PNAS* **103 (5)**, 1621-1626

Coghill, I.D., Brown, S., Cottle, D.L., McGrath, M.J., Robinson, P.A., Nandurkar, H.H., Dyson, J.M., Mitchell, C.A. (2003). FHL3 is an actin-binding protein that regulates α-actinin-mediated actin bundling. *J Biol Chem* **278 (26)**, 24139-24152

Cole, R.A., Fowler, J.E. (2006). Polarized growth: maintaining focus at the tip. *Curr Opin Cell Biol* **9**, 579-588

Cong, F., Varmus, H. (2004). Nuclear-cytoplasmic shuttling of axin regulates subcellular localization of β-catenin. *PNAS* **101 (9)**, 2882-2887

Davis, A.J., Im, Y.J., Dubin, J.S., Tomer, K.B., Boss, W.F. (2007). *Arabidopsis* phosphatidylinositol phosphate kinase 1 binds F-actin and recruits phosphatidylinositol 4-kinase β1 to the actin cytoskeleton. *J Biol Chem* **282 (19)**, 14121-14131

Decreux, A., Messiaen, J. (2005). Wall-associated kinase WAK1 interacts with cell wall pectins in a calcium-induces conformation. *Plant Cell Physiol* **46 (2)**, 268-278

Derksen, J., Knuiman, B., Hoedemaekers, K., Guyon, A., Bonhomme, S., Pierson, E.S. (2002). Growth and cellular organization of *Arabidopsis* pollen tubes in vitro. *Sex Plant Reprod* **15**, 133-139

Downes, B.P., Stupar, R.M., Gingerich, D.J., Vierstra, R.D. (2003). The HECT ubiquitin-protein ligase (UPL) family in *Arabidopsis*: UPL3 has a specific role in trichome development. *Plant J.* **35**, 729-742

Dowd, P.E., Coursol, S., Skirpan, A.L., Kao, T.H., Gilroy, S. (2006). Petunia phospholipase c1 is involved in pollen tube growth. *Plant Cell* **18**,1438-1453

Dresselhaus, T. (2006). Cell-cell communication during double fertilization. *Curr Opin Plant Biol* **9**, 41-47

Dresselhaus, T., Srilunchang, K.-o., Leljak-Levanić, D., Schreiber, D.N., Garg P. (2006). The fertilization induced DNA replication factor MCM6 of maize shuttles between cytoplasm and nucleus, and is essential for plant growth and development. *Plant Physiol* **140**, 512-527

Drews, G.N., Yadegari, R. (2002). Development and function of the angiosperm female gametophyte. *Annu Rev Genet* **36**, 99-124

Drøbak, B.K., Watkins, P.A.C., Valenta, R., Dove, S.K., Lloyd, C.W., Staiger, C.J. (1994). Inhibition of plant membrane phosphoinositide phospholipase C by the actin-binding protein profilin. *Plant J* **6**, 389-400

Drøbak, B.K., Franklin-Tong, V.E., Staiger, C.J. (2004). The role of the actin cytoskeleton in plant cell signaling. *New Phytologist* **163,** 13-30

D´Souza, C., Chavrier, P. (2006). ARF proteins: roles in membrane traffic and beyond. *Nat Rev Mol Cell Biol* **7**, 347-358

Eisenmann, D.M. (2005). Wnt signaling. *WormBook*, ed. The *C. elegans* Research Community, WormBook, doi/10.1895/wormbook.1.7.1, http://www.wormbook.org.

Edwards, D.C., Sanders, L.C., Bokoch, G.M., Gill, G.N. (1999). Activation of LIM-kinase by Pak1 couples Rac/Cdc42 GTPase signaling to actin cytoskeletal dynamics. *Nat Cell Biol* **1**, 253-259

Faix, J., Grosse, R. (2006). Staying in shape with formins. *Dev Cell* **10,** 693-706

Fagotto, F., Glück, U., Gumbiner, B.M. (1998). Nuclear localization signal-independent and importin/karyopherin-independent nuclear import of β-catenin. *Curr Biol* **8**, 181-190

Faure, J.-E., Rotman, N., Fortune, P., Dumas, C. (2002). Fertilization in *Arabidopsis thaliana* wild type: Developmental stages and time course. *Plant J* **30**(**4**), 481-488

Fernandez-Borja, M., Janssen, L., Verwoerd, D., Hordijk, P., Neefjes, J. (2005). RhoB regulates endosome transport by promoting actin assembly on endosomal membranes through Dia1. *J Cell Sci* **118**, 2661-2607

Fischer, U., Men, S., Grebe, M. (2004). Lipid function in plant cell polarity. *Curr Opin Plant Biol* **7**, 670-676

Fu, Y., Yuan, M., Huang B.-Q., Yang, H.-Y., Zee, S.-Y. (2000). Changes in actin organization in the living egg apparatus of *Torenia fournieri* during fertilization. *Sex Plant Reprod* **12**, 315-322

Fu, Y., Wu, G., Yang, Z. (2001). Rop GTPase-dependent dynamics of tip-localized F-actin controls tip growth in pollen tubes. *J Cell Biol* **152**, 1019-1032

Gibbon, B.C., Kovar, D.R., Staiger, C.J. (1999). Latrunculin B has different effects on pollen germination and tube growth. *Plant Cell* **11**, 2349-2363

Goldberg, R.B., Beals, T.P., Sanders, P.M. (1993). Anther development: Basic principles and practical applications. *Plant Cell* **5**, 1217-1229

González-Lamothe, R., Tsitsigiannis, D.I., Ludwig, A.A., Panicot, M., Shirasu, K., Jones, J.D.G. (2006). The U-Box protein CMPG1 is required for efficient activation of defense mechanisms triggered by multiple resistance genes in tobacco and tomato. *Plant Cell* **18**, 1067-1083

Groß-Hardt, R., Kägi, C., Baumann, N., Moore, J.M., Baskar, R., Gagliano, W.B., Jürgens, G., Grossniklaus, U. (2007). LACHESIS restricts gametic cell fate in the female gametophyte of *Arabidopsis*. *PLoS Biology* **5 (3)**, e47

Gu, T., Mazzurco, M., Sulaman, W., Matias, D.D., Goring, D.R. (1998). Binding of an arm repeat protein to the kinase domain of the S-locus receptor kinase. *Proc Natl Acad Sci USA* **95**, 382-387

Gu, Y., Vernoud, V., Fu, Y., Yang, Z. (2003). ROP GTPase regulation of pollen tube growth through the dynamics of tip-localized F-actin. *J Exp Bot* **54 (380)**, 93-101

Gu, Y., Fu, Y., Dowd, D., Li, S., Vernoud, V., Gilroy, S., Yang, Z. (2005). A Rho family GTPase controls actin dynamics and tip growth via two counteracting downstream pathways in pollen tubes. *J Cell Biol* **169 (1)**, 127-138

Gu, Y., Li, S., Lord, E.M., Yang, Z. (2006). Members of a novel class of *Arabidopsis* Rho Guanine Nucleotide Exchange Factors control Rho GTPase-dependent polar growth. *Plant Cell* **18**, 366-381

Hable, W.E., Miller, N.R., Kropf, D.L. (2003). Polarity establishment requires dynamic actin in fucoid zygotes. *Protoplasma* **221**, 193-204

Hadfield, K.A., Bennett, A.B. (1998). Polygalacturonases: Many genes in search of a function. *Plant Physiol* **117**, 337–343

Haecker, A., Groß-Hardt, R., Geiges, B., Sarkar, A., Breuninger, H., Herrmann, M., Laux, T. (2004). Expression dynamics of WOX genes marks the cell fate decisions during embryonic patterning in *Arabidopsis thaliana. Development* **131**, 657-668

Hall, A. (1998) Rho GTPases and the Actin Cytoskeleton. *Science* **279**, 509-514

Hatzfeld, M. (1999). The Armadillo family of structural proteins. *Int Rev Cytol* **186**, 179-224

Hatzfeld, M. (2007). Plakophilins: Multifunctional proteins or just regulators of desmosomal adhesion? *Biochim Biophys Acta* **1773**, 69-77

Hepler, P.K., Vidali, L., Cheung, A.Y. (2001). Polarized cell growth in higher plants. *Annu Rev Cell Dev Biol* **17**, 159-187

Hepler, P., Lovy-Wheeler, A. (2006). Oscillatory calcium and proton gradients in growing pollen tubes. *Plant Physiol online* **4**, Essay 15.1

Heslop-Harrison, Y., Heslop-Harrison, J. (1992). Germination of monocolpate angiosperm pollen: evolution of the actin cytoskeleton and wall during hydration, activation and tube emergence. *Ann Bot* **69**, 385-394

Higashiyama, T., Yabe, S., Sasaki, N., Nishimura, Y., Myiagishima, S.-y., Kuroiwa, H., Kuroiwa, T. (2001). Pollen tube attraction by the synergid cell. *Science* **293**, 1480-1483

Higashiyama, T., Hamamura, Y. (2008). Gametophytic pollen tube guidance. *Sex Plant Reprod* **21 (1)**, 17-26

Honys, D., Twell, D. (2004). Transcriptome analysis of haploid male gametophyte development in *Arabidopsis. Genome Biol* **5**, R85

Hood, J.K., Silver, P.A. (2000). Diverse nuclear transport pathways regulate cell proliferation and oncogenesis. *Biochim Biophys Acta Rev Canc* **1471 (1)**, 31-41

Howden, R., Park, S.K., Moore, J.M., Orme, J., Grossniklaus, U., Twell, D. (1998). Selection of T-DNA-tagged male and female gametophytic mutants by segregation distortion in *Arabidopsis*. *Genetics*, 621-631

Huang, B.-Q., Sheridan, W.F. (1994). Female gametophyte development in maize: microtubular organization and embryo sac polarity. *Plant Cell* **6**, 845-861

Huang, B.-Q., Sheridan, W.F. (1998). Actin coronas in normal and indeterminate gametophyte1 embryo sacs of maize. *Sex Plant Reprod* **11**, 257-264

Huang, B.-Q., Fu, Y., Zee, S.Y., Hepler, P.K. (1999). Three-dimensional organization and dynamic changes of the actin cytoskeleton in embryo sacs of *Zea mays* and *Torenia fournieri. Protoplasma* **209**, 105-119

Huang, S., Blanchoins, L., Kovar, D.R., Staiger, C.J. (2003). *Arabidopsis* capping protein (AtCP) is a heterodimer that regulates assembly of the barbed ends of actin filaments. *J Biol Chem* **278 (45)**, 44832-44842

Huang, S., Jin, L., Du, J., Li, H., Zhao, Q., Ou, G., Ao, G., Yuan, M. (2007). SB401, a pollen-specific protein from *Solanum berthaultii*, binds to and bundles microtubules and F-actin. *Plant J* **51(3)**, 406-418

Huber, A.H., Nelson, W.J., Weis, W.I. (1997). Three-dimensional structure of the armadillo repeat region of β-catenin. *Cell* **90**, 871-882

Huber, A.H., Weis, W.I. (2001). The structure of the beta-catenin/E-cadherin complex and the molecular basis of diverse ligand recognition by beta-catenin. *Cell* **105**, 391-402

Huck, N., Moore, J.M., Federer, M., Grossniklaus, U. (2003). The *Arabidopsis* mutant *feronia* disrupts the female gametophytic control of pollen tube reception. *Development* **130**, 2149-2159

Huson, D.H., Bryant, D. (2006). Application of phylogenetic networks in evolutionary studies. *Mol Biol Evol* **23**, 254-267

Hussey, P.J., Deeks, M.J., Hawkins, T.J., Ketelaar, T. (2004). Polar cell growth and the cytoskeleton biology. in *Polarity in plants* (ed, K. Lindsey), pp. 1-50. Blackwell publishing, Oxford, UK

Hwang, J.-U., Gu, Y., Lee, Y.-J., Yang, Z. (2005). Oscillatory ROP GTPase activation leads the oscillatory polarized growth of pollen tubes. *Mol Biol Cell* **16**, 5385-5399

Ingouff, M., Fitz Gerald, J.N., Guérin, C., Robert, H., Sørensen, M.B., Van Damme, D., Geelen, D., Blanchoin, L., Berger, F. (2005). Plant formin AtFH5 is an evolutionarily conserved actin nucleator involved in cytokinesis. *Nat Cell Biol* **7 (4)**, 374-380

Ingouff, M., Hamamura, Y., Gourgues, M., Higashiyama, T., Berger, F. (2007). Distinct dynamics of HISTONE3 variants between the two fertilization products in plants. *Curr Biol* **17**, 1032-1037

Iyer, K., Bürkle, L., Auerbach, D., Thaminy, S., Dinkel, M., Engels, K., Stagljar, I. (2005). Utilizing the Split-Ubiquitin Membrane Yeast Two-Hybrid system to identify protein-protein interactions of integral membrane proteins. *Sci STKE* **275**, pl3

Johnson-Brousseau, S., McCormick, S. (2004). A compendium of methods useful for characterizing *Arabidopsis* pollen mutants and gametophytically- expressed genes. *Plant J* **39**, 761-775

Johnston, A.J., Meier, P., Gheyselinck, J., Wuest, S.E.J., Federer, M., Schlagenhauf, E., Becker, J.D., Grossniklaus, U. (2007). Genetic subtraction profiling identifies genes essential for *Arabidopsis* reproduction and reveals interaction between the female gametophyte and the maternal sporophyte. *Genome Biol* **8**, R204

Jones, D.T., Taylor, W.R., Thornton, J.M. (1992). The rapid generation of mutation data matrices from protein sequences. *Comput Appl Biosci* **8**, 275-282

Jones-Rhoades, M.W., Borevitz, J.O., Preuss, D. (2007). Genome-wide expression profiling of the *Arabidopsis* female gametophyte identifies families of small, secreted proteins. *PLoS Genet* **3 (10)**, e171

Kaothien, P., Han Ok, S., Shuai, B., Wengier, D., Cotter, R., Kelley, D., Kiriakopolos, S., Muschietti, J., McCormick, S. (2005). Kinase partner protein interacts with the LePRK1 and LePRK2 receptor kinases and plays a role in polarized pollen tube growth. *Plant J* **42**, 492-503

Karner, C., Wharton, K.A., Carroll, T.J. (2006). Apical–basal polarity, Wnt signaling and vertebrate organogenesis. *Semin Cell Dev Biol* **17**, 214-222

Kerschen, A., Napoli, C.A., Jorgensen, R.A., Müller, A.E. (2004). Effectiveness of RNA interference in transgenic plants. *FEBS Lett* **566**, 223-228

Kim, S., Choi, H., Ryu, H., Park, J.H., Kim M.D., Kim, S.Y. (2004). ARIA, an *Arabidopsis* arm repeat protein interacting with a transcriptional regulator of abscisic acid-responsive gene expression, is a novel abscisic acid signalling component. *Plant Physiol* **136**, 3639-3648

Kobe, B. (1999). Autoinhibition by an internal nuclear localization signal revealed by the crystal structure of mammalian importin alpha. *Nat Struct Biol* **6**, 388-397

Kohorn, B.D. (2000). Plasma membrane-cell wall contacts. *Plant Physiol* **124,** 31-38

Koncz, C., Schell, J. (1986). The promoter of the TL-DNA gene 5 controls the tissue-specific expression of chimaeric genes carried by a novel type of *Agrobacterium* vector. *Mol Gen Genet* **204**, 383-396

Konstantinopoulos, P.A., Karamouzis, M.V., Papavassiliou, A.G. (2007). Post-translational modifications and regulation of the RAS superfamily of GTPases as anticancer targets. *Nat Rev Drug Discov* **6**, 541-555

Kost, B., Spielhofer, P., Chua, N.-H. (1998). A GFP-mouse talin fusion protein labels actin filaments *in vivo* and visualizes the actin cytoskeleton in growing pollen tubes. *Plant J* **16 (3)**, 393-401

Kost, B., Lemichez, E., Spielhofer, P., Hong, Y., Tolias, K., Carpenter, C., Chua, N.-H. (1999). Rac homologues and compartmentalized phosphatidylinositol 4,5-bisphosphate act in a common pathway to regulate polar pollen tube growth. *J Cell Biol* **145 (2)**, 317-330

Kost, B. (2008). Spatial control of Rho (Rac-Rop) signaling in tip growing plant cells. *Trends Cell Biol* **18**, 119-127

Kovar, D.R. (2006). Molecular details of formin-mediated actin assembly. *Curr Opin Cell Biol* **18**, 11-17

Kusano, H., Testerink, C., Vermeer, J.E.M., Tsuge, T., Shimada, H., Oka, A., Munnik, T., Aoyama, T. (2008). The *Arabidopsis* phosphatidylinositol phosphate 5-kinase PIP5K3 is a key regulator of root hair tip growth. *Plant Cell* **20**, 367-380

Lalanne, E., Michaelidis, C., Moore, J.M., Gagliano, W., Johnson, A., Patel, R., Howden, R., Vielle-Calzada, J.-P., Grossniklaus, U., Twell, D. (2004). Analysis of transposon insertion mutants highlights the diversity of mechanisms underlying male progamic development in *Arabidopsis. Genetics* **167**, 1975-1986

Latres, E., Chiaur, D.S., Pagano, M. (1999). The human F box protein β-Trcp associates with the Cul1/Skp1 complex and regulates the stability of β-catenin. *Oncogene* **18**, 849-854

Laux, T., Jürgens, G. (1997). Embryogenesis: A new start in life. *Plant Cell* **9 (7)**, 989-1000

Le, Q., Gutiérrez-Marcos, J.F., Costa, L.M., Meyer, S., Dickinson, H.G., Lörz, H., Kranz, E., Scholten, S. (2005). Construction and screening of subtracted cDNA libraries from limited populations of plant cells: a comparative analysis of gene expression between maize egg cells and central cells. *Plant J* **44**, 167-178

Lennon, K.A., Lord, E.M. (2000). In vivo pollen tube cell of *Arabidopsis thaliana.* I. Tube cell cytoplasm and wall. *Protoplasma* **214**, 45-56

Li, H., Lin, Y., Heath, R.M., Zhu, M.X., Yang, Z. (1999). Control of pollen tube tip growth by a Rop GTPase-dependent pathway that leads to tip-localized calcium influx. *Plant Cell* **11**, 1731-1742

Li, S., Blanchoin, L., Yang, Z., Lord, E.M. (2003). The putative *Arabidopsis* ARP2/3 complex controls leaf cell morphogenesis. *Plant Physiol* **132**, 2034-2044

Liu, C.-m., Meinke, D.W. (1998). The titan mutants of *Arabidopsis* are disrupted in mitosis and cell cycle control during seed development. *Plant J* **16 (1)**, 21-31

Liu, P., Sherman-Broyles, S., Nasrallah, M.E., Nasrallah, J.B. (2007). A cryptic modifier causing transient self-incompatibility in *Arabidopsis thaliana*. *Curr Biol* **17**, 734-740

Lord, E.M., Russell, S.D. (2002). The mechanisms of pollination and fertilization in plants. *Annu Rev Cell Dev Biol* **18**, 81-105

Lovy-Wheeler, A., Wilsen, K.L., Baskin, T.I., Hepler, P.K. (2005). Enhanced fixation reveals the apical cortical fringe of actin filaments as a consistent feature of the pollen tube. *Planta* **221**, 95-104

Macara, I.G. (2001). Transport into and out of the Nucleus. *Microbiol Mol Biol Rev* **65**, 570-594

Malhó, R., Liu, Q., Monteiro, D., Rato, C., Camacho, L., Dinis, A. (2006). Signalling pathways in pollen germination and tube growth. *Protoplasma* **228**, 21-30

Mansfield, S.G. and Bowman, J.L. (1994) Ovules. In: *Arabidopsis: An atlas of morphology and development* (ed. Bowman J.L.), Chapter 5, 299-331. Springer-Verlag New York, Inc.

Márton, M.L., Cordts, S., Broadhvest, J., Dresselhaus, T. (2005). Micropylar pollen tube guidance by Egg Apparatus 1 of Maize. *Science* **307**, 573-576

Mathur, J., Mathur, N., Kirik, V., Kernebeck, B., Srinivas, B.P., Hülskamp, M. (2003a). *Arabidopsis* CROOKED encodes for the smallest subunit of the ARP2/3 complex and controls cell shape by region specific fine F-actin formation. *Development* **130**, 3137-3146

Mathur J., Mathur, N., Kernebeck, B., Hülskamp, M. (2003b). Mutations in actin-related proteins 2 and 3 affect cell shape development in Arabidopsis. *Plant Cell* **15**, 1632-1645

McCormick, S. (1993). Male gametophyte development. *Plant Cell* **5**, 1265-1275

McCormick, S. (2004). Control of male gametophyte development. *Plant Cell* **16**, 142-153

Molendijk, A.J., Bischoff, F., Rajendrakumar, C.S.V., Friml, J., Braun, M., Gilroy, S., Palme, K. (2001). *Arabidopsis thaliana* Rop GTPases are localized to tips of root hairs and control polar growth. *EMBO J* **20 (11)**, 2779-2788

Monteiro, D., Liu, Q., Lisboa, S., Scherer, G.E.F., Quader, H., Malhó, R. (2005). Phosphoinositides and phosphatidic acid regulate pollen tube growth and reorientation through modulation of $[Ca^{2+}]_c$ and membrane secretion. *J Exp Bot* **56 (416)**, 1665–1674

Moretti, S., Armougom, F., Wallace, I.M., Higgins, D.G., Jongeneel, C.V., Notredame, C. (2007). The M-Coffee web server: a meta-method for computing multiple sequence alignments by combining alternative alignment methods. *Nucleic Acids Res* **35,** 645-648

Mudgil, Y., Shiu, S.-H., Stone, S.L., Salt, J.N., Goring, D.R. (2004). A large complement of the predicted *Arabidopsis* ARM repeat proteins are members of the U-box E3 ubiquitin ligase family. *Plant Physiol* **134**, 59-66

Murashige T. and Skoog F. (1962). A revised medium for rapid growth and bioassays with tobacco tissue cultures. *Physiol Plant* **15**, 473-497

Nacry, P., Mayer, U., Jürgens, G. (2000). Genetic dissection of cytokinesis. *Plant Mol Biol* **43**, 719-733

Nawashin, S. (1898). Resultate einer Revision der Befruchtungsvorgänge bei *Lillium martagon* und *Fritillaria tenella*. *Bulletin de l´Académie Impériale des Sciences de St. Pétersbourg Series* **59**, 377-382

Nicholas, K.B., Nicholas H.B. Jr., Deerfield, D.W. II. (1997). GeneDoc: analysis and visualization of genetic variation. *Embnew News* **4**, 14

Niessen, C., Yap, A. (2006). Another job for the talented p120-catenin. *Cell* **127 (5)**, 875-877

Niogret, M.-F., Dubald, M., Mandaron, P., Mache, R. (1991). Characterization of pollen polygalacturonase encoded by several cDNA clones in maize. *Plant Mol Biol* **17**, 1155-1164

Nishiyama, T., Fujita, T., Shin-I, T., Seki, M., Nishide, H., Uchiyama, I., Kamiya, A., Carnici, P., Hayashizaki, Y., Shinozaki, K., Kohara, Y., Hasebe, M. (2003). Comparative genomics of *Physcomitrella patens* gametophytic transcriptome and *Arabidopsis thalianna*: implication for land plant evolution. *PNAS* **100 (13)**, 8007-8012

Odell, J.T., Nagy, F., and Chua, N.-H. (1985). Identification of DNA sequences required for activity of cauliflower mosaic virus 35S promoter. *Nature* **313**, 810-812

O'Neill, S.D. (1997). Pollination regulation of flower development. *Annu Rev Plant Physiol Plant Mol Biol* **48**, 547-574

Ovečka, M., Lang. I., Baluška, F., Ismail, A., Illeš, P., Lichtscheidl, I.K. (2005). Endocytosis and vesicle trafficking during tip growth of root hairs. *Protoplasma* **226**, 39-54

Oxford, G., Theodorscu, D. (2003). The role of Ras superfamily proteins in bladder cancer progression. *J Urol* **170**, 1987-1993

Pagnussat, G.C., Yu, H.-J., Ngo, Q.A., Rajani, S., Mayalagu, S., Johnson, C.S., Capron, A., Xie, L.-F., Ye, D., Sundaresan, V. (2005). Genetic and molecular identification of genes required for female gametophyte development and function in *Arabidopsis*. *Development* **132**, 603-614

Palanivelu, R., Preuss, D. (2000). Pollen tube targeting and axon guidance: parallels in tip growth mechanisms. *Trends Cell Biol* **10**, 517-524

Pandey, S., Assmann, M. (2004). The *Arabidopsis* putative G protein-coupled receptor GCR1 interacts with the G protein α subunit GPA1 and regulates abscisic acid signaling. *Plant Cell* **16**, 1616-1632

Pang, S.Z., DeBoer, D.L., Wan, Y., Ye, G., Layton, J.G., Neher, M.K., Armstrong, C.L., Fry, J.E., Hinchee, M.A., Fromm, M.E. (1996). An improved green fluorescent protein gene as a vital marker in plants. *Plant Physiol* **112**, 893-900

Paves, H. and Truve, E. (2004). Incorporation of mammalian actin into microfilaments in plant cell nucleus. *BMC Plant Biol* **4**, 7

Pawloski, L.C., Kandasamy, M.K., Meagher, R.B. (2006). The late pollen actins are essential for normal male and female development in *Arabidopsis*. *Plant Mol Biol* **62**, 881-896

Perera, I.Y., Davis, A.J., Ju Im, Y., Boss, W.F. (2007). The plant phosphoinositide pathway: identifying and characterizing flux limiting enzymes. in *Current Advances in the Biochemistry and Cell Biology of Plant Lipids.* (ed, C.Benning, J.Ohlrogge), pp. 80-86. Aardvark Global Publishing Company, LLC Salt Lake City, UT

Pfeifer, M., Wieschaus, E. (1990). The segment polarity gene *armadillo* encodes a functionally modular protein that is the *Drosophila* homolog of human Plakoglobin. *Cell* **63**, 1167-1176

Pfeifer, M., Berg, S., Reynolds, A.B. (1994). A repeating amino acid motif shared by proteins with diverse cellular roles. *Cell* **76**, 789-791

Pfeifer, M., Polakis, P. (2000). Wnt Signaling in oncogenesis and embryogenesis: a look outside the nucleus. *Science* **287**, 1606-1609

Poon, I.K.H., Jans, D.A. (2005). Regulation of nuclear transport: central role in development and transformation? *Traffic* **6**, 173-186

Preuss, M.L., Schmitz, A.J., Thole, J.M., Bonner, H.K., Otegui, M.S., Nielsen, E. (2006). A role for the RabA4b effector protein PI-4Kβ1 in polarized expansion of root hair cells in *Arabidopsis thaliana*. *J Cell Biol* **172**, 991-998

Ren, H., Xiang, Y. (2007). The function of actin-binding proteins in pollen tube growth. *Protoplasma* **230**, 171-182

Riggleman, B., Wieschaus, E., Schedl, P. (1989). Molecular analysis of the *armadillo* locus: uniformly distributed transcripts and a protein with novel internal repeats are associated with a *Drosophila* segment polarity gene. *Gene Dev* **3**, 96-113

Rohila, J.S., Chen, M., Chen, S., Chen, J., Cerny, R., Dardick, C., Canlas, P., Xu, X., Gribskov, M., Kanrar, S., Zhu, J.-K., Ronald, P., Fromm, M.E. (2006). Protein–protein interactions of tandem affinity purification-tagged protein kinases in rice. *Plant J* **46**, 1-13

Russell, S. D. (1993). The egg cell: Development and role in fertilization and early embryogenesis. *Plant Cell* **5**, 1349-1359

Saedler, R., Mathur, N., Srinivas, B.P., Kernebeck, B., Hülskamp, M., Mathur, J. (2004). Actin control over microtubules suggested by DISTORTED2 encoding the Arabidopsis ARPC2 subunit homolog. *Plant Cell Physiol* **45**, 813-822

Saitou, N., Nei, M. (1987). The neighbor-joining method: A new method for reconstructing phylogenetic trees. *Mol Biol Evol* **4**, 406-425

Sakai, T., Honing, H. van der, Nishioka, M., Uehara, Y., Takahashi, M., Fujisawa, N., Saji, K., Seki, M., Shinozaki, K., Jones, M.A., Smirnoff, N., Okada, K., Wasteneys, G.O. (2008). Armadillo repeat-containing kinesins and a NIMA-related kinase are required for epidermal cell morphogenesis in Arabidopsis. *Plant J* **53**, 157-171

Samaj, J., Müller, J., Beck, M., Böhm, N., Menzel, D. (2006) Vesicular trafficking, cytoskeleton and signalling in root hairs and pollen tubes. *Trends Plant Sci* **11**, 594-600

Sambrook, J., Fritsch, E.F., Maniatis, T. (1989). Molecular cloning: A laboratory manual (2nd edition). Cold Spring Harbor Laboratory Press, N.Y.

Sanchez, A.M., Bosch, M., Bots, M., Nieuwland, J., Feron, R., Mariani, C. (2004). Pistil factors controlling pollination. *Plant Cell* **16**, 98-106

Schneitz, K., Hülskamp, M., Pruitt, R.E. (1995). Wild-type ovule development in *Arabidopsis thaliana*: a light microscope study of cleared whole-mount tissue. *Plant J* **7 (5)**, 731-749

Schneitz, K., Hülskamp, M., Kopczak, S.D., Pruitt, R.E. (1997). Dissection of sexual organ ontogenesis: a genetic analysis of ovule development in *Arabidopsis thaliana*. *Development* **124**, 1367-1376

Scholl, R.L., May, S.T., and Ware, D.H. (2000). Seed and molecular resources for *Arabidopsis*. *Plant Physiol* **124**, 1477-1480

Sheahan, M.B., Staiger, C.J., Rose, R.J., McCurda, D.W. (2004). A green fluorescent protein fusion to actin-binding domain 2 of *Arabidopsis* fimbrin highlights new features of a dynamic actin cytoskeleton in live plant cells. *Plant Physiol* **136**, 3968-3978

Sheoran, I.S., Sproule, K.A., Olson, D.J.H., Ross, A.R.S., Sawhney, V.K. (2006). Proteome profile and functional classification of proteins in *Arabidopsis thaliana* (Landsberg erecta) mature pollen. *Sex Plant Reprod* **19**, 185-196

Smyth D.R., Bowman J.L. and Meyerowitz E.M. (1990). Early flower development in *Arabidopsis*. *Plant cell* **2**, 755-767

Sonobe, S., Shibaoka, H. (1989). Cortical fine actin filaments in higher plant cells visualized by rhodamine-phalloidin after pretreament with m-maleimidobenzoyl N-hydroxysuccinimide ester. *Protoplasma* **148**, 80-86

Sprunck, S., Baumann, U., Edwards, K., Langridge, P., Dresselhaus, T. (2005). The transcript composition of the egg cell changes significantly following fertilization in wheat (*Triticum aestivum* L.). *Plant J* **41**, 660-672

Städeli, R., Hoffmans, R., Basler, K. (2006). Transcription under the control of nuclear Arm/β-catenin. *Curr Biol* **16 (10)**, R378-R385

Staiger, C.J., Blanchoin, L. (2006). Actin dynamics: old friends with new stories. *Curr Opin Plant Biol* **9**, 554-562

Steffen, J.G., Kang, I.-H., Macfarlane, J., Drews, G.N. (2007). Identification of genes expressed in the *Arabidopsis* female gametophyte. *Plant J* **51 (2)**, 281-292

Steinmann, T., Geldner, N., Grebe, M., Mangold, S., Jackson, C.L., Paris, S., Gälweiler, L., Palme, K., Jürgens, G. (1999). Coordinated polar localization of auxin efflux carrier PIN1 by GNOM ARF GEF. *Science* **286**, 316-318

Stone, S.L., Anderson, E.M., Mullen, R.T., Goring, D.R. (2003). ARC1 is an E3 ubiquitin ligase and promotes the ubiquitination of proteins during the rejection of self-incompatible *Brassica* pollen. *Plant cell* **15**, 885-898

Strasburger, E. (1879). Die Angiospermen und die Gymnospermen. Jena, Germany: Fischer.

Sumi, T., Matsumoto, K., Takai, Y., Nakamura, T. (1999). Cofilin phosphorylation and actin cytoskeletal dynamics regulated by Rho- and Cdc42-activated LIM-kinase 2. *J Cell Biol* **147 (7)**, 1519-1532

Sun, Q.-Y., Schatten, H. (2006). Regulation of dynamic events by microfilaments during oocyte maturation and fertilization. *Reproduction* **131**, 193-205

Sunilkumar, G., Mohr, L., Lopata-Finch, E., Emani C., Rathore, K.S. (2002). Developmental and tissue-specific expression of CaMV 35S promoter in cotton as revealed by GFP. *Plant Mol Biol* **50**, 463-474

Taunton, J. (2001). Actin filament nucleation by endosomes, lysosomes and secretory vesicles. *Curr Opin Cell Biol* **13 (1)**, 85-91

Taylor, L.P., Hepler, P.K. (1997).Pollen germination and tube growth. *Annu Rev Plant Physiol Plant Mol Biol* **48**, 461-491

Thole, J.M., Vermeer, J.E.M., Zhang, Y., Gadella, Jr., T.W.J., Nielsen, E. (2008). *ROOT HAIR DEFECTIVE4* encodes a phosphatidylinositol-4-phosphate phosphatase required for proper root hair development in *Arabidopsis thaliana. Plant Cell* **20**, 381-395

Thomas, C., Hoffmann, C., Dieterle, M., von Troys, M., Ampe, C., Steinmetz, A. (2006a). Tobacco WLIM1 is a novel F-actin binding protein involved in actin cytoskeleton remodelling. *Plant Cell* **18**, 2194-2206

Thomas, S.G., Huang, S., Li, S., Staiger, C.J., Franklin-Tong, V.E. (2006b). Actin depolymerization is sufficient to induce programmed cell death in self-incompatible pollen. *J Cell Biol* **174 (2)**, 221-229

Torki, M., Mandaron, P., Thomas, F., Quigley, F., Mache, R., Falconet, D. (1999). Differential expression of a polygalacturonase gene family in *Arabidopsis thaliana*. *MGG* **261**, 948-952

Vancanneyt, G., Schmidt, R., O'Connor-Sanchez, A., Willmitzer, L., Rocha-Sosa, M. (1990). Construction of an intron-containing marker gene: Splicing of the intron in transgenic plants and its use in monitoring early events in *Agrobacterium*-mediated plant transformation. *Mol Gen Genet* **220 (2)**, 245-250

Veeman, M.T., Axelrod, J.D., Moon, R.T. (2003). A second canon: functions and mechanisms of β-catenin-independent Wnt signaling. *Dev Cell* **5**, 367-377

Verica, J.A., He, Z. (2002). The cell wall-associated kinase (WAK) and WAK-like kinase gene family. *Plant Physiol* **129 (2)**, 455-459

Vidali, L., Hepler, P.K. (2001). Actin and pollen tube growth. *Protoplasma* **215**, 64-76

Vielle-Calzada, J.-P., Baskar, R., Grossniklaus, U. (2000). Delayed activation of the paternal genome during seed development. *Nature* **404**, 91-94

Vincent, P., Chua, M., Nogue, F., Fairbrother, A., Mekeel, H., Xu, Y., Allen, N., Bibikova, T.N., Gilroy, S., Bankaitis, V.A. (2005). A Sec14p-nodulin domain phosphatidylinositol transfer protein polarizes membrane growth of *Arabidopsis thaliana* root hairs. *JCB* **168 (5)**, 801-812

Wang, B., Pelletier, J., Massaad, M.J., Herscovics, A., Shore, G.C. (2004). The yeast split-ubiquitin membrane protein two-hybrid screen identifies BAP31 as a regulator of the turnover of endoplasmic reticulum-associated protein tyrosine phosphatase-like B. *Mol Cell Biol* **24 (7)**, 2767-2778

Wang, B., Pelletier, J., Massaad, M.J., Herscovics, A., Shore, G.C. (2004). The yeast split-ubiquitin membrane protein two-hybrid screen identifies BAP31 as a regulator of the turnover of endoplasmic reticulum-associated protein tyrosine phosphatase-like B. *Mol Cell Biol* **24 (7)**, 2767-2778

Wang, Q., Kong, L., Hao, H., Wang, X., Lin, J., Samaj, J., Baluska, F. (2005). Effects of Brefeldin A on pollen germination and tube growth. Antagonistic effects on endocytosis and secretion. *Plant Physiol* **139**, 1692-1703

Webb, M.C., Gunning, B.E.S. (1994). Embryo sac development in *Arabidopsis thaliana*. II. The cytoskeleton during megagametogenesis. *Sex Plant Reprod* **7**, 153-163

Weins, A., Schwarz, K., Faul, C., Barisoni, L., Linke, W.A., Mundel, P. (2001). Differentiation- and stress-dependent nuclear cytoplasmic redistribution of myopodin, a novel actin-bundling protein. *J Cell Biol* **155 (3)**, 393-403

Weterings, K., Russell, S.D. (2004). Experimental analysis of the fertilization process. *Plant Cell* **16**, 107-118

Wikramanayake, A.H., Wallingford, J.B. (2006) The Wnt signaling pathway: A focus on its role in establishing polarity of cells, tissues and organs. *Semin Cell Dev Biol* **17**, 155-156

Wilkinson, J.E., Twell, D., Lindsey, K. (1997). Activities of CaMV 35S and nos promoters in pollen: implications for field release of transgenic plants. *J Exp Bot* **48**, 265-275

Willert, K., Jones, K.A. (2006). Wnt signalling: is the party in the nucleus? *Gene Dev* **20**, 1394-1404

Wilsen, K.L., Lovy-Wheeler, A., Voigt, B., Menzel, D., Kunkel, J.G., Hepler, P.K. (2006). Imaging the actin cytoskeleton in growing pollen tubes. *Sex Plant Reprod* **9**, 51-62

Woodcock, D.M., Crowther, P.J., Doherty, J., Jefferson, S., DeCruz, E., Noyer-Weidner, M., Smith, S.S., Michael, M.Z., Graham, M.W. (1989). Quantitative evaluation of *Escherichia coli* host strains for tolerance to cytosine methylation in plasmid and phage recombinants. *Nucl Acids Res* **17**, 3469-3478

Wu, G., Li, H., Yang, Z. (2000). *Arabidopsis* RopGAPs are a novel family of Rho GTPase-activating proteins that require the Cdc42/Rac-interactive binding motif for Rop-specific GTPase stimulation. *Plant Physiol* **124**,1625-1636

Xiang, C., Han, P., Oliver, D.J. (1999). *In solium* selection for *Arabidopsis* transformants resistant to kanamycin. *Plant Mol Biol Rep* **17**, 59-65

Xiong, Y., Kotake, Y. (2006). No exit strategy? No problem: APC inhibits β-catenin inside the nucleus. *Gene Dev* **20**, 637-642

Xu, J., Scheres, B. (2005). Dissection of *Arabidopsis* ADP-RIBOSYLATION FACTOR 1 function in epidermal cell polarity. *Plant Cell* **17**, 525-536

Yadegari, R., Drews, G.N. (2004). Female gametophyte development. *Plant Cell* **16**, 133-141

Yanagisawa S., Schmidt R.J. (1999). Diversity and similarity among recognition sequences of Dof transcription factors. *Plant J* **17**, 209-214

Yanagisawa, M., Huveldt, D., Kreinest, P., Lohse, C.M., Cheville, J.C., Parker, A.S., Copland, J.A., Anastasiadis, P.Z. (2008). A p120 catenin isoform switch affects Rho activity, induces tumor cell invasion and predicts metastatic disease. *J Biol Chem*, paper in press, published online ahead of print April 11, 2008

Yang, C.W., Gonzalez-Lamothe, R., Ewan, R.A., Rowland, O. Yoshioka, H., Shenton, M., Ye, H. O´Donell, E., Jones, J.D., Sadanandom A. (2006a). The E3 Ubiqiutin ligase activity of *Arabidopsis* PLANT U-BOX17 and its functional tobacco homolog ACRE276 are required for cell death and defense. *Plant Cell* **18**, 1084-1098

Yang, G., Gao, P., Zhang, H., Huang, S., Zheng, Z.-L. (2007). A mutation in MRH2 kinesin enhances the root hair tip growth defect caused by constitutively activated ROP2 small GTPase in *Arabidopsis*. *PLoS ONE* **2 (10)**, e1074. doi:10.1371/journal.pone.0001074

Yang, H., Kaur, N., Kiriakopolos, S., McCormick, S. (2006b). EST generation and analysis towards identifying female gametophyte-specific genes in *Zea mays* L. *Planta* **224 (5)**, 1004-1014

Ye, X.-L., Yeung, E.C., Zee, S.-Y. (2002). Sperm movment during double fertilization of a flowering plant, *Phaius tankervilliae*. *Planta* **215**, 60-66

Yoon, G.M., Dowd, P.E., Gilroy, S., McCubbin, A.G. (2006). Calcium dependent protein kinase isoforms in Petunia have distinct functions in pollen tube growth, including regulating polarity. *Plant Cell* **18**, 867-878

Yu, H.-J., Hogan, P., Sundaresan, V. (2005). Analysis of the female gametophyte transcriptome of *Arabidopsis* by comparative expression profiling. *Plant Physiol* **139**, 1853-1869

Zeng, L.-R., Qu, S., Bordeos, A., Yang, C., Baraoidan, M., Yan, H., Xie, Q., Nahm, B.H., Leung, H., Wang, G.-L. (2004). Spotted leaf11, a negative regulator of plant cell death and defense, encodes a U-box/Armadillo repeat protein endowed with E3 Ubiquitin ligase activity. *Plant Cell* **16**, 2795-2808

Zhang, S.-D., Kassis, J., Olde, B., Mellerick, D.M., Odenwald, **W.F.** (1996). Pollux, a novel *Drosophila* adhesion molecule, belongs to a family of proteins expressed in plants, yeast, nematodes and man. *Gene Dev* **10**, 1108-1119

Zhao, H., Ren, H. (2006). Rop1Ps promote actin cytoskeleton dynamics and control the tip growth of lily pollen tube. *Sex Plant Reprod* **19**, 83-91

Zheng, Z.-L., Yang, Z. (2000) The Rop GTPase switch turns on polar growth in pollen. *Trends Plant Sci* **5 (7)**, 298-303

Zhurinsky, J., Shtutman, M., Ben-Ze´ev, A. (2000). Plakoglobin and beta-catenin: protein interactions, regulation and biological roles. *J Cell Sci* **113 (18)**, 3127-3139

7. APPENDIX

7.1 Primer

Table 7.1.1: List of primers used for expression analysis

Name	Orien-tation	Sequence	Annealing temperature (°C)	Additional ingredients	Product size (bp)
Act3 fw	5´->3´	GAT TTG GCA TCA CAC TTT CTA CAA TG	58-60	-	757w/ Intron 655w/o Intron
Act3 rev	3´->5´	GTT CCA CCA CTG AGC ACA ATG	58-60	-	
ARO1fw	5´->3´	TGA GTA TTT AGG TCT CCC TC	54	4% DMSO	239
ARO1rev	3´->5´	GCC GCG TTT TCT TGA CCT TCC	54	4% DMSO	
ARO2fw	5´->3´	AGC GCA TCC AAG ACT CG	57	4% DMSO	679
ARO2rev	3´->5´	AAG CCC ATT CCA ACA CTG	57	4% DMSO	
ARO3fw	5´->3´	AAT GGC GAG TAA AAT CAG TAG TAG	54	4% DMSO	219
ARO3rev	3´->5´	GGT ATC TTT TCC GGG GGT TTA	54	4% DMSO	
ARO4fw	5´->3´	TCG GCT TGC TCA AAT GCT TAG AAC ACT	57	4% DMSO	519
ARO4rev	3´->5´	GAT TTG CCC CTC CGC CGA TGA A	57	4% DMSO	

Table 7.1.2:List of primers used for T-DNA insertion mutants

Name	Orien-tation	Sequence	Annealing temperature (°C)	Additional ingredients	Product size (bp)
ARO1-1LP	5´->3´	CAA GTT AGA CAA GCA TTG GAA CC	52	-	1059
ARO1-1RP	3´->5´	TTT CAC AAT ATC CGC CAT GAG	52	-	
ARO1-2LP	5´->3´	CAG AGA CAC GTA GGA GCC AAG	52	-	1073
ARO1-2RP	3´->5´	AAG CTG GTG TCC TTG ACT GTG	52	-	
ARO1-3LP	5´->3´	GCTTGCACGTGACAATGATCG	59	10% DMSO	1109
ARO1-3RP	3´->5´	GCTTCACGAGTGGTCCAATGA	59		
ARO1-4LP	5´->3´	TAC CAC AAG CCG TGC CAA CTT	59	10% DMSO	1067
ARO1-4RP	3´->5´	CGA TCA TCG AGA GAG CCT GTG A	59		
ARO2LP	5´->3´	GCT CCA CGC TCT CAG GAT CAC	59	10% DMSO	1194
ARO2RP	3´->5´	TTT CGC AGG TTC GGT GAA TGT	59		
ARO3LP	5´->3´	CAT TGG AAC ACA CGT GGA AAT CA	61	-	1099
ARO3RP	3´->5´	AAC GAG GAG GAG GAC GAC GAT	61	-	
ARO4LP	5´->3´	CTT TCG ATT TTG GTT CTC ACG	52	-	1032
ARO4RP	3´->5´	CCT CTC CTT CTT GAA ATT CCC	52	-	
LBa1	3´->5´	TGG TTC ACG TAG TGG GCC ATC G	52-61	-	*
LBb1	3´->5´	GCG TGG ACC GCT TGC TGC AAC T	52-61	-	*
T-D fw	5´->3´	TCG GCC GTT GCT GTC GTA ATG ATA	61	-	403
T-D rev	3´->5´	GAC TGT GGC CGG CTG GGT GTG	61	-	

*Fragment size dependent on the second primer used for each reaction

Table 7.1.3: List of primers used for generation of constructs

Name	Orien-tation	Sequence	Annealing temperature (°C)	Additional ingredients	Product size (bp)
ARO1p fw	5´->3´	TAA AGa gat ctA AGC TGG TGT C	56	4% DMSO	720
ARO1p rev	3´->5´	CGC CAT Gag atc tAA CAA TCA A	56	4% DMSO	
ARO1 GFP fw	5´->3´	TTG Tcc tag gTC ATG GCG GAT ATT GTG AAA CAG	58	4% DMSO	2015
ARO1 GFP rev	3´->5´	CGT Ccc tag gCA ATG AAA TCC TCT TGA CCC TC	58	4% DMSO	
ARO2 GFP fw	5´->3´	CTG Acc tag gCG ATG GCA GAC ATC GTC AAG	58	4% DMSO	1976
ARO2 GFP rev	3´->5´	AAT Acc tag gCA ATT GAA ATT GTA ACC CTT TGA TCC	58	4% DMSO	
PAro1F	5´->3´	CTC Tcg gcc gcg ATC TAA GCT GGT GT	*	-	714
PAro1R	3´->5´	CCC Cac tag tAA CAA TCA AGA AAC TC	*	-	
EC1-PF	5´->3´	CTC Tcg gcc gCC TTA TGA TTT CTT C	*	-	481
EC1-PR	3´->5´	CCC Cgg atc cTT CTC AAC AGA TTG ATA A	*	-	
ARO-Bam	3´->5´	ccc GGA TCC TCT CTT CCT TTA ATG C	*	-	Eco / Bam:307 Eco/ Mlu:309
ARO-Eco	5´->3´	ccc cgA ATT CCG GCG GAT AA	*	-	
ARO-Mlu	3´->5´	ctc tAC GCG TCT CTC TTC CTT TAA TGC	*	-	

*Primers were designed and used by the DNA cloning service, Hamburg.

Table 7.1.4: List of primers used for yeast two hybrid screen

Name	Orien-tation	Sequence	Annealing temperature (°C)	Additional ingredients	Product size (bp)
Y2H/Aro1 NcoI	5´->3´	TTC cca tgg CGG ATA TTG TGA AAC AG	57	10% DMSO 1M Betain	2005
Y2H/Aro1 SmaI	3´->5´	ccc ggg CAT ATA TCA ATG AAA TCC TCT TGA	57	10% DMSO 1M Betain	
Y2H/Act3 NcoI	5´->3´	TCC TCG AGA GTA GAc cat ggC TGA T	55	-	1157
Y2H/Act3 SmaI	3´->5´	GGC TTC ccc ggg AGC AGA CTT AAC T	55	-	
Y2H/Act4 NcoI	5´->3´	CCA GAT TGA Acc atg gCG GAC GGT G	60	10% DMSO 1M Betain	1139
Y2H/Act4 SmaI	3´->5´	GAc ccg ggA TTA GAA GCA TTT CCT ATG C	60	10% DMSO 1M Betain	
Y2H/Act7 NcoI	5´->3´	AAG TGA Acc atg gCC GAT GGT GAG G	55	-	1137
Y2H/Act7 SmaI	3´->5´	ccc ggg TAG AAG CAT TTC CTG TGA AC	55	-	
Y2H/GFP NcoI	5´->3´	cca tgg GCA AGG GCG AGG AAC TGT T	55	-	910
Y2H/GFP SmaI	3´->5´	GAT Ccc cgg gTC ACT TGT AGA GTT CAT CC	55	-	

Table 7.1.5: List of primers used for ARO1-RNAi plants

Name	Orien-tation	Sequence	Annealing temperature (°C)	Additional ingredients	Product size (bp)
bar biV fw	5´->3´	CCG TAC CGA GCC GCA GGA AC	64	-	444
bar biV rev	3´->5´	CAG ATC TCG GTG ACG GGC AGG AC	64	-	
iF2 rev	3´->5´	CCA CCA ACC CAC CAG AAA	54	4%DMSO	1108
P106325 fw 1	5´->3´	TGC CTT ATG ATT TCT TCG GTT TC	54	4%DMSO	

Table 7.1.6: List of primers used for sequencing

Name	Orien-tation	Sequence	Annealing temperature (°C)
A1prom5´	3´->5´	CTT GTT CGT TTT AAT AAC TCA TGA	58
A1prom3´	5´->3´	CGA TCA AAG CCA CCA TCT TCA	58
GUS start rev	3´->5´	ATC CAG ACT GAA TGC CCA CA	60
GFP seq	3´->5´	CCA GTT CCA CCA GGA TTG	60
Ubi 1	5´->3´	CTG TTT CTT TTG TCG ATG C	57
3´AD seq	3´->5´	AGATGGTGCACGATGCACAG	*
3´DNA-BD seq	3´->5´	ATCATAAATCATAAGAAATTCGCC	*
5´LD amplier	5´->3´	CTA TTC GAT GAT GAA GAT ACC CCA CCA AAC CC	*
3´LD amplier	3´->5´	GTG AAC TTG CGG GGT TTT TCA GTA TCT ACG AT	*
M13 fw	5´->3´	CGT TTT ACA ACG TCG TGA CTG GG	53-60
M13 rev	3´->5´	CCT GTG TGA AAT TGT TAT CCG CT	53-60
T7 seq	5´->3´	TAATACGACTCACTATAGGGC	*

*Primers were designed by Clontech, Saint-Germain-en-Laye, France and used for sequencing by 4base lab, Reutlingen

7.2 Yeast two hybrid screen cDNA inserts

Table 7.2: Gene matches found for cDNA fragments from yeast two hybrid screen with pollen cDNA library. Blue clones showed strong activation of the *lacZ* reporter, orange clones intermediate activation.

Gene	cDNA fragment isolated from clone
PGA3, At3g07820	1-E-5, 1-E-12, 2-A-8, 2-A-9, 2-C-6, 2-G-1, 3-E-5, 4-B-7, 4-C-1, 4-E-3, 4-F-11, 4-F-12, 5-A-2, 5-A-4, 5-H-1, 6-A-3, 6-B-1, 6-B-11, 6-B-12, 6-C-1, 6-C-2, 6-C-8, 6-E-1, 6-F-8, 6-G-1, 7-A-7, 7-A-9, 7-D-2, 7-H-2, 8-A-2,
Polygalacturonase, At5g48140	5-G-3, 8-D-4
Polygalacturonase, At2g23900	5-C-10, 6-A-2
SKS13 copper ion binding, At3g13400	3-C-4, 4-C-12, 6-C-6, 6-E-7
Pectin esterase family, At5g 07430	8-A-4
No hit	5-B-4, 5-C-11, 7-E-4

7.3 Vector cards

7.3.1 pMG-2002

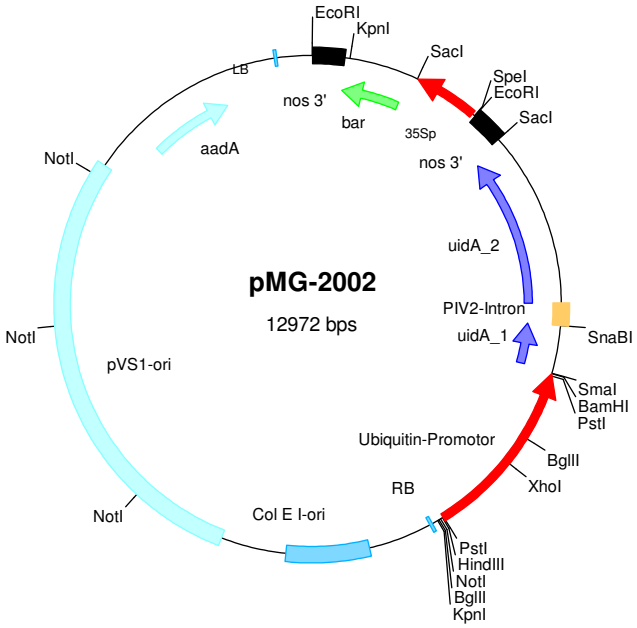

7.3.2 *AtARO1p::GUS*

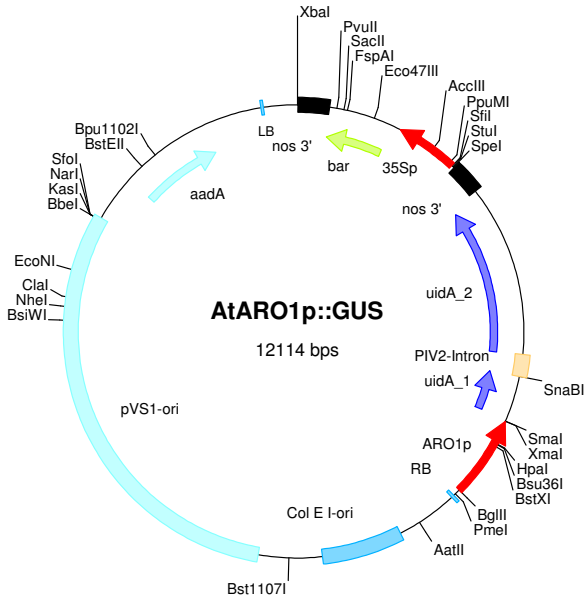

7.3.3 pLNU-GFP

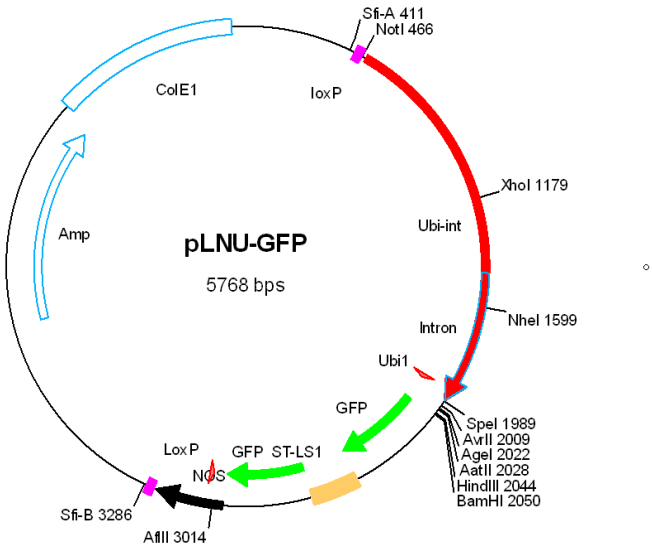

7.3.4 *UBIp::AtARO1-GFP* and *UBIp::AtARO2-GFP*

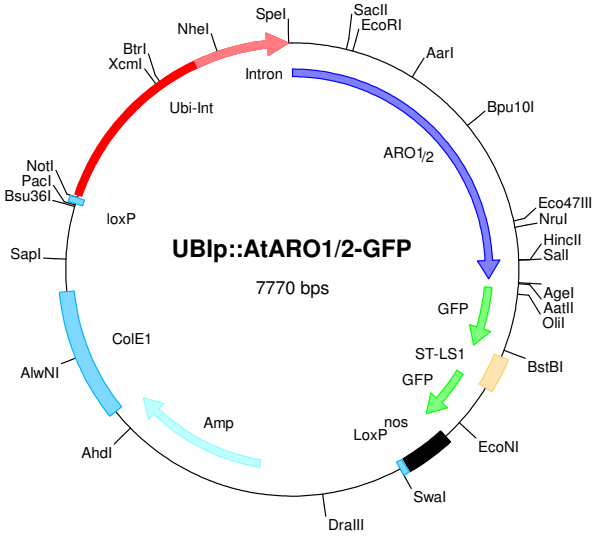

7.3.5 pLNU-*35Sp::AtARO1-GFP*

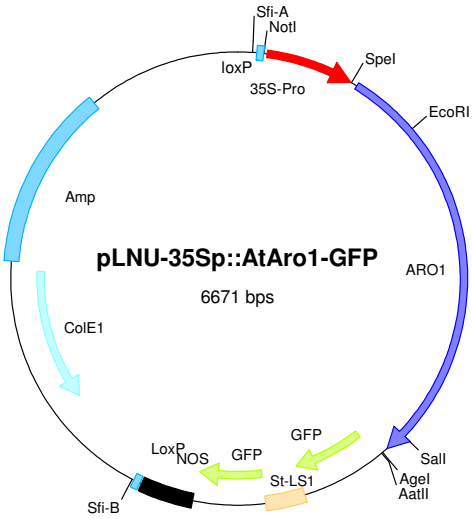

7.3.6 95P-Nos*35Sp::AtARO1-GFP*

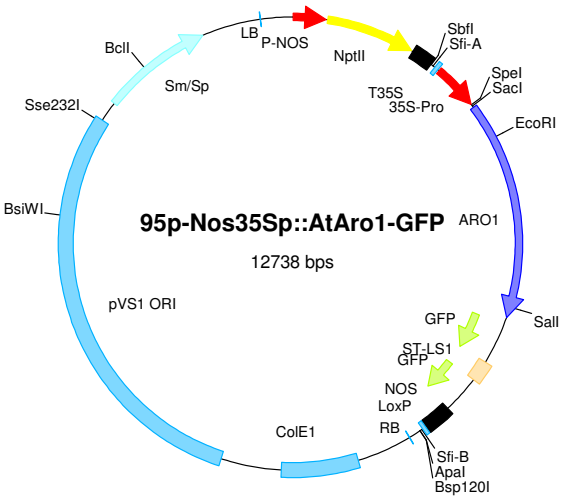

7.3.7 pLNU-*AtARO1p::AtARO1-GFP*

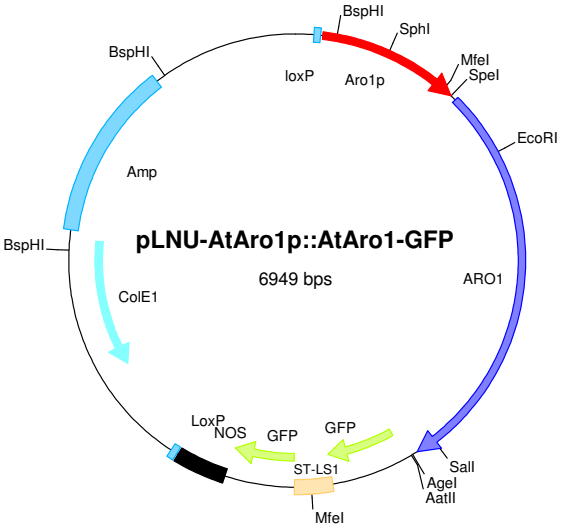

7.3.8 95P-Nos*AtARO1p::AtARO1-GFP*

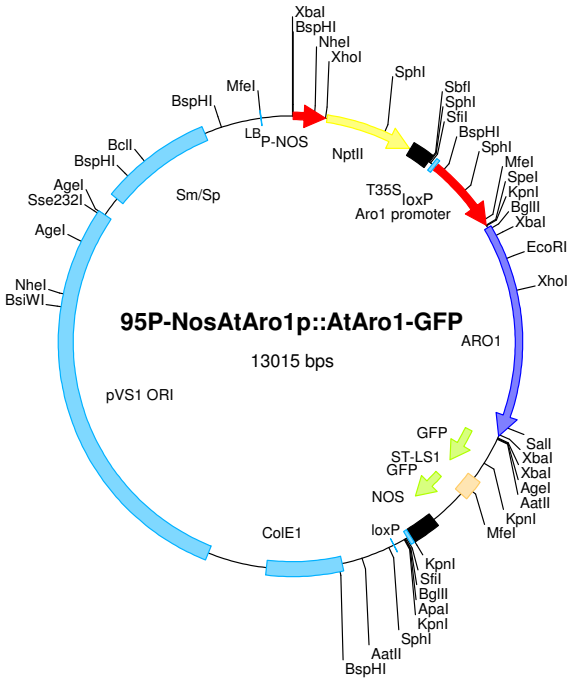

7.3.9 pUBI-iF2

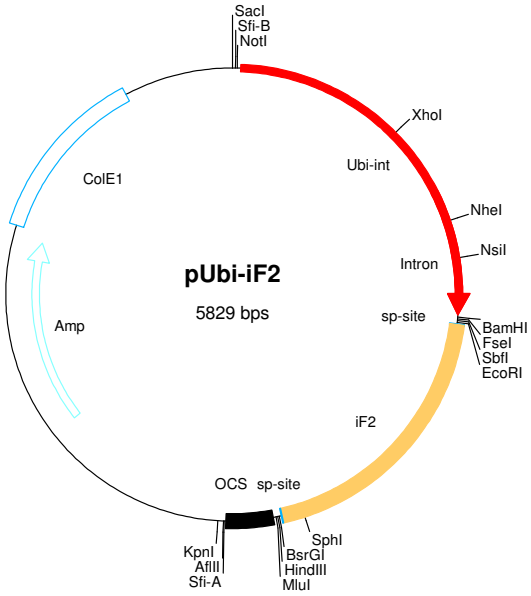

7.3.10 *pEC1-iF2*

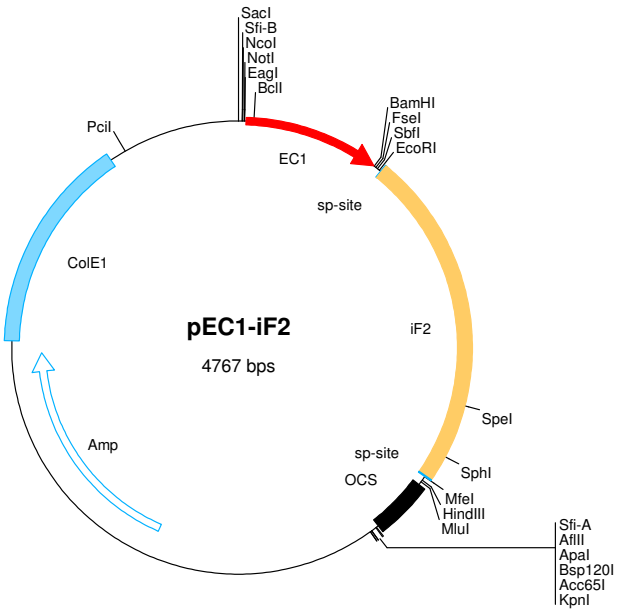

7.3.11 *pEC1-ARO1*-AS

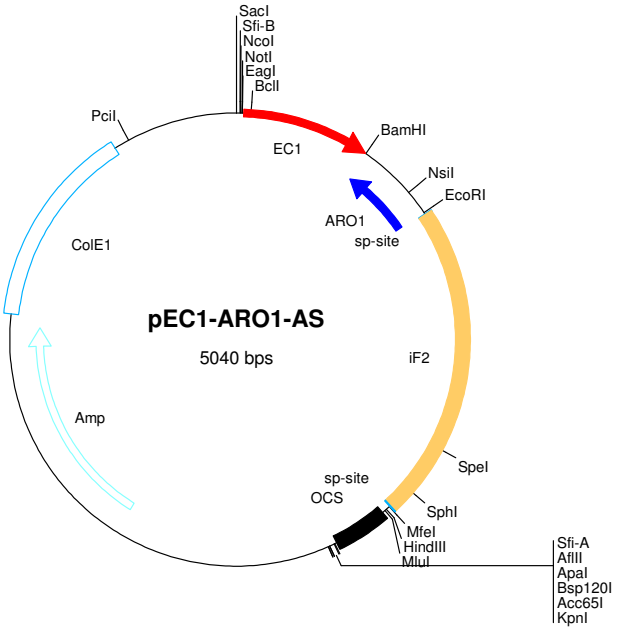

7.3.12 *pEC1-ARO1*-RNAi

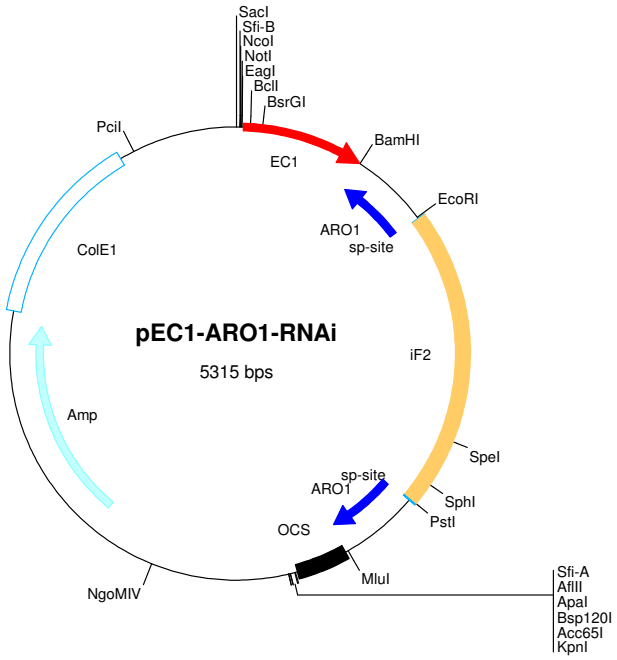

7.3.13 p7N*EC1p::ARO1-RNAi*

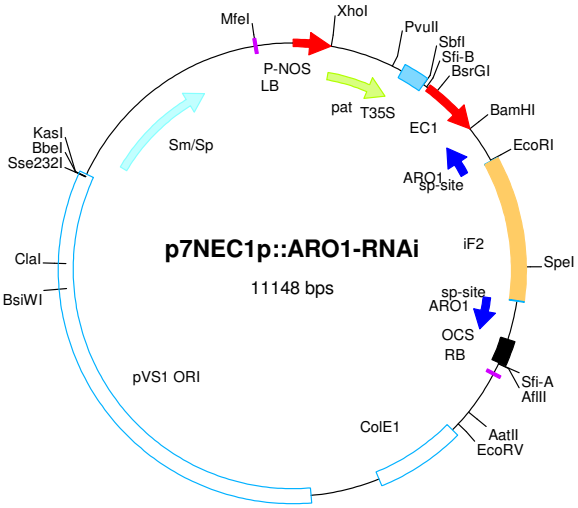

ACKNOWLEDGEMENTS

First of all I am grateful to Prof. Dr. Thomas Dresselhaus for giving me the opportunity to work in his group and providing laboratory and research facilities. I also thank him for the possibility to participate at international conferences and for the evaluation of my thesis.

I would like to thank Dr. Stefanie Sprunck for providing me with this interesting project and her support and supervision during my PhD thesis. I thank her for giving me always new ideas, for interesting discussions during the past years and for correcting my thesis.

I thank Prof. Dr. E. Kerkhoff for being an expert of my thesis.

I thank Manfred Gahrtz for valuable discussions and corrections of part of my thesis.

A warm thanks goes to all former members of the “Golden Lab” in Hamburg, Jörg Bantin, Preeti Garg, Mihaela Márton, Dunja Leljak-Levanic, Hanna Heidemann and Eva Thiemann for the friendly and supporting atmosphere.

Further I would like to thank everybody who shared the time with me during the move to Regensburg and in our new “Blue Lab”, Birgit Bellmann, Irina Kliwer, née Kempel, Nadia Krohn, Jeab Srilunchang, Lucija Soljic, Andreas Lausser, Svenja Rademacher, Monika Kammerer, Annemarie Taffner, Michaela Leyh, Anna Helminger, JongSu An and Kwang-Il Ri.

I would like to thank Veronika Mrosek and Uschi Reinitz for coping with all bureaucratic matters and Günther Peissig for taking care of my plants and collecting tons of seeds.

I would like to thank Lucija Soljic for sharing her egg cell microarray data with me and Guido Grossmann for the introduction into the confocal microscope and to the bavarian traditions.

I am grateful to Mr. Quader, Elke Woelken and Rudolf Reimers, who helped me with the confocal microscope in Hamburg. Fred Berger kindly provided the marker line H3.3-mRFP1. I acknowledge Rainer Merkl for assistance with alignments and phylogenetic trees.

The German Research Council (DFG) is acknowledged for financial support (grant DR 334/5-2).

Special and big thanks go to my wonderful parents Karita and Wolfgang Gebert and my sister Corinna as well as my grandma Helga Schütt, who supported me during my whole studies and never stopped believing in me. From all my heart, I thank Marc for being there for me during all this times, for building me up when times were difficult and for his patience, understanding and love.

Eidesstattliche Erklärung

Ich erkläre hiermit an Eides statt, dass ich die vorliegende Arbeit ohne unzulässige Hilfe Dritter und ohne Benutzung anderer als der angegebenen Hilfsmittel angefertigt habe; die aus anderen Quellen direkt oder indirekt übernommenen Daten und Konzepte sind unter Angabe des Literaturzitates gekennzeichnet.

Regensburg, den 23.05.08

Parts of this work are reported in:

Gebert, M., Dresselhaus, T. and Sprunck, S. F-actin organization and pollen tube tip growth is dependent on the gametophyte– specific Armadillo repeat protein AtARO1 (submitted)

Plant gametophyte transcriptional control sequences (2008)
Inventors: Gebert, M., Dresselhaus, T., Sprunck, S.;
Applicants: Gebert, M., Dresselhaus, T., Sprunck, S.,
Australian Center for Plant Functional Genomics; PCT-filed Nov. 11, 2007